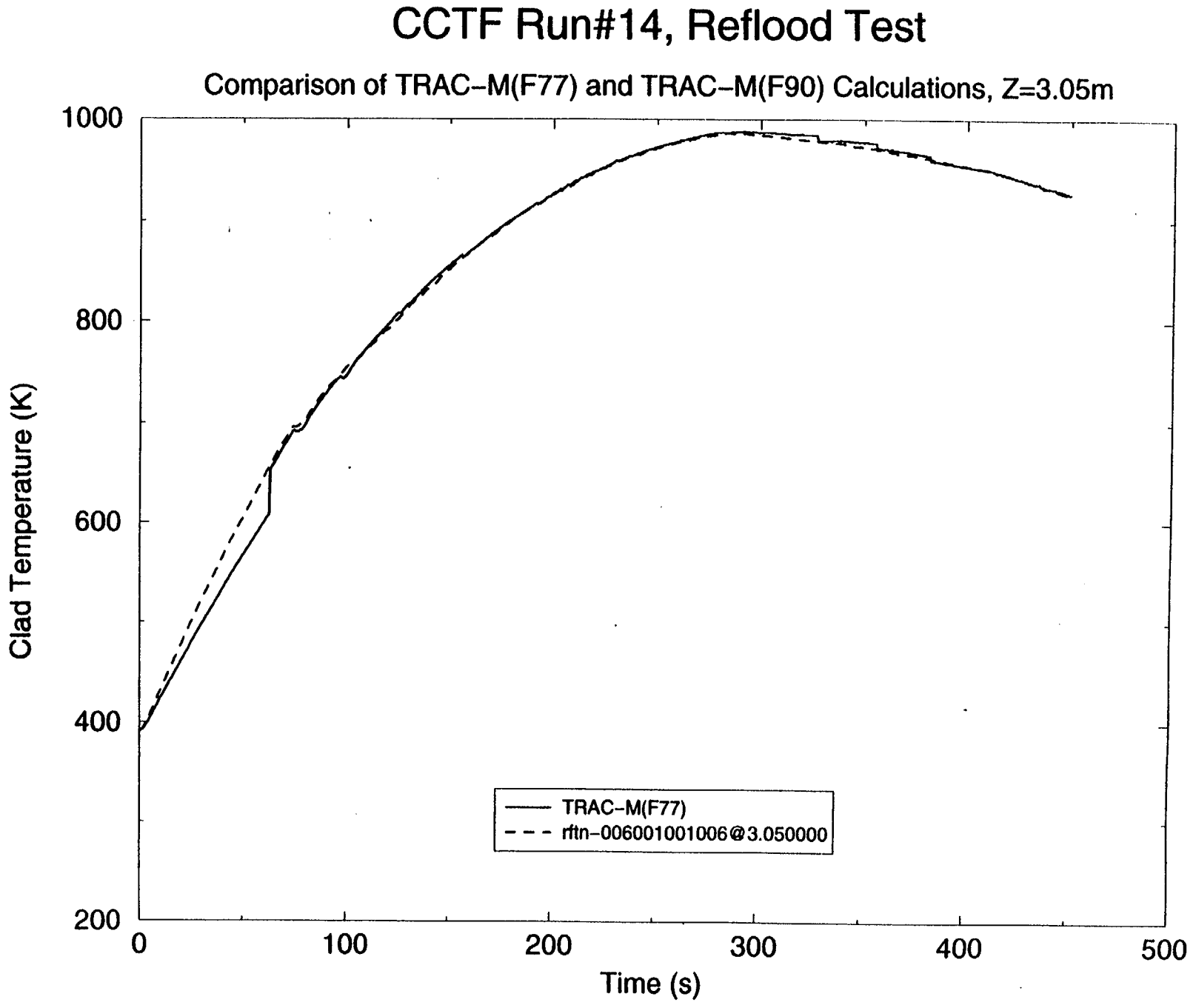

**Figure 4.4.52 CCTF Run 14, Reflood Test –
Comparison of TRAC-M(F77) and TRAC-M(F90) Calculations (Z=3.05m)**

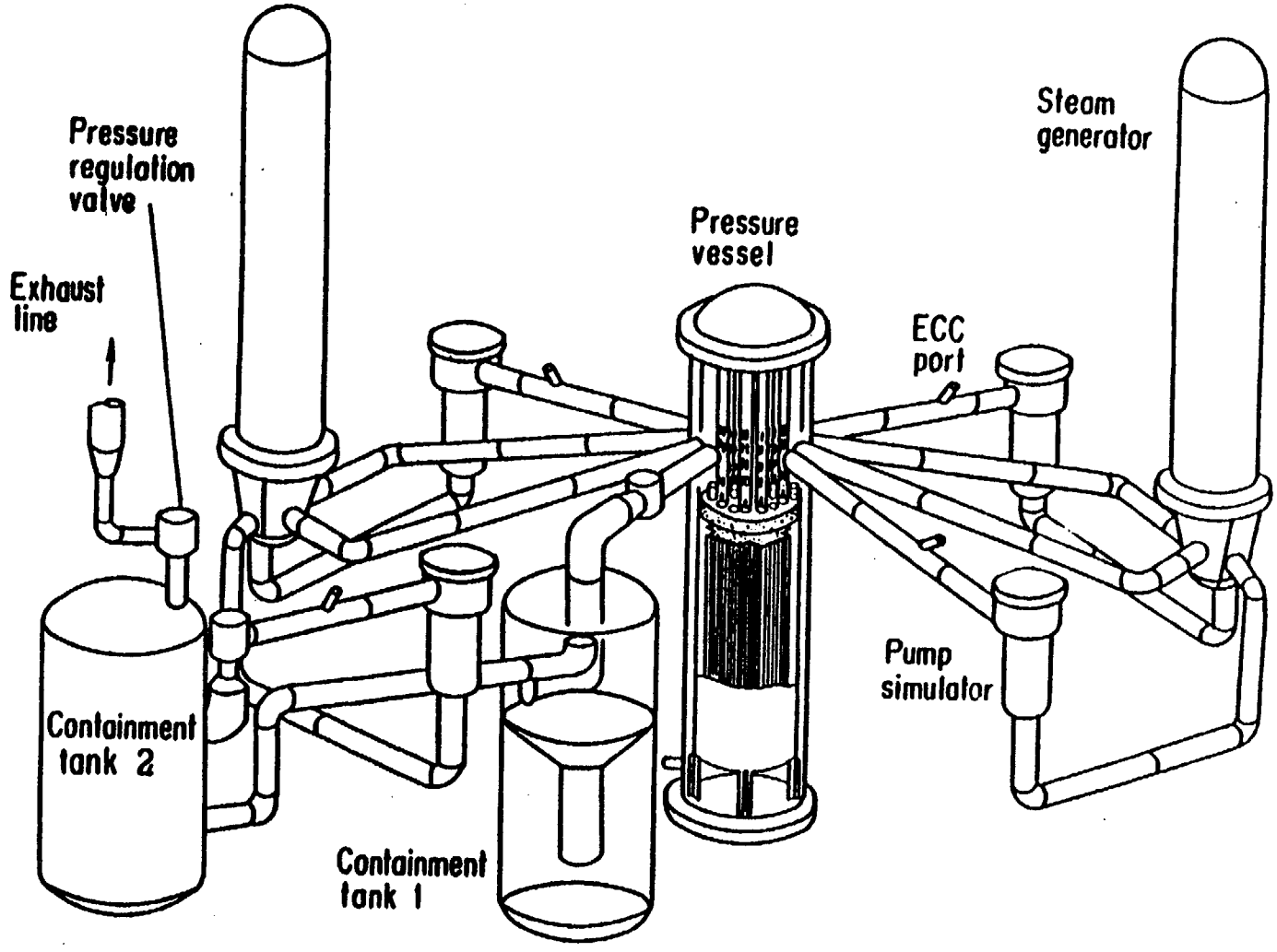

Figure 4.4.53 Isometric View of CCTF

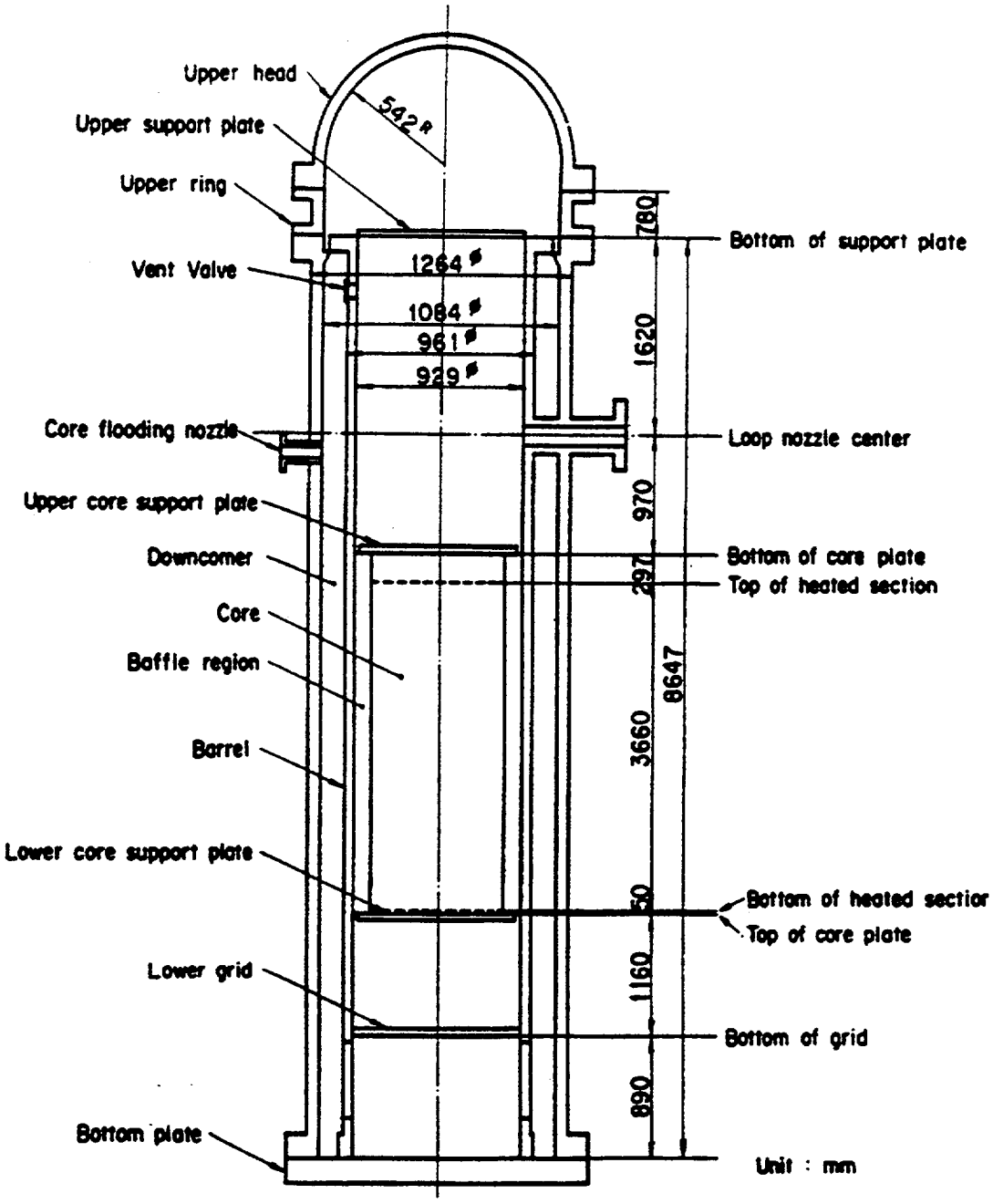

Figure 4.4.54 CCTF Pressure Vessel

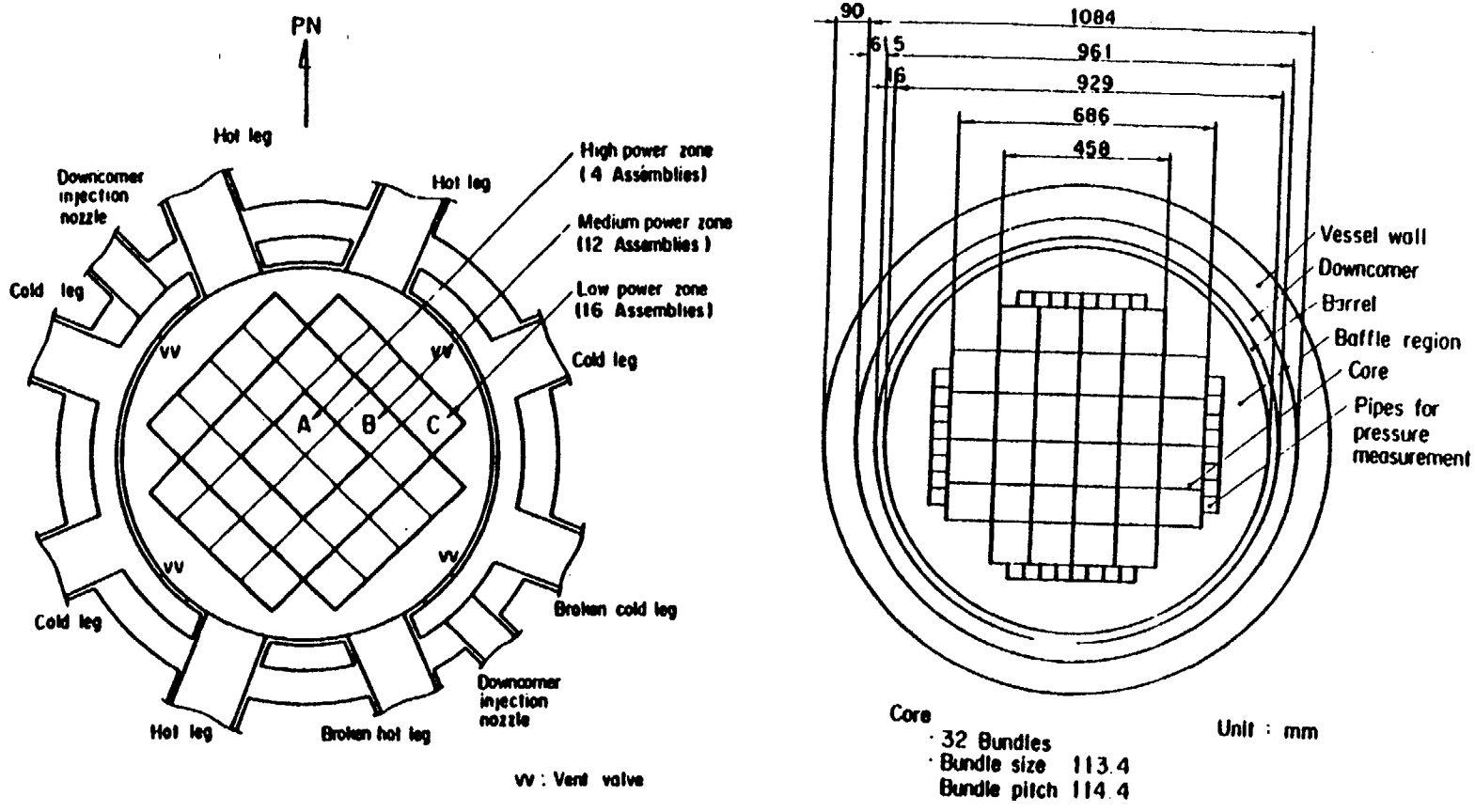

Figure 4.4.55 Cross-Sections of the CCTF Pressure Vessel

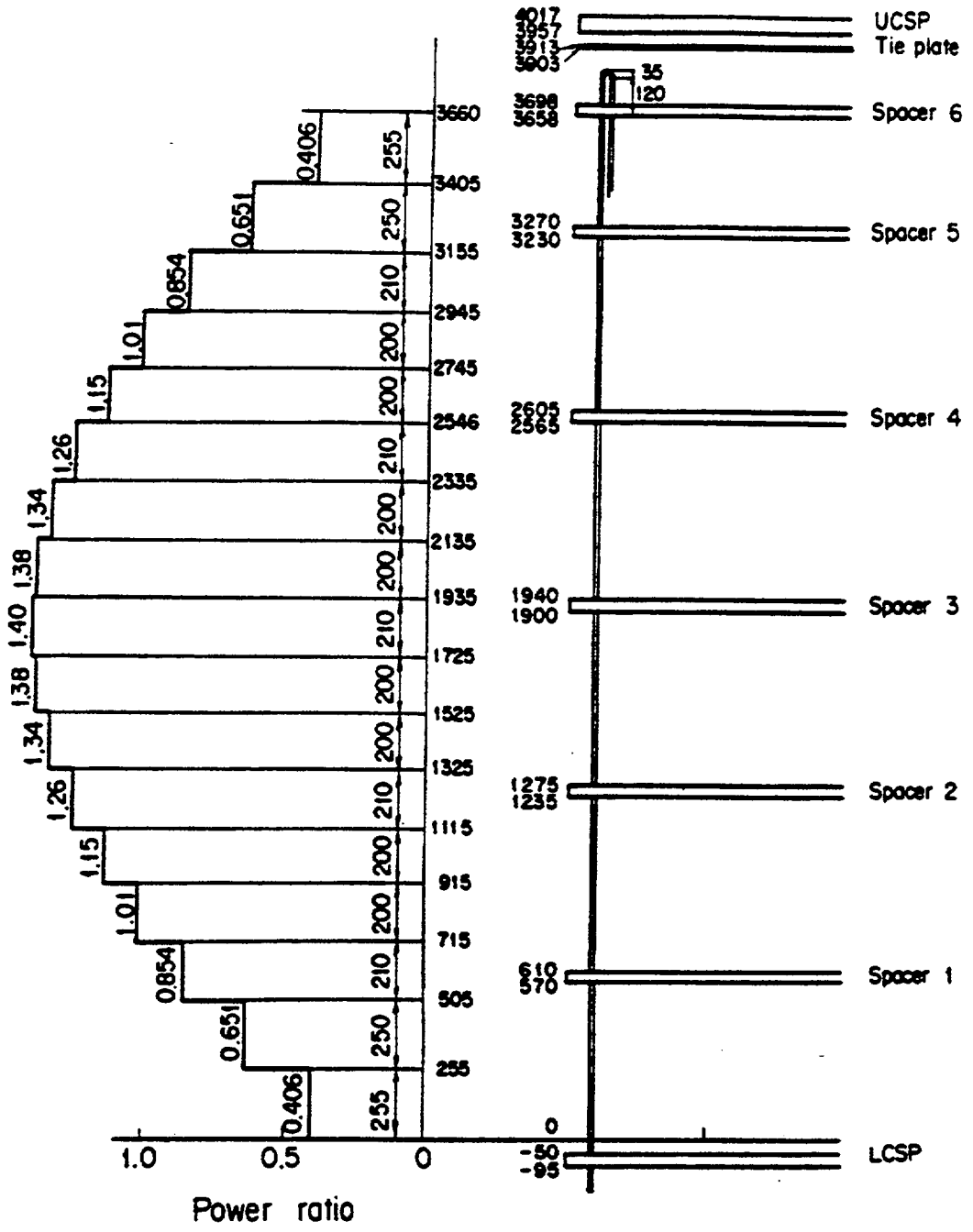

Figure 4.4.56 CCTF Heater-Rod Axial Power Profile

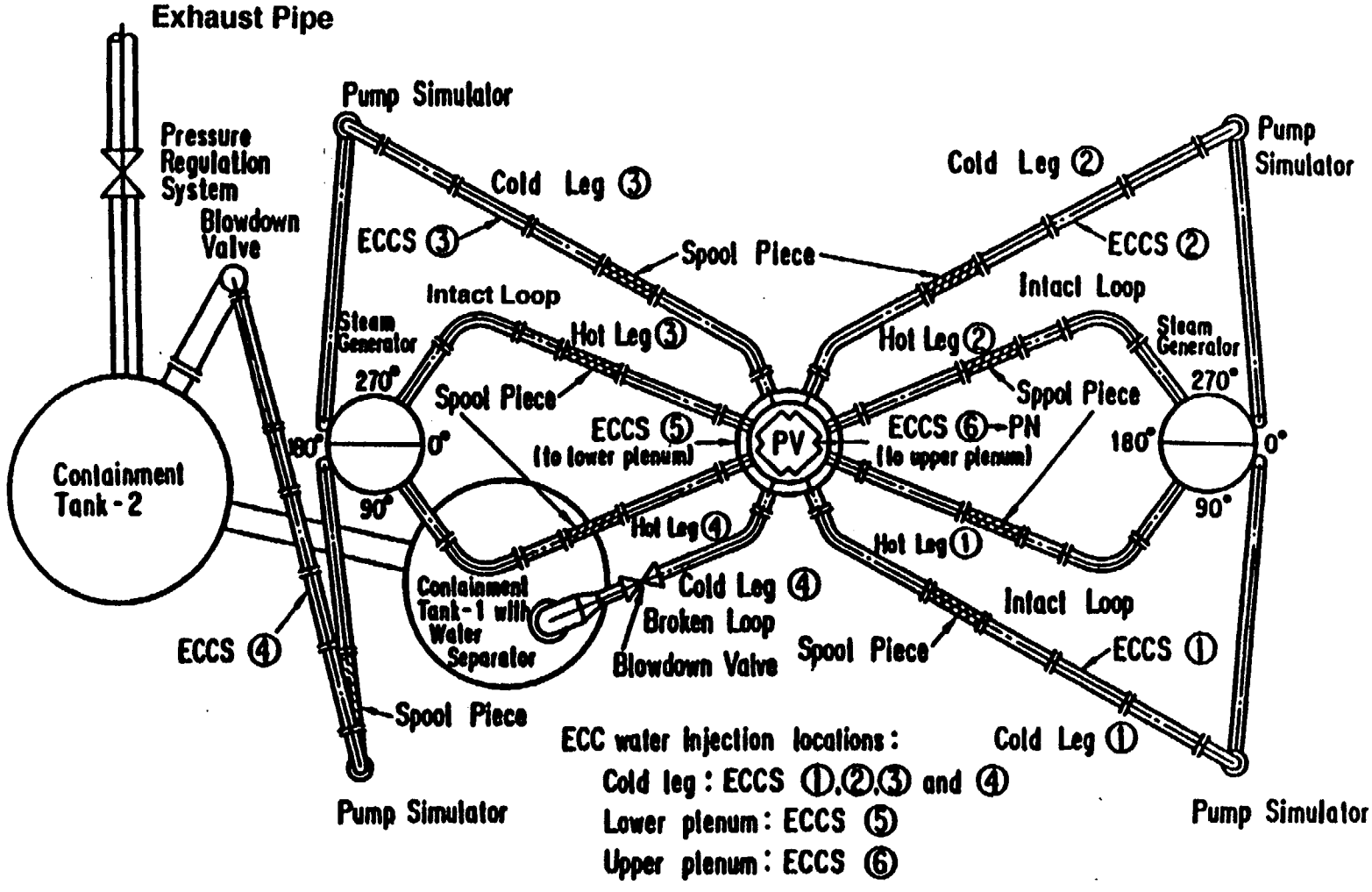

Figure 4.4.57 Top View of Primary-Loop Piping Layout

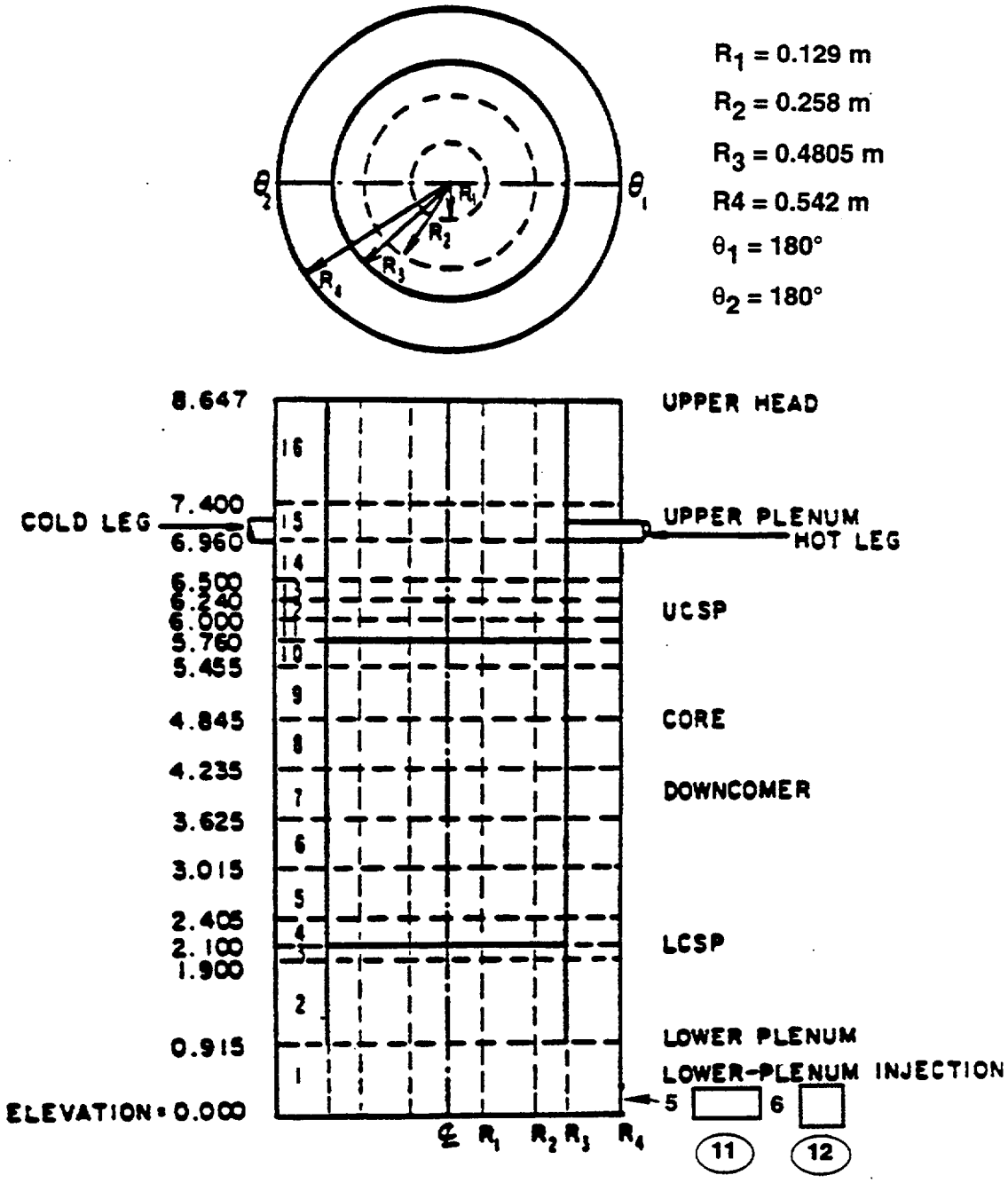

Figure 4.4.58 CCTF Pressure Vessel Noding: 2-Theta Model

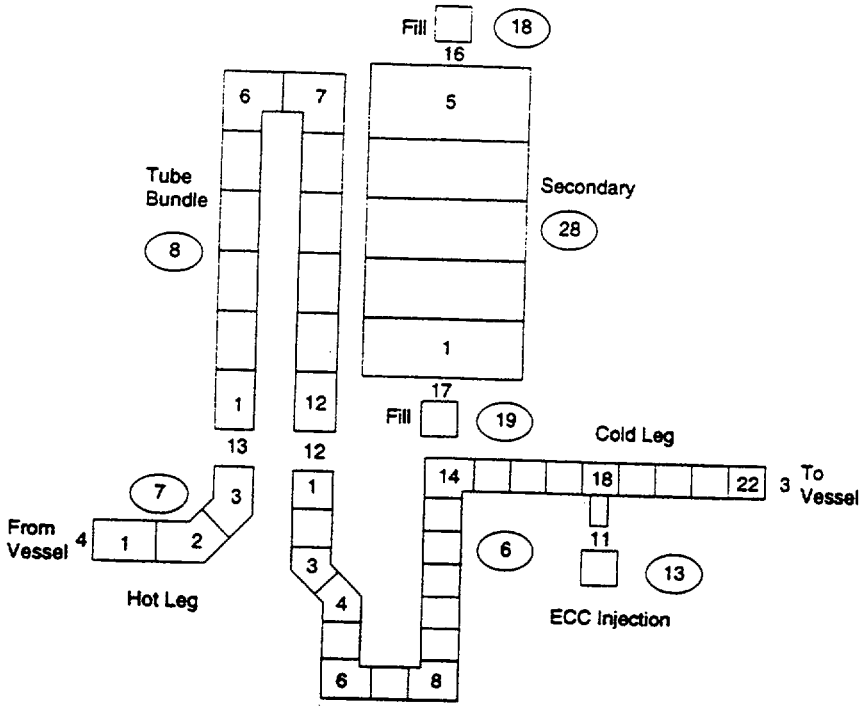

Figure 4.4.59 CCTF Intact-Loop Noding

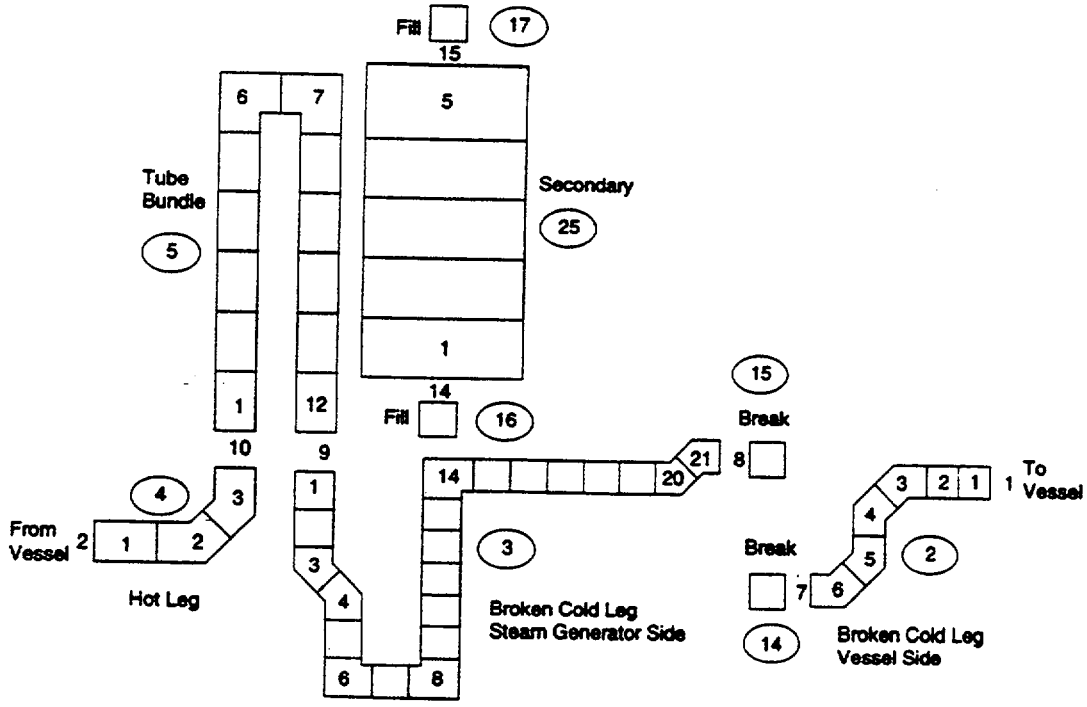

Figure 4.4.60 CCTF Broken-Loop Noding

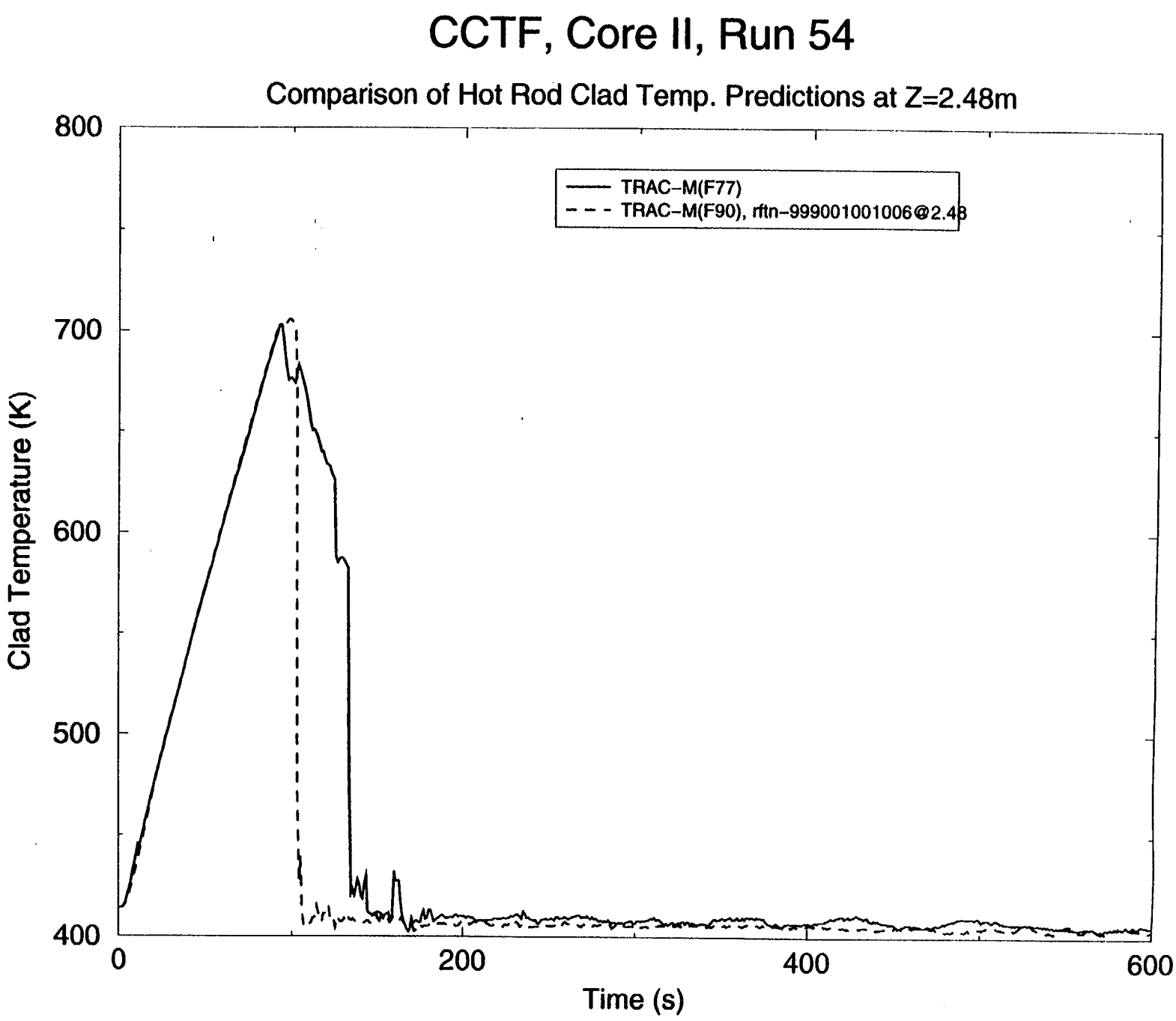

Figure 4.4.61 CCTF, Core II, Run 54 –
Comparison of Hot Rod Clad Temperature Predictions at Z = 2.48 m

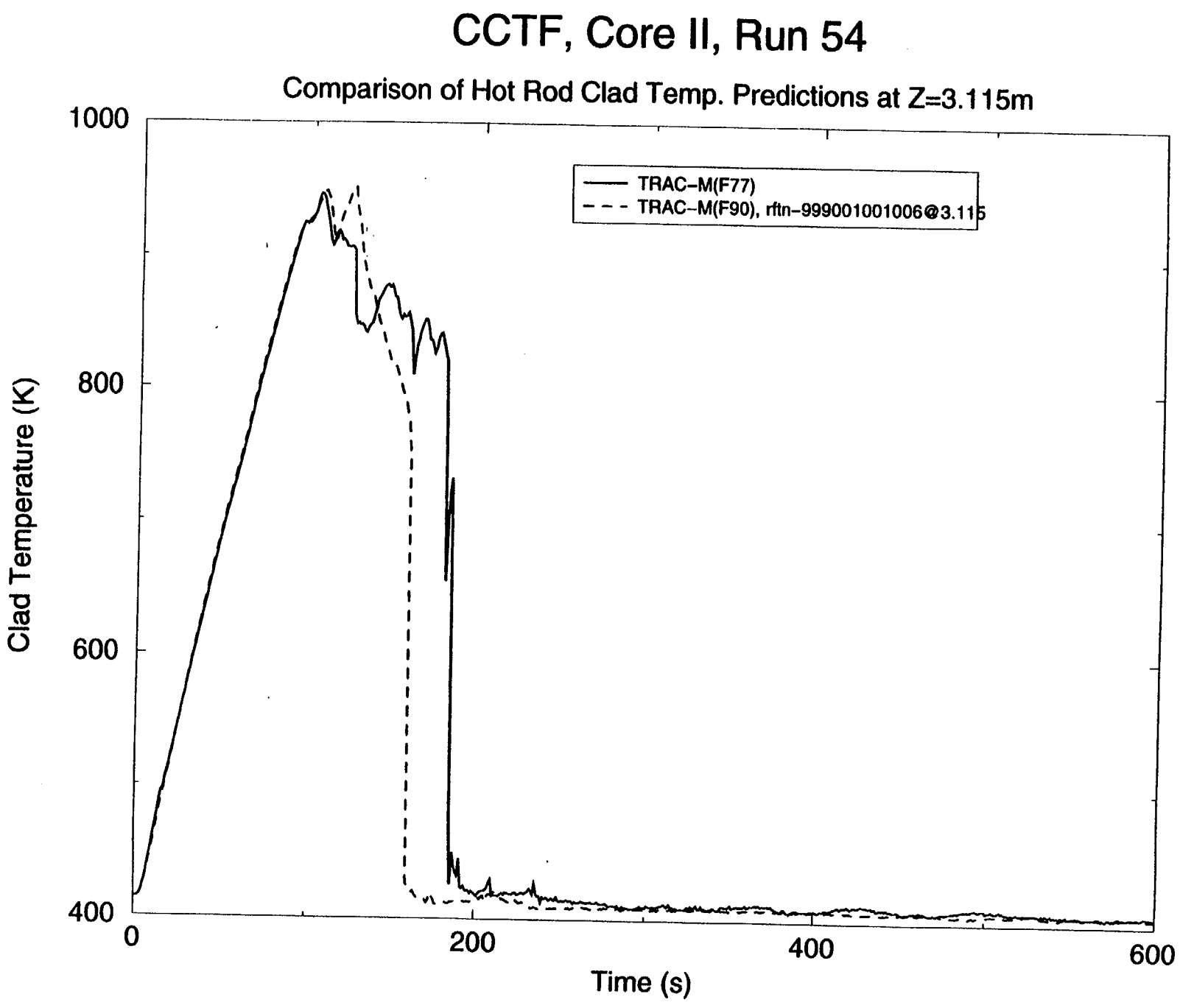

Figure 4.4.62 CCTF, Core II, Run 54 –
Comparison of Hot Rod Clad Temperature Predictions at Z = 3.115 m

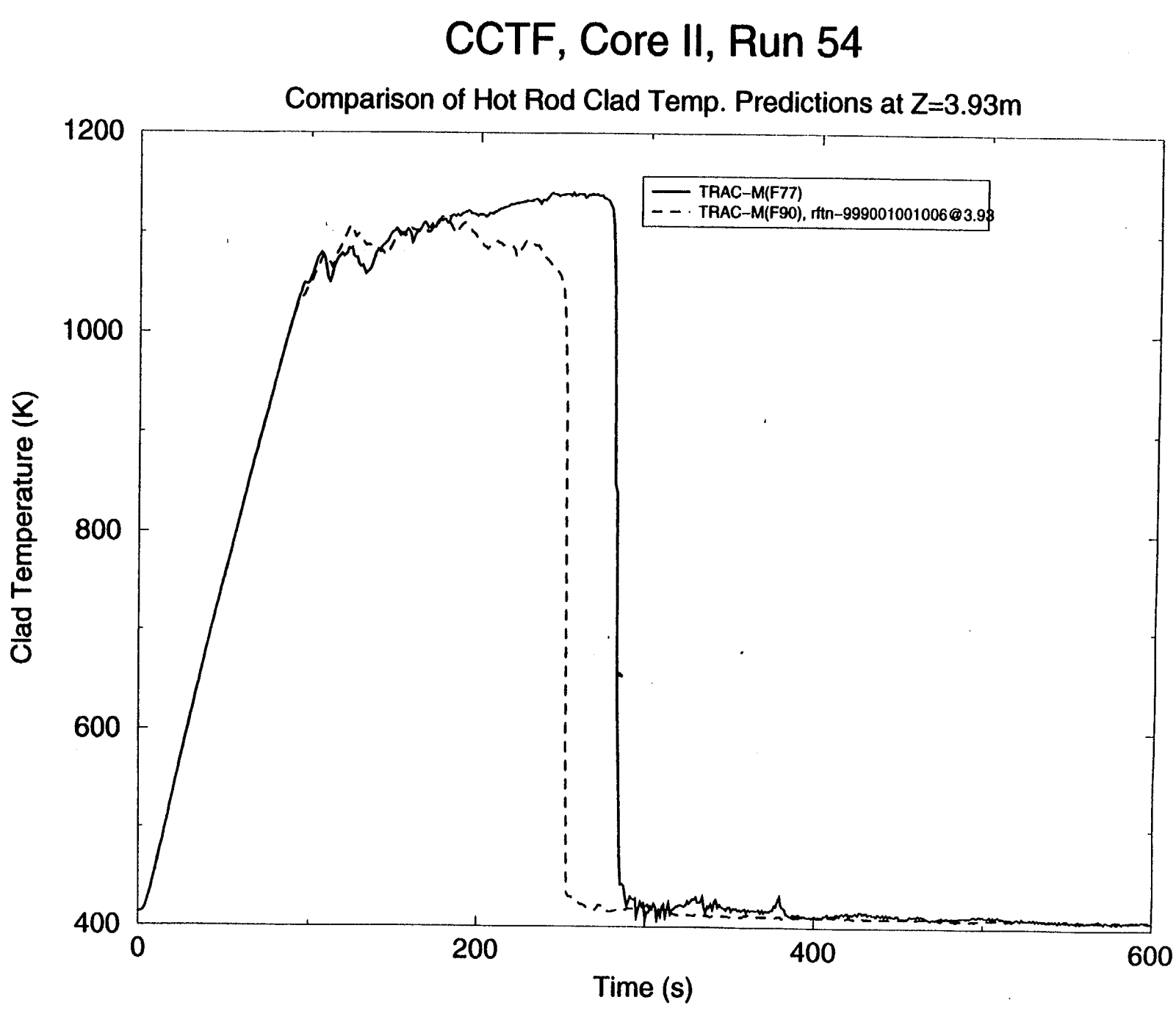

Figure 4.4.63 CCTF, Core II, Run 54 –
Comparison of Hot Rod Clad Temperature Predictions at Z = 3.93 m

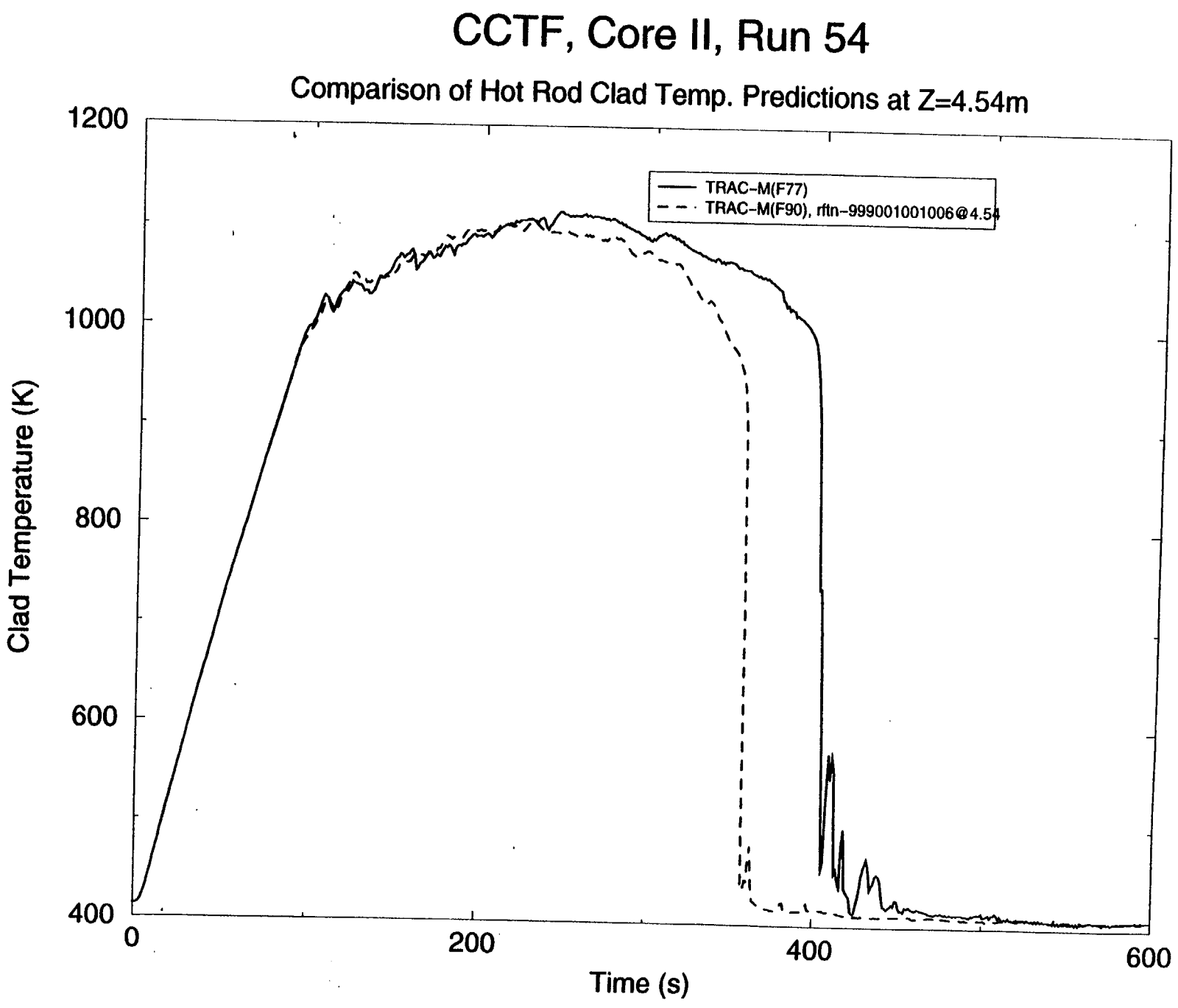

Figure 4.4.64 CCTF, Core II, Run 54 –
Comparison of Hot Rod Clad Temperature Predictions at Z = 4.54 m

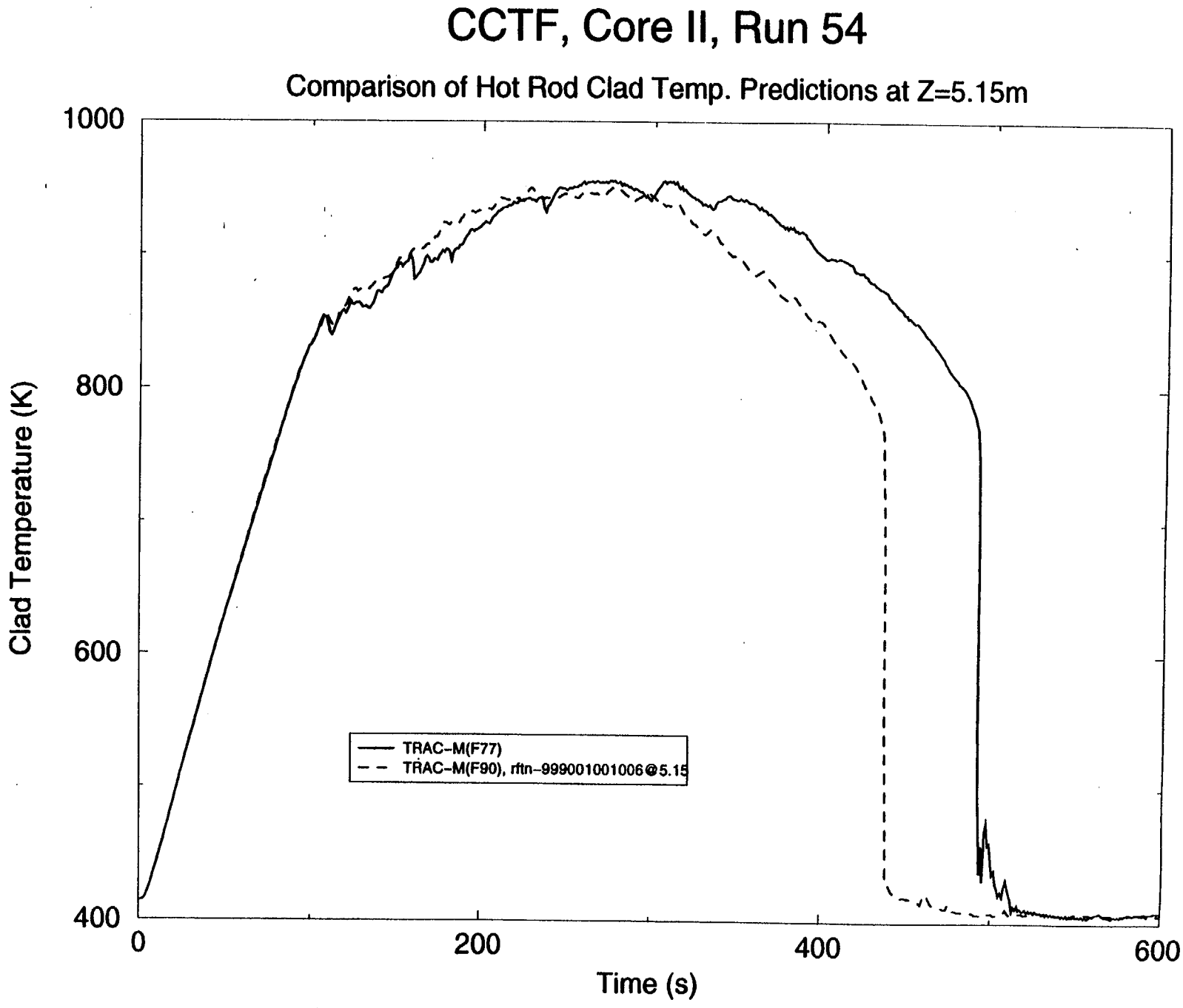

Figure 4.4.65 CCTF, Core II, Run 54 –
Comparison of Hot Rod Clad Temperature Predictions at Z = 5.15 m

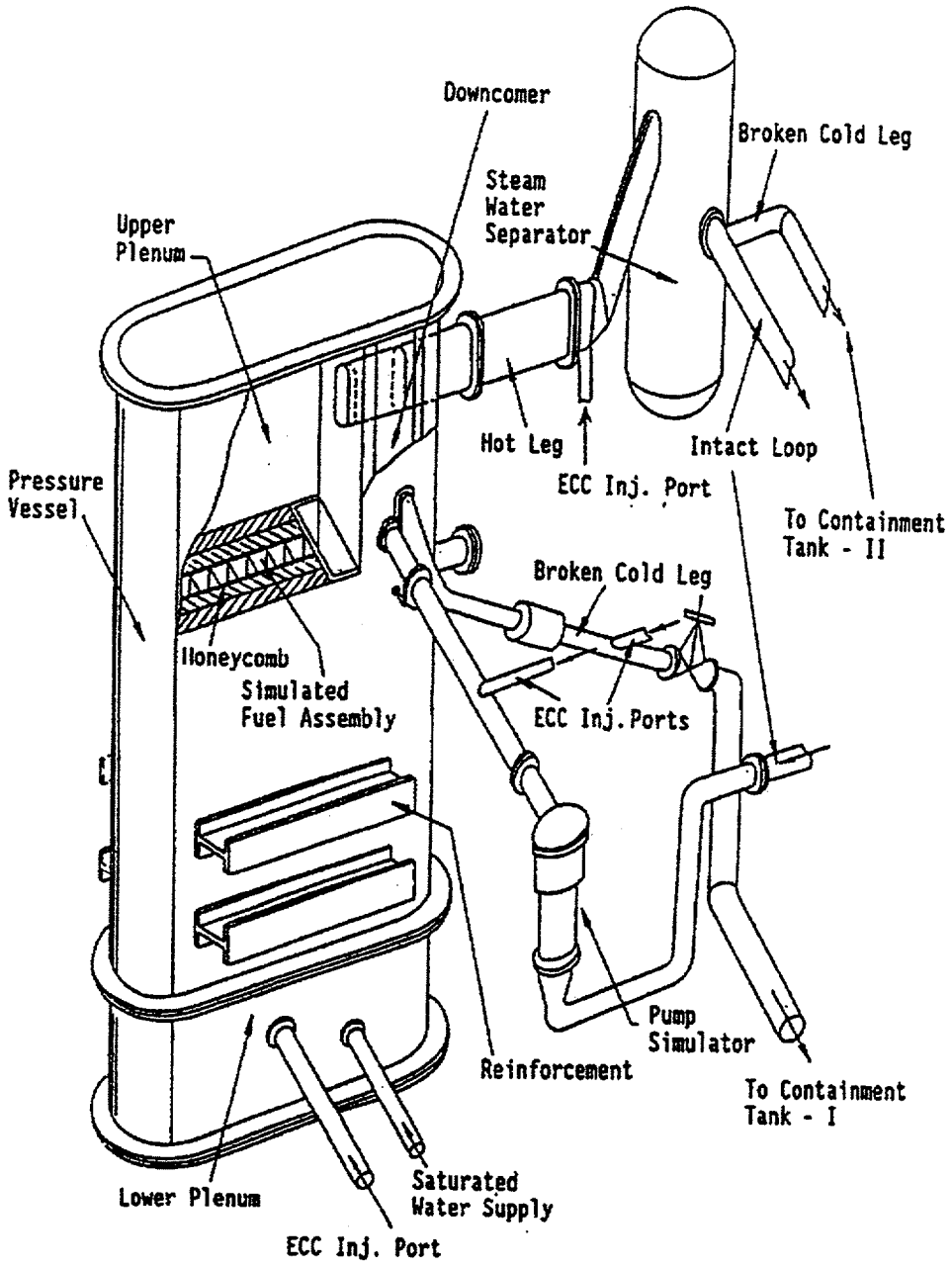

Figure 4.4.66 Overview of the Slab Core Test Facility

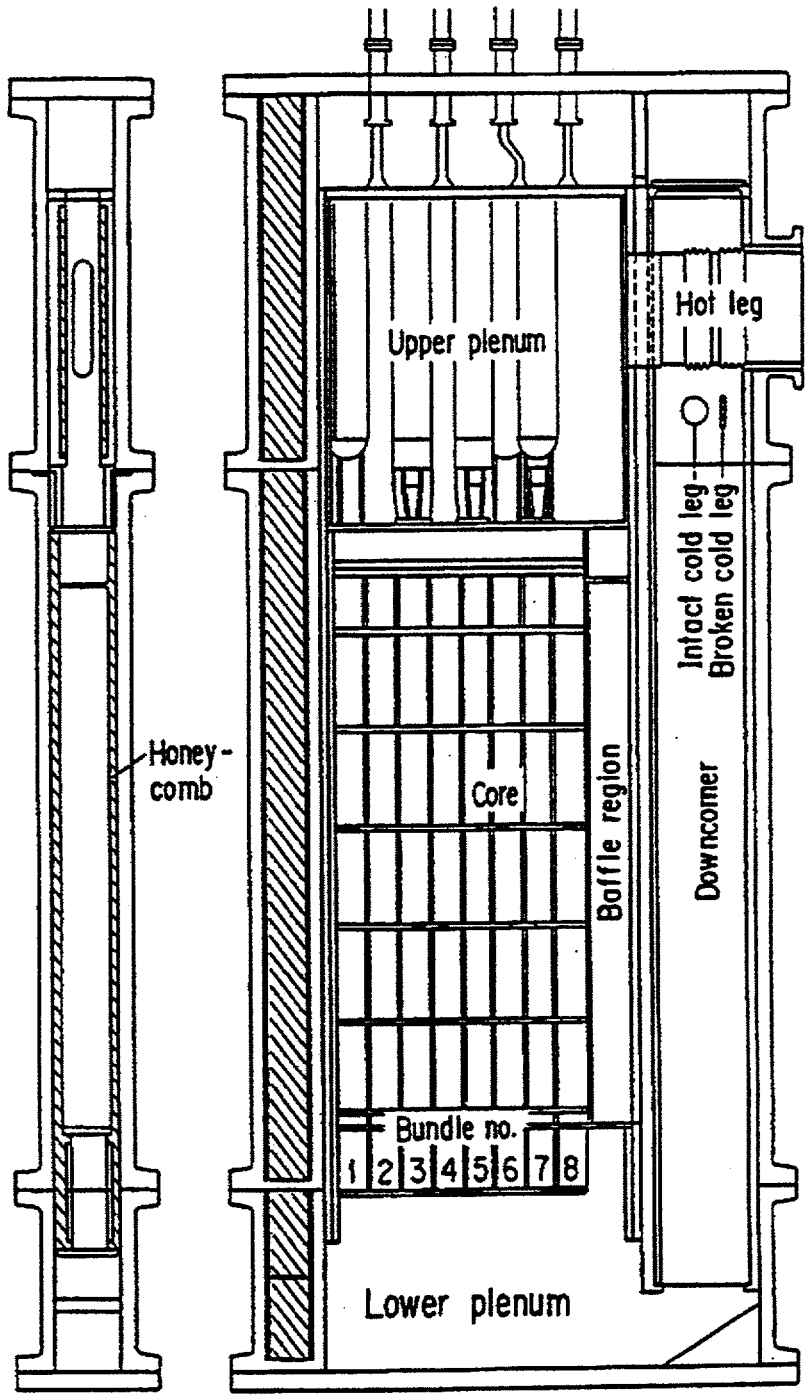

Figure 4.4.67 Vertical Cross-Section View of SCTF Pressure Vessel

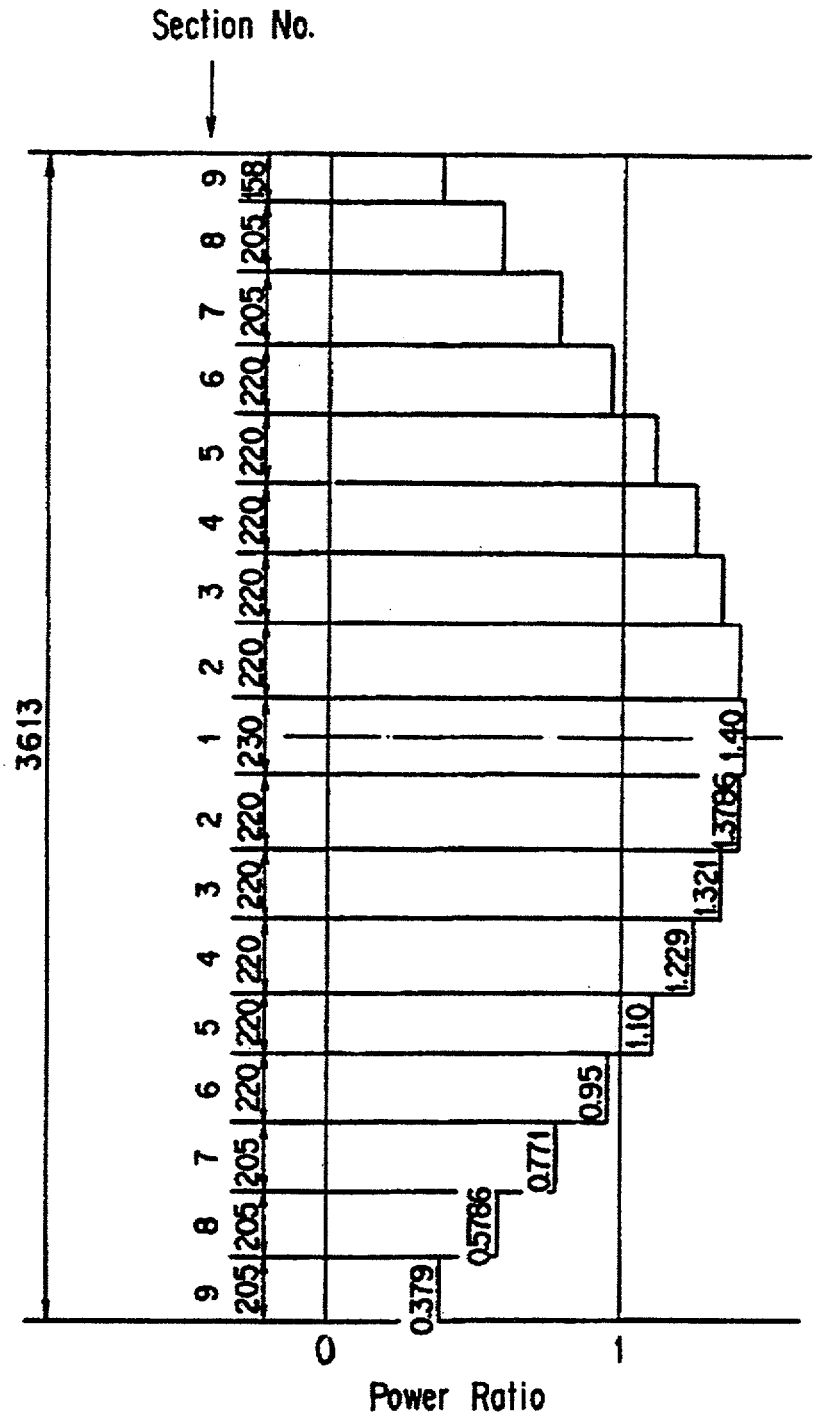

Figure 4.4.68 Axial Power Distribution of Heater Rods

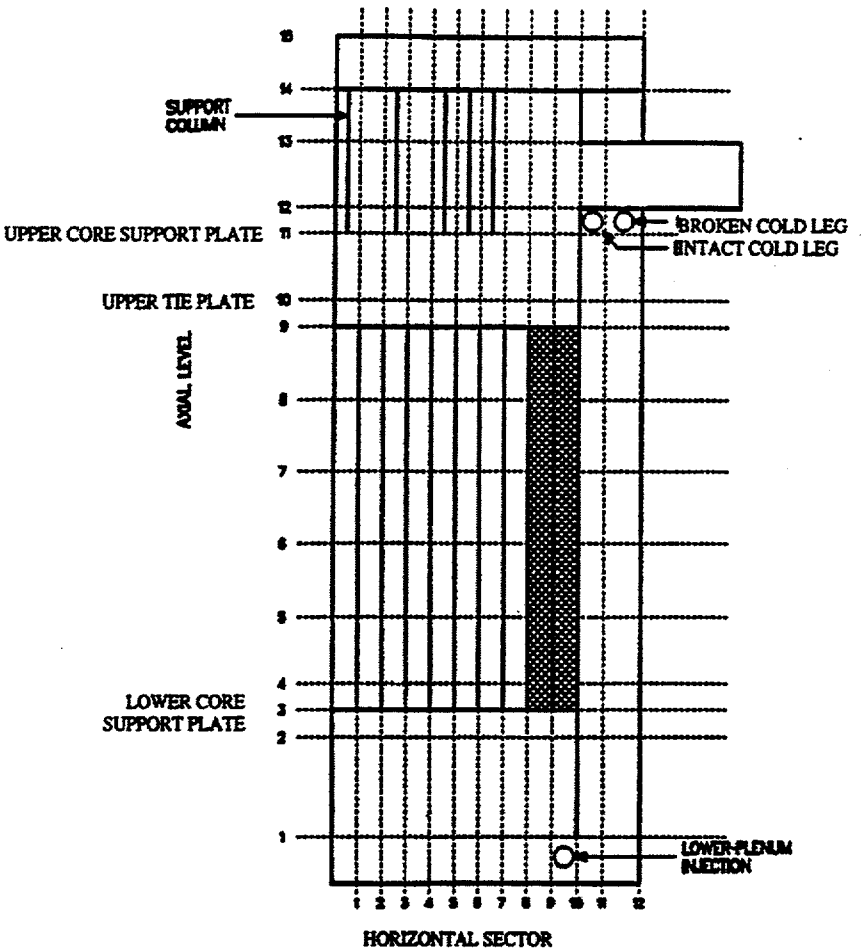

Axial Level	Elevation (m)	Horizontal Sector	Distance (m)
1	0.502	1	0.23
2	1.432	2	0.46
3	1.719	3	0.69
4	1.9595	4	0.92
5	2.6245	5	1.15
6	3.2895	6	1.38
7	3.9545	7	1.61
8	4.6195	8	1.84
9	5.332	9	2.017
10	5.748	10	2.334
11	6.337	11	2.667
12	6.822	12	3.020
13	7.559		
14	7.996		
15	8.657		

Figure 4.4.69 Pressure Vessel Noding Diagram

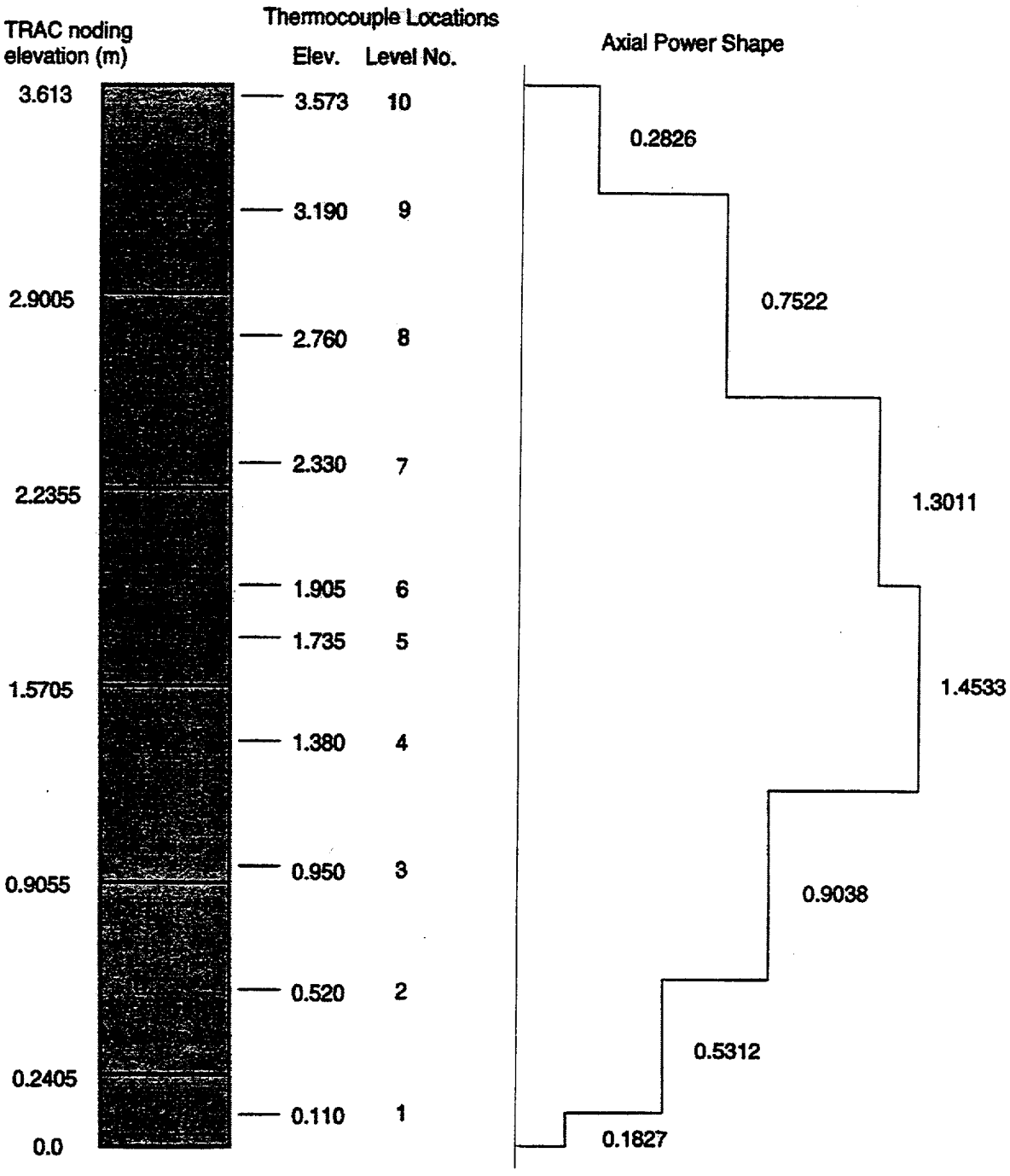

Figure 4.4.70 TRAC Heater-Rod Noding, Thermocouple Locations, and Modeled Axial Power Shape

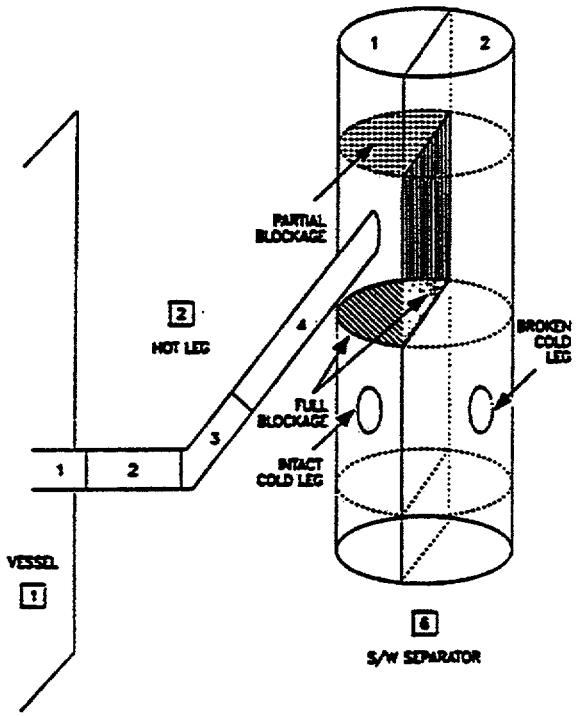

Figure 4.4.71 Hot-Leg and S/W-Separator Noding Diagram

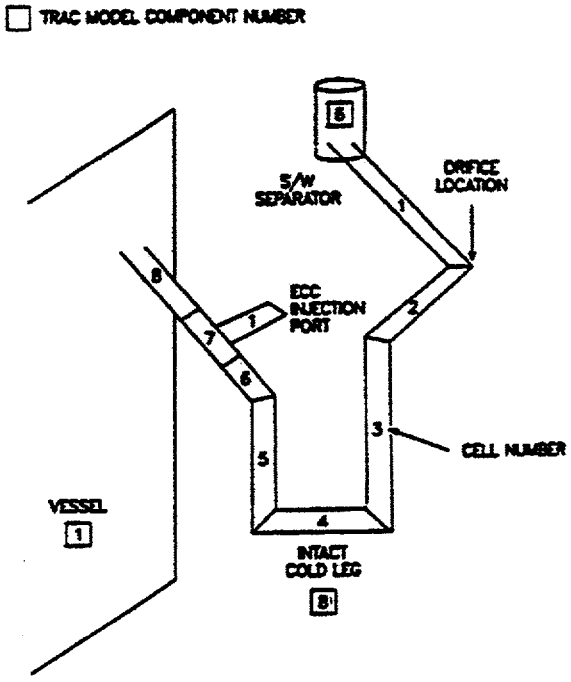

Figure 4.4.72 Intact Cold-Leg Noding Diagram

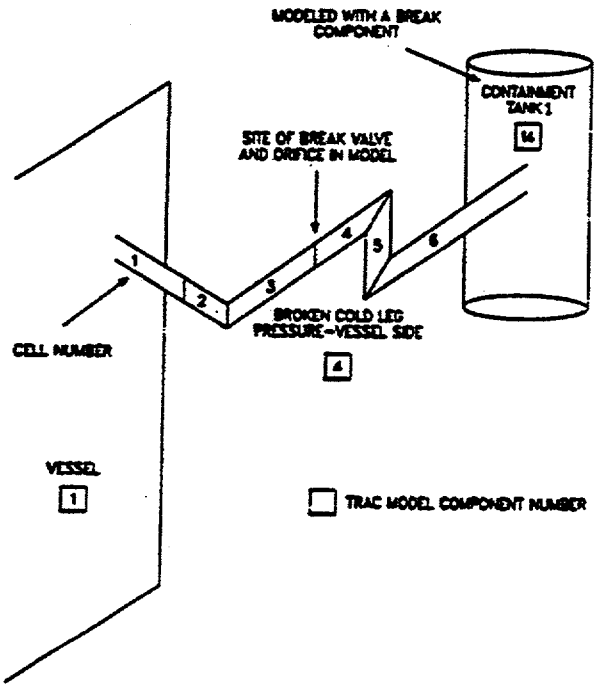

Figure 4.4.73 Broken Cold-Leg Noding from Pressure Vessel to Containment Tank 1

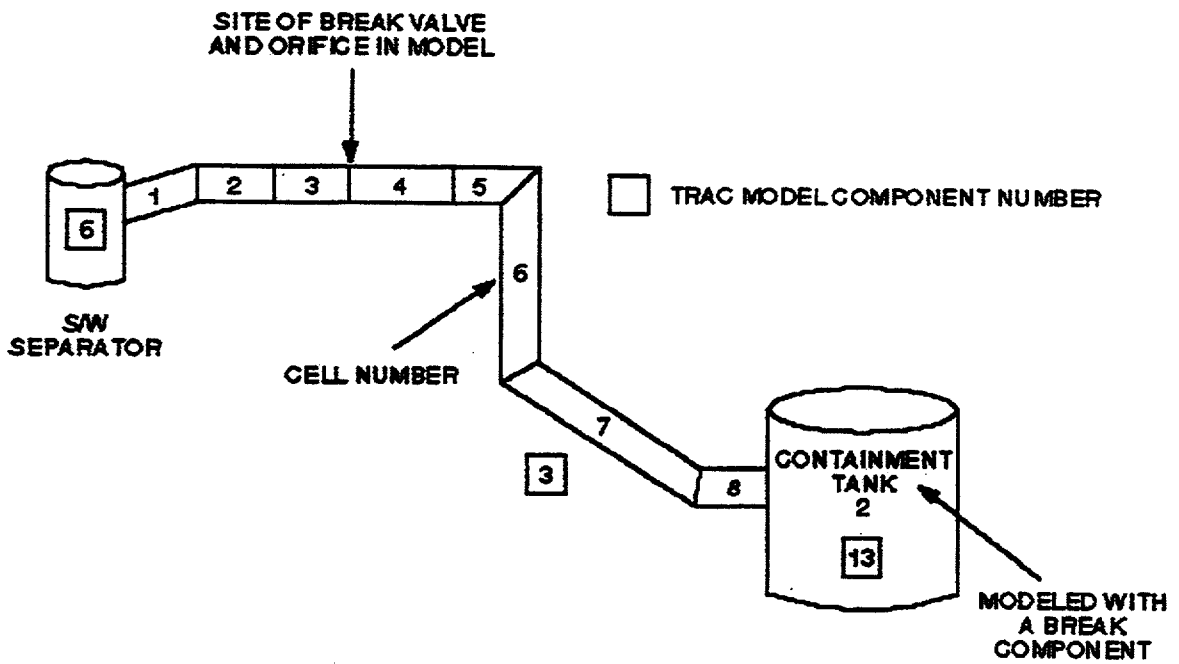

Figure 4.4.74 Broken Cold-Leg Noding from S/W Separator to Containment Tank 2

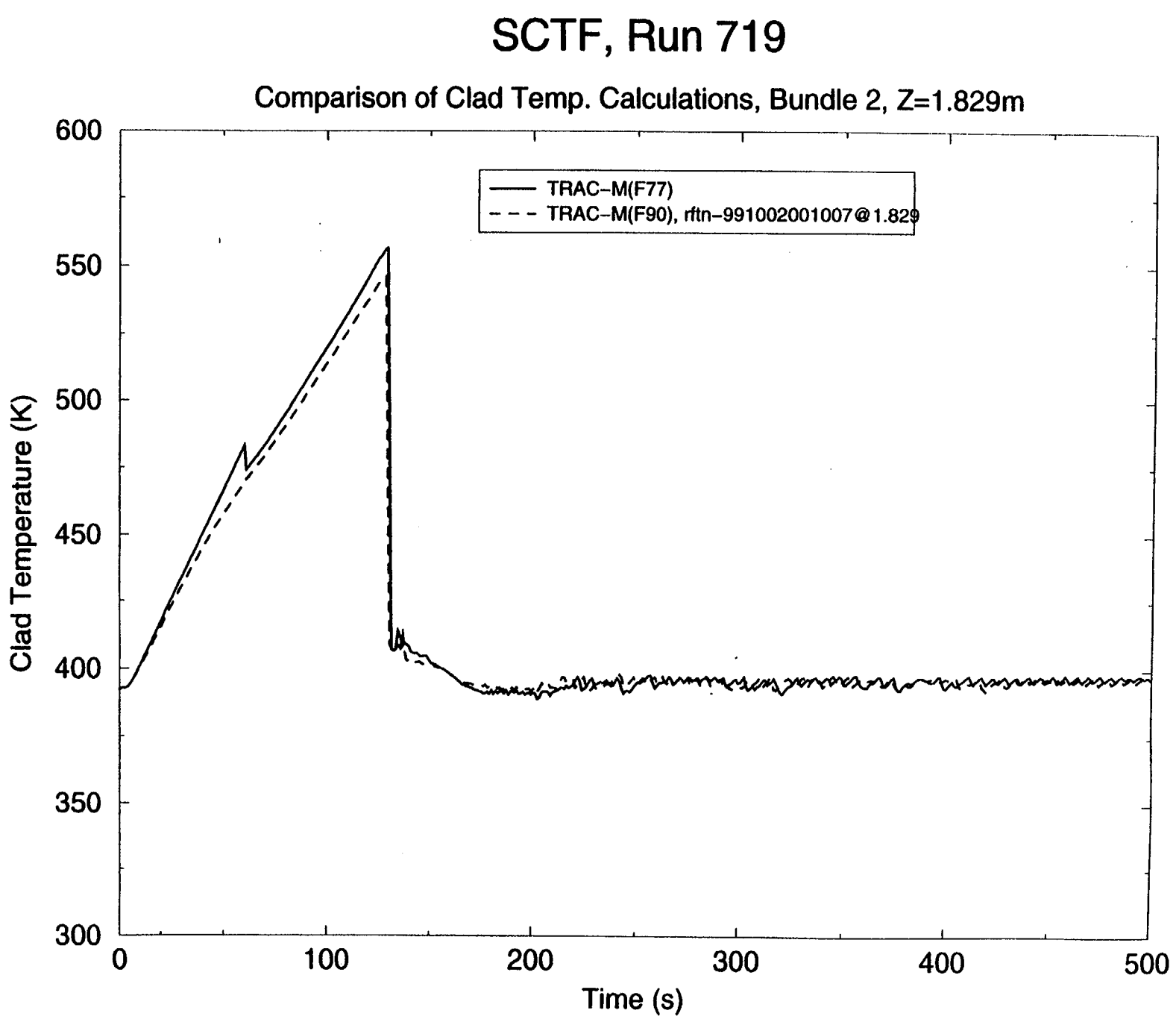

Figure 4.4.75 SCTF, Run 719 – Comparison of Clad Temperature Calculations, Bundle 2 (Z = 1.829 m)

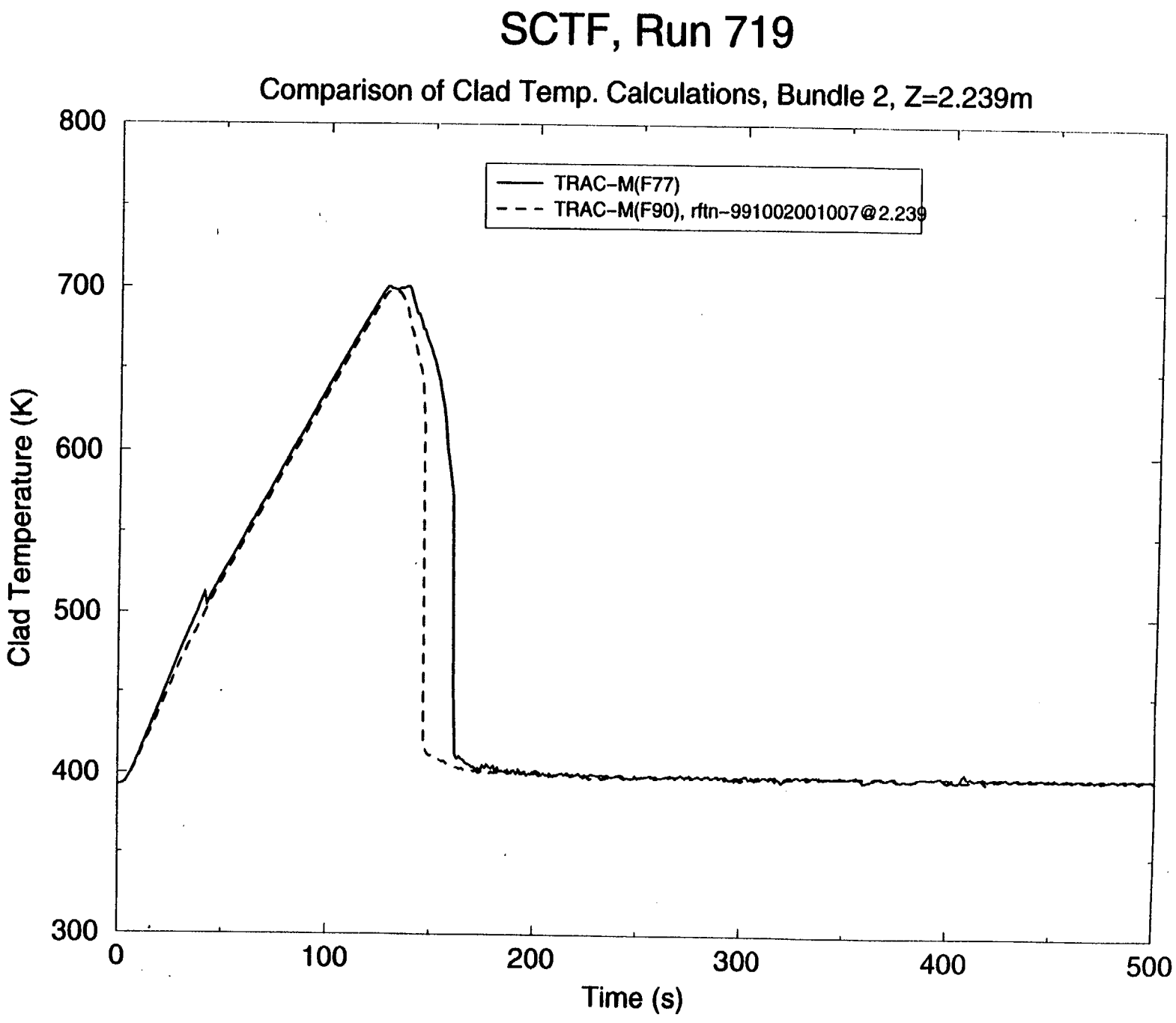

Figure 4.4.76 SCTF, Run 719 – Comparison of Clad Temperature Calculations, Bundle 2 (Z = 2.239 m)

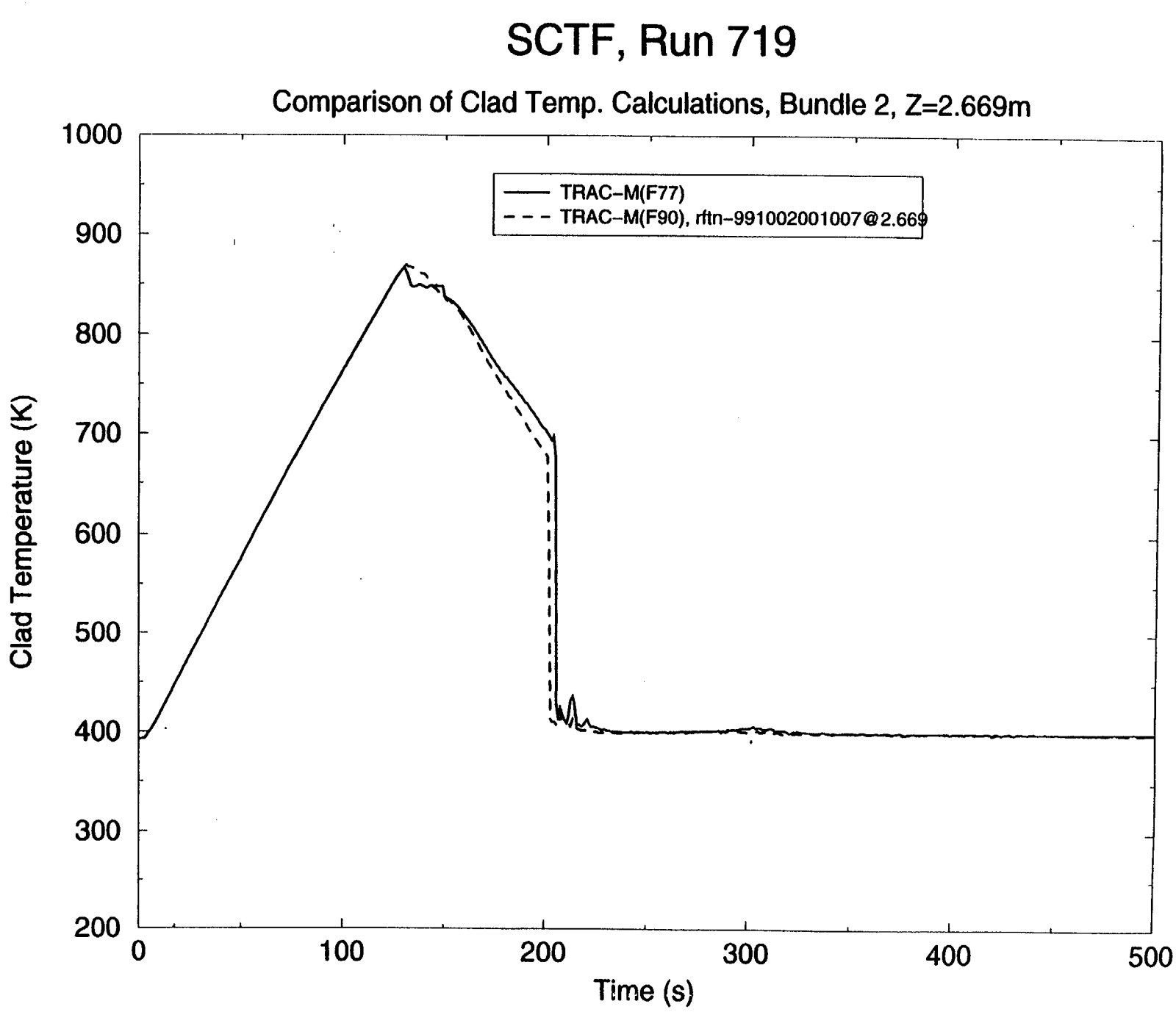

Figure 4.4.77 SCTF, Run 719 – Comparison of Clad Temperture Calculations, Bundle 2 (Z = 2.669 m)

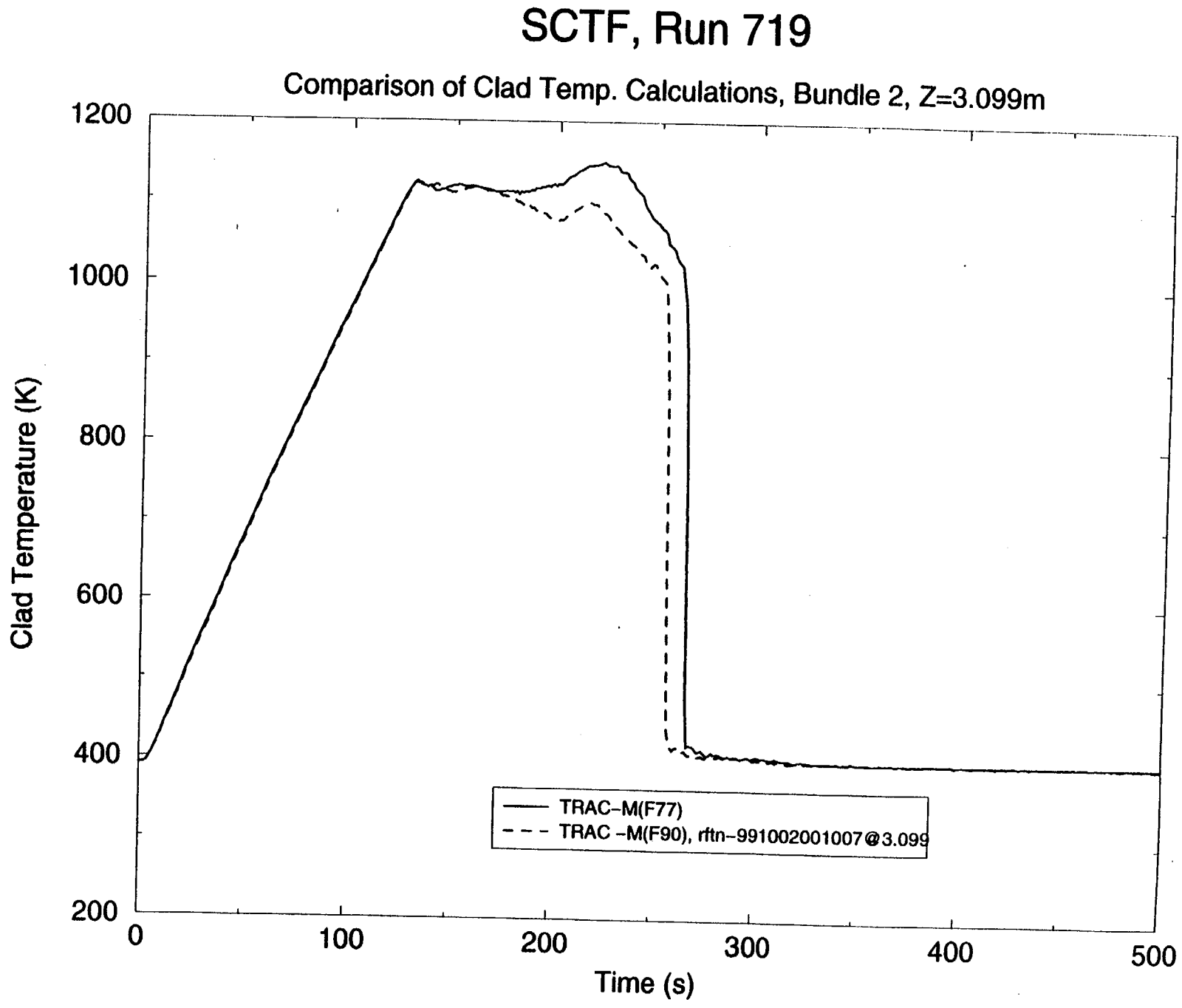

Figure 4.4.78 SCTF, Run 719 – Comparison of Clad Temperature Calculations, Bundle 2 (Z = 3.099 m)

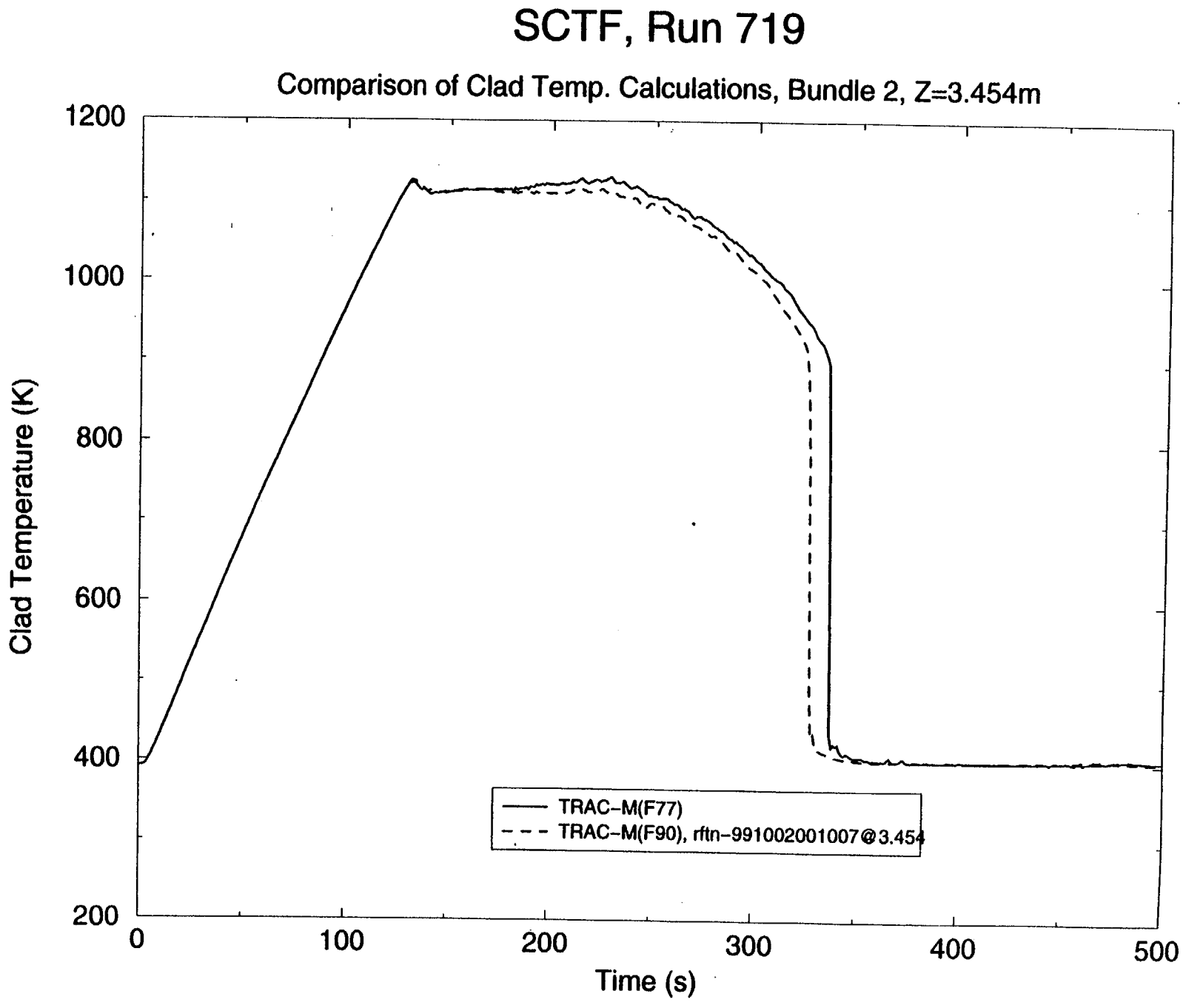

Figure 4.4.79 SCTF, Run 719 – Comparison of Clad Temperature Calculations, Bundle 2 (Z = 3.454 m)

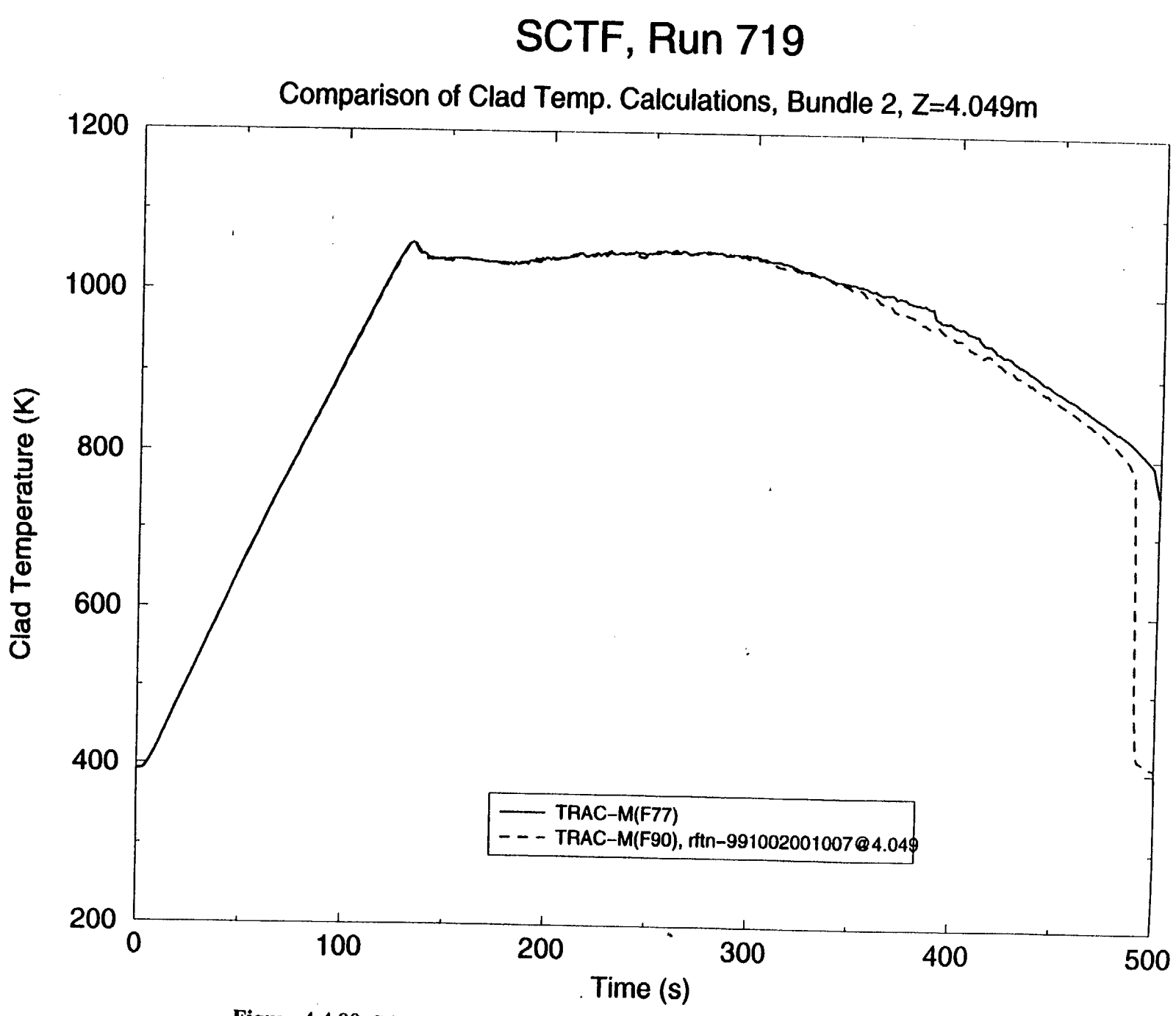

Figure 4.4.80 SCTF, Run 719 – Comparison of Clad Temperature Calculations, Bundle 2 (Z = 4.049 m)

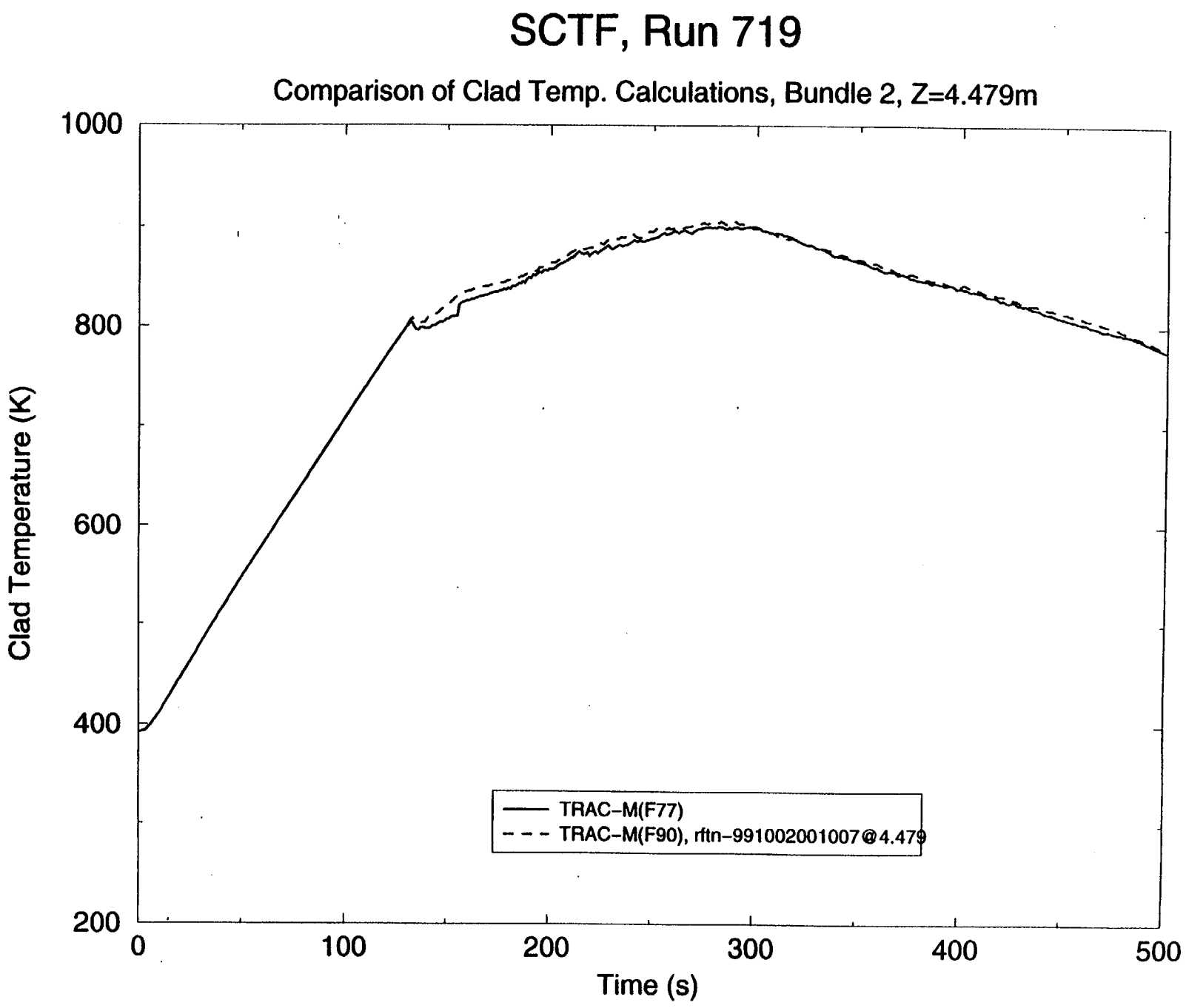

Figure 4.4.81 SCTF, Run 719 – Comparison of Clad Temperature Calculations, Bundle 2 (Z = 4.479 m)

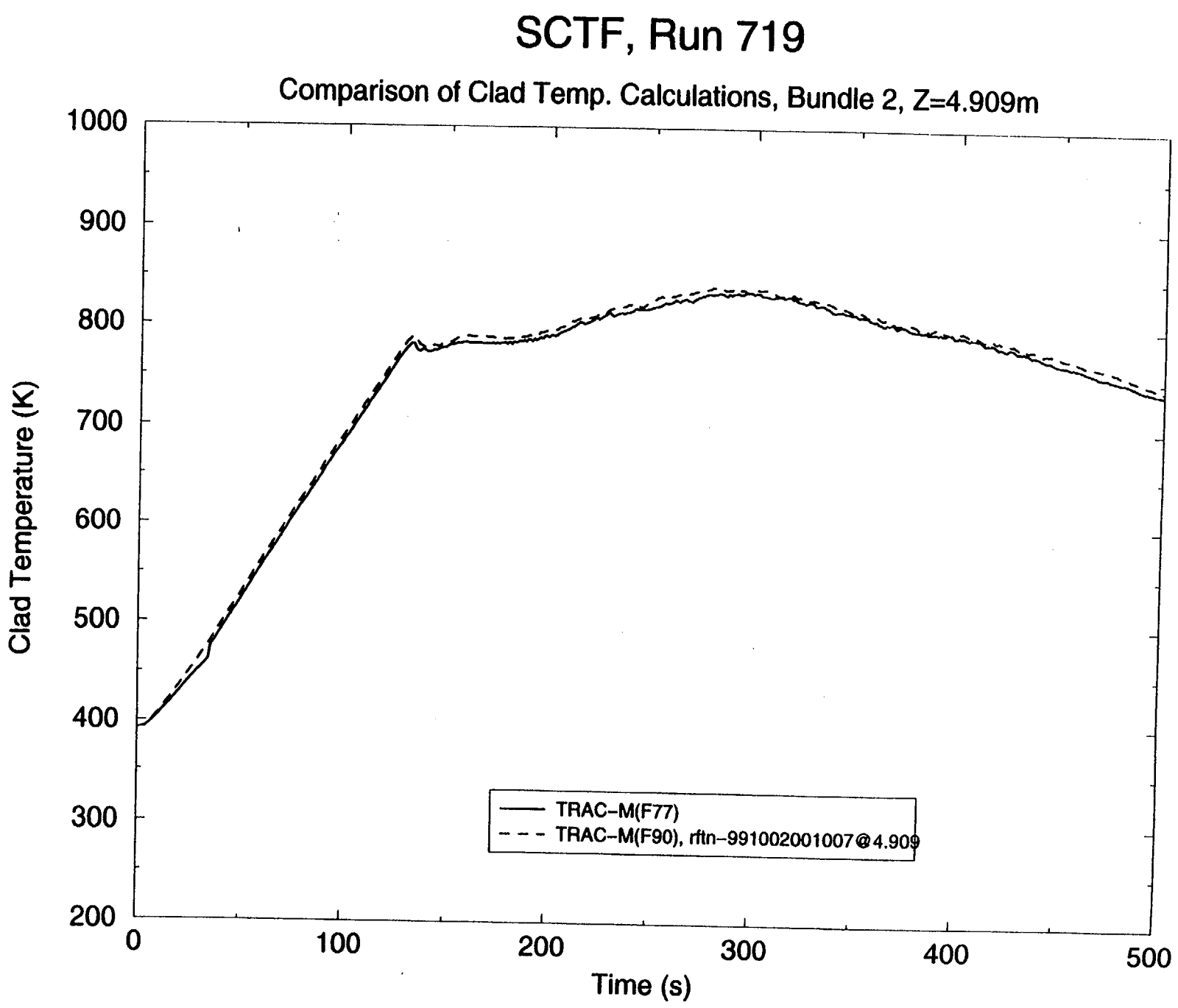

Figure 4.4.82 SCTF, Run 719 – Comparison of Clad Temperature Calculations, Bundle 2 (Z = 4.909 m)

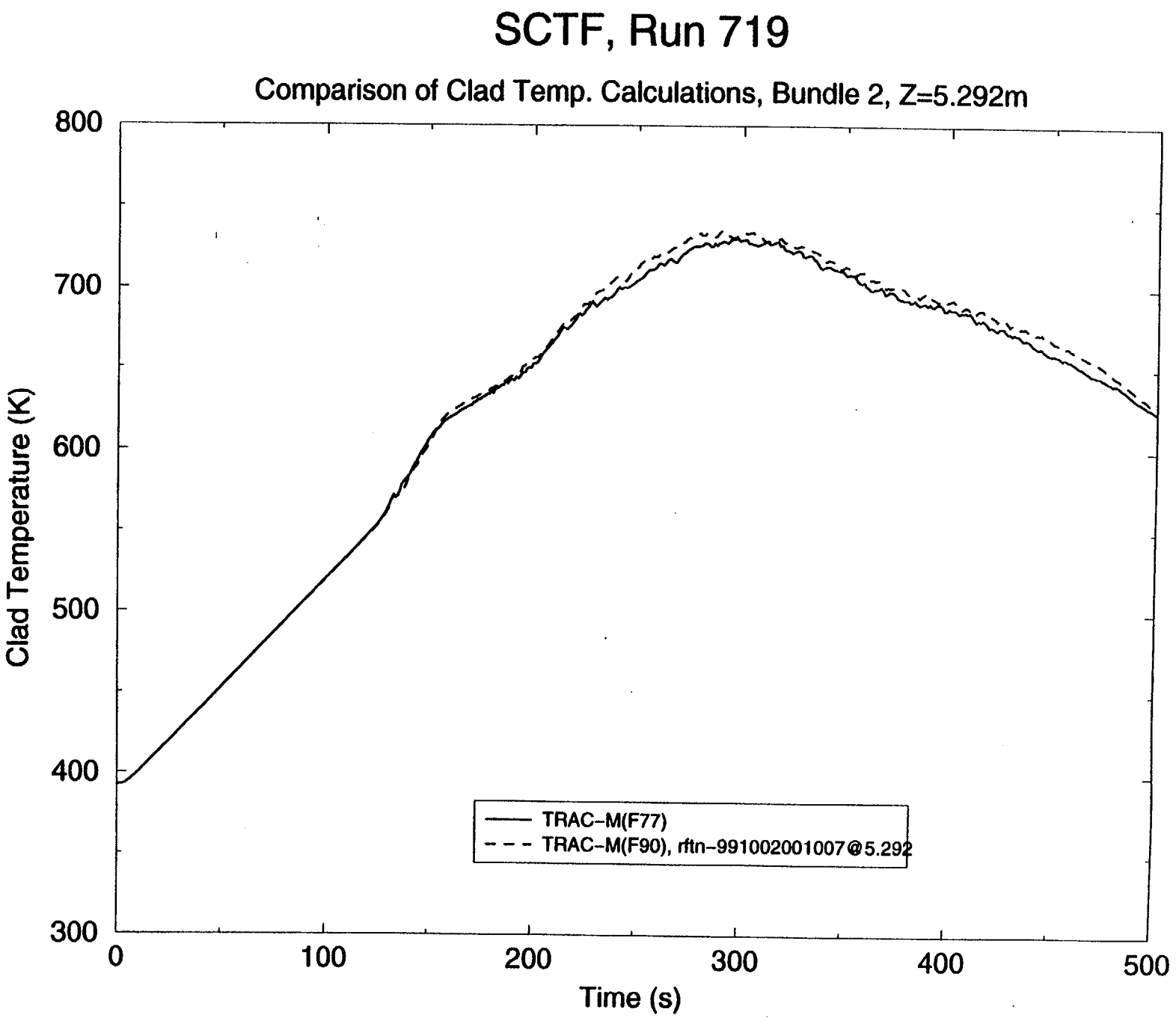

Figure 4.4.83 SCTF, Run 719 – Comparison of Clad Temperature Calculations, Bundle 2 (Z = 5.292 m)

4.5 Flow Patterns in Cold Legs During ECC Injection

During a LOCA, subcooled ECC interacts with steam in the primary loops near the injection nozzles, and the steam is partially or completely condensed by the ECC. The extent of condensation strongly affects the flow regime in the loop, as well as the delivery of ECC water to the vessel. Depending on the flow conditions, water plugs (which completely fill the pipe cross-section) can form.

UPTF Tests 8, 9, 25B, and 26 investigated the flow patterns in the reactor coolant loops for typical LOCA flow conditions. These tests included ECC injection into only the cold legs, only the hot legs, and both the hot legs and cold legs. They intended to investigate loop flow patterns at full scale, and to determine the T/H boundary conditions for the transition between the different flow regimes.

4.5.1 Upper-Plenum Test Facility (UPTF), Cold Leg Flow Test 8, Phase B, Part 1

The Upper-Plenum Test Facility (UPTF), described in Ref. 4.4.8, is a full-scale model of a four-loop 1300-MWe PWR, which includes the reactor vessel, downcomer, lower plenum, core simulation, upper plenum, and four loops with pump and steam generator simulation. A flow diagram of the system and an overview of the test facility are shown in Figs. 4.5.1 and 4.5.2. Major dimensions of the facility are shown in Fig. 4.5.3, and a plan view of the test vessel is shown in Fig. 4.5.4. The T/H feedback of the containment is modeled using a containment simulator. The test vessel, core barrel, and internals are a full-size simulation of a PWR with four full-scale hot and cold legs modeling three intact loops and one broken loop. Both cold and hot leg breaks can be investigated with ECC injection into the intact and broken loop cold and/or hot legs and into the vessel downcomer. The steam produced in a real core and the liquid entrained by this steam flow are simulated by direct steam injection and by liquid presence in the core simulator. Steam production on the primary side of an intact steam generator is simulated by direct steam injection into each intact loop steam generator simulator.

4.5.2 Test Procedure

UPTF Test 8 is a separate effects test (SET) to investigate the T/H phenomena that occur in the loops of a PWR as a result of ACC and low-pressure ECC liquid injection in the cold legs during the end-of-blowdown, refill, and reflood phases of a postulated LOCA. Pressure and fluid oscillations can occur in the loops when induced by steam condensation on the ECC injected subcooled liquid. In a reactor with cold leg ECC injection, liquid plugs form in the cold leg when the ECC injection rate and the liquid subcooling are large. The formation and movement of these plugs were predicted by TRAC before they were experimentally observed.

The goals of UPTF Test 8 were to investigate the loop flow pattern, and to quantify the T/H boundary conditions that lead to pressure and flow oscillations in the loops where ECC liquid is injected. Test 8 consisted of two test runs or phases that differed only in the pump simulator flow resistance set in loop 2. In phase A (Run 112), the pump simulator K-factor was set to 10, and in phase B (Run 111), a K-factor of 18 was used; both referenced to a pipe diameter of 0.75 m. Each of the phases consisted of two parts, including cold leg ECC injection in Part 1 and hot leg ECC injection in Part 2. The TRAC calculation presented herein models Part 1 of Phase B, cold leg ECC injection. The system test configuration for this test is depicted in Fig. 4.5.5. The flow

parameters that determine liquid plug formation and oscillation in loop 2 are of special interest in this test.

The hot leg and cold leg break valves of broken-loop 4 were both open. The loop-1 pump simulator was closed to model full blockage and no flow. The loop-2 and loop-3 pump simulators were set to a stroke of 108 mm (K factor of 18.0 for a 0.750-m pipe diameter) in an attempt to model partial blockage and to establish a 0.25-bar differential pressure between the upper plenum and downcomer. Broken loop 4 had a throttle plate with an inner diameter of 0.411 m (K factor of 18.2 for a 0.750-m pipe diameter) installed in the 0.750-m diameter hot leg pipe between the steam/water separator and break valve to simulate the flow resistance of a partially blocked pump.

Core simulator steam injection was initiated at 23 s into the test with a 2-s ramp to 115.3 kg/s, where it was then held constant for 200 s. No steam generator simulator steam injection took place during this test. The loop-2 cold leg ECC injection was initiated at 27 s into the test with a 4-s ramp to 600 kg/s, where it was then varied through a series of 30-s time interval steps starting at 600 kg/s and decreasing to 80 kg/s.

The initial to transient conditions of UPTF Test 8, Phase B, Part 1, Run 111 (hereafter referred to as UPTF8B) are shown in Table 4.5.1. Saturated steam was initially present throughout the primary system, except for liquid in the lower plenum, core, and downcomer of the vessel at a height of 4.2 m from the vessel bottom and in the intact loop, steam generator simulator, and broken loop steam/water separator drains. Liquid was drained from the vessel whenever the level exceeded 4.2 m.

4.5.3 TRAC Model

The TRAC-M(F77) and TRAC-M(F90) models of the UPTF primary system used in this assessment are based on the TRAC-PF1/MOD1 Code Scalability, Applicability, and Uncertainty (CSAU) model. The vessel model for the MOD1 assessment contained 2 radial rings, 4 azimuthal sectors, and 13 axial levels. Several changes were made in the flow areas of the cells in the vessel, as follows:

- The model for the 0.411-m diameter throttle plate in the broken loop-4 hot leg pipe of 0.750 m diameter was changed to a forward and reverse friction factor of 0.14928 at the 0.411-m diameter interface (a K factor of 18.2 for a 0.750-m diameter pipe), as specified for the test.

- The initial pressure of saturated steam throughout the primary system at 23 s into the experiment, when the TRAC calculation of the transient is initiated, had been defined to be the nominal containment simulator pressure of 400 kPa (4 bar). This was changed to the measured steam pressure of 375 kPa in the upper plenum and downcomer of the vessel at 23 s. During the transient, the constant pressure of 400 kPa defined as input to the containment simulator was changed to the measured pressure at the top of the vessel downcomer. This was done to better approximate the actual time-dependent pressure boundary condition of the containment. The vessel downcomer steam pressure is approximately the same as the containment simulator steam pressure because little flow resistance occurs in the broken loop-4 cold leg between their locations. The containment pressure was modeled with two time-dependent pressure boundary components, one connected to the broken hot leg and the other

connected to the broken cold leg. A 1-s time delay was applied to the initial pressure pulse from core simulator steam injection before ECC injection.

- The average liquid level in the lower plenum, core, and downcomer of the vessel, with an initial height of 4.38 m, had been specified to be held at 4.3 to 4.4 m during the transient by a trip-controlled liquid drain from the vessel. This procedure attempted to maintain a constant liquid inventory in the vessel. This was changed to maintain the measured liquid height in the lower plenum and core, with an initial height of 4.2 m, by a trip-controlled liquid drain from the vessel during the transient.

Noding diagrams for the TRAC model of the UPTF are shown in Figs. 4.5.6 through 4.5.14. The vessel axial noding is shown in Fig. 4.5.6. The vessel model consists of 13 axial levels, 4 azimuthal sectors, and 2 radial rings for a total of 104 computational cells. The azimuthal and radial noding distribution for the vessel is shown in Fig. 4.5.7. The core is represented by the inner ring, and the downcomer is represented by the outer ring.

Figs. 4.5.8 through 4.5.10 show the noding for Loops 1, 2, and 3. In each loop, the hot leg is modeled with a TEE component; the steam generator simulator is modeled with a combination of four TEE components and one VALVE component; and the crossover pipe, pump simulator, and cold leg are modeled with another TEE component. Steam injection into the top of the steam generator simulator is modeled with TEE and FILL components. This FILL component can be controlled by the mass flow of liquid in the hot leg. The drain line from the bottom of the secondary side of the middle TEE to the steam generator simulator inlet plenum is modeled with another TEE and VALVE component. The pump simulator is modeled with a flow area restriction and the correct volumes associated with the pump simulator component. ECC injection is modeled in both the hot and cold legs with the TEE and FILL components. The FILL components can invoke a time-dependent programmed ECC flow if desired. Loop-1 and Loop-3 noding are identical. In Loop-2, the pressurizer in the hot leg required the addition of an extra TEE component. This FILL also may use a preprogrammed type steam flow.

Figs. 4.5.11 and 4.5.12 show the broken loop-4 hot and cold leg noding. The broken loop cold leg model is composed of a VALVE component to model the main break valve, a TEE component to model the bottom of the steam generator simulator, and another TEE component to model the steam/water separator and piping to the containment. The bottom of the steam generator simulator drain line is modeled to the drain tank valve. This drain line drains off accumulated liquid during the course of the transient. The broken loop hot leg is modeled with a TEE component for the hot leg, another TEE component for the steam generator simulator, and a VALVE component for piping run out to the containment tank. The containment tank is modeled with two BREAK components. These components provide a transient pressure boundary condition. Drain lines from the bottom of the vessel to the drain tank were completely modeled, and are shown in Fig. 4.5.13.

The core steam/water injection sources are modeled by four individual TEE components shown in Fig. 4.5.14, each of which is connected to one of the four core cells at the vessel level 6. The TEE components are able to combine the steam input from a feedback injection with the preprogrammed steam/water input. The preprogrammed steam/water input was provided to Los Alamos by Kraftwerk Union Aktiengesellschaft (KWU). The walls between the UPTF

injection zones are solid; therefore, TRAC incorporates a zero flow area in the radial and azimuthal direction at level 6. Because the steam is injected in the radial direction at this level, it will impact the walls and lose its radial momentum. To model this effect in the TRAC input, the S/W injection sources are directed radially.

4.5.4 Comparison of TRAC-M(F77) and TRAC-M(F90) Predictions

Calculations were performed using both TRAC-M(F77) and TRAC-M(F90). TRAC-M(F90) did not run on the Silicon Graphics (SGI) platform, and failed to perform calculations giving the error message of iteration failure. The code did run on the Digital Equipment Corporation (DEC)-Alpha platform, and comparisons are made using the resulting calculations.

Figs. 4.5.15 through 4.5.20 show comparisons of various parameters calculated during the ECC injection. These figures do not show experimental data, since the data were obtained under the 2-D/3-D program, and are restricted to the use of program participants. When an agreement with other partners is reached to release these data, this report will be revised to include comparisons of experimental data with code predictions.*

Figs. 4.5.15 and 4.5.16 show the variation of pressures calculated in the downcomer and upper plenum of the vessel respectively. Fig. 4.5.17 illustrates how the vessel liquid level changes during the injection. Fig. 4.5.18 shows how the liquid temperatures vary downstream of the injection point. Figs. 4.5.19 and 4.5.20 illustrate how steam flows vary in loops 3 and 2, respectively. All of these calculations show that the agreement between the predictions generated by the two codes is either "Excellent" or "Reasonable." Some differences exist between the predictions in some areas; however, considering the error corrections that have been implemented in TRAC-M(F90), the conversion from TRAC-M(F77) has been successful for this application.

4.5.5 Conclusions

The conversion from TRAC-M(F77) has been successful for this application. However, there is some code robustness problem, since the calculations could only be performed on the DEC-alpha platform.

---

* See footnote on page 4-79.

Table 4.5.1 Transient Conditions

Parameters	Value
Vessel and containment initial pressure	375.0 kPa
Vessel lower plenum liquid level	2.4–4.2 m
Steam generator simulator steam injection	0.0 kg s^{-1}
Core simulator steam injection	0.0–115.3 kg s^{-1}
Core simulator steam temperature	416.1 K
Loop-2 cold leg ECC liquid injection	0.0–600.0 kg s^{-1}
Loop-2 cold leg ECC liquid temperature	311.0 K
Loops 1 and 3 cold leg ECC liquid injection	0.0 kg s^{-1}
Loops 1, 2, 3, and 4 hot leg ECC liquid injection	0.0 kg s^{-1}
Loop-1 fully blocked pump K factor	infinity
Loop-2 partially blocked pump K factor	18.0
Loop-3 partially blocked pump K factor	18.0
Broken loop 4 throttle plate K factor	18.2
Broken loop 4 hot and cold leg break valves	open

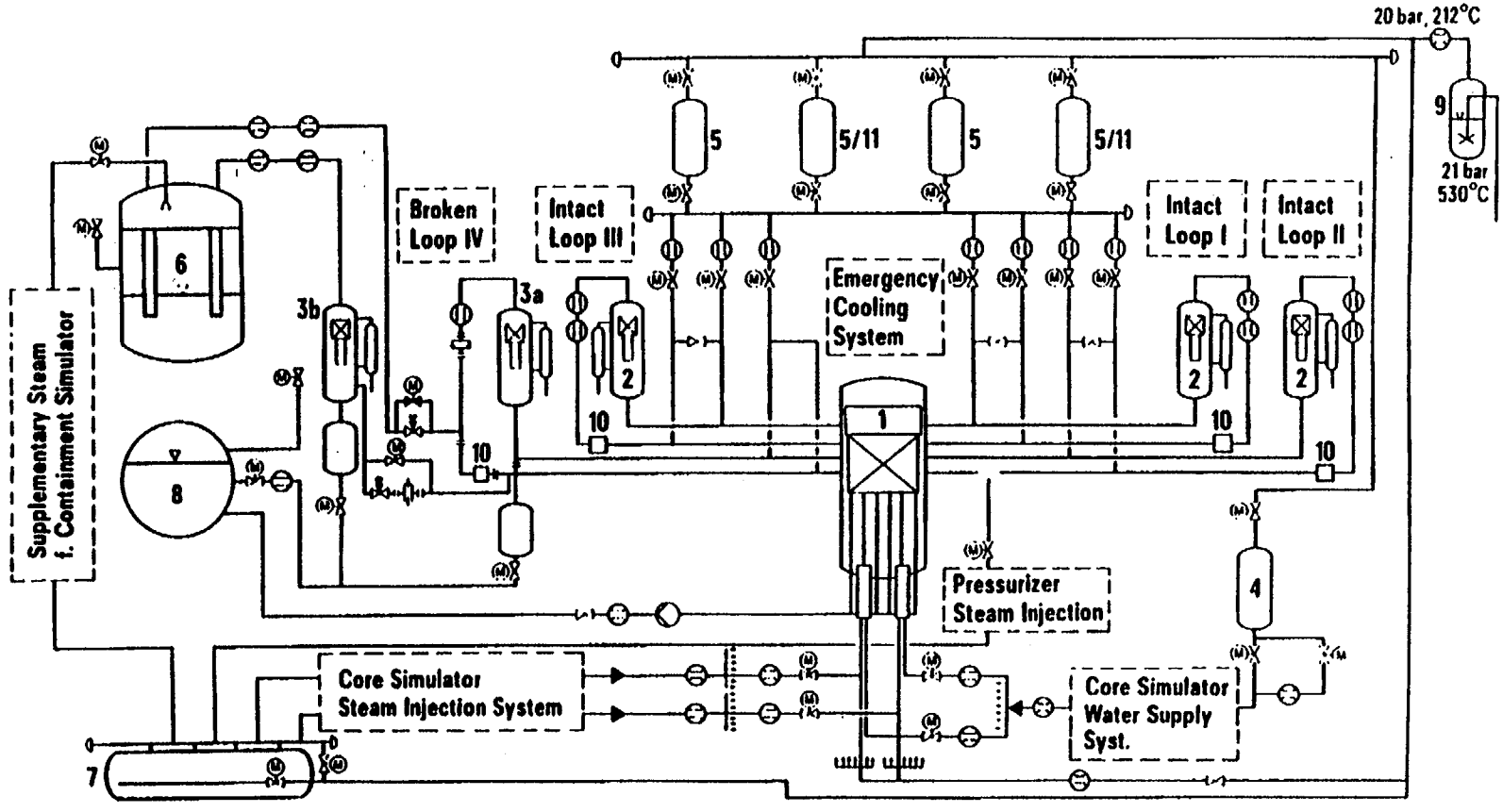

Figure 4.5.1 UPTF Flow Diagram

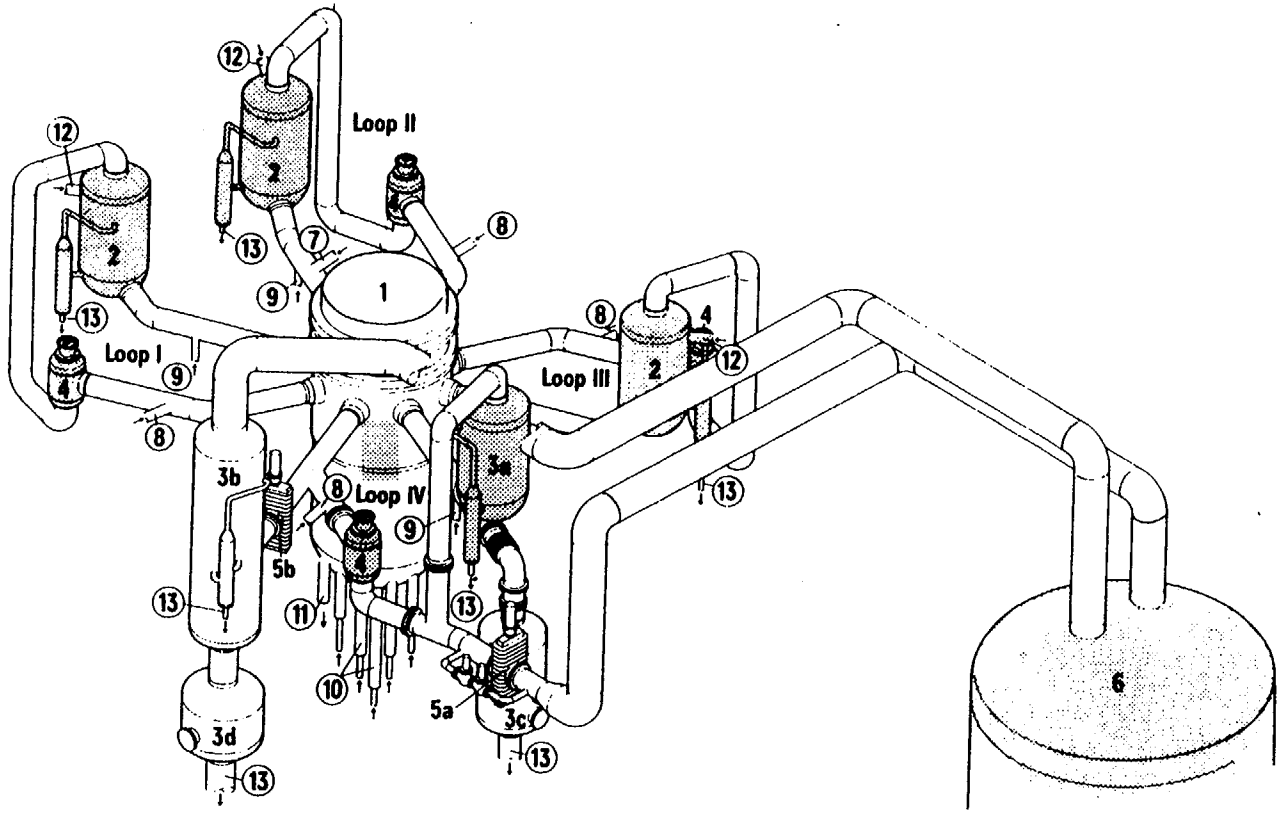

1 Test Vessel
2 Steam Generator Simulator (Intact Loop)
3a Steam Generator Simulator/ Water Separator (Broken Loop Hot Leg)
3b Water Separator (Broken Loop Cold Leg)
3c Drainage Vessel for Hot Leg
3d Drainage Vessel for Cold Leg
4 Pump Simulator
5a Break Valve (Hot Leg)
5b Break Valve (Cold Leg)
6 Containment Simulator

(7) Surgeline-Nozzle
(8) ECC-Injection Nozzles (Cold Leg)
(9) ECC-Injection Nozzles (Hot Leg)
(10) Core Simulator Injection Nozzle
(11) TV-Drainage Nozzle
(12) Steam Injection Nozzle
(13) Drainage Nozzle

Simulator

Figure 4.5.2 UPTF Primary System

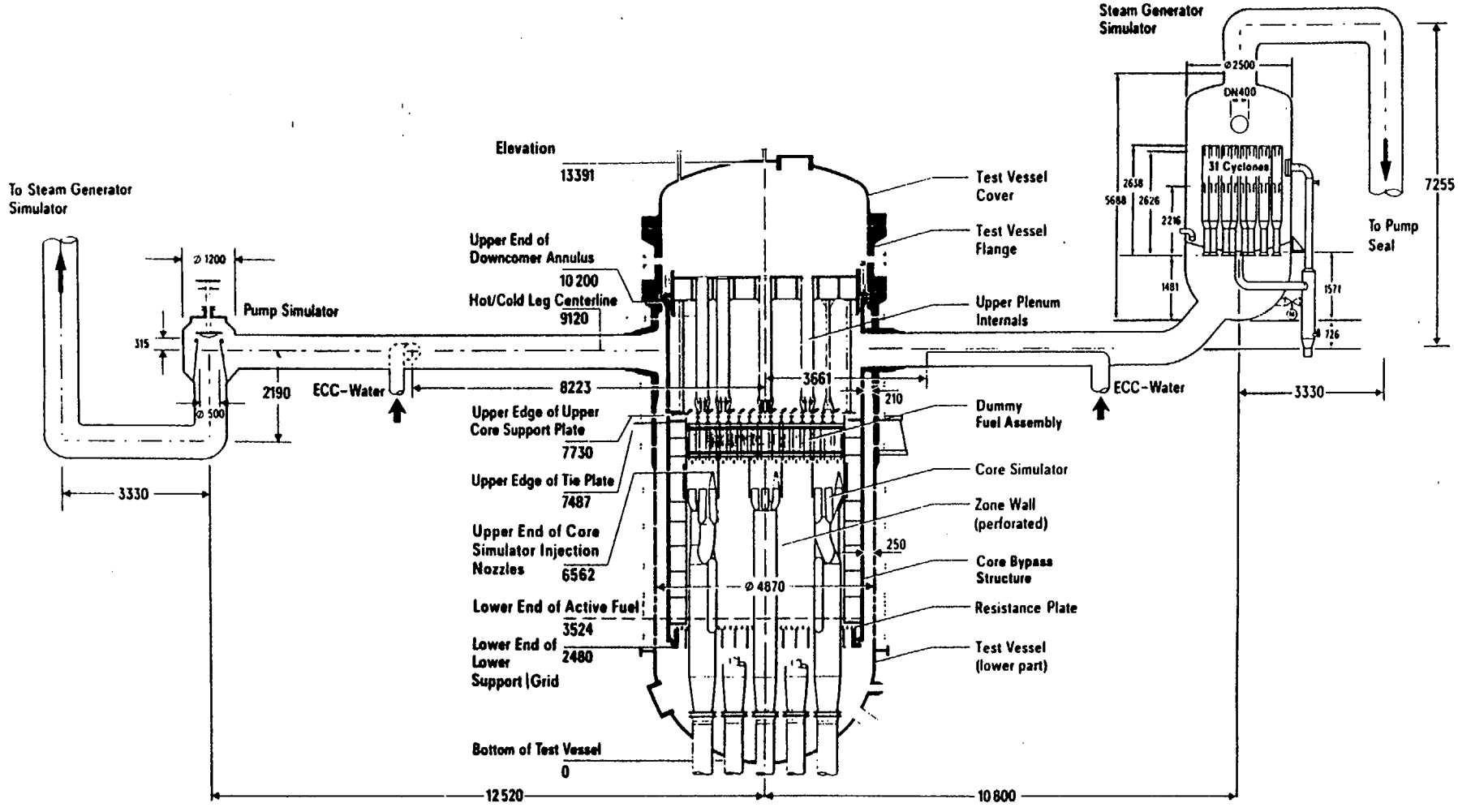

Figure 4.5.3 Major Dimensions of the UPTF Primary System

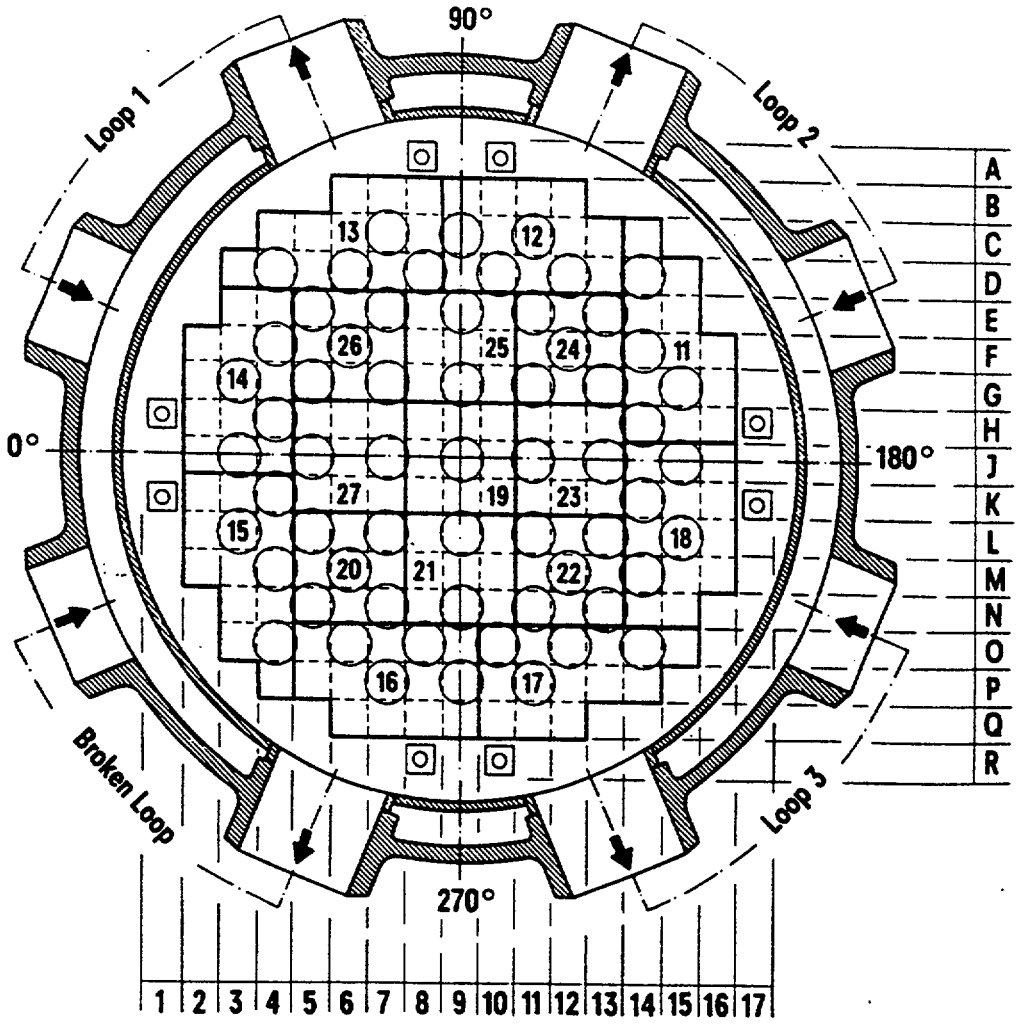

Figure 4.5.4 Plan View of UPTF Test Vessel

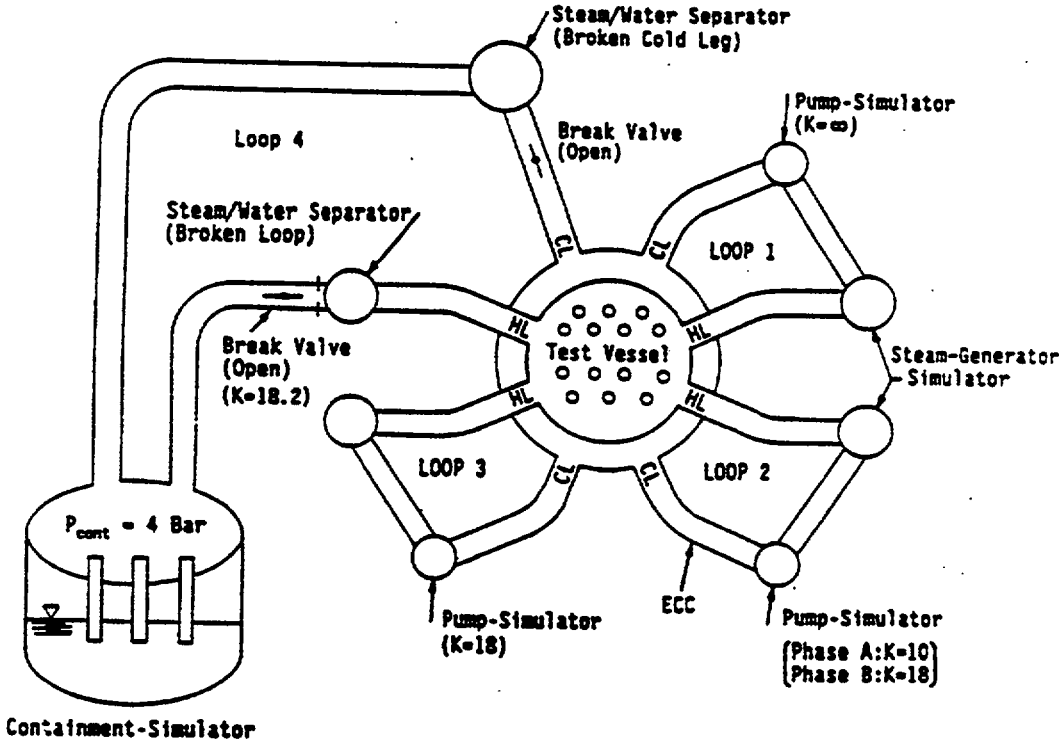

Figure 4.5.5 System Configuration for UPTF Test 8, Part 1

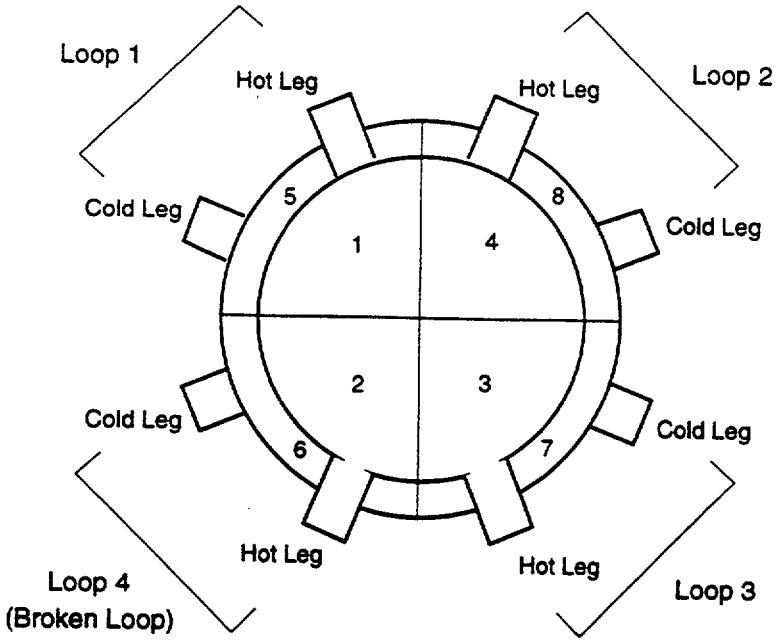

Figure 4.5.7 UPTF8B Vessel Model Plan View

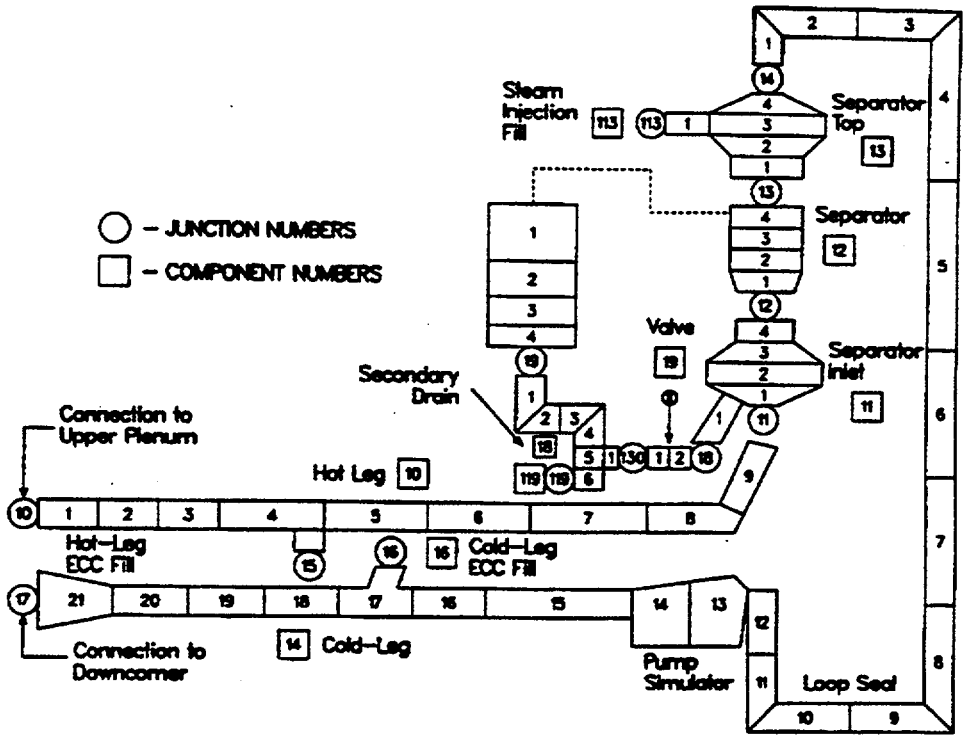

Figure 4.5.8 UPTF Loop-1 Noding Diagram

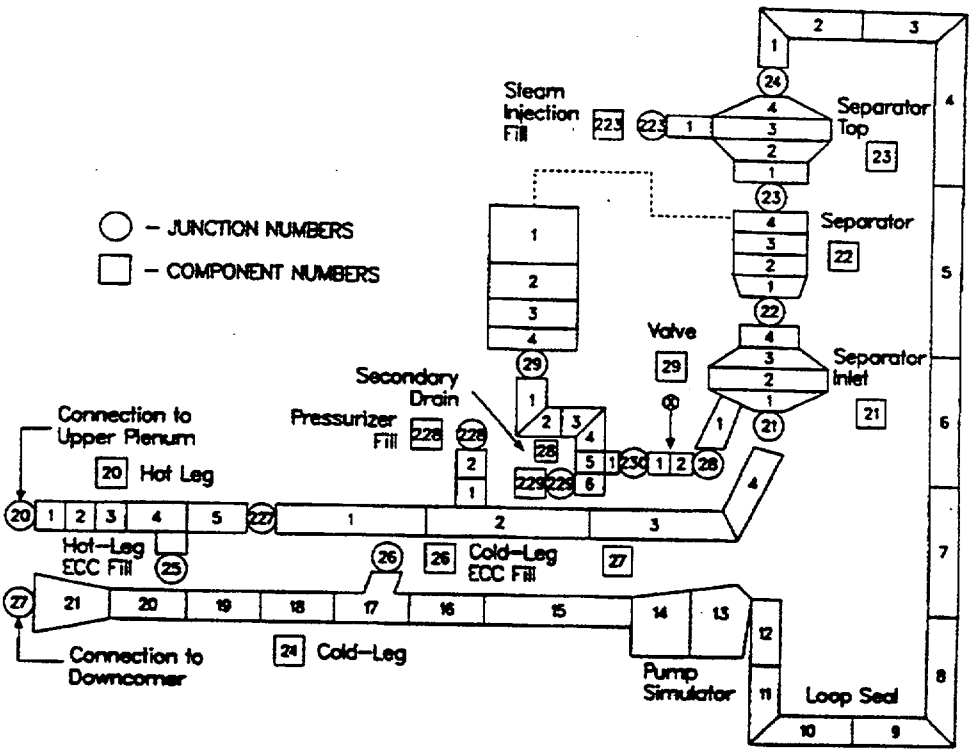

Figure 4.5.9 UPTF Loop-2 Noding Diagram

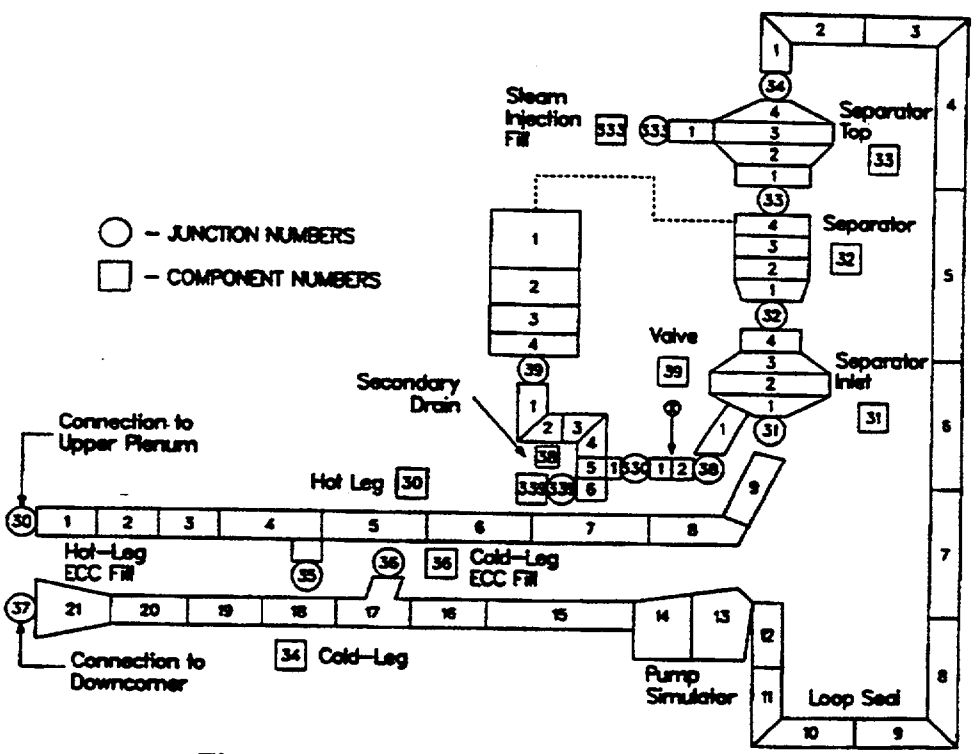

Figure 4.5.10 UPTF Loop-3 Noding Diagram

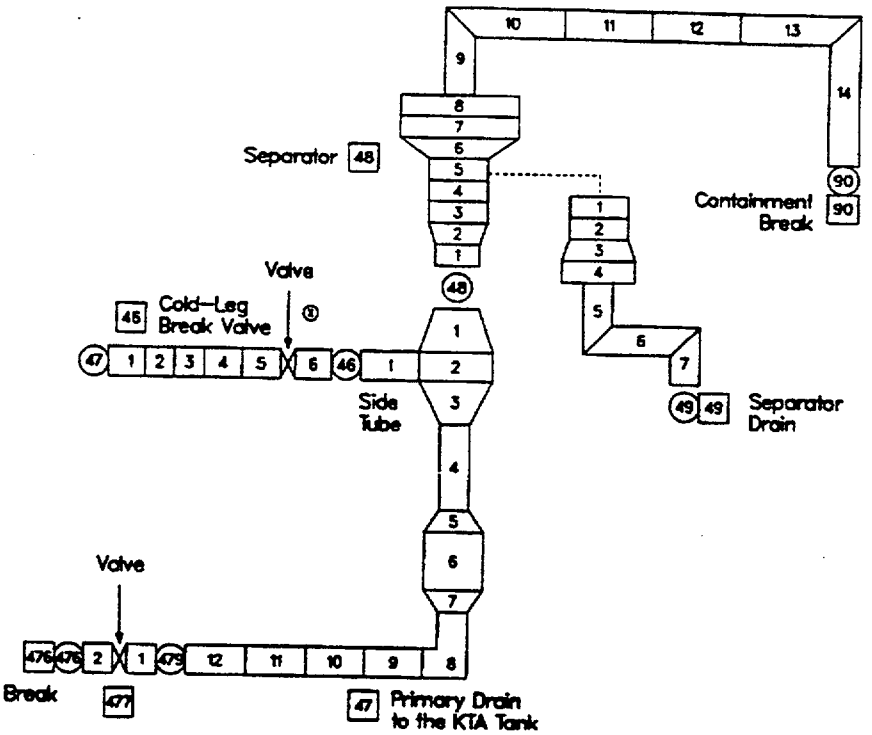

Figure 4.5.11 UPTF Broken-Loop-4 Cold-Leg Noding Diagram

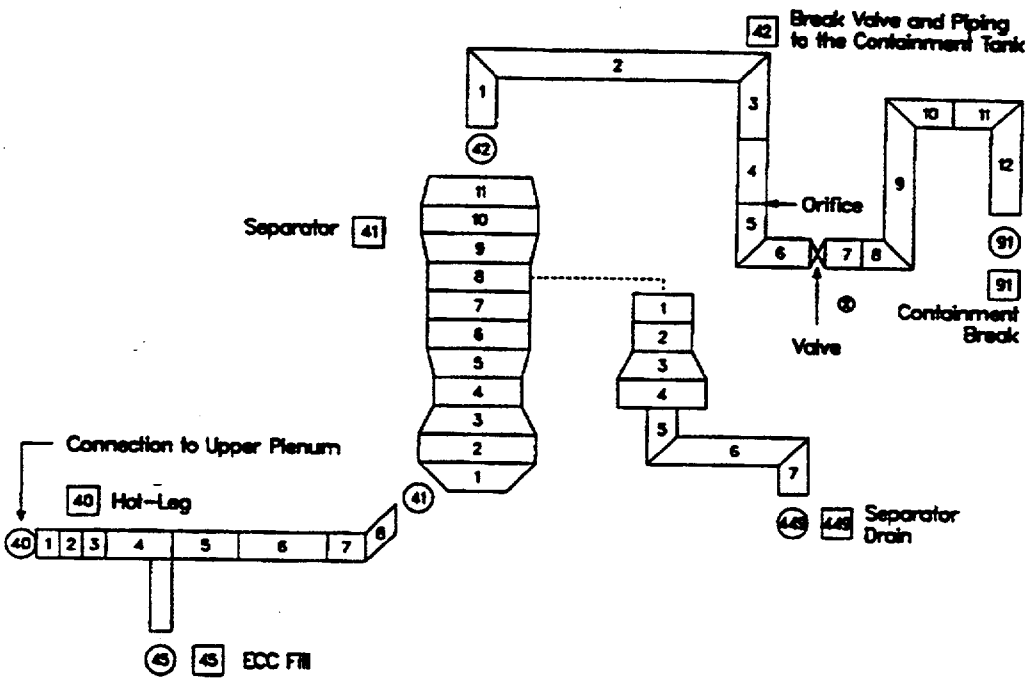

Figure 4.5.12 UPTF Broken-Loop-4 Hot-Leg Noding Diagram

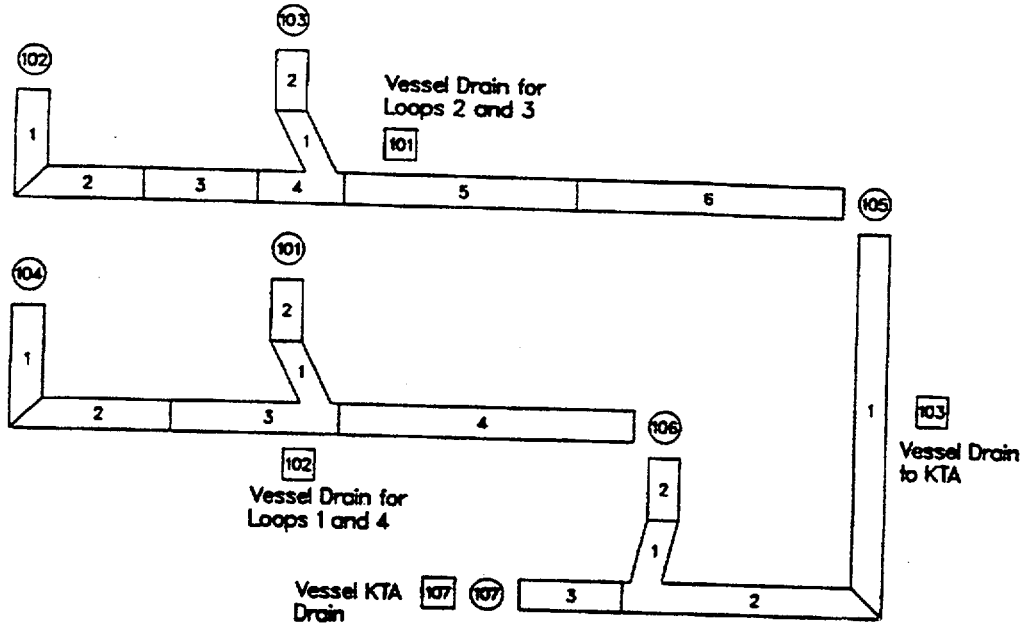

Figure 4.5.13 UPTF Water Drainage System Noding Diagram

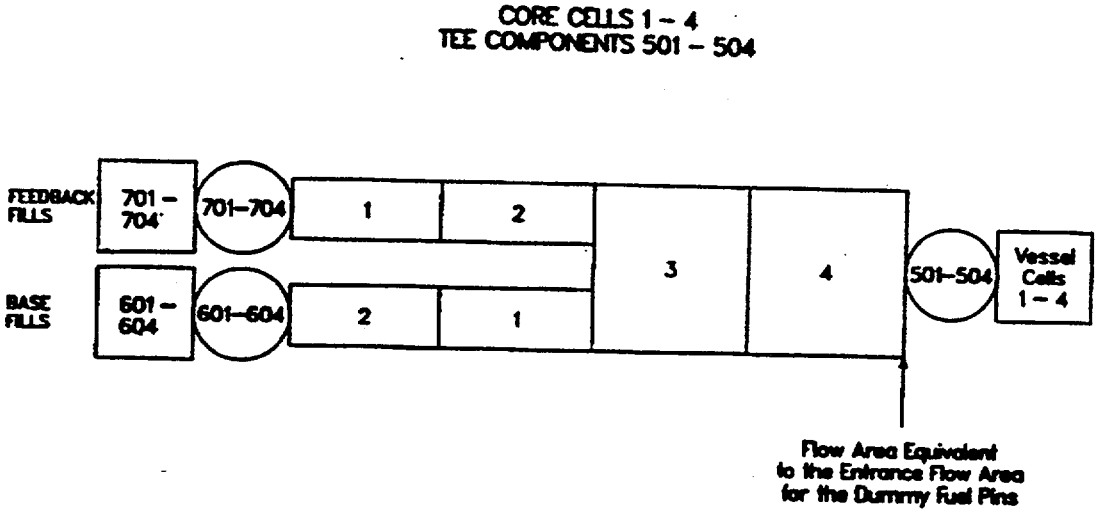

Figure 4.5.14 UPTF Core-Simulator-Injection Noding Diagram

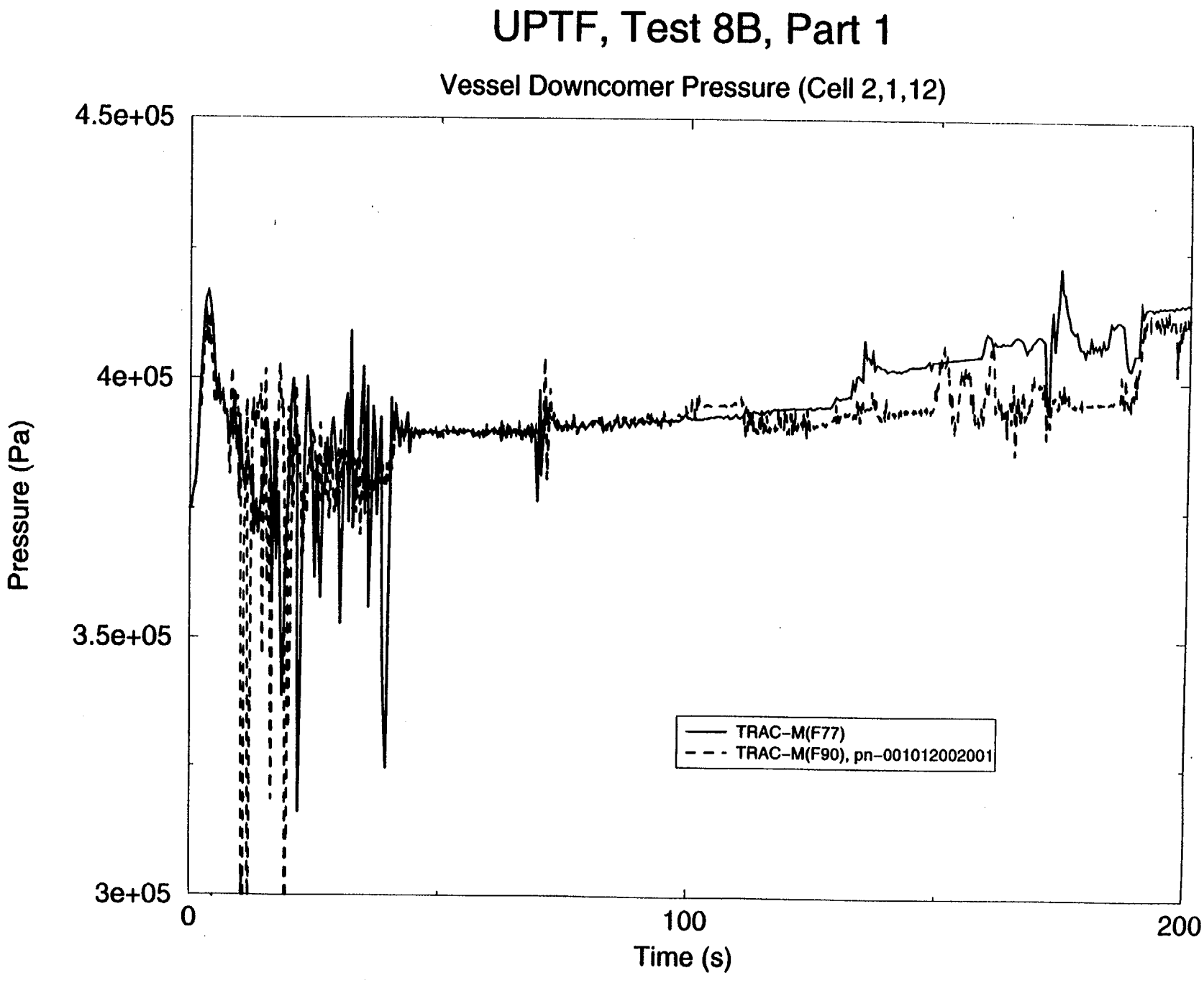

Figure 4.5.15 UPTF, Test 8B, Part 1 – Vessel Downcomer Pressure (Cell 2, 1, 12)

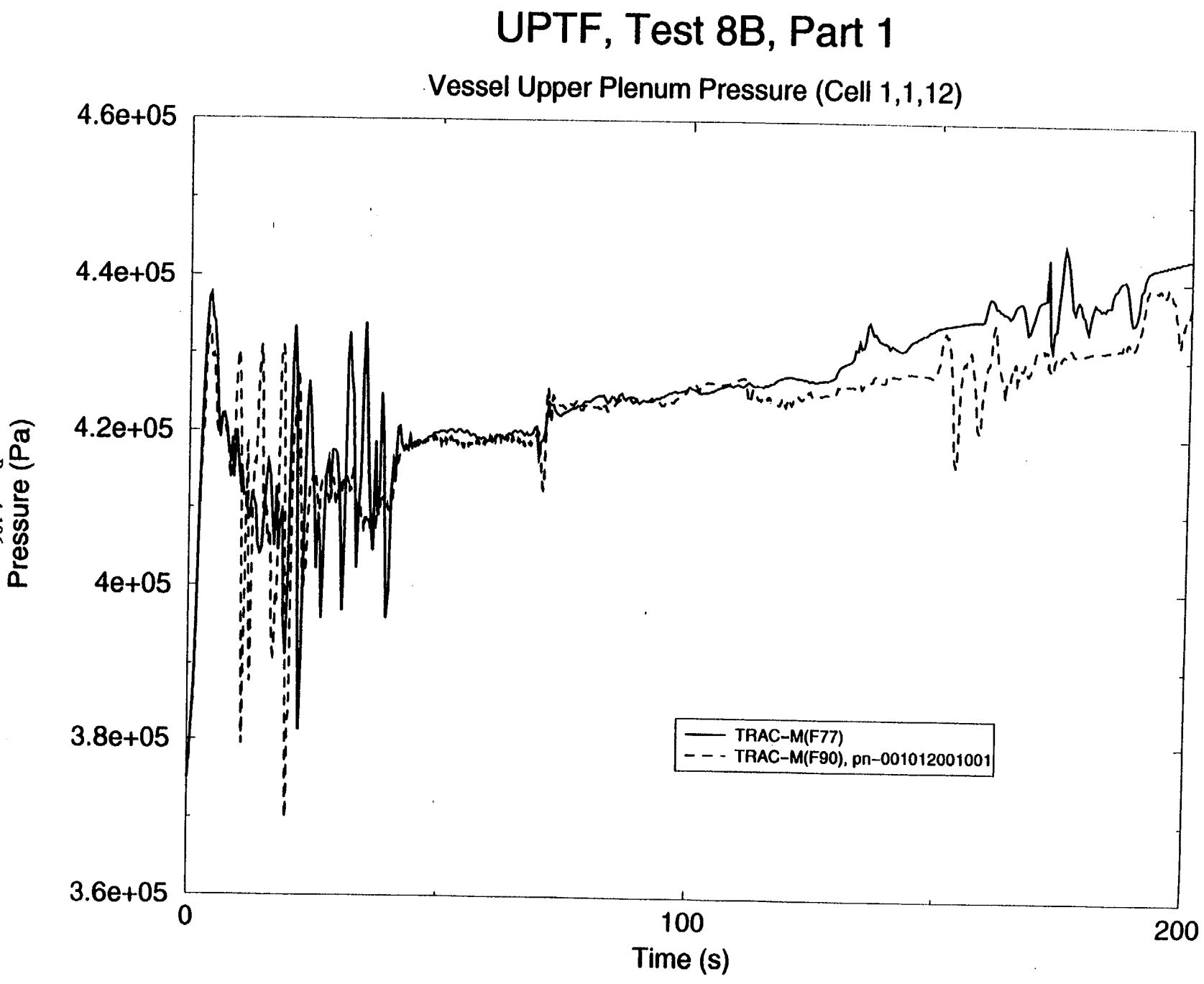

Figure 4.5.16 UPTF, Test 8B, Part 1 – Vessel Upper Plenum Pressure (Cell 1, 1, 12)

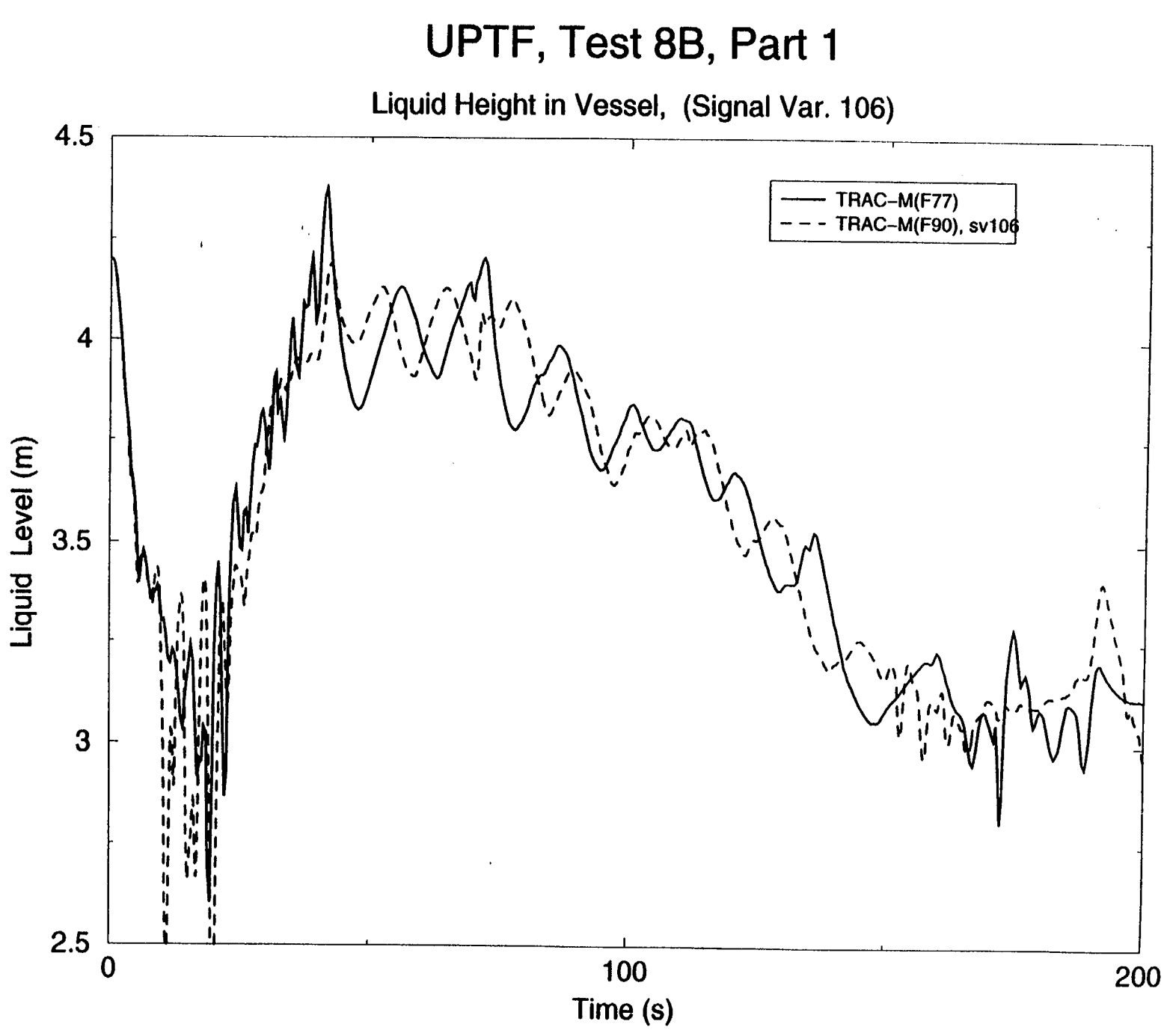

Figure 4.5.17 UPTF, Test 8B, Part 1 – Liquid Height in Vessel (Signal Var. 106)

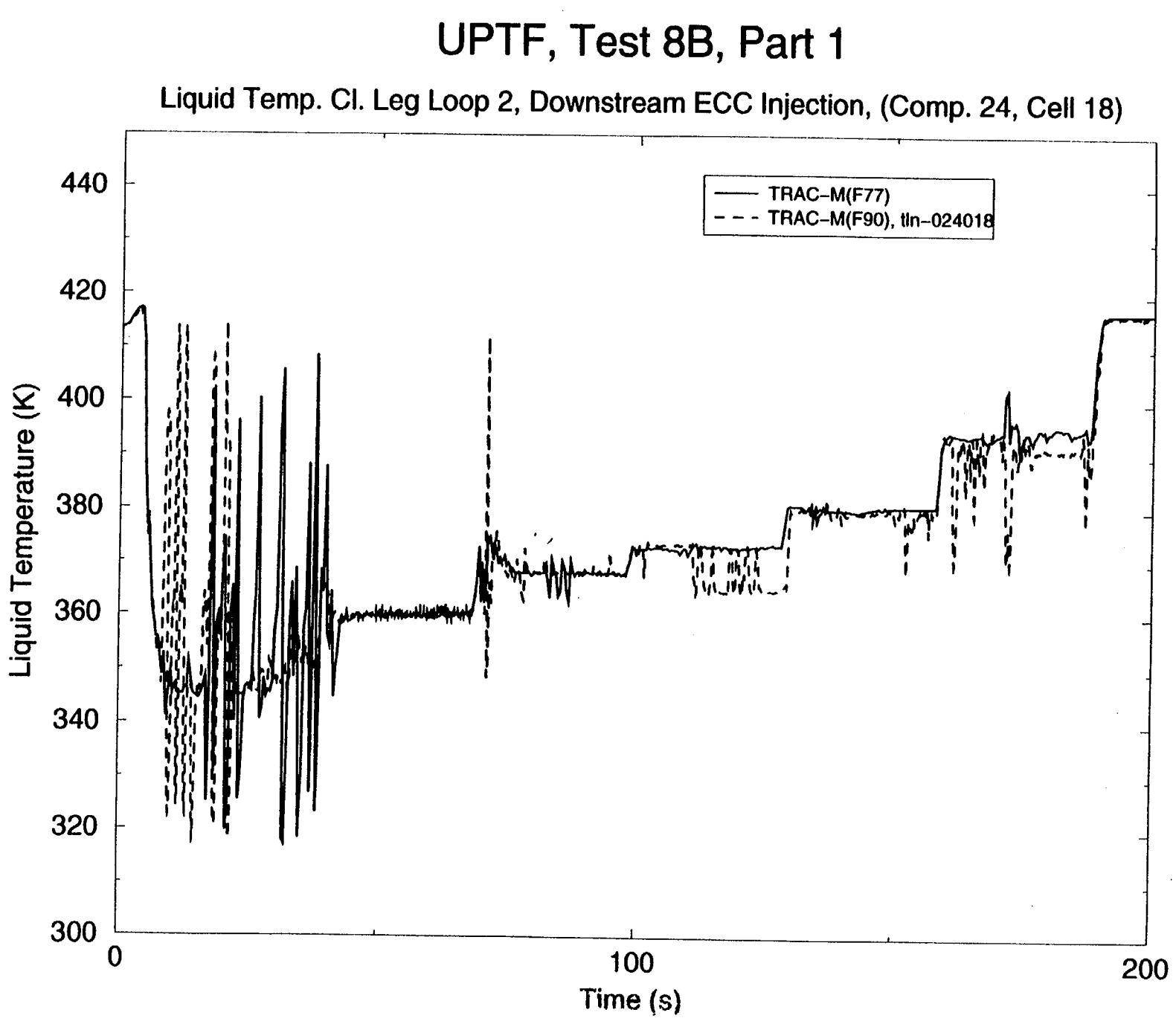

Figure 4.5.18 UPTF, Test 8B, Part 1 – Liquid Temperature Cold Leg Loop 2, Downstream ECC Injection (Comp. 24, Cell 18)

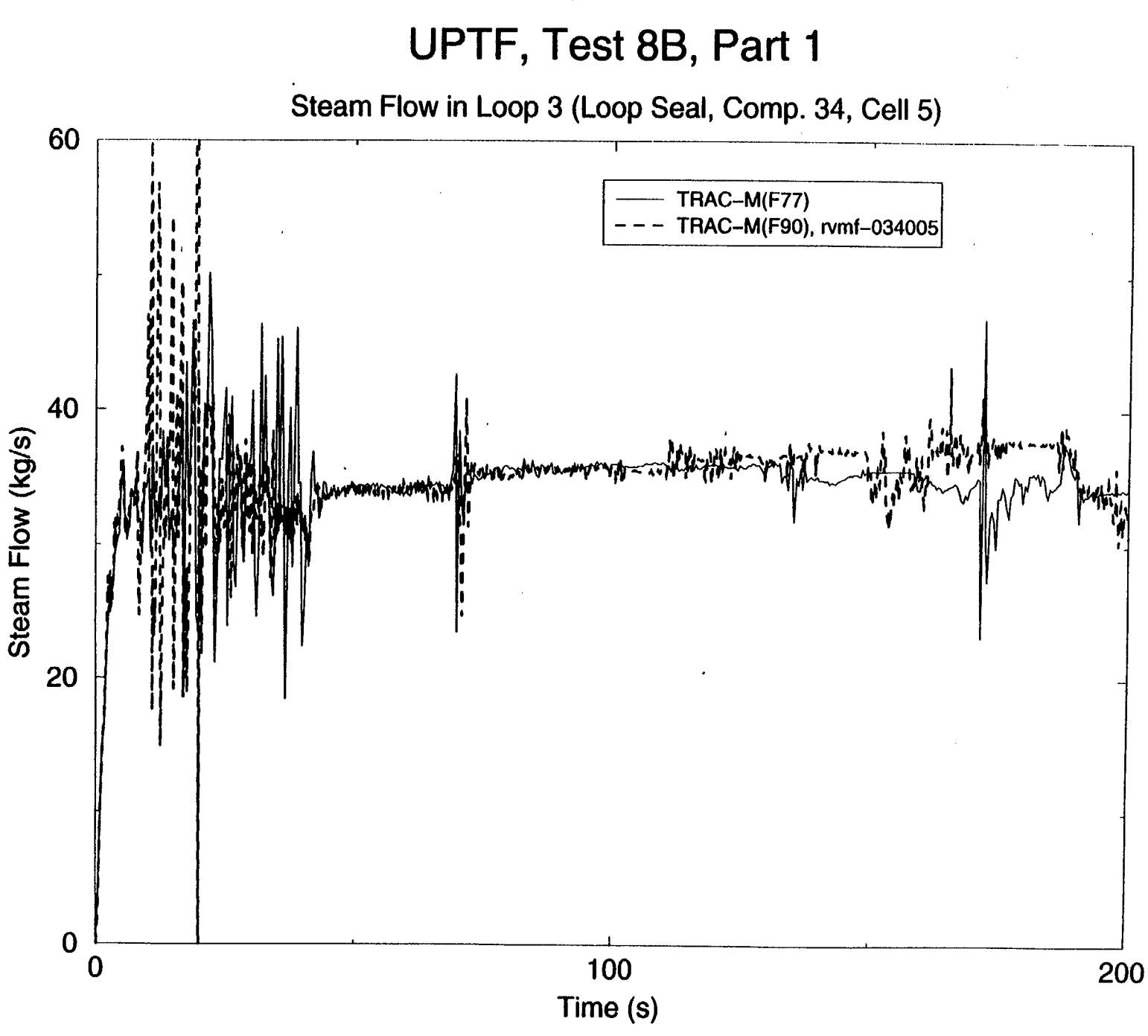

Figure 4.5.19 UPTF, Test 8B, Part 1 – Steam Flow in Loop 3 (Loop Seal, Comp. 34, Cell 5)

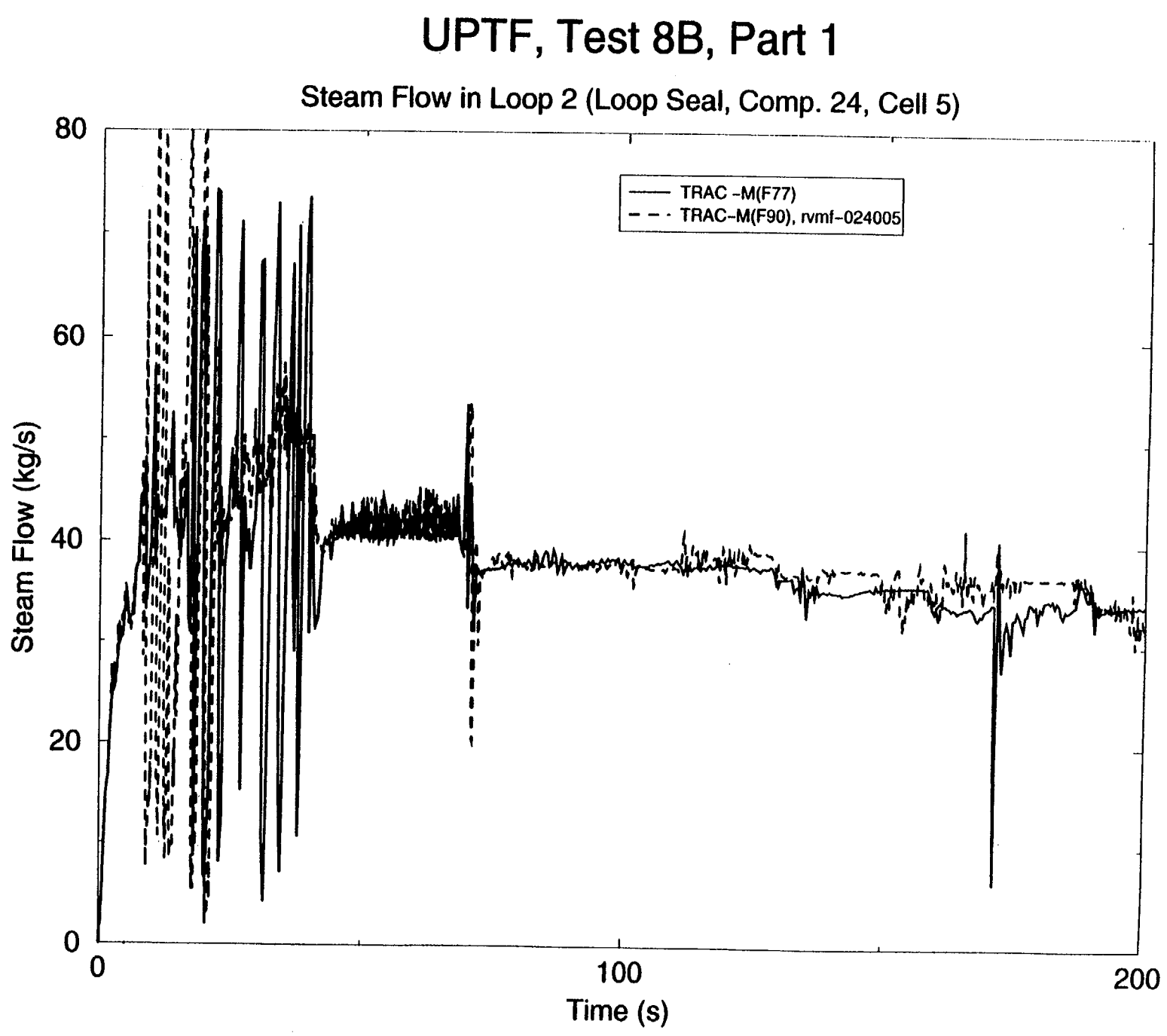

Figure 4.5.20 UPTF, Test 8B, Part 1 – Steam Flow in Loop 2 (Loop Seal, Comp. 24, Cell 5)

4.6 ECC Bypass and Downcomer and Lower Plenum Refill

During the end of blowdown, steam flows up the downcomer to escape from the broken cold leg. Because of the flashing and entrainment in the lower plenum, the downcomer upflow may have two distinct phases. This upflow initially tends to prevent the ECC from flowing down the downcomer to refill the vessel. The upflow can carry some or all of the ECC water that is injected into the cold legs directly out the broken cold leg (i.e., ECC bypass). Subscale tests have shown that, at a certain steam or two-phase upflow, ECC starts to be delivered to the lower plenum. The objective of the UPTF-6 testing was to investigate downcomer flooding behavior.

4.6.1 Upper Plenum Test Facility (UPTF) Downcomer Test 6, Run 133

The UPTF, described in Ref. 4.4.8, is a full-scale model of a four-loop, 1300-MWe PWR, which includes the reactor vessel, downcomer, lower plenum, core simulation, upper plenum, and four loops with pump and steam generator simulation. A flow diagram of the system and an overview of the test facility are shown in Figs. 4.6.1 and 4.6.2, respectively. Major dimensions of the facility are shown in Fig. 4.6.3, and a plan view of the test vessel is shown in Fig. 4.6.4. The T/H feedback of the containment is modeled using a containment simulator. The test vessel, core barrel, and internals are a full-size simulation of a PWR with four full-scale hot and cold legs modeling three intact loops and one broken loop. Both hot and cold leg breaks can be investigated with ECC injection into the hot and/or cold legs of the intact and broken loops, and into the vessel downcomer. The steam produced in a real core, and the liquid entrained by this steam flow, are simulated by direct steam injection and by liquid presence in the core simulator. Steam production on the primary side of an intact steam generator is simulated by direct steam injection into the steam generator simulator of each intact loop.

4.6.2 Test Procedure

UPTF Test 6 is a separate effects test (SET) to investigate the ECC bypass phenomenon in the lower plenum and downcomer of a US/Japanese PWR. A series of five steady-state runs (Runs 131, 132, 133, 135, and 136) was conducted under similar boundary conditions (ECC cold leg injection, and intact loops blocked at pump simulators) to investigate the steam/water CCFL behavior in the full-scale downcomer of a PWR. The goals of this test series were to establish test points on a flooding curve, determine scale and geometry effects on downcomer ECC bypass behavior, and provide full-scale test data for code assessment. The total ECC injection flow rate was held constant at ~1500 kg/s (about 500 kg/s from each intact cold leg), while the steam injection flow rates ranged from 100 to 500 kg/s.

The system configuration for all five tests in this series (see Fig. 4.6.5) was as follows:

- closed intact loop pump simulators
- closed hot leg break valve
- fully open cold leg break valve

At the start of each test, the primary system is filled with steam only, and there is no water in the lower plenum. The primary system pressure corresponds to the containment pressure, and the

primary structures are heated to the saturation temperature of the maximum pressure expected during the test. ECC water is injected into the intact loop cold leg, and nitrogen is injected into the ECC water. Steam is injected into the core simulator and the steam generator simulators of the intact loop.

4.6.3 TRAC Model

Noding diagrams for the TRAC model are shown in Figs. 4.6.6 through 4.6.14. The vessel axial noding is shown in Fig. 4.6.6. The vessel model consists of 13 axial levels, 8 azimuthal sectors, and 3 radial rings. The azimuthal and radial noding distribution for the vessel is shown in Fig. 4.6.7. The core is represented by the inner two rings, and the downcomer is represented by the outer ring.

Figs. 4.6.8 through 4.6.10 show the noding for Loops 1, 2, and 3, respectively. In each loop, the hot leg is modeled with a TEE component; the steam generator simulator is modeled with a combination of four TEE components and one VALVE component; and the crossover pipe, pump simulator, and cold leg are modeled with another TEE component. Steam injection into the top of the steam generator simulator is modeled with TEE and FILL components. This FILL component can be controlled by the mass flow of liquid in the hot leg. The drain line from the bottom of the secondary side of the middle TEE to the steam generator simulator inlet plenum is modeled with another TEE and VALVE component. The pump simulator is modeled with a flow area restriction and the correct volumes associated with the pump simulator component. ECC injection is modeled in both the hot and cold legs with the TEE and FILL components. If desired, the FILL components can invoke a time-dependent programmed ECC flow. The Loop 1 and Loop 3 noding are identical. In Loop 2, the pressurizer in the hot leg required the addition of an extra TEE component. This FILL component also may use a preprogrammed type steam flow.

Figs. 4.6.11 and 4.6.12 show the hot and cold leg noding, for the broken loop 4, respectively. The broken loop cold leg model is composed of a VALVE component to model the main break valve, a TEE component to model the bottom of the steam generator simulator, and another TEE component to model the steam/water separator and piping to the containment. The bottom of the steam generator simulator drain line is modeled to the drain tank valve. This drain line drains off accumulated liquid during the course of the transient. The broken loop hot leg is modeled with a TEE component for the hot leg, another TEE component for the steam generator simulator, and a VALVE component for piping run out to the containment tank. The containment tank is modeled with two BREAK components. These components provide a transient pressure boundary condition. Drain lines from the bottom of the vessel to the drain tank were completely modeled, and are shown in Fig. 4.6.13.

The core steam/water injection sources are modeled by 16 individual TEE components, each of which has the same noding shown in Fig. 4.6.14. Each component is connected to one of the 16 core cells at the vessel Level 6. The TEE components are able to combine the steam input from a feedback injection with the preprogrammed steam/water input. For UPTF Test 6, there is no feedback injection flow. The walls between the UPTF injection zones are solid; therefore, TRAC incorporates a zero flow area in the radial and azimuthal direction at Level 6. Because the steam is injected in the radial direction at this level, it will impact the walls and lose its radial momentum. To model this effect in the TRAC input, the steam/water injection sources are directed radially.

4.6.4 Comparison of TRAC-M(F77) and TRAC-M(F90) Calculations

TRAC-M(F77) and TRAC-M(F90) analyses are performed for Run 133, which corresponded to a steam injection flow rate of 110 kg/s. The test conditions for Run 133 are presented in Table 4.6.1.

The intact loops are blocked at the pump simulators, so the steam flow from the steam generator simulators is forced to flow through the hot legs, down into the vessel, and up the downcomer. Therefore, the total amount of steam that flows up the downcomer is ~200 kg/s for this test. The steam flow is held fairly constant throughout the test.

Calculations are performed using both TRAC-M(F77) and TRAC-M(F90), and the results are compared in Figs. 4.6.15 through 4.6.21. Since UPTF test data are restricted to 2-D/3-D program participants, these figures compare code-to-code results, and this report does not contain any graphics of the test data. Agreements between code calculations are considered "Excellent" for this test.*

Figs. 4.6.15 through 4.6.17 illustrate code calculations of pressure, liquid temperature, and vapor temperature at mid-elevation of the downcomer as the ECC water is injected into the vessel. Figs. 4.6.18 through 4.6.20 show code calculations of vapor fraction at the bottom, mid, and top elevations of the downcomer showing the refill process. Fig. 4.6.21 shows how the vessel mass increases as the ECC is injected.

4.6.5 Conclusions

The conversion from TRAC-M(F77) to TRAC-M(F90) has been successful for this type of application.

---

* See footnote on page 4-79.

Table 4.6.1 Initial Test Conditions

Initial pressure in downcomer	257 kPa
Downcomer wall temperature	460 K
Lower plenum water inventory	0 kg
Pressure in drywell	256 kPa
ECC temperature	388–390 K
Total ECC injection rate	1473 kg/s
Total nitrogen injection rate	1 kg/s
Total core simulator steam mass flow rate	110 kg/s
Steam generator simulators steam mass flow rate (each)	29–33 kg/s

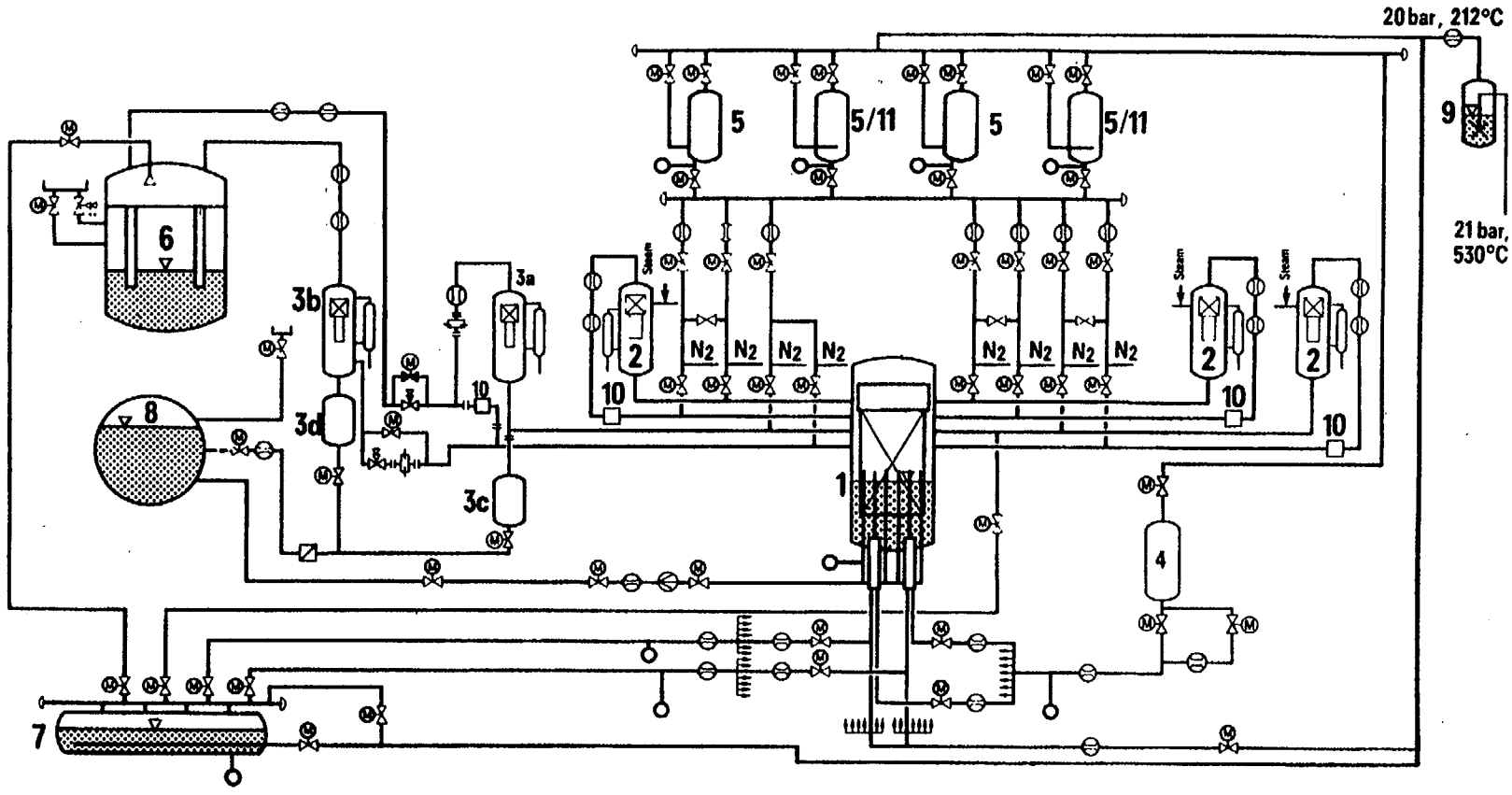

1 Test Vessel
2 Steam Generator Simulator (Intact Loop)
3a Steam Generator Simulator/ Water Separator (Broken Loop Hot Leg)
3b Water Separator (Broken Loop Cold Leg)
3c Drainage Vessel for Hot Leg
3d Drainage Vessel for Cold Leg
4 Hot Water Storage Tank
5 Accumulatur
6 Containment Simulator
7 Steam Storage Tank
8 Water Collecting Tank
9 Steam Cooler
10 Pump Simulator
11 N_2-Tank
○ Sample

Figure 4.6.1 UPTF Flow Diagram

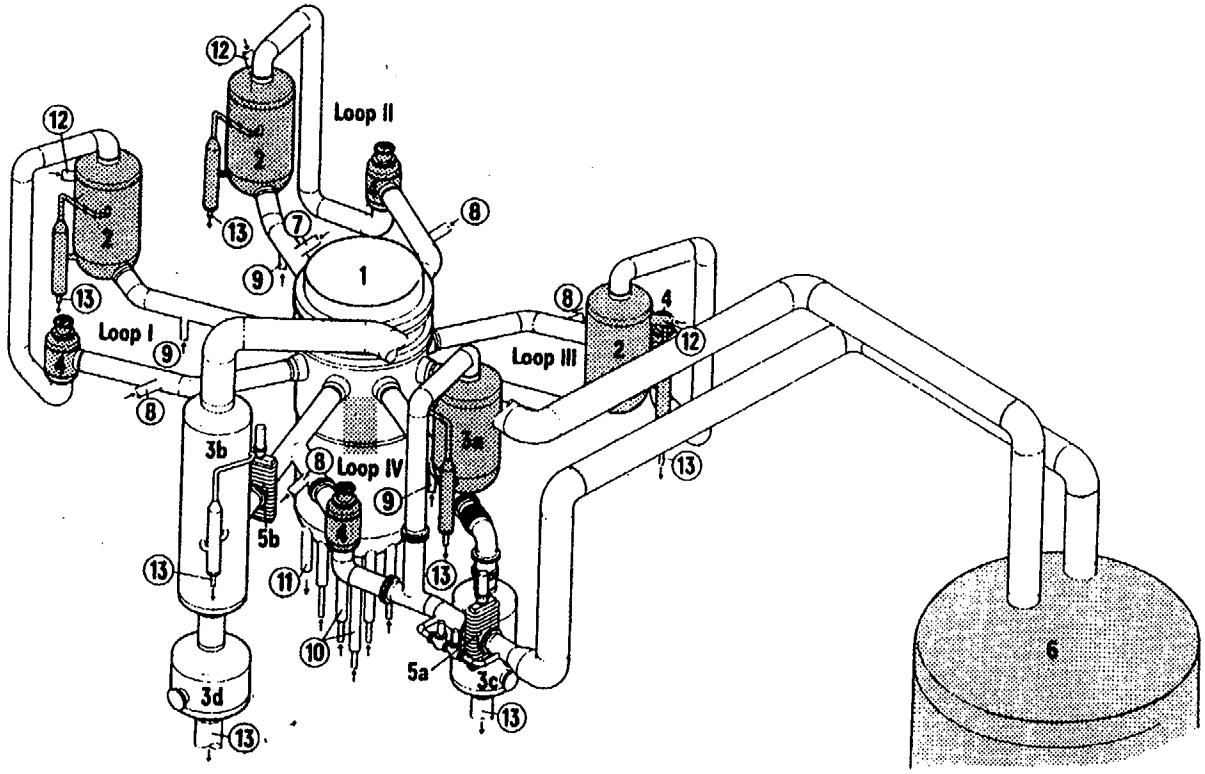

1 Test Vessel
2 Steam Generator Simulator (Intact Loop)
3a Steam Generator Simulator/ Water Separator (Broken Loop Hot Leg)
3b Water Separator (Broken Loop Cold Leg)
3c Drainage Vessel for Hot Leg
3d Drainage Vessel for Cold Leg
4 Pump Simulator
5a Break Valve (Hot Leg)
5b Break Valve (Cold Leg)
6 Containment Simulator

(7) Surgeline-Nozzle
(8) ECC-Injection Nozzles (Cold Leg)
(9) ECC-Injection Nozzles (Hot Leg)
(10) Core Simulator Injection Nozzle
(11) TV-Drainage Nozzle
(12) Steam Injection Nozzle
(13) Drainage Nozzle

Simulator

Figure 4.6.2 Overview of UPTF Primary System

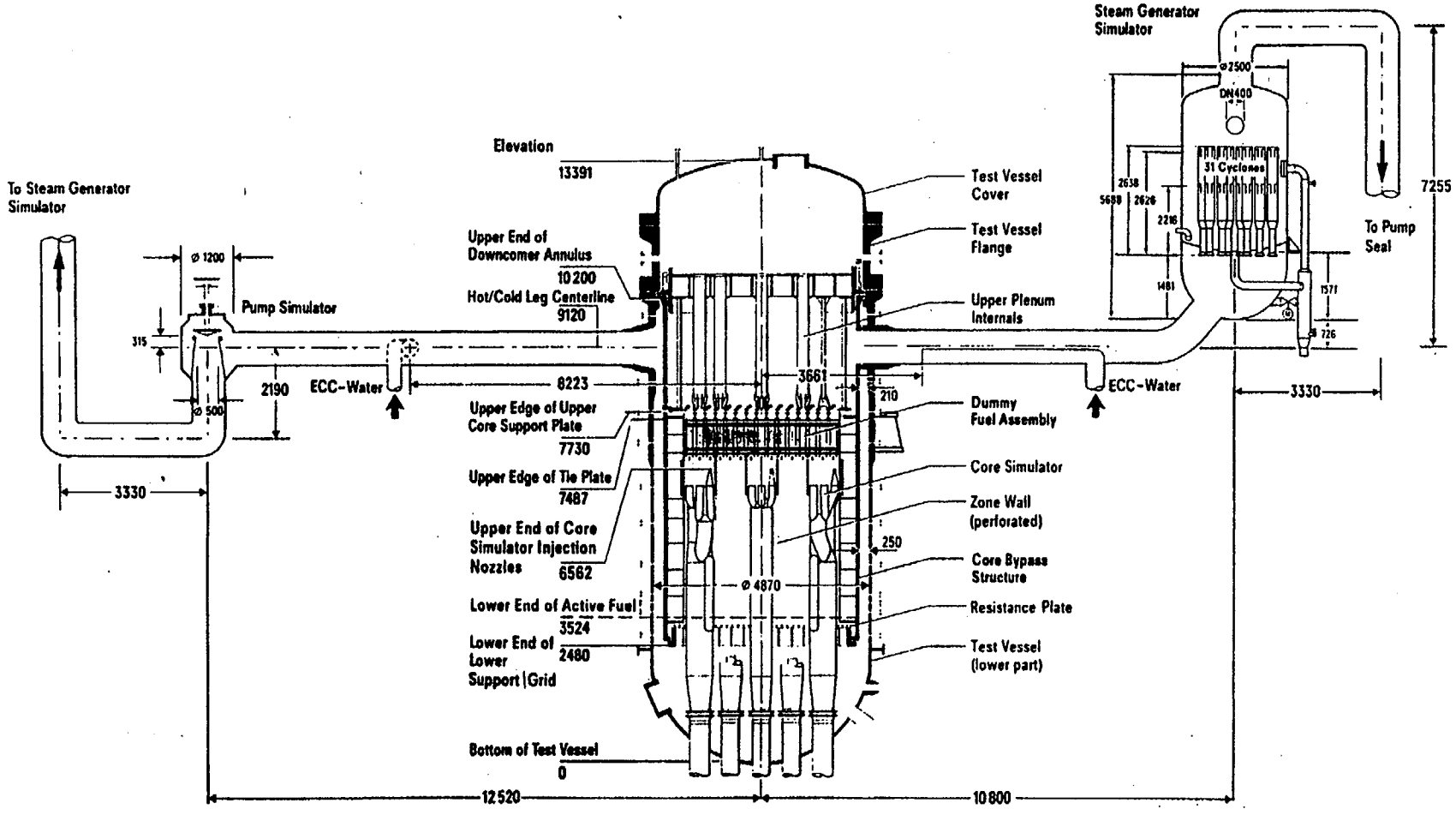

Figure 4.6.3 Major Dimensions of the UPTF Primary System

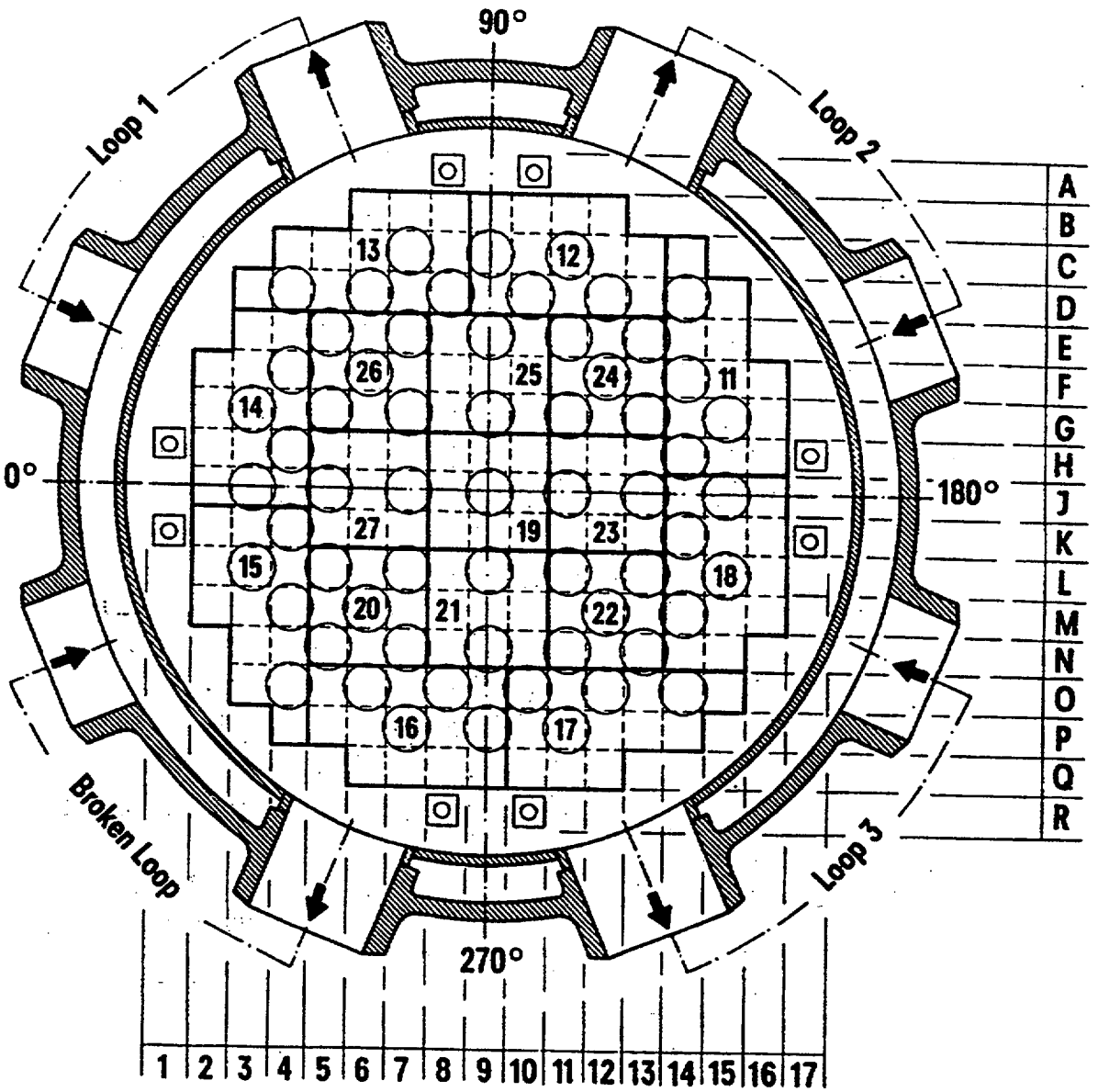

Figure 4.6.4 Plan View of UPTF Test Vessel

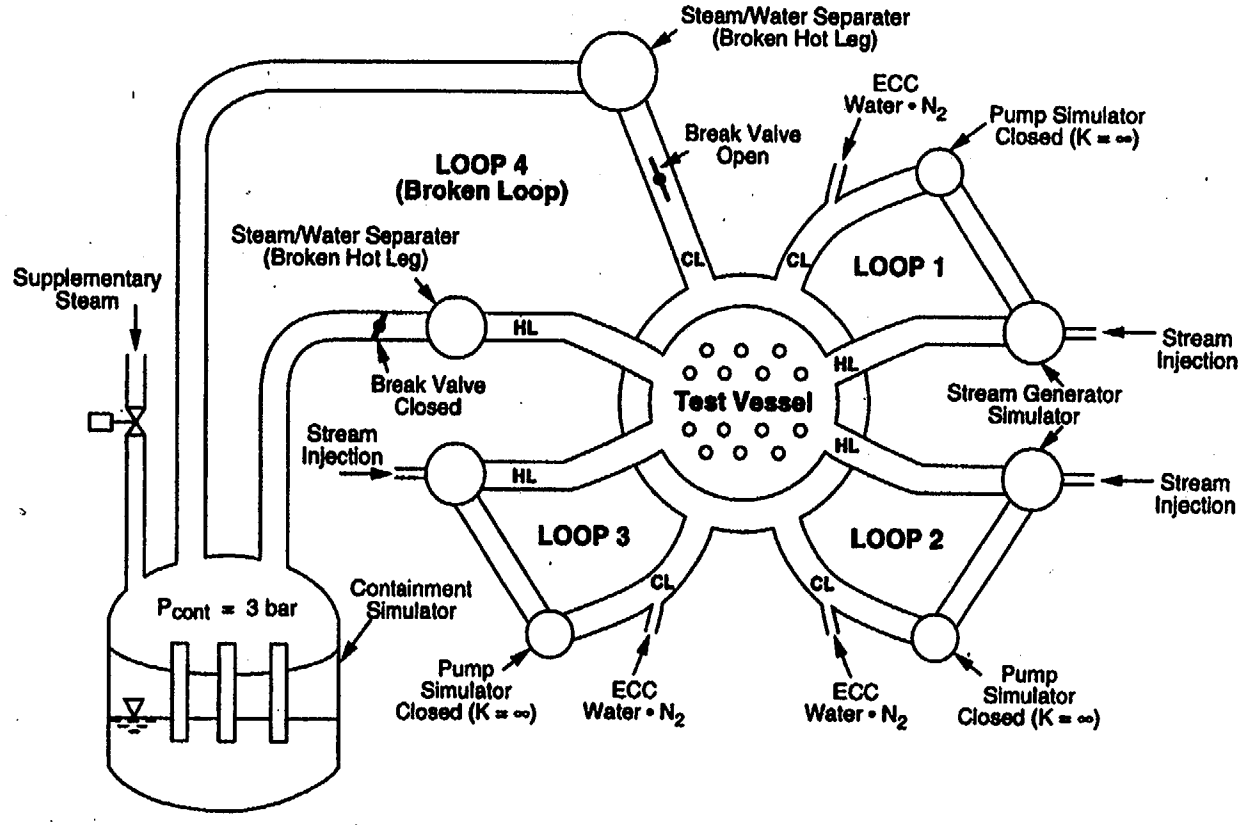

Figure 4.6.5 System Configuration for UPTF Test 6

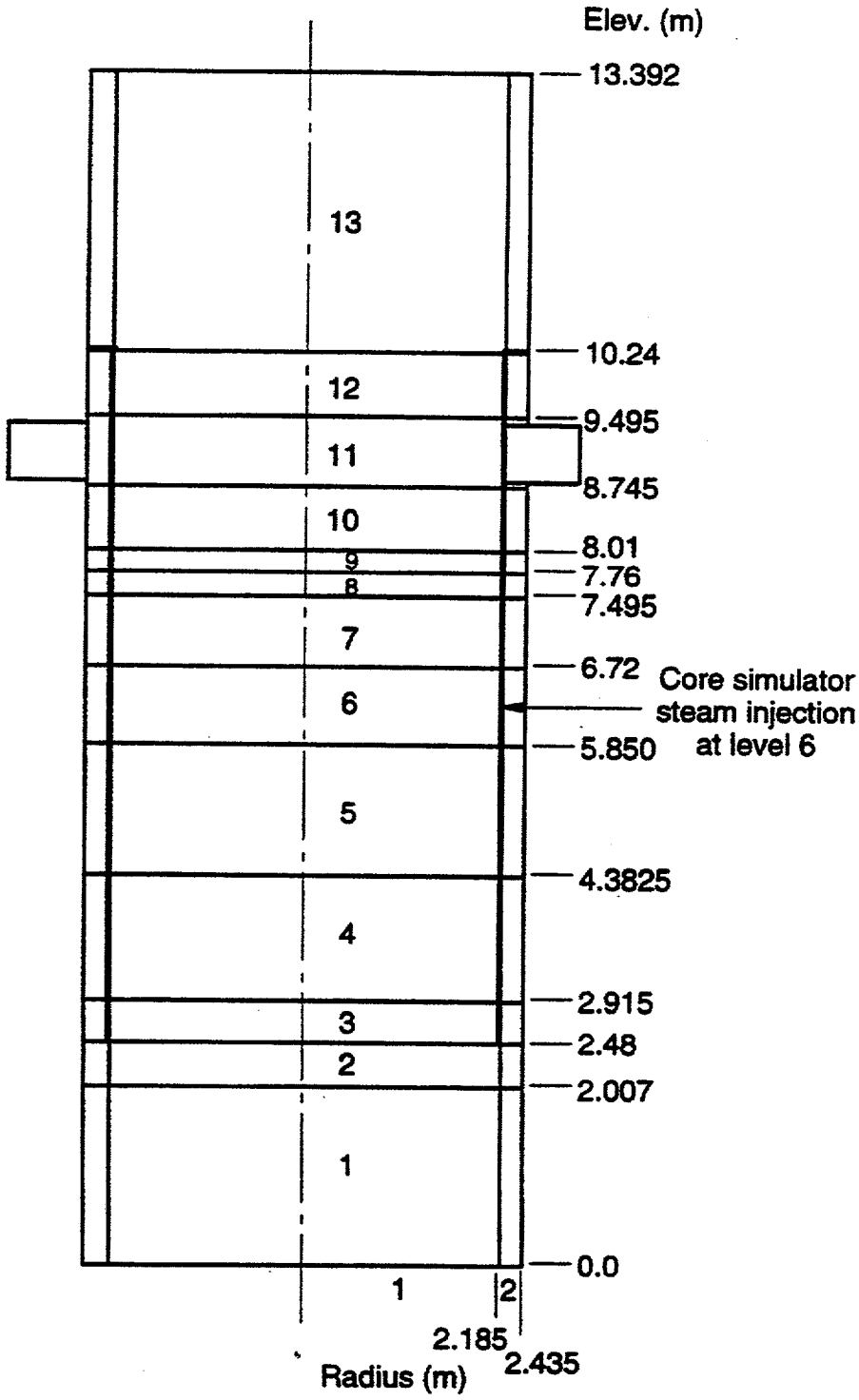

Figure 4.6.6 Vessel Model Elevation View for UPTF Test 6

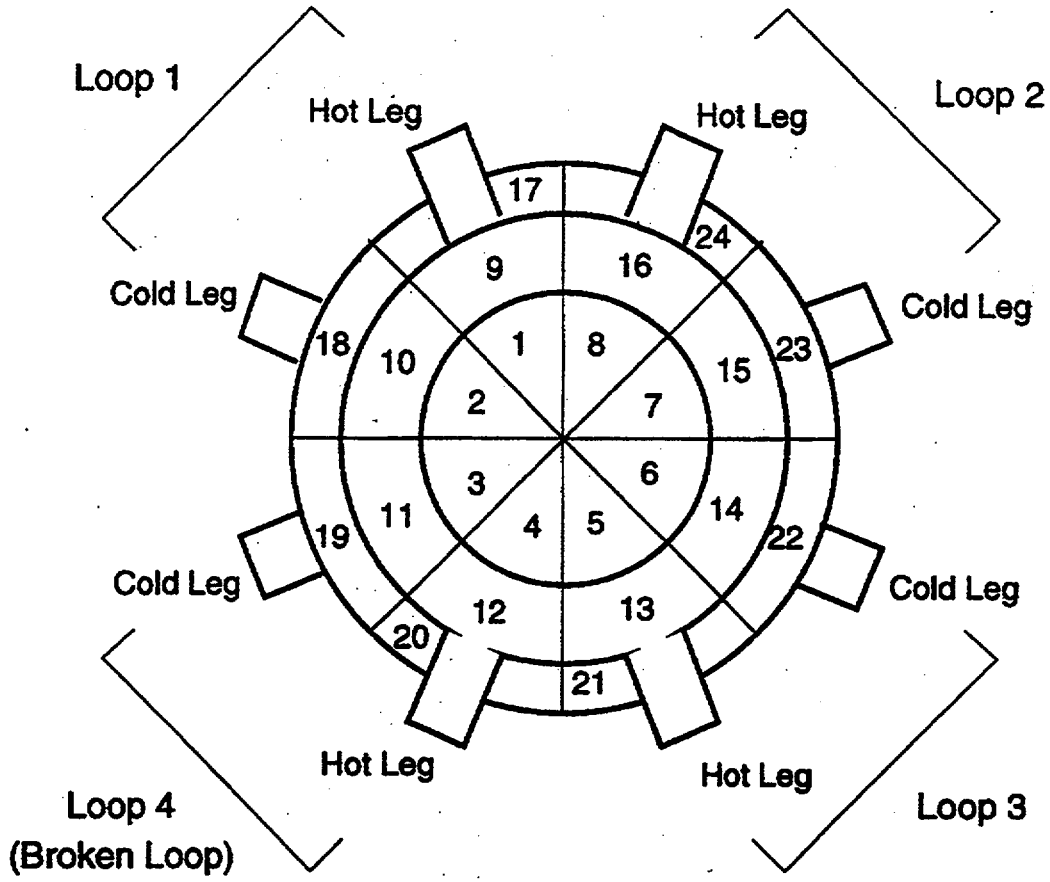

Figure 4.6.7 Vessel Model Plan View for UPTF Test 6

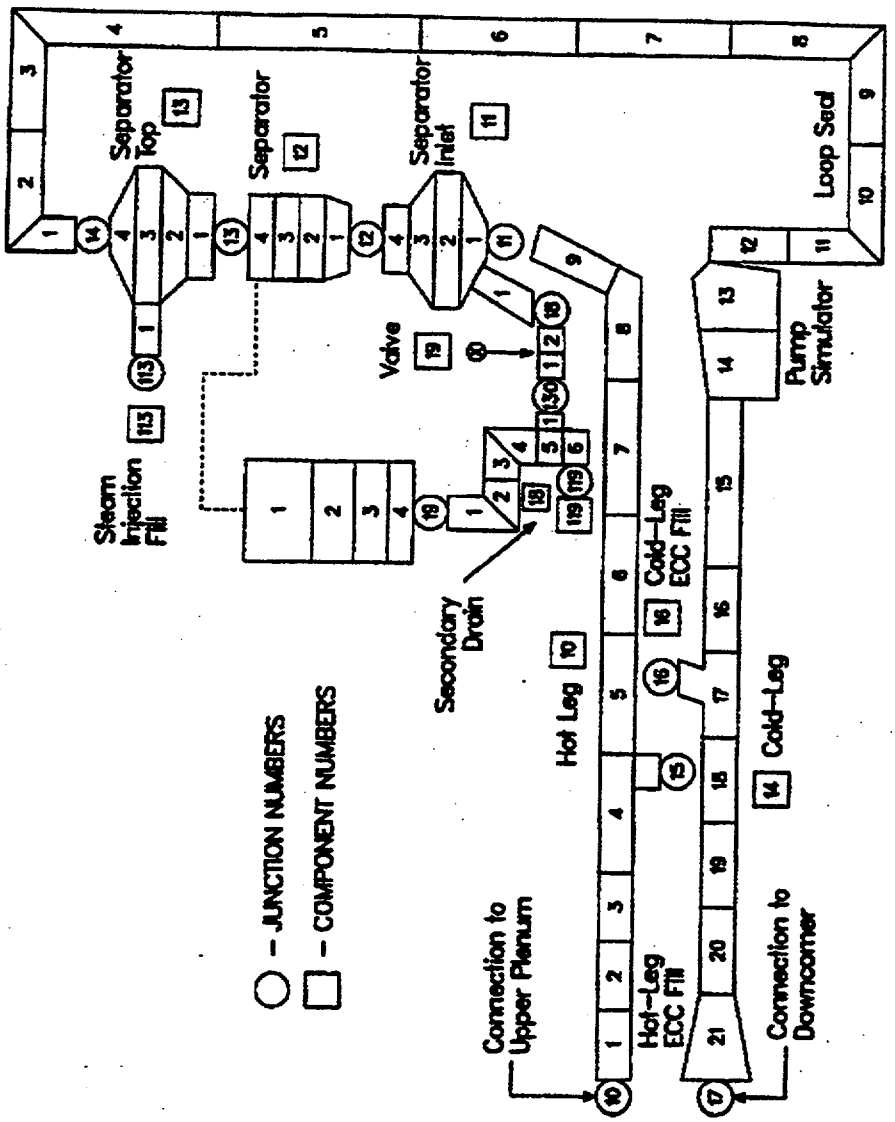

Figure 4.6.8 UPTF Loop-1 Noding Diagram

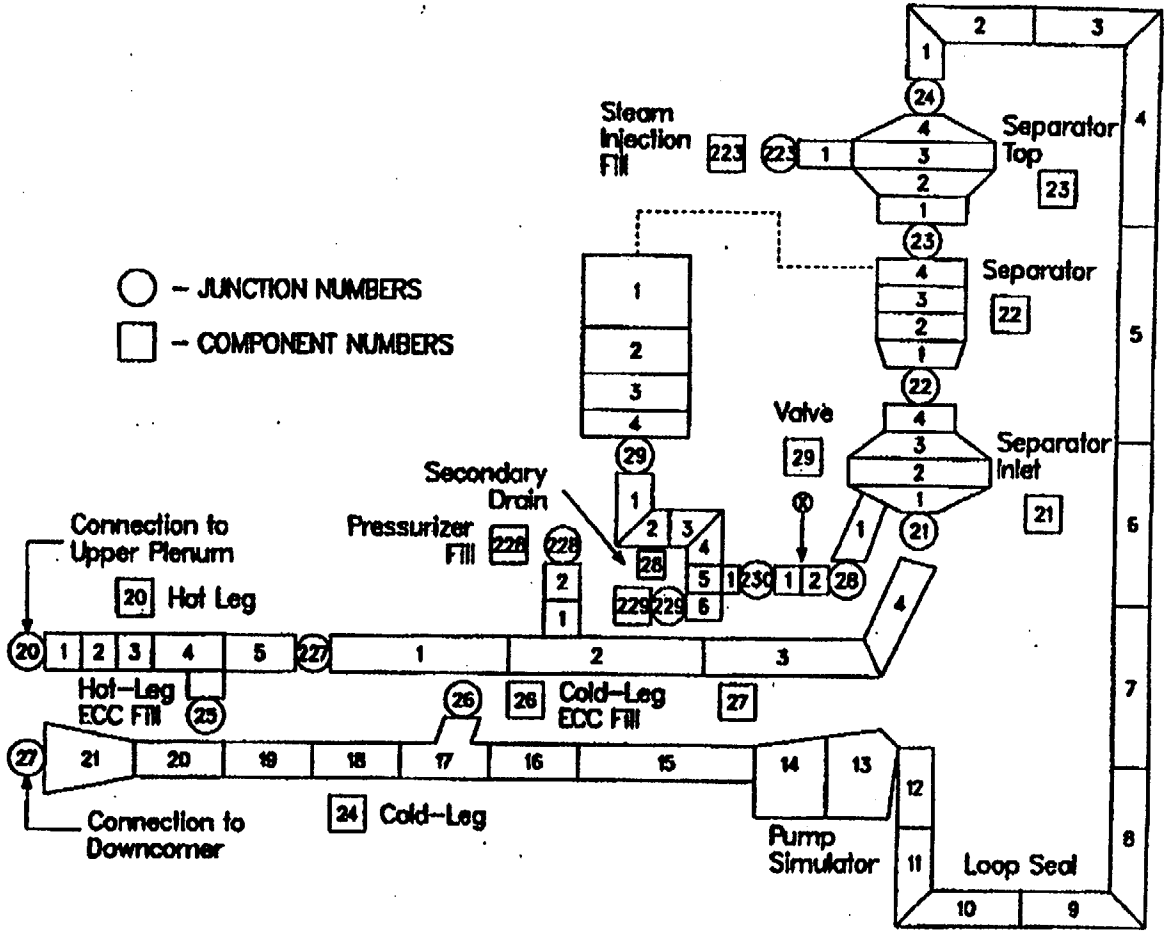

Figure 4.6.9 UPTF Loop-2 Noding Diagram

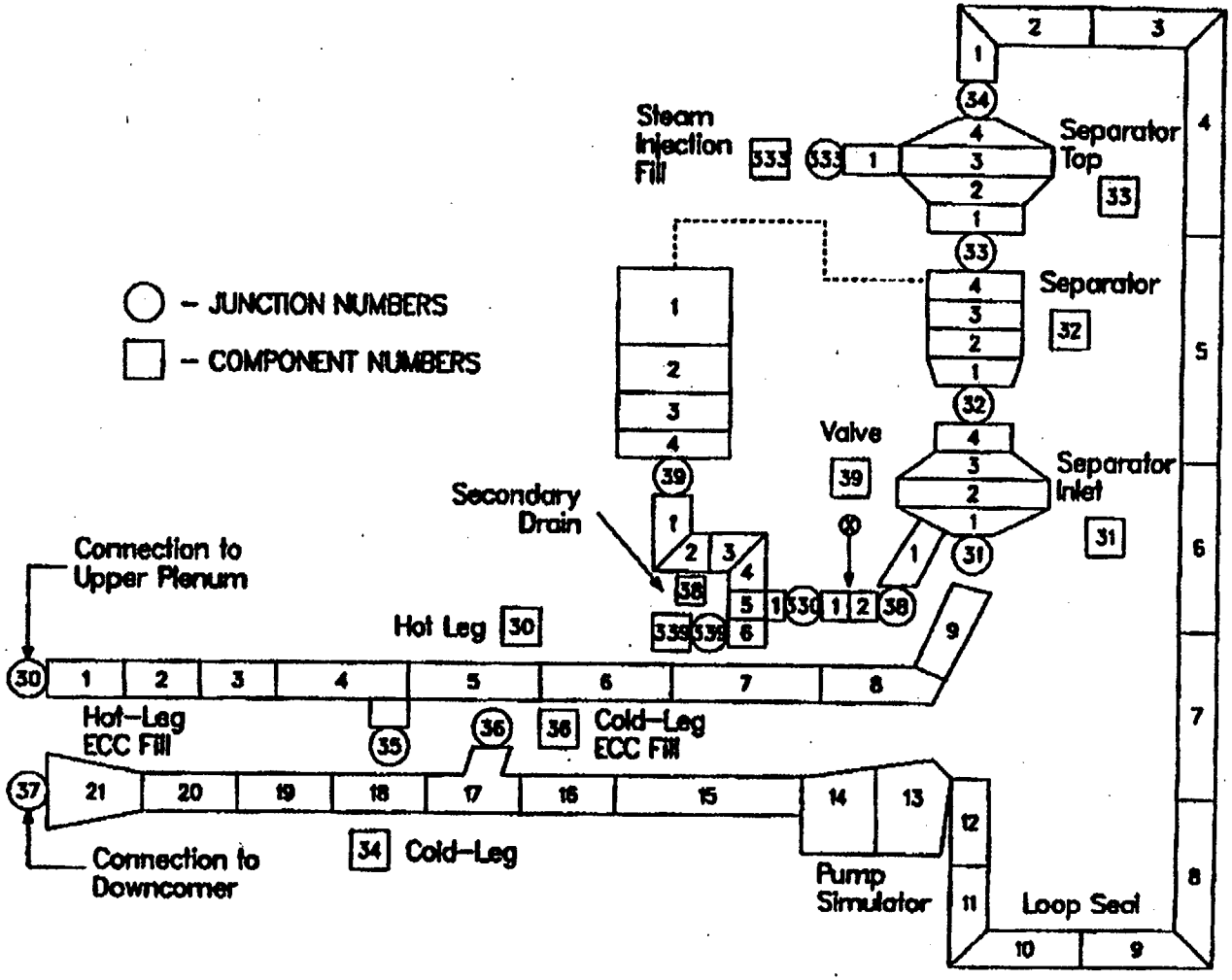

Figure 4.6.10 UPTF Loop-3 Noding Diagram

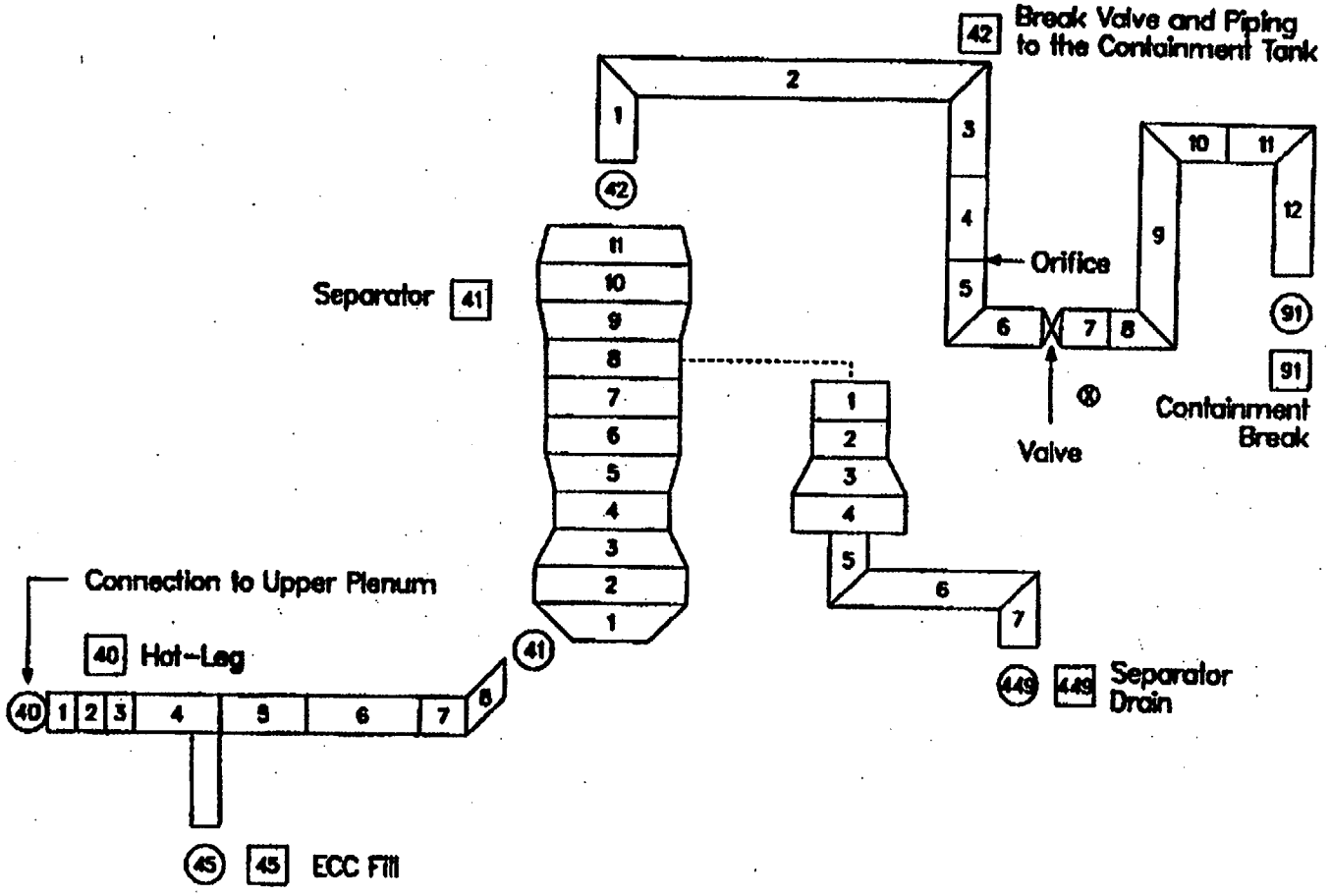

Figure 4.6.11 UPTF Loop-4 Broken-Hot-Leg Noding Diagram

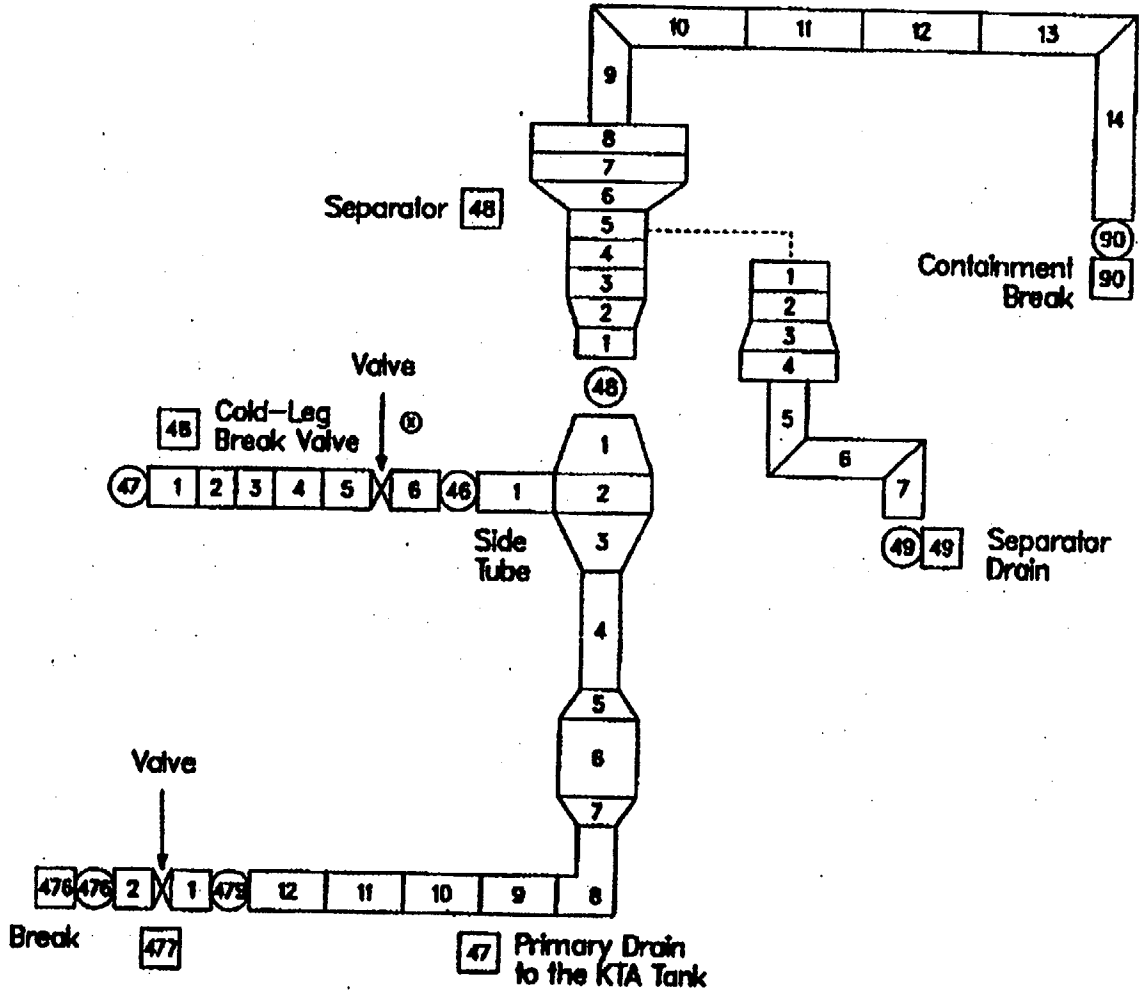

Figure 4.6.12 UPTF Loop-4 Broken-Cold-Leg Noding Diagram

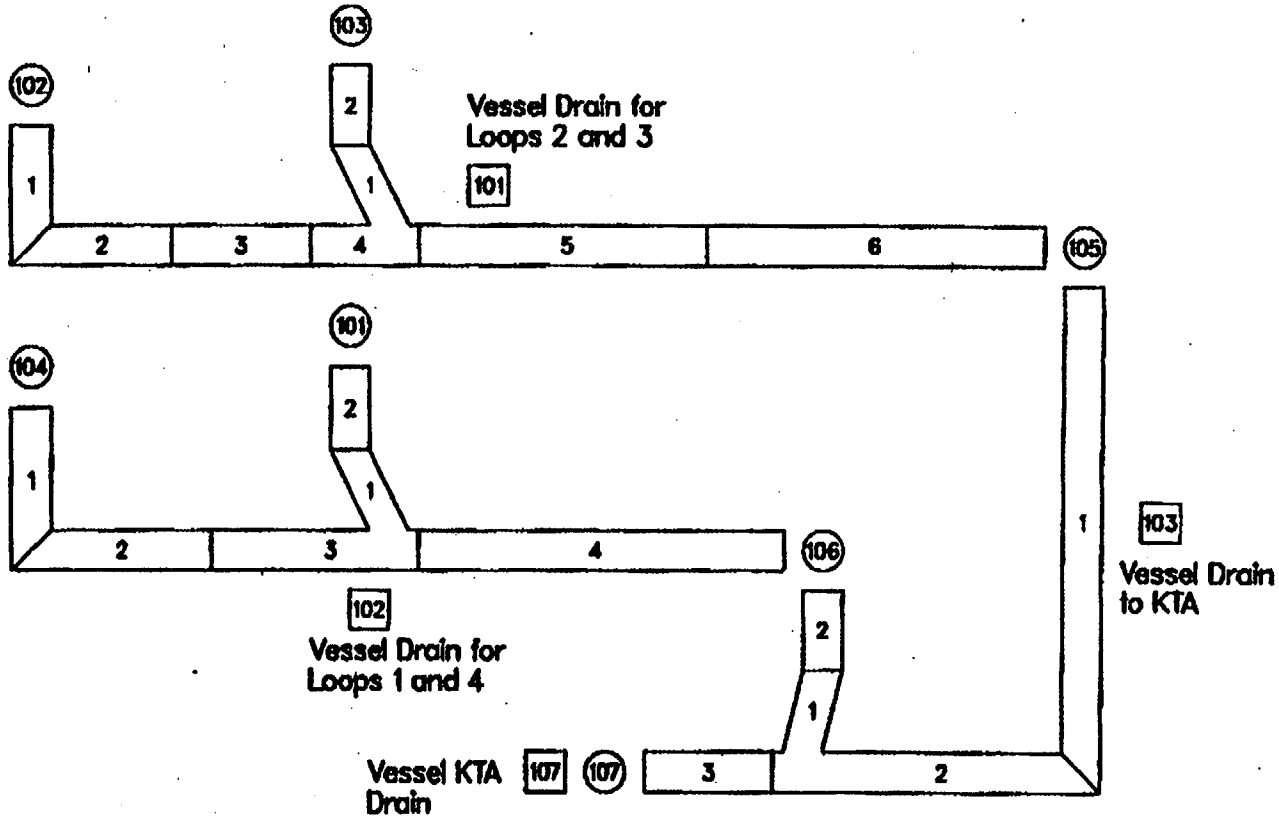

Figure 4.6.13 UPTF Water Drainage System Noding Diagram

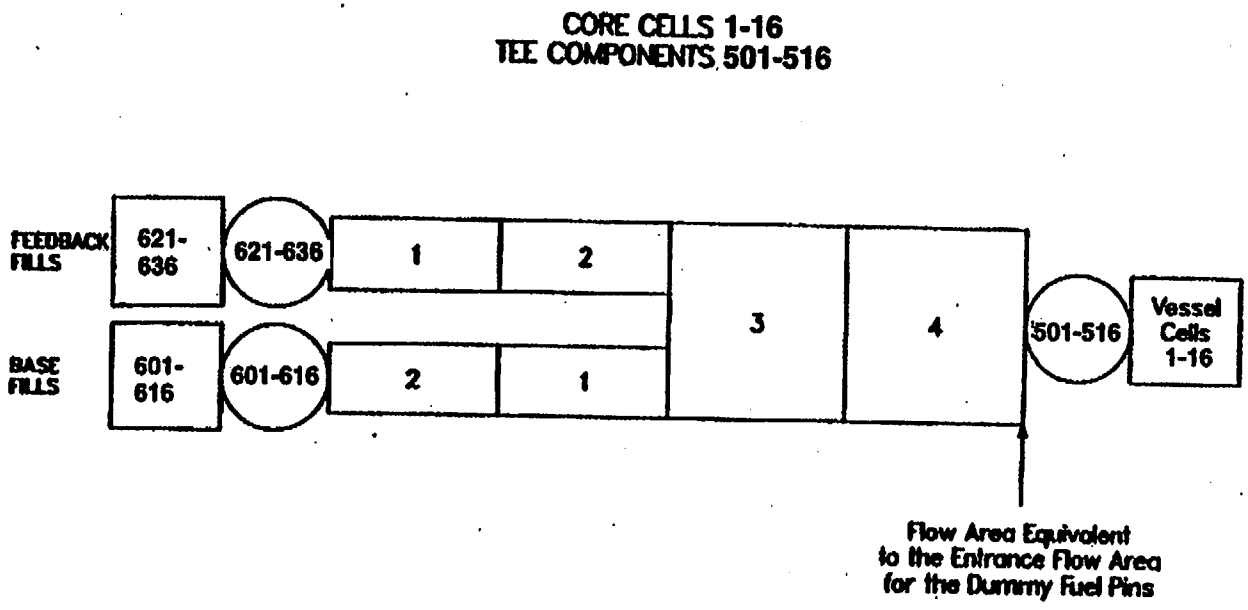

Figure 4.6.14 UPTF Core-Simulator-Injection Noding Diagram

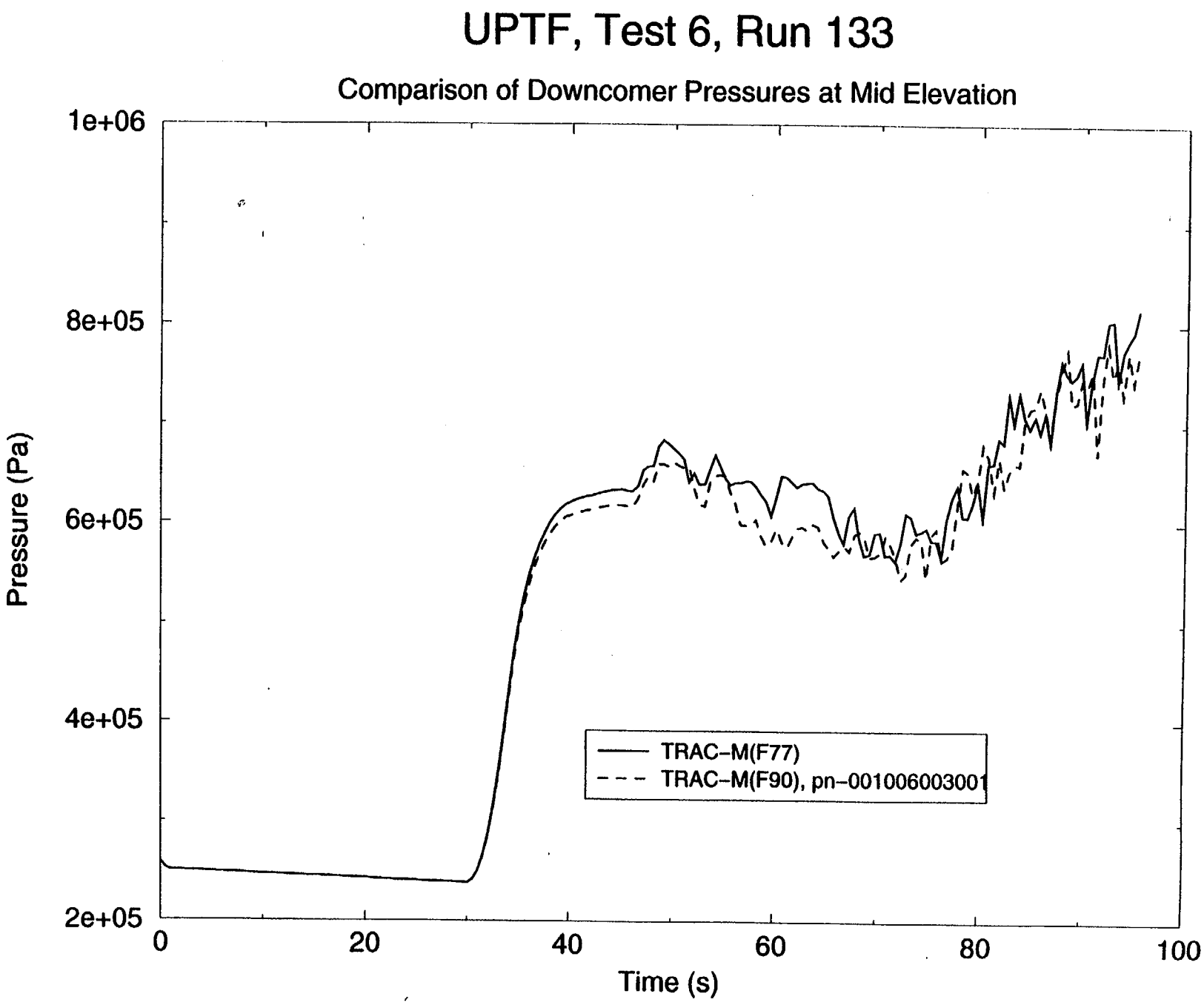

Figure 4.6.15 UPTF, Test 6, Run 133 – Comparison of Downcomer Pressures at Mid-Elevation

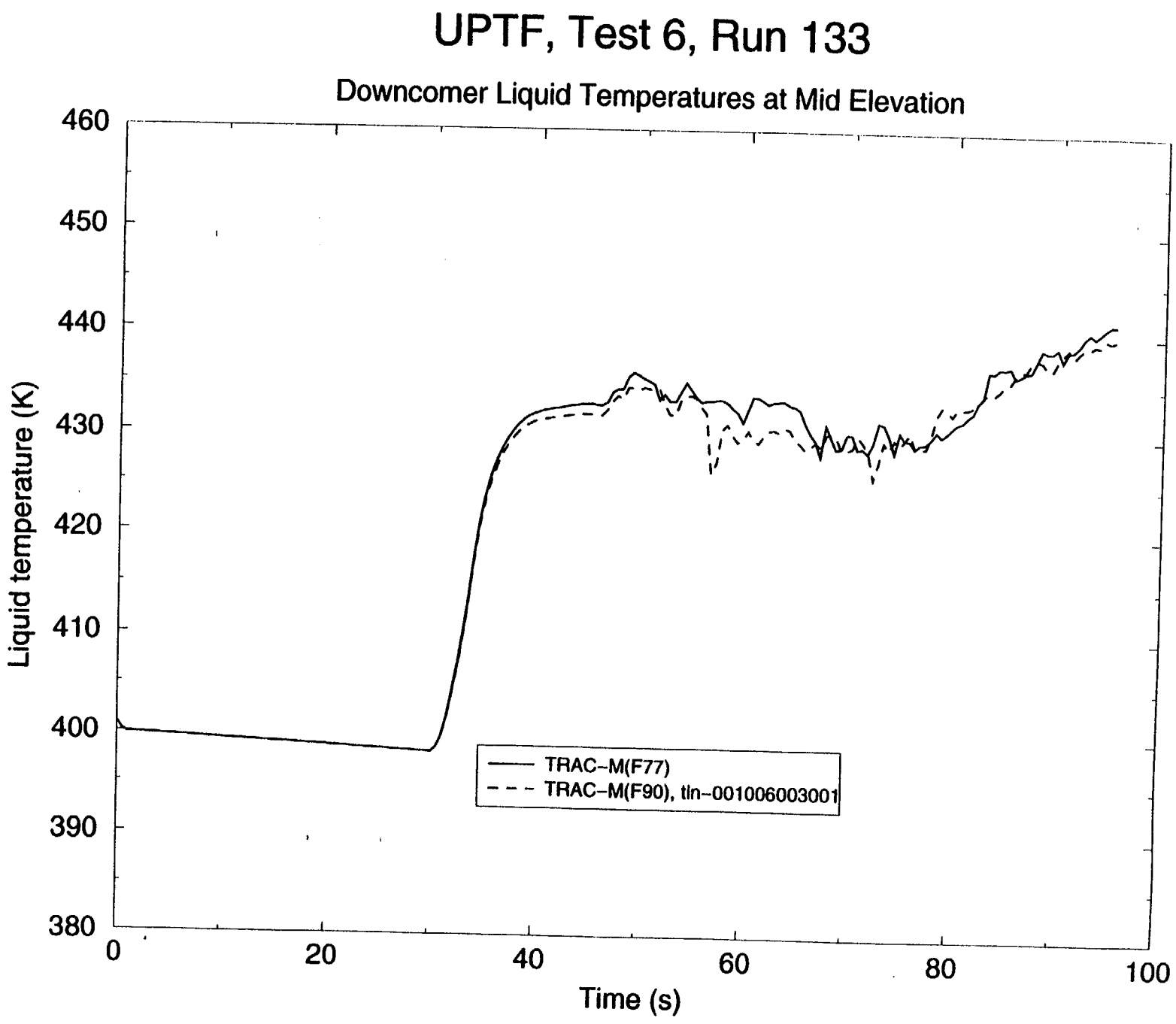

Figure 4.6.16 UPTF, Test 6, Run 133 – Downcomer Liquid Temperatures at Mid-Elevation

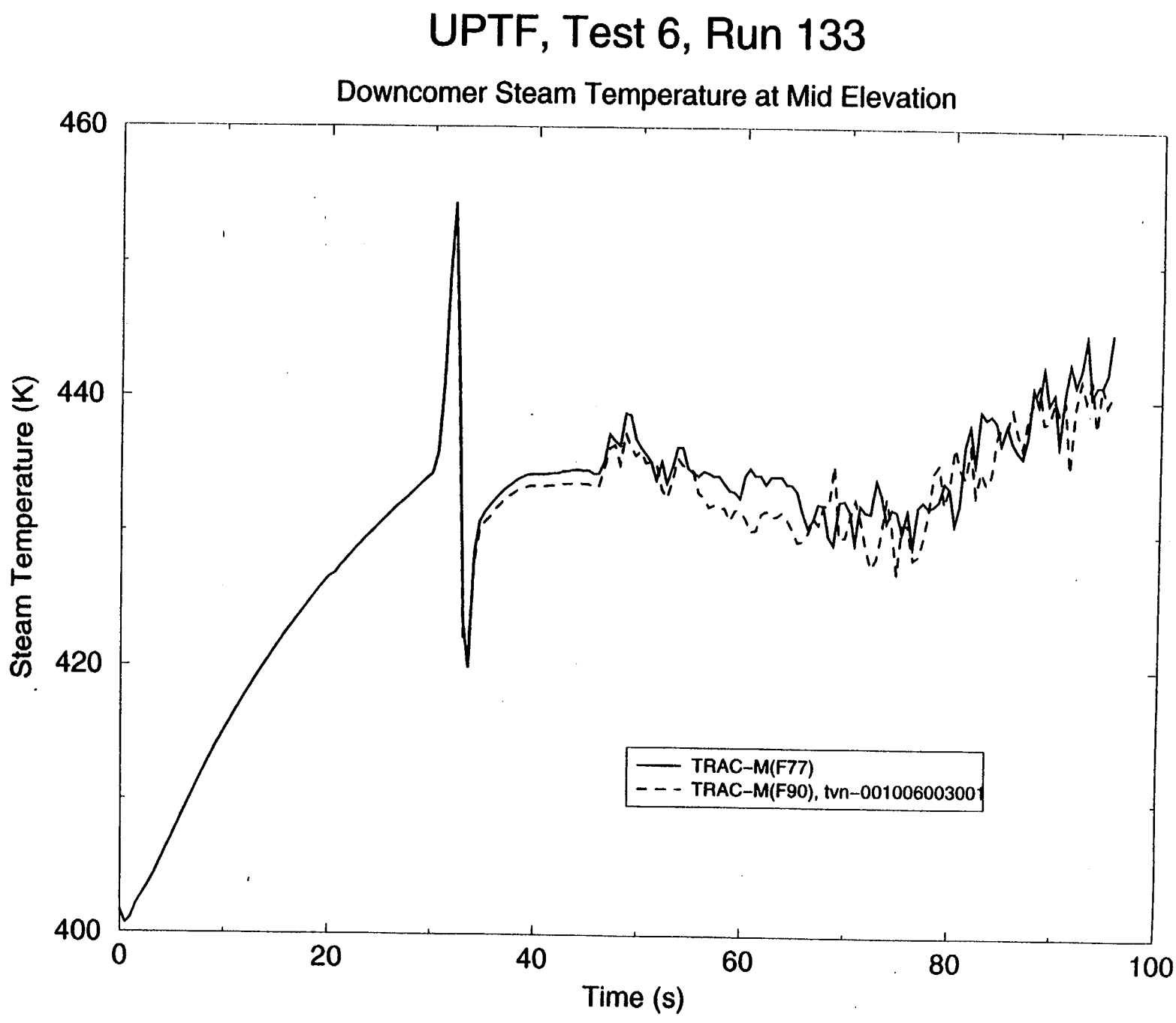

Figure 4.6.17 UPTF, Test 6, Run 133 – Downcomer Steam Temperature at Mid-Elevation

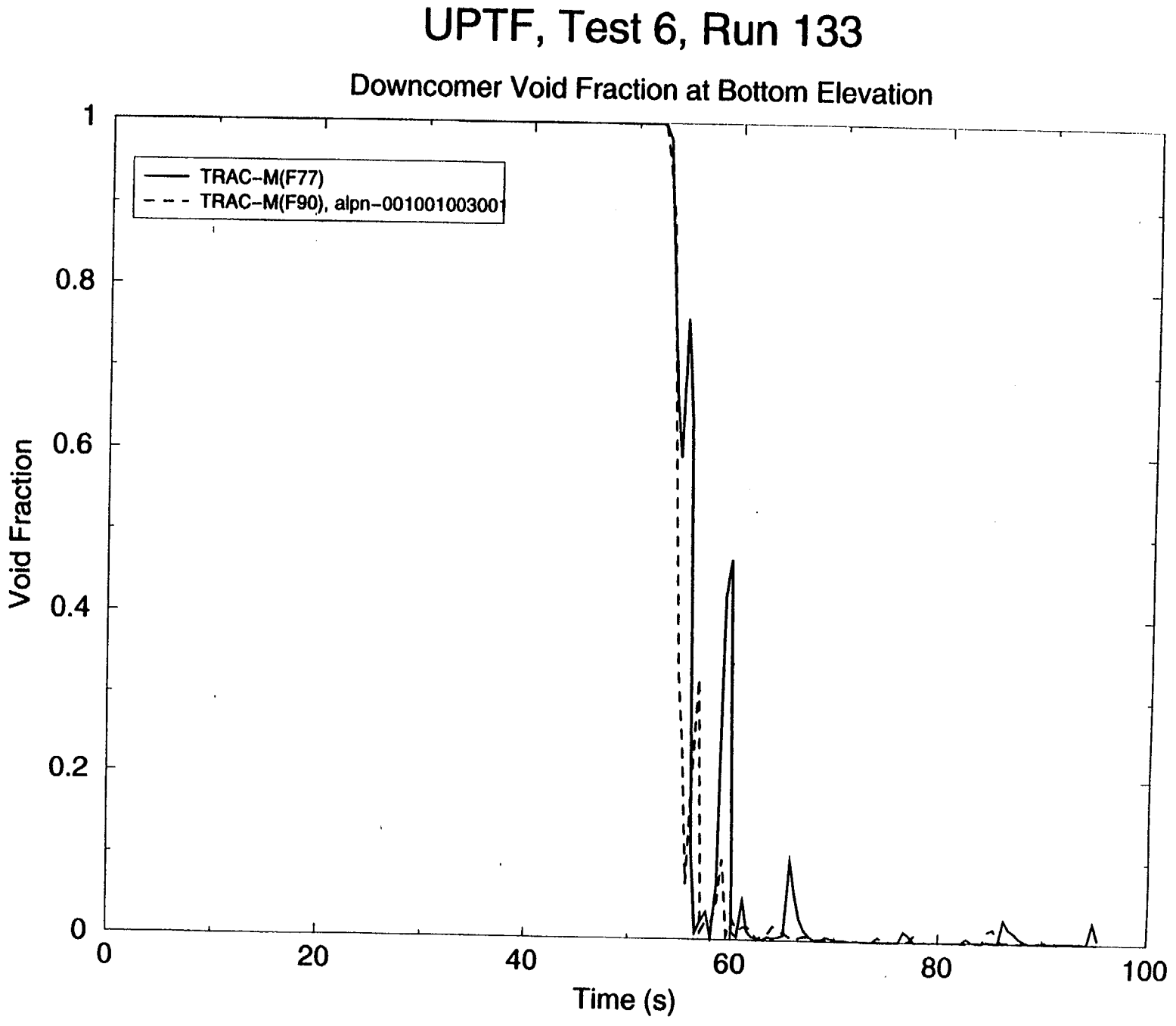

Figure 4.6.18 UPTF, Test 6, Run 133 – Downcomer Void Fraction at Bottom Elevation

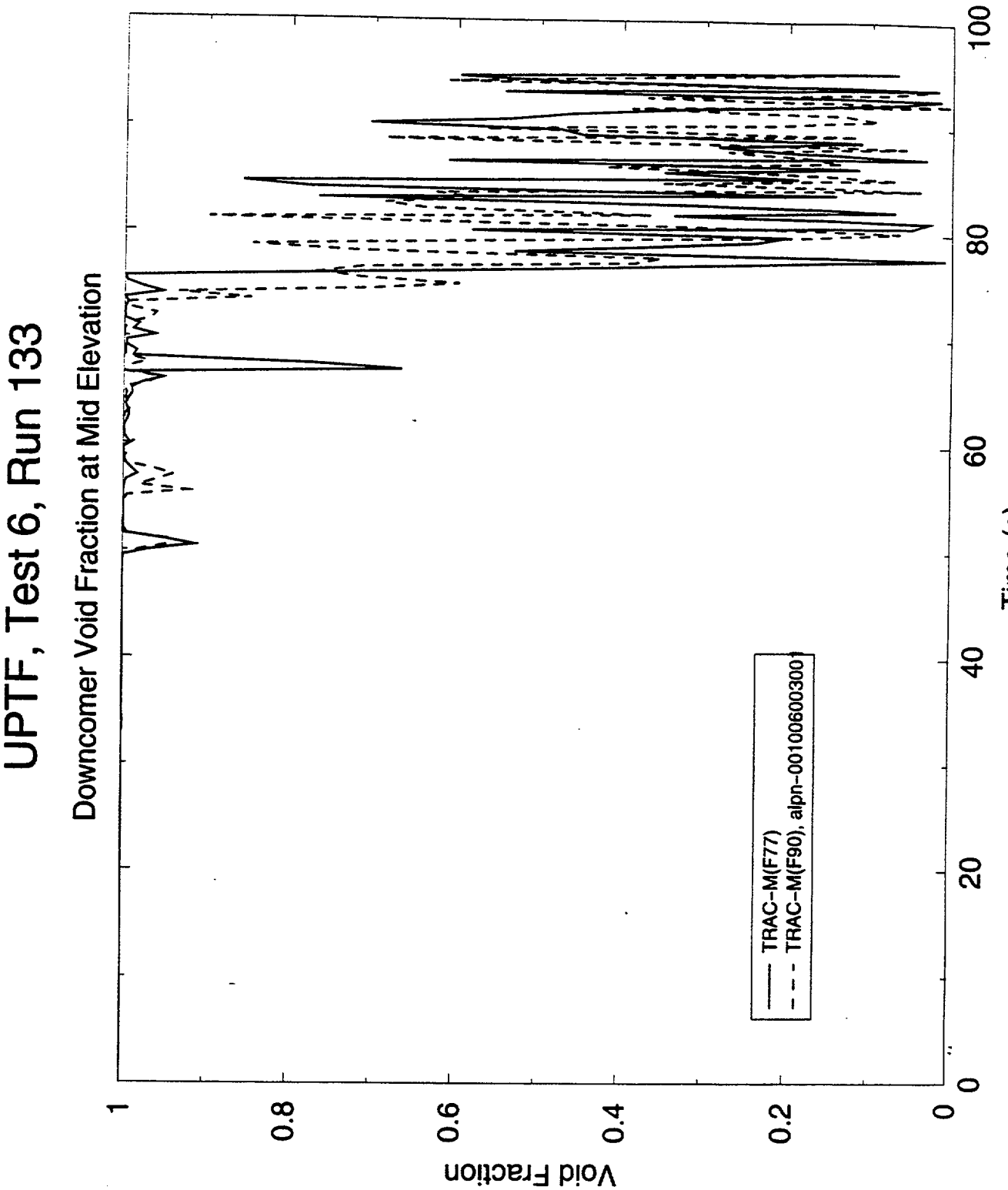

Figure 4.6.19 UPTF, Test 6, Run 133 – Downcomer Void Fraction at Mid-Elevation

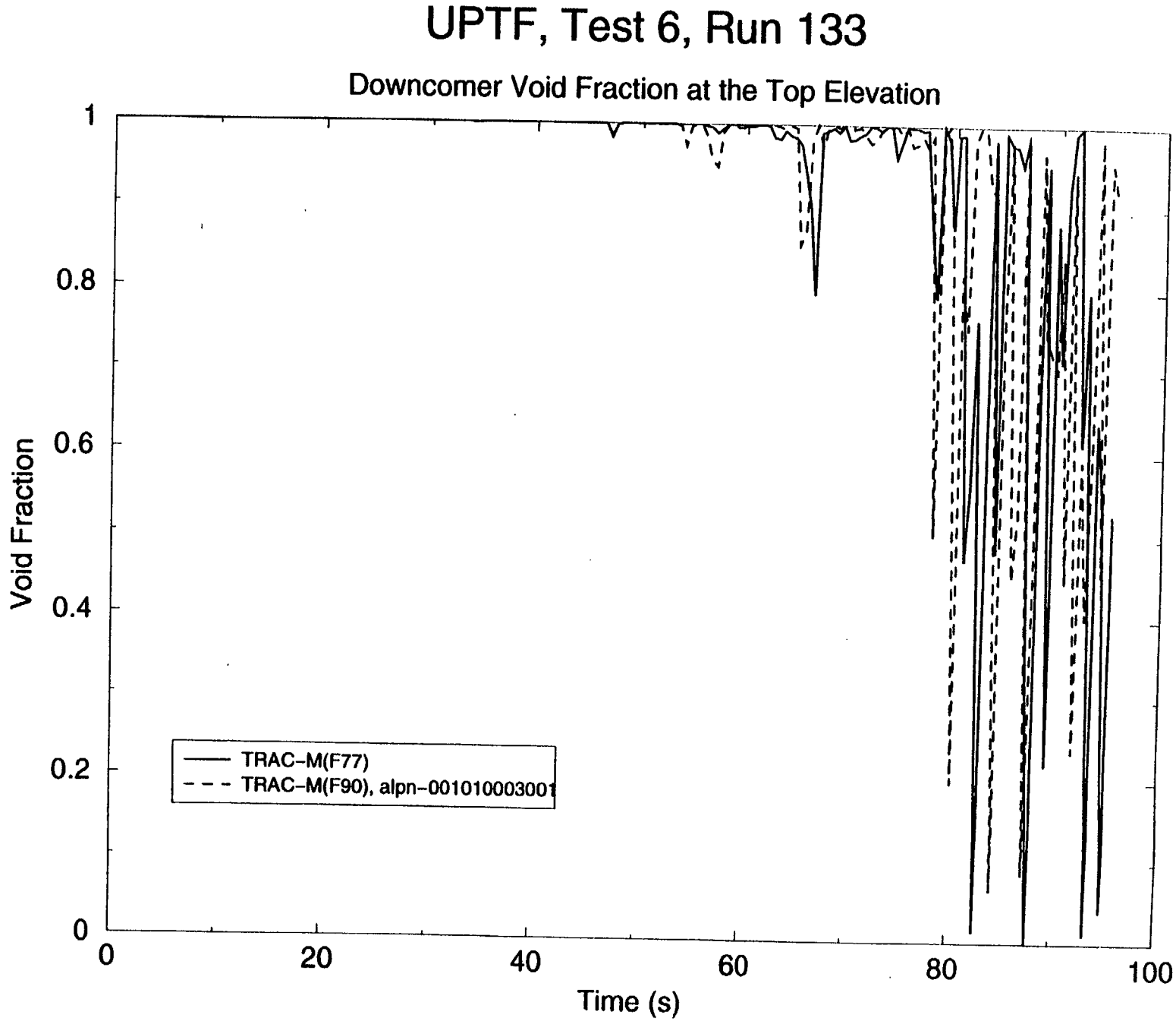

Figure 4.6.20 UPTF, Test 6, Run 133 – Downcomer Void Fraction at the Top Elevation

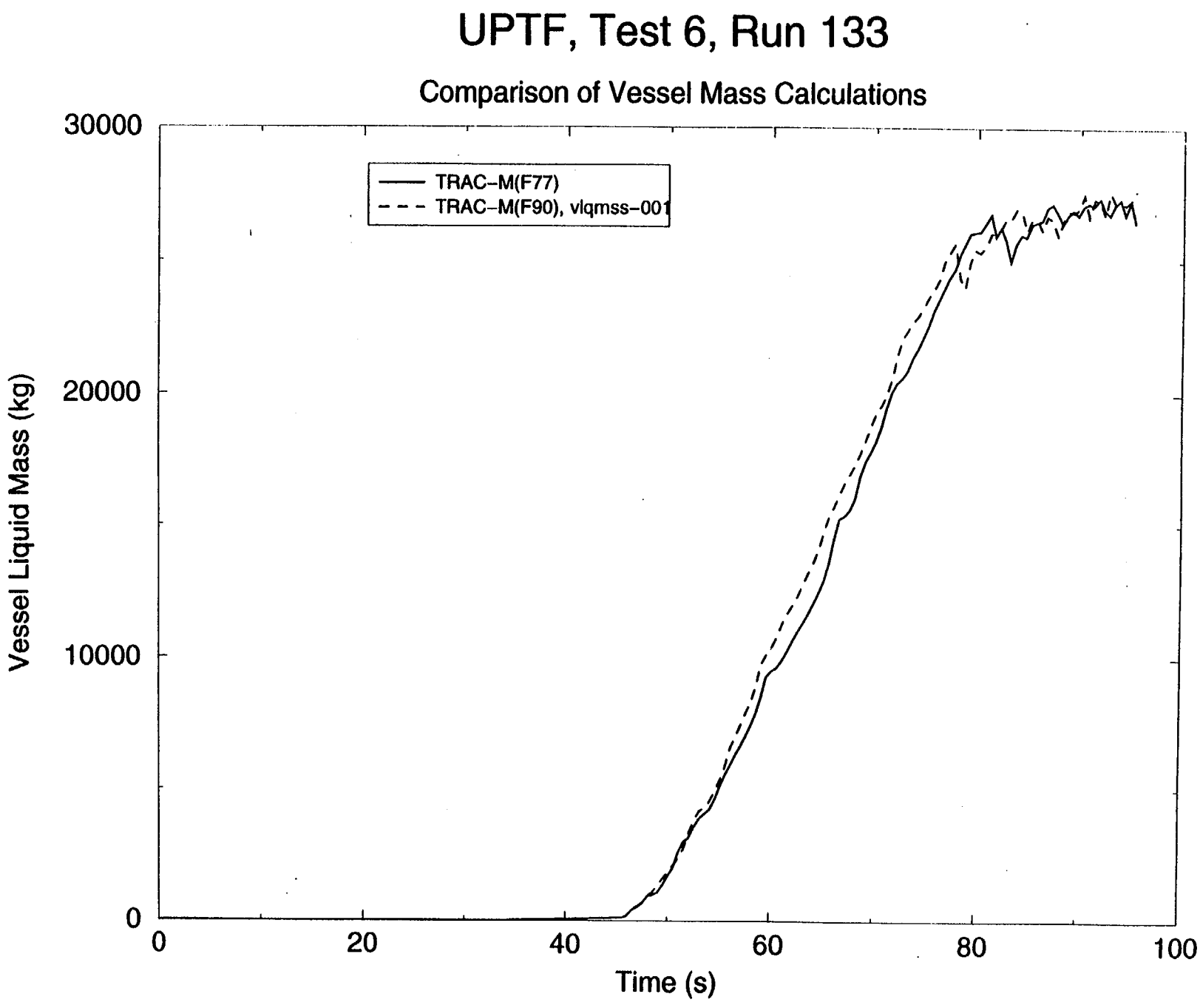

Figure 4.6.21 UPTF, Test 6, Run 133 – Comparison of Vessel Mass Calculations

4.7 Steam Cooling

The phenomenon that occurs during steam cooling is rather simple. During some part of the transient, the reactor core is assumed to be full of steam with no liquid present. The incoming flow from the core inlet is also assumed to be steam. The question is whether the incoming steam flow can cool the fuel assemblies. Hence, the capability required from the codes is proper modeling of heat transfer in a convective single-phase flow. The next level of requirements is that trends and important parameters should be predicted with acceptable accuracy.

4.7.1 FLECHT-SEASET Test 32753

Steam cooling tests were conducted in the FLECHT-SEASET facility in order to simulate steam cooling conditions in a PWR. The test facility is described in Section 4.4.2.1 of this report. Tests were initiated by pressurizing and preheating the rod bundle and associated piping with steam that was slightly superheated. Once the test section was heated above the saturation temperature, the rod power was turned on to a preset value, and was kept constant while the steam flow was initiated.

The quantitative success metric will be based on the experimental spread of the clad temperature data, which will be plotted and examined. Fig. 4.7.1 shows the scatter of thermocouple readings at Z = 1.52 m elevation in Run 32753. The spread of the data is within 70K. (There is one outlier trace that is giving incorrect measurements. This thermocouple trace will not be included in the uncertainty band.) This spread is attributed to the natural circulation occurring within the test section because of heat losses from the walls and effects of unheated tubes where steam probes and instruments are located. (Locations of unheated rods are shown in Fig. 4.4.11.)

If clad temperatures are predicted within 70K, the predictions will be considered "Excellent." However, it should be noted that data above Z = 1.52 m elevation were not used for comparisons. Severe rod bundle distortions occurred above this elevation, and a majority of the heater rod temperatures did not attain their steady-state values according to Ref. 4.7.1. Because of these distortions, many runs were not usable.

4.7.2 TRAC Input Model for FLECHT-SEASET Steam Cooling Run 32753

The TRAC input model schematic used to model steam cooling for FLECHT-SEASET Run 32753 is similar to the one used for Forced Reflood Run 31504 (as described in Section 4.4.2.3 of this report) with the exception that the power applied to the test section remained constant with time, and the heater rod was nodalized finer than in Run 31504 in order to bring the cell interfaces to thermocouple locations for accurate comparisons of code predictions with test data. As in the case of Run 31504, the input deck does not model heat losses from the test section to the environment. Details of the input deck are presented in Ref. 4.7.2.

4.7.3 Comparison of the TRAC-M(F77) and TRAC-M(F90) Calculations with Experimental Data from FLECHT-SEASET Run 32753

Calculations were performed using both TRAC-M(F77) and TRAC-M(F90), and the results were compared with experimental data. Table 4.7.1 lists the initial test conditions for Run 32753,

and Fig. 4.7.2 compares the predictions by TRAC-M(F77) and TRAC-M(F90) and the test data. Comparisons show that agreements between the predictions and the test data at different elevations are well within the uncertainty band of 70K, up to the elevation of 1.52 m. (As stated above, because of severe rod bundle distortions, comparisons are made only up to the elevation of 1.52 m.) At this elevation, the differences between code predictions and the thermocouple trace grow to approximately 70K. The thermocouple trace represents the average of the traces in Fig. 4.7.1. Hence, the agreement is slightly out of the bound of uncertainty, and will be considered "Reasonable." One reason for this slight difference is that the input deck does not model heat losses from the test section, so a slight bias for hotter predictions is expected.

Examining Fig. 4.7.2, one can conclude that the trend of the test data (i.e., the asymptotic approach to the steady-state values at different elevations) is very well predicted. Code-to-code differences in the predictions are approximately null, as expected.

4.7.4 Conclusions

This assessment shows that both TRAC-M(F77) and TRAC-M(F90) predict the single-phase convective flow heat transfer correctly and with acceptable accuracy. The agreement between the predictions and the test data is "Excellent" to "Reasonable," and it is believed that "Excellent" agreement throughout the entire region of valid testing may be obtained by modeling the input deck in greater detail.

The comparison of the predictions shows that the conversion from TRAC-M(F77) to TRAC-M(F90) has been successful for this type of application.

REFERENCES

4.7.1 Wong, S., and L.E. Hochreiter, NUREG/CR-1533, "Analysis of FLECHT-SEASET Unblocked Steam Cooling and Boiloff Tests," NRC: Washington, D.C. January 1981.

4.7.2 Odar, F., NUREG-1744, "Assessment of the TRAC-M Codes Using FLECHT-SEASET Reflood and Steam Cooling Data," NRC: Washington, D.C. May 2001.

Table 4.7.1 Initial Conditions for FLECHT-SEASET Run 32753

Parameter	Test Condition Value
Upper Plenum Pressure	0.28 MPa
Initial Rod Wall Temperature	408 K
Rod Peak Power	0.205 kw/m
Inlet Flow Rate	0.36 kg/sec
Coolant Temperature	405 K
Bundle Radial Profile	Uniform

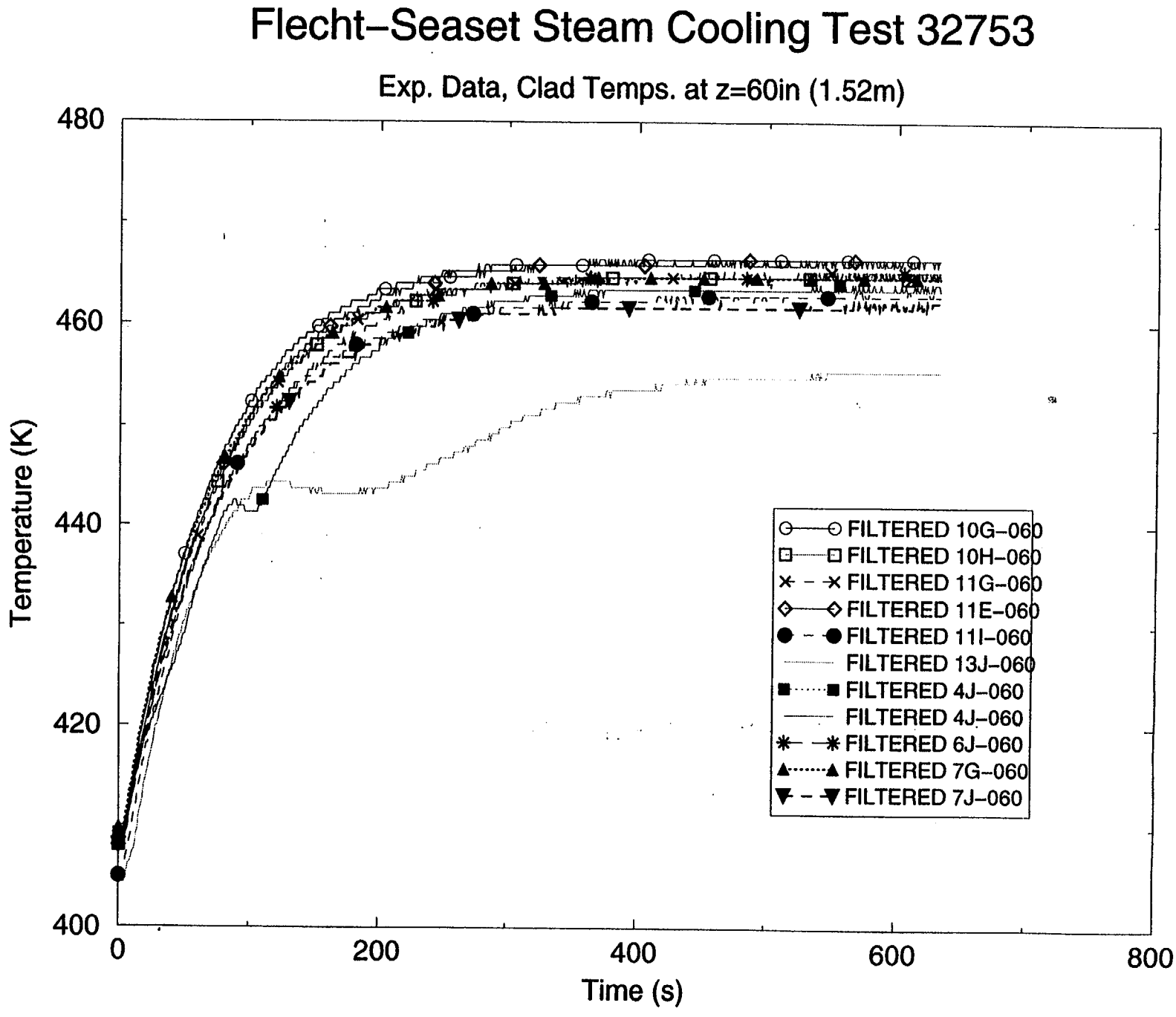

Figure 4.7.1 Experimental Data, Clad Temperatures at Z = 1.52 m

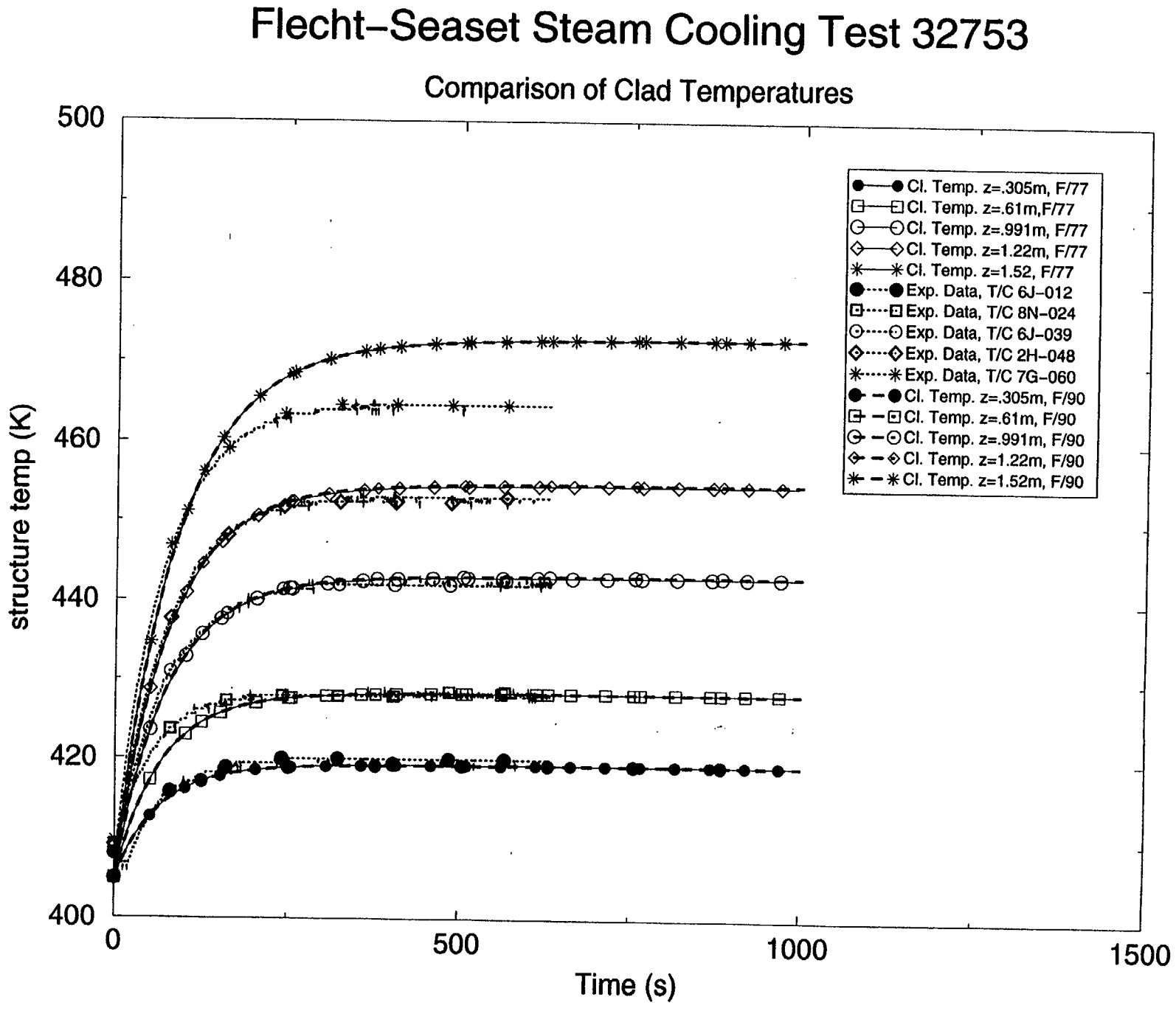

Figure 4.7.2 Comparison of Predicted and Measured Clad Temperatures

4.8 Loss-of-Fluid Test (LOFT), Test L2-6 (Large-Break LOCA)

The Loss-of-Fluid Test (LOFT) facility was designed, constructed, and operated by the Idaho National Engineering Laboratory under the sponsorship of the NRC. The LOFT facility contained a nuclear core, and was designed to simulate the major components and system responses of a commercial PWR during LOCAs and anticipated transients caused by abnormal PWR operations. A number of experimental series were run in the LOFT, including nonnuclear LB experiments; nuclear LB, intermediate-break (IB), and SBLOCA experiments; nuclear anticipated transient experiments; and nuclear anticipated transients with multiple failures. The LOFT test used in this assessment, L2-6, simulated a 200% cold leg break combined with a loss-of-offsite power (LOSP) at the start of the test.

4.8.1 Facility Description

The LOFT facility was a fully operational PWR with instrumentation to measure and provide data on the T/H conditions throughout the system. The facility was configured to represent a 1/60-scale-by-power (1/44 by volume) model of a typical 3000-MW(t) commercial four-loop PWR. An overview and piping schematic of the LOFT facility are shown in Figs. 4.8.1 and 4.8.2, respectively. References 4.8.1 and 4.8.2 provide descriptions of the LOFT facility in general, and the primary system in particular.

The LOFT experimental system consisted of five major systems, including the reactor, primary coolant, blowdown suppression, emergency core cooling, and secondary coolant. These systems were heavily instrumented to provide continuous monitoring of the nuclear, thermal, hydraulic, and structural processes occurring during the LOFT experiments.

The reactor system consisted of the reactor vessel and head, core support barrel, upper and lower core support structures, flow skirt, reactor vessel fillers, and nuclear core. The 1.68-m LOFT core was rated at 50 MW(t), and was designed to have the same physical properties as a PWR core. The core contained two basic fuel assembly configurations, square and triangular. The square fuel assemblies contained 225 fuel rod locations, 21 of which were occupied by guide tubes. The triangular assemblies contained 78 fuel rod locations, 8 of which were occupied by guide tubes.

The primary coolant system consisted of two coolant loops connected to the reactor system. Three PWR primary coolant loops were simulated by the single, intact loop in the LOFT experimental system. This single LOFT loop was scaled to have the same volume-to-power ratio as the three PWR loops. The broken loop in the LOFT experimental system simulated the fourth PWR primary coolant loop where the break was postulated to occur. The intact loop contained a steam generator, primary coolant pumps, pressurizer, primary coolant venturi (flow measuring device), and intact loop piping. The intact loop active steam generator, shown in Fig. 4.8.3, had a secondary side that consists of a U-tube boiler section, a steam dome, and a downcomer. The steam generator secondary side was connected to a main steam flow control valve (MSFCV), condenser, feedwater pump, auxiliary feedwater pump, and a feedwater flow control valve.

The blowdown suppression system simulated the containment backpressure response of a commercial PWR during LOCAs, and provided containment for the blowdown effluent. The major system components were the blowdown suppression header and downcomers, blowdown suppression tank, and blowdown suppression tank spray system.

The facility's ECCS simulated a commercial plant ECCS. This system included two ECCS trains, each of which contained a high-pressure injection system (HPIS), an accumulator (ACC) system, and a low-pressure injection system (LPIS).

The LOFT facility was highly instrumented. A partial list of the measured parameters includes coolant temperature; coolant level; coolant velocity, momentum, and flow direction; coolant density; coolant pressure; coolant flows; differential pressure; pump speed; and metal temperatures. The available instrumentation is summarized in Ref. 4.8.2.

4.8.2 Test Procedure

Test L2-6 simulated a 200% cold leg break combined with a LOSP at the start of the transient. The reactor was brought to a power level of 46 MW, and was maintained at that level until the blowdown was initiated. The conditions in the intact loop were established to provide a 247.8-kg/s flow with temperature and pressure in the hot leg at 589 K and 15.09 MPa, respectively, at the time of blowdown initiation.

ECC injection was directed to the intact loop cold leg at a system pressure of 4.11 MPa at 17.5 s. In order to simulate the LOSP, the primary coolant pumps were tripped at 0.8 s, after which they coasted down under the influence of the flywheels. When the pump speed dropped below 73.54 rad/s, the flywheel uncoupled from the pump, thereby effectively reducing the pump's moment of inertia. The assumption of LOSP at the initiation of the transient resulted in a delay in the availability of the HPIS and LPIS. The HPIS injection was initiated at 21.8 s, and the LPIS injection was initiated at 34.8 s. The experiment operating specifications (Ref. 4.8.3) and quick-look report (Ref. 4.8.4) document the initial test conditions and its operation.

The behavior of Test L2-6 was similar to that of earlier Tests L2-2 (Ref. 4.8.5) and L2-3 (Ref. 4.8.6), in which the pumps ran at approximately constant speed throughout the test. The most significant differences occurred in the core during the first ~11 s. Because of the higher power level in Test L2-6, the peak clad temperatures (PCTs) were higher (e.g., 1074 K vs ~900 K in Test L2-3). Test L2-6 exhibited the same early core rewet that was observed in Tests L2-2 and L2-3. However, in Test L2-6, rapid quenches were observed from cladding temperatures as high as 1074 K. In addition, the early rewet progressed only to a core elevation of 1.113 to 1.245 m before a second temperature increase began, whereas Tests L2-2 and L2-3 exhibited complete quenching of the entire core during the early rewet.

4.8.3 TRAC Model

Noding diagrams of the TRAC representation of the LOFT facility are shown in Figs. 4.8.4, through 4.8.7. As shown in Fig. 4.8.4, the VESSEL component is used to model the reactor vessel and internals. The component is divided into 12 axial levels, 4 radial rings, and 4 azimuthal sectors. The lower plenum is modeled with two axial levels, while the upper plenum resides in the first three radial sectors of Level 12. The core resides in the first 3 radial sectors of Levels 4 through 8, and the downcomer resides in radial sector 4 of Levels 3 through 11. The intact and broken hot leg and cold leg connections to the VESSEL component are at axial Level 11. The VESSEL connections to the intact and broken loops are shown in the horizontal cross-sectional view in Fig. 4.8.4.

The ECCS for LOFT L2-6 was modeled by a PIPE capped by a BREAK to model the accumulator, a VALVE to model the accumulator check valve, one pipe each for the HPIS and LPIS lines with the flow conditions specified by FILLs, and a plenum to receive the ACC, LPIS, and HPIS flows.

To ensure consistency with the earlier calculations, the input model specifies that the reflood model is tripped on at 20 s.

4.8.4 Comparison of Calculated and Measured Results

The calculations of LOFT Test L2-6 were performed using TRAC-M(F77) Version 5.5 (Ref. 1.2), and the results were compared with the calculations generated by TRAC-M(F90). Both cases used the newrfd=1 option. Ref. 1.2 demonstrated that the grid spacer model should not be used because it results in excessive and nonphysical heat transfer processes in the upper portions of the core. Therefore, the grid spacer model was not included in the deck for LOFT Test L2-6.

Table 4.8.1 presents the calculated steady-state conditions from which the transient calculation was initiated, as well as the initial test data. The constrained steady-state input feature in TRAC was used to drive the solution to the specified loop flow rate, secondary side pressure, and cold leg temperature. The calculated and observed sequence of events during the transient are presented in Table 4.8.2.

A comparison of the pressurizer pressures calculated by both codes and the test data is shown in Fig. 4.8.8. The agreement between the predictions generated by both codes and test data is "Excellent" to "Reasonable" up to 10 s, after which both TRAC calculations indicate a faster depressurization than do the test data. Both TRAC calculations are in "Excellent" agreement with each other; however, the agreement with the test data is minimal from 10 to 25 ~ 30 s into the transient. After 30 s, the agreement with the test data is "Reasonable," as is the agreement between the two TRAC pressure calculations.

Figs. 4.8.9 and 4.8.10 present comparisons of the calculated and measured broken loop mass flow rates at hot and cold leg locations, respectively. Agreements between the test data and code predictions are "Excellent" to "Reasonable" for the entire transient. During the subcooled blowdown, both codes predict the spike and surge of two-phase fluid during the two-phase blowdown. During the reflood (i.e., after ~10s), TRAC-M(F77) calculates slugs of flow through the break similar to the experimental data. However, the data indicate flow variations of higher magnitudes and frequencies. The integrals of break flow rates for this period of time seem to show that TRAC-M(F77) predicts higher inventory loss than the data would indicate.

The agreements between the two code predictions in Figs. 4.8.9 and 4.8.10 until ~25 s are "Excellent." They deviate from each other after 25 s (as shown in Fig. 4.8.10) during the reflood period; however, given certain differences between the choked flow models of the two codes, the agreement between the two TRAC calculations after 25 s seems reasonable.

Figs. 4.8.11 and 4.8.12 present comparisons of the calculated and measured intact loop mass flow rates at hot and cold leg locations, respectively. Calculations from both codes are in "Excellent" to "Reasonable" agreement with the test data. In Fig. 4.8.11, the data show large spikes in mass flow in the intact cold leg because of ACC injection. Although both codes predict

some spikes, their magnitude is not as large as indicated by the test data. Overall, agreement between the code calculations and the test data is judged to be "Excellent" to "Reasonable," as is the agreement between the code predictions.

Figure 4.8.13 shows a comparison of calculated and measured rod clad temperatures at 0.6943 m elevation from the bottom of the fuel. The input deck was constructed to reference the calculations of fuel properties to the bottom of the vessel. The difference in the elevations between the bottom of the fuel and the bottom of the vessel is 1.248 m (as shown in Fig. 4.8.4). In order to plot the temperature variation with time at 0.6943 m elevation, the increment of 1.248 m was added in the XMGR plotting software.

Figure 4.8.13 shows that both codes predict clad temperatures higher than the experimental data indicate. The first peak is predicted higher, and the quench from the first peak is not predicted. The reflood was activated by the user at 20 s. The final quench predictions reasonably agree with the data. As discussed in Section 4.4.2, the physics of reflood including grid spacer effects is not adequately modeled in the codes, so it is expected that predictions by both codes would be inadequate. Hence, there are some differences between the code predictions and the test data.

The agreement between the two code predictions is "Excellent" to "Reasonable," although there are some differences between the code predictions from 20 s to 50 s. This is the time when reflood takes place, and there were some differences in break flow rate predictions during this period (as shown in Fig. 4.8.10). TRAC-M(F77) predicts a higher break flow rate with slugs of liquid coming out. This could be the reason for higher clad temperatures by TRAC-M(F77).

4.8.5 Conclusions

The prediction of reflood by both codes is not accurate. However, both codes predicted flow rates in both broken and intact loops reasonably well, and the results show "Excellent" to "Reasonable" agreement between the two sets of predictions.

REFERENCES

4.8.1 Reeder, D.L., "LOFT System and Test Description (5.5-ft Nuclear Core 1 LOCES)," Idaho National Engineering Laboratory Report TREE-1208, NUREG/CR-0247, July 1978.

4.8.2 Nalezny, C.L., NUREG/CR-3214, "Summary of Nuclear Regulatory Commission's LOFT Program Experiments," NRC: Washington, D.C. July 1983.

4.8.3 Feldman, E.M., "OECD LOFT Project Experiment Specification Document, Cold Leg Large-Break Experiment LP-02-6," Idaho National Engineering Laboratory Report OECD LOFT-T-3402, July 1983.

4.8.4 Adams, J.P., K.G. Condie, and D.L. Batt, "Quick-Look Report on OECD LOFT Experiment LP-02-6," Idaho National Engineering Laboratory Report OECD LOFT-T-3404, October 1983.

4.8.5 McCormick-Barger, M., "Experimental Data Report for LOFT Power Ascension Experiment L2-2," Idaho National Engineering Laboratory Report TREE-1322, NUREG/CR-0492, February 1979.

4.8.6 Prassinos, P.G., B.M. Galusha, and D.B. Engelman, "Experimental Data Report for LOFT Power Ascension Experiment L2-3," Idaho National Engineering Laboratory Report TREE-1326, NUREG/CR-0792, July 1979.

Table 4.8.1 LOFT Test L2-6 Initial Conditions and Initial Test Data

Parameter	Measured	Uncertainty	TRAC-M (F77)	TRAC-M (F90)
Reactor power (MW)	46.000	±1.20	47.00	47.00
Intact loop mass flow (kg/s)	248.700	±2.60	248.00	248.00
Hot leg pressure (MPa)	15.090	±0.08	15.03	15.03
Hot leg temperature (K)	589.000	±1.10	591.00	591.60
Cold leg temperature (K)	555.900	±1.10	556.70	557.20
Steam generator pressure (MPa)	5.620	±0.10	5.62	5.62

Table 4.8.2 LOFT Test L2-6 Sequence of Events

	Time (s)		
Event	**Test**	**TRAC-M(F77)**	**TRAC-M(F90)**
Break initiated	0.0	0.0*	0.0*
Reactor scrammed	0.1	0.1*	0.1*
Primary coolant pumps tripped	0.8	0.8*	0.8*
Accumulator A injection initiated	17.5	15.0	13.8
HPIS injection initiated	21.8	21.8*	21.8*
LPIS injection initiated	34.8	34.8*	34.8*

*User-input values

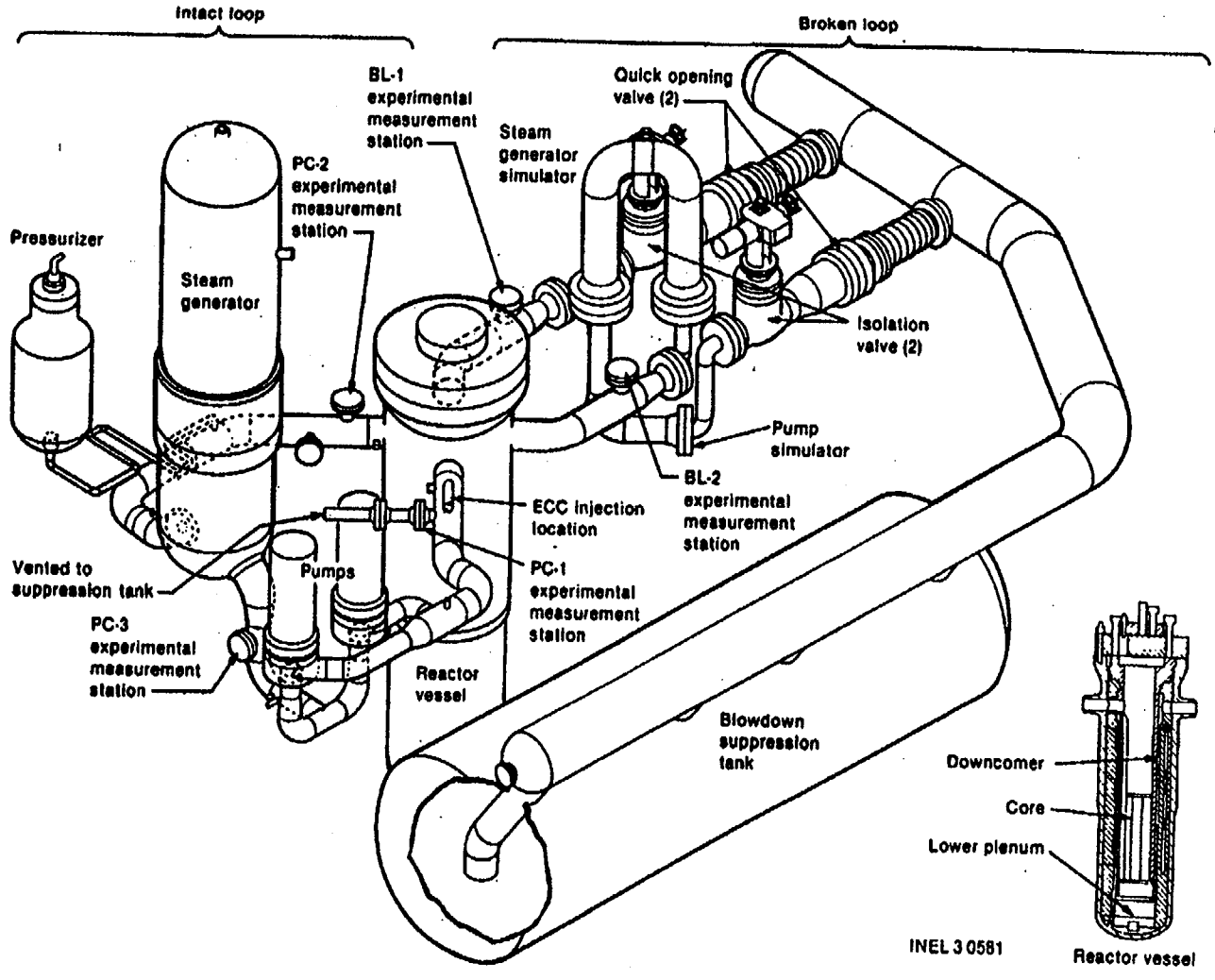

Figure 4.8.1 Overview of the LOFT Facility

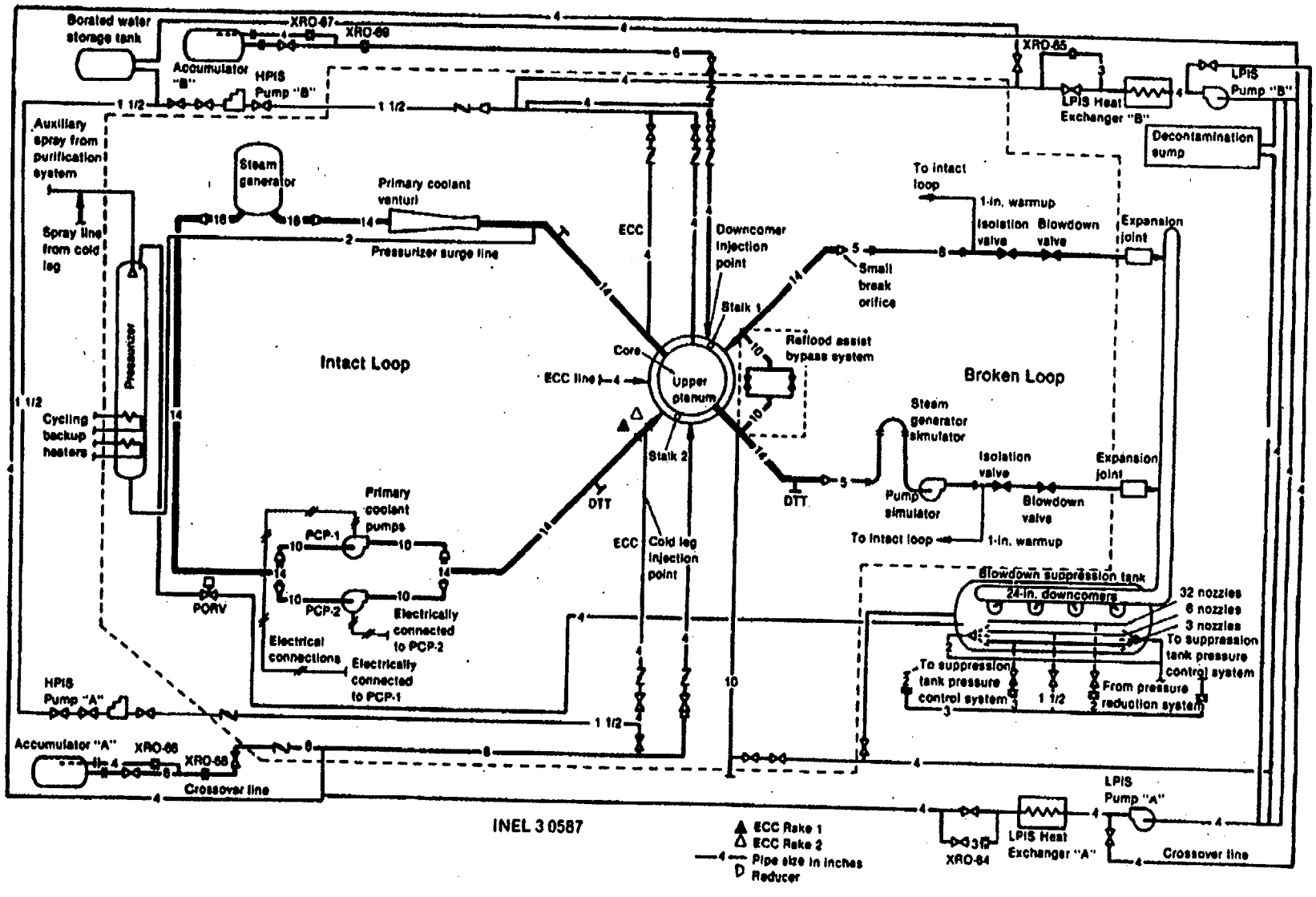

Figure 4.8.2 Piping Schematic of the LOFT Facility

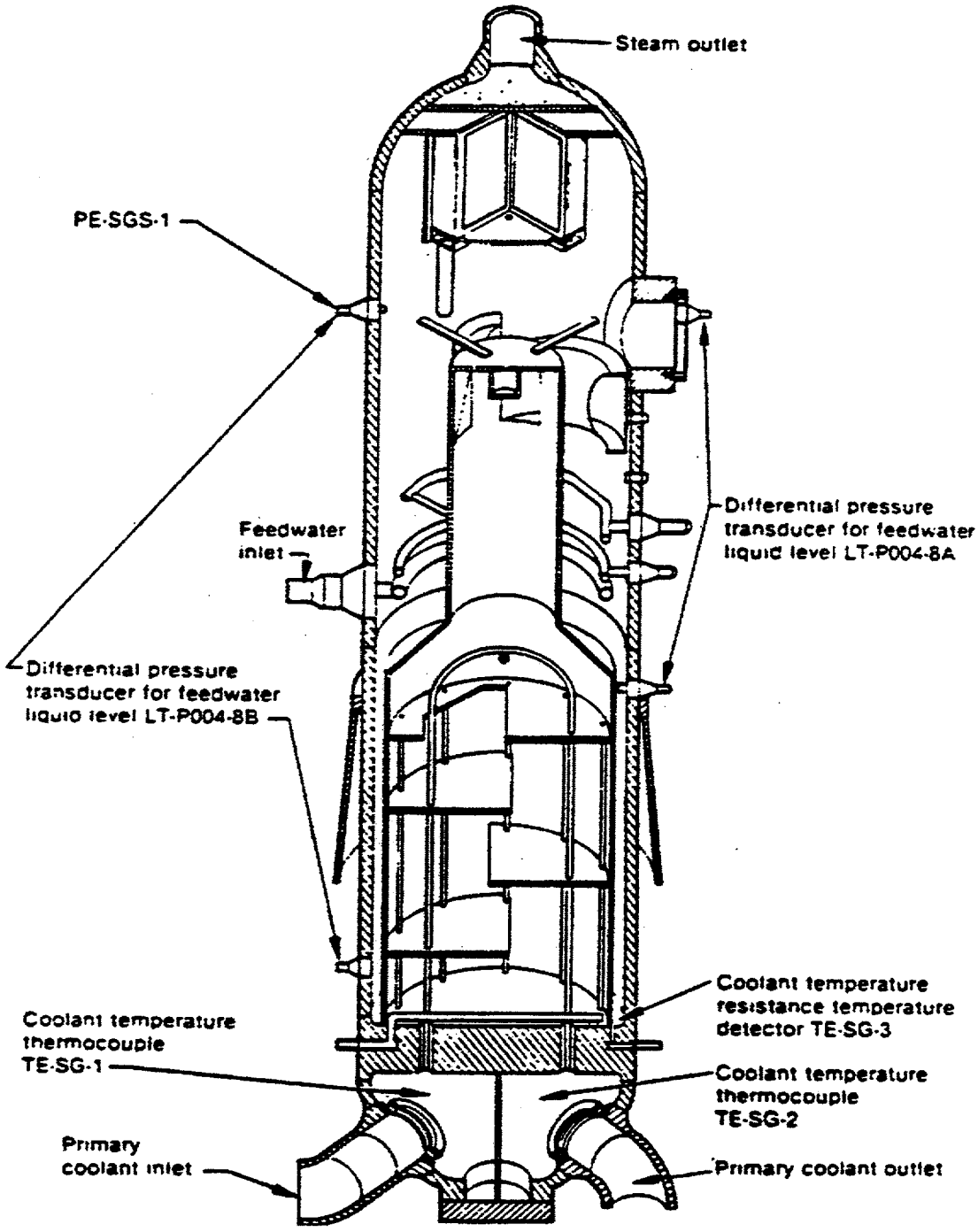

Figure 4.8.3 Intact-Loop Steam Generator in the LOFT Facility

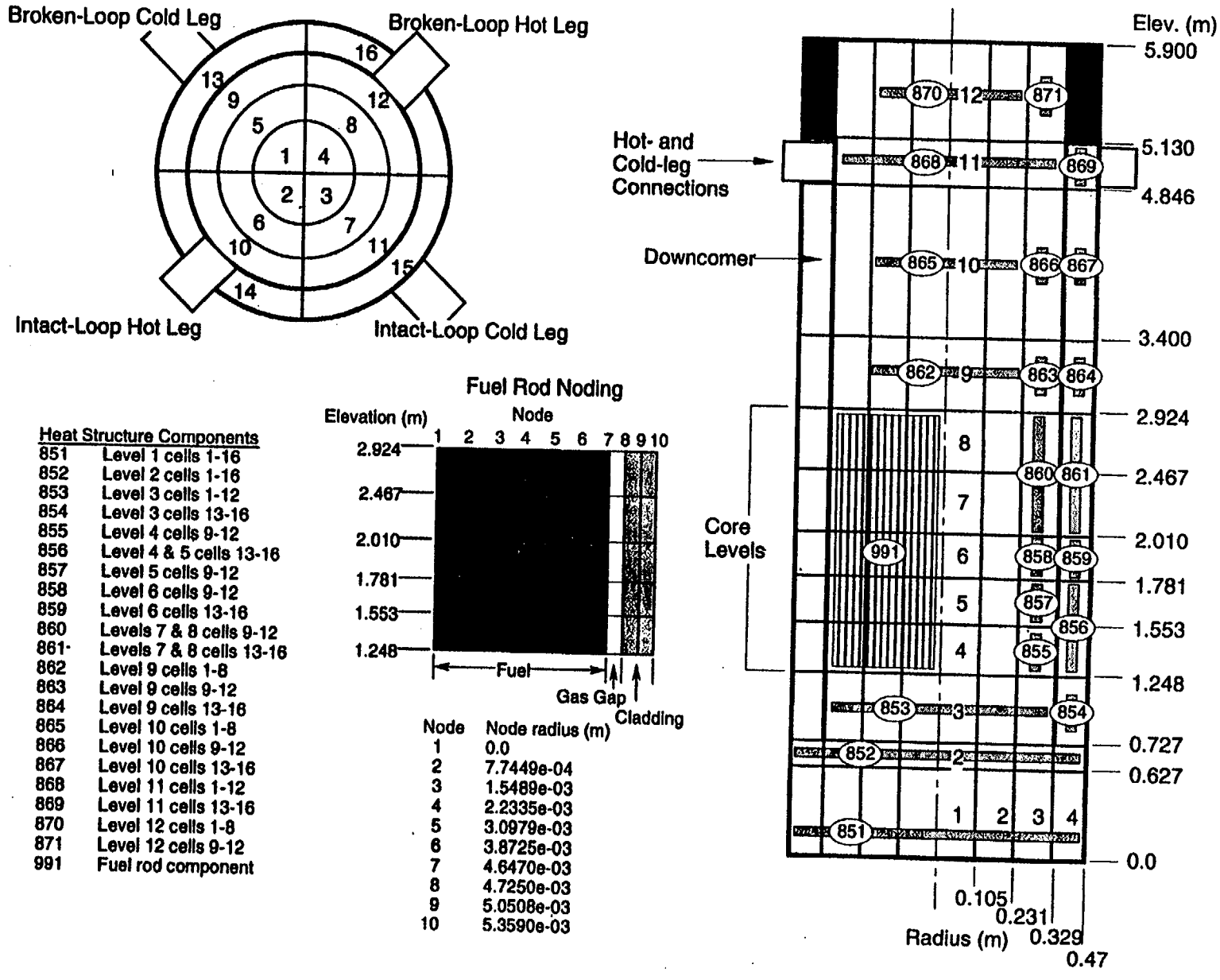

Heat Structure Components	
851	Level 1 cells 1-16
852	Level 2 cells 1-16
853	Level 3 cells 1-12
854	Level 3 cells 13-16
855	Level 4 cells 9-12
856	Level 4 & 5 cells 13-16
857	Level 5 cells 9-12
858	Level 6 cells 9-12
859	Level 6 cells 13-16
860	Levels 7 & 8 cells 9-12
861	Levels 7 & 8 cells 13-16
862	Level 9 cells 1-8
863	Level 9 cells 9-12
864	Level 9 cells 13-16
865	Level 10 cells 1-8
866	Level 10 cells 9-12
867	Level 10 cells 13-16
868	Level 11 cells 1-12
869	Level 11 cells 13-16
870	Level 12 cells 1-8
871	Level 12 cells 9-12
991	Fuel rod component

Node	Node radius (m)
1	0.0
2	7.7449e-04
3	1.5489e-03
4	2.2335e-03
5	3.0979e-03
6	3.8725e-03
7	4.6470e-03
8	4.7250e-03
9	5.0508e-03
10	5.3590e-03

Figure 4.8.4 LOFT L2-6 Reactor Vessel Noding Diagram

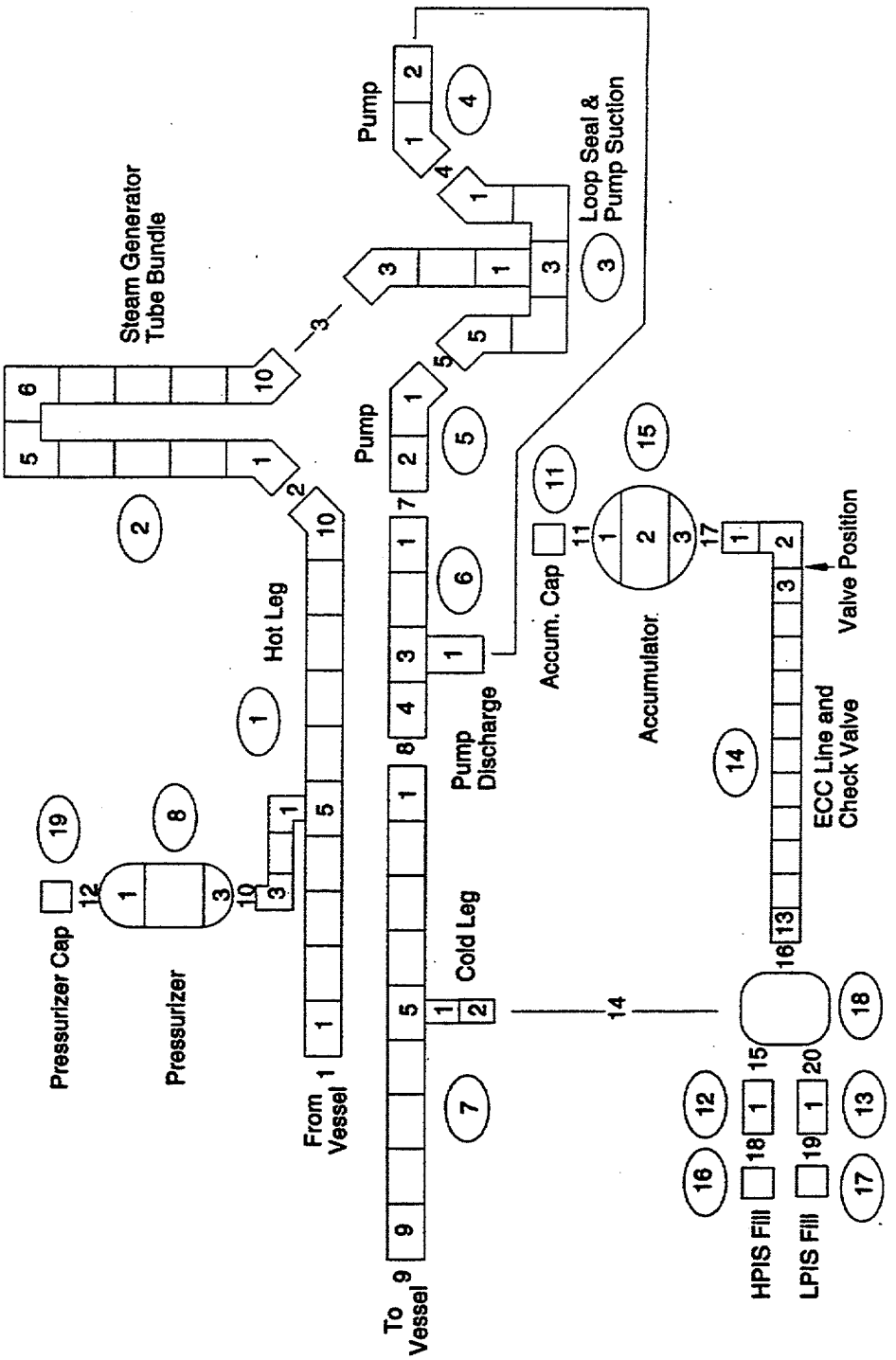

Figure 4.8.5 LOFT L2-6 Intact-Loop Noding Diagram

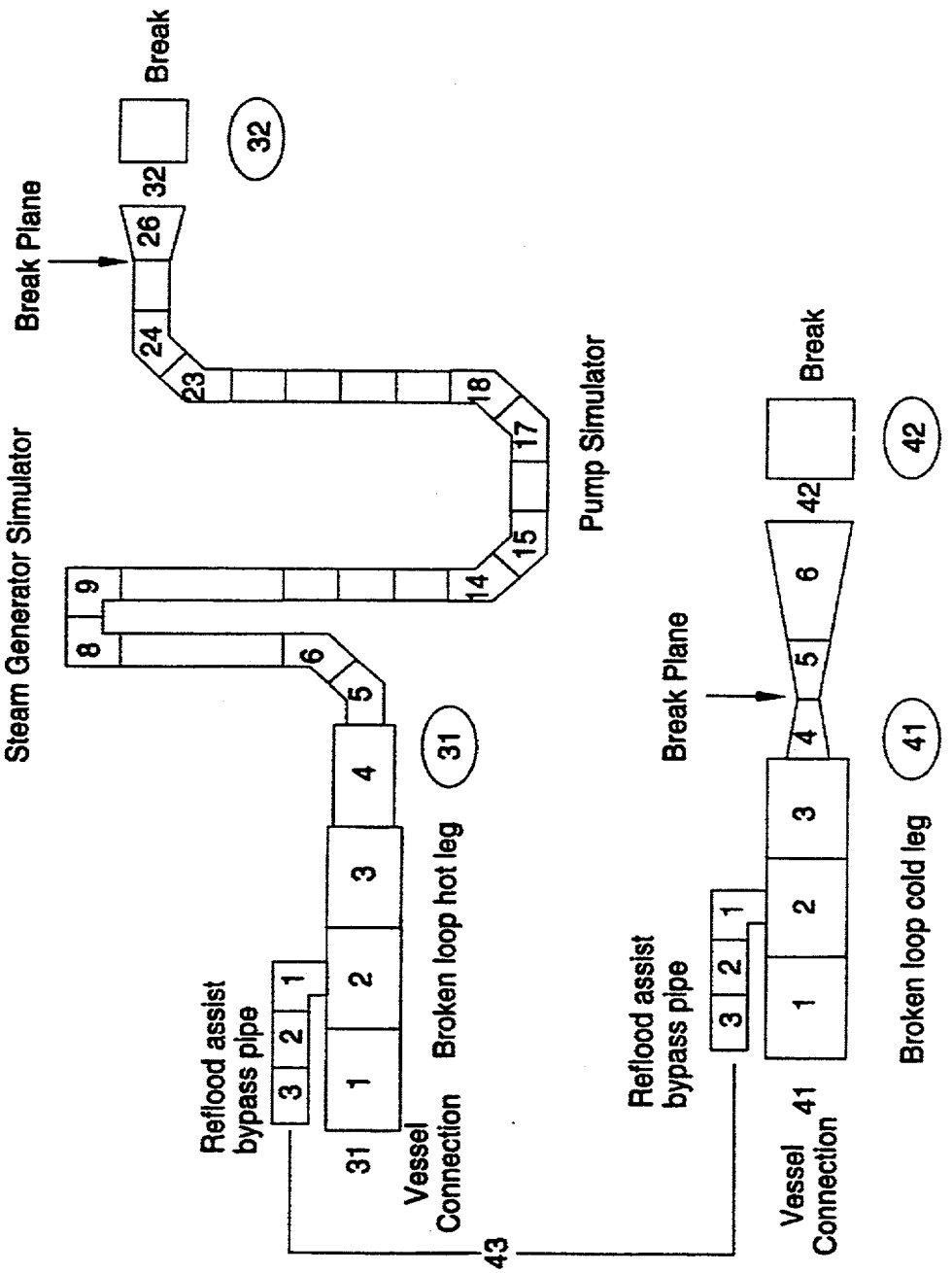

Figure 4.8.6 LOFT L2-6 Broken-Loop Noding Diagram

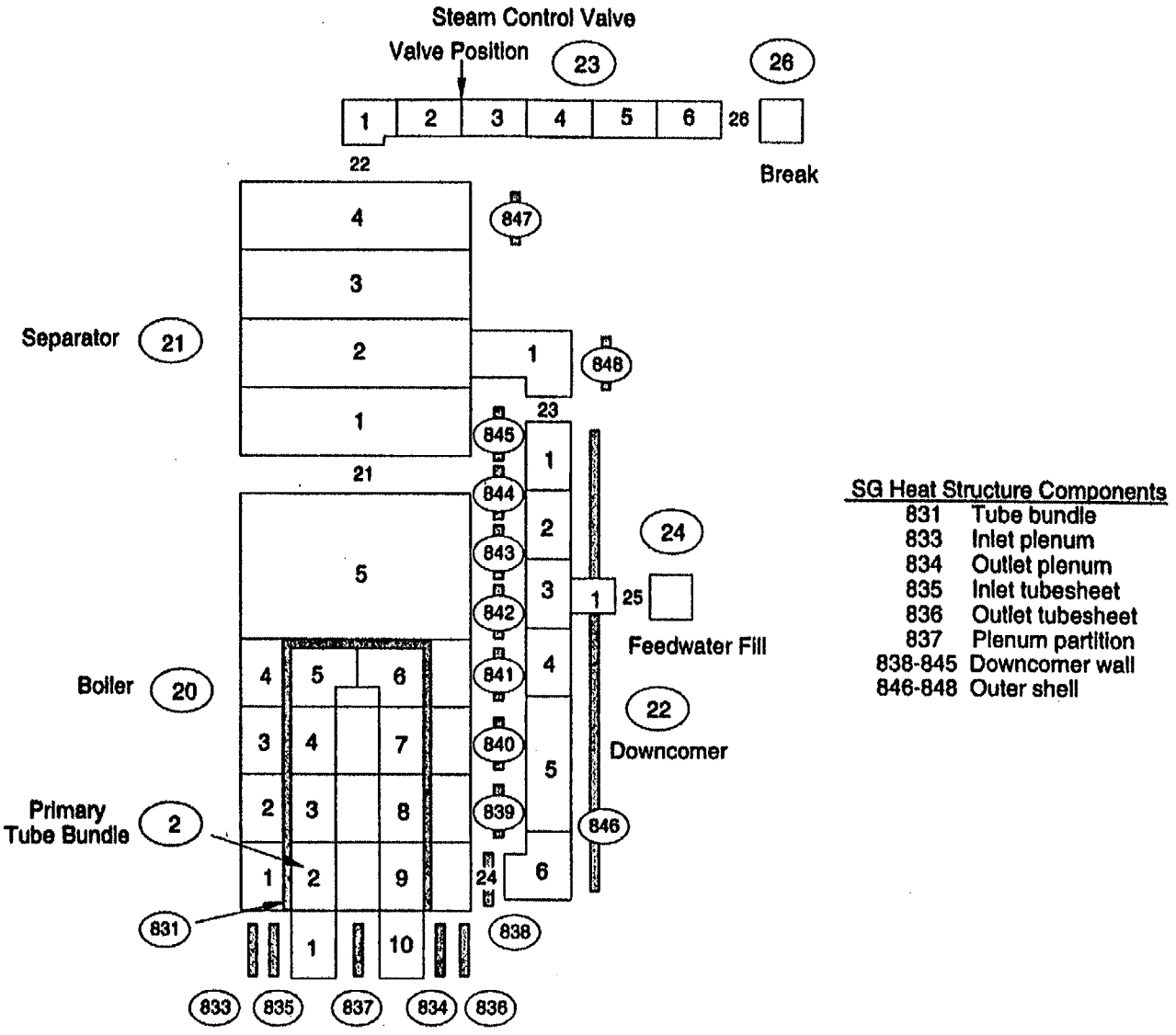

Figure 4.8.7 LOFT L2-6 Steam-Generator Noding Diagram

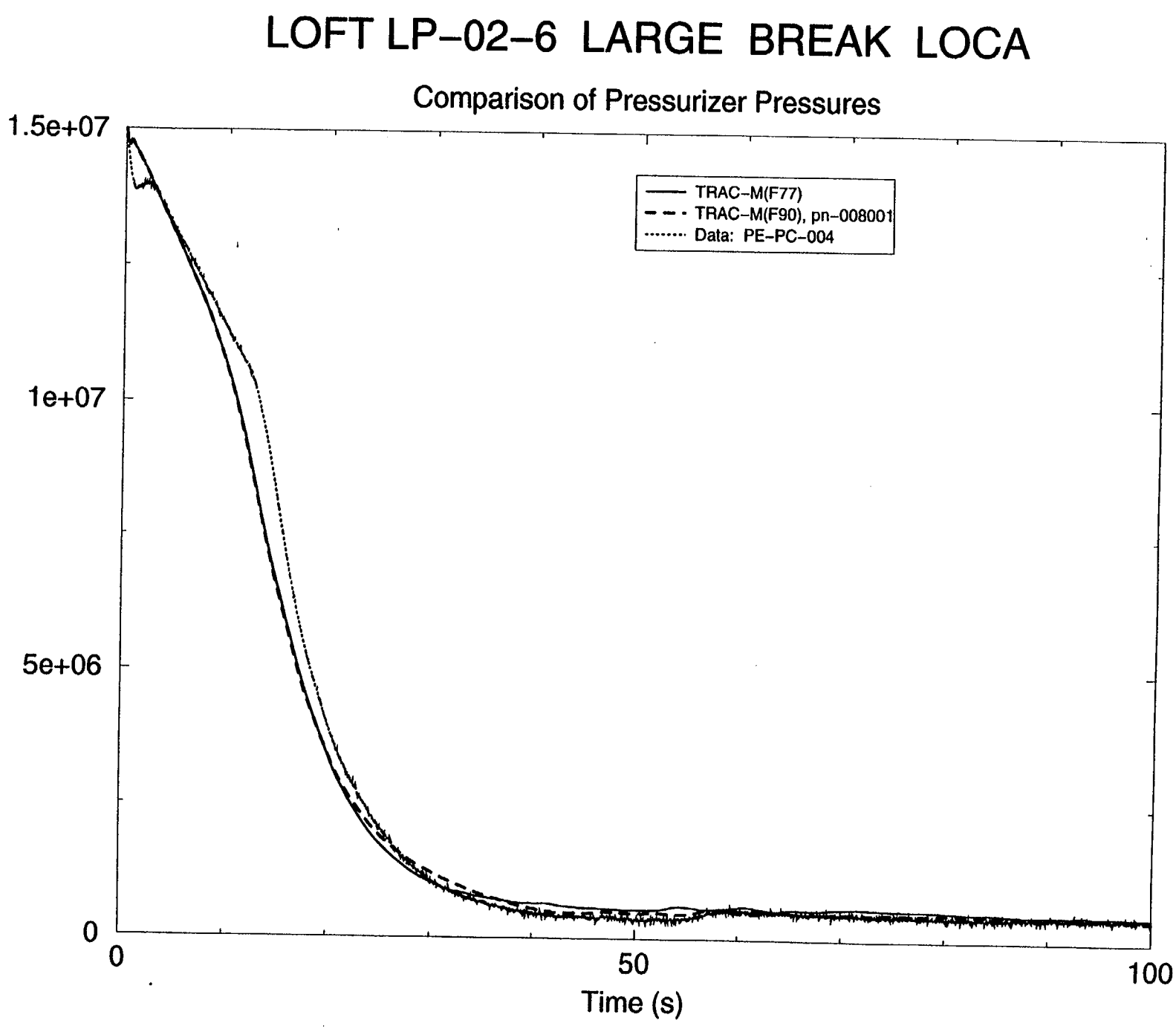

Figure 4.8.8 Comparison of Calculated and Measured Pressurizer Pressures

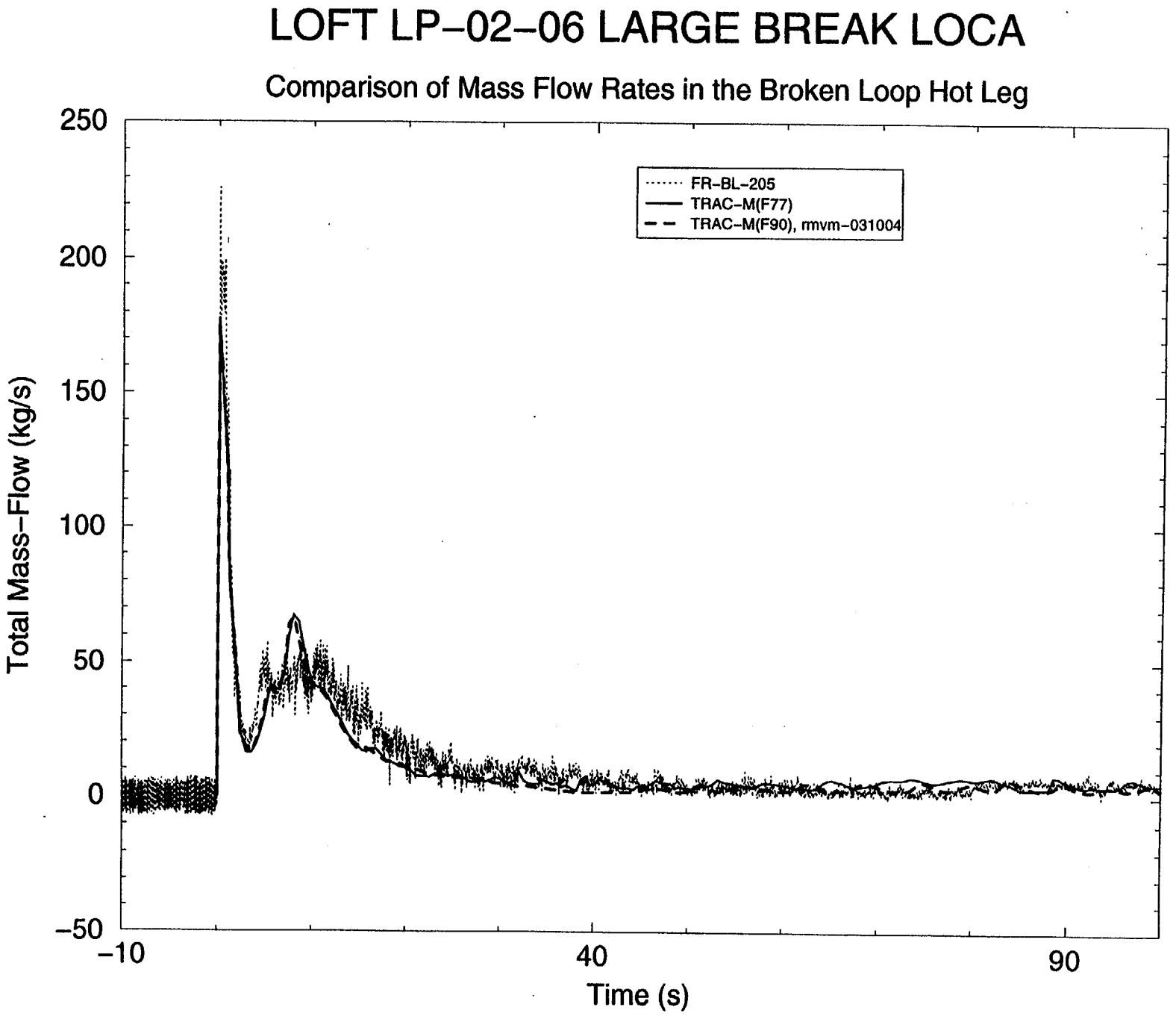

Figure 4.8.9 Comparison of Calculated and Measured Broken-Loop Hot Leg Mass Flow Rates

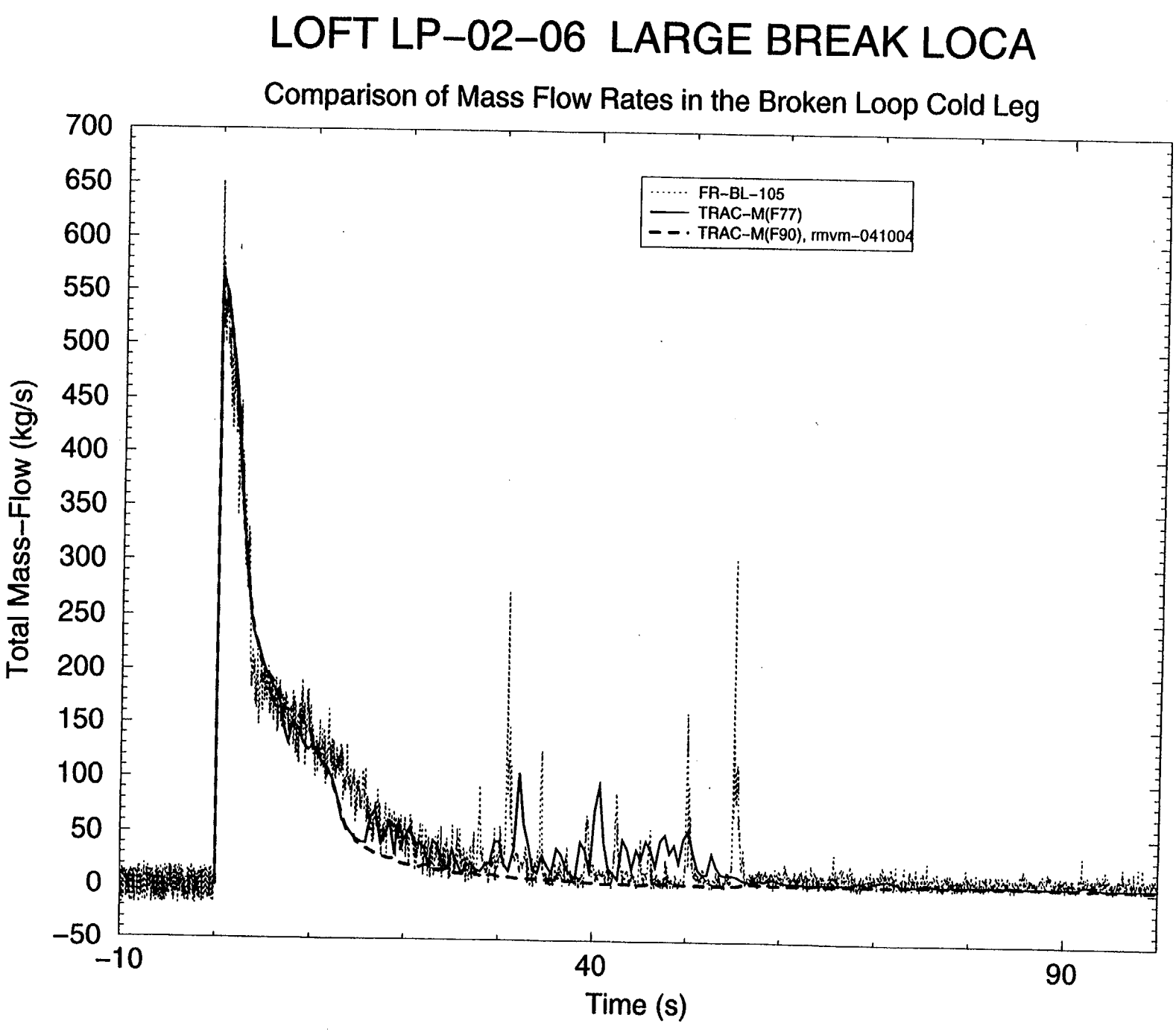

Figure 4.8.10 Comparison of Calculated and Measured Broken-Loop Cold Leg Mass Flow Rates

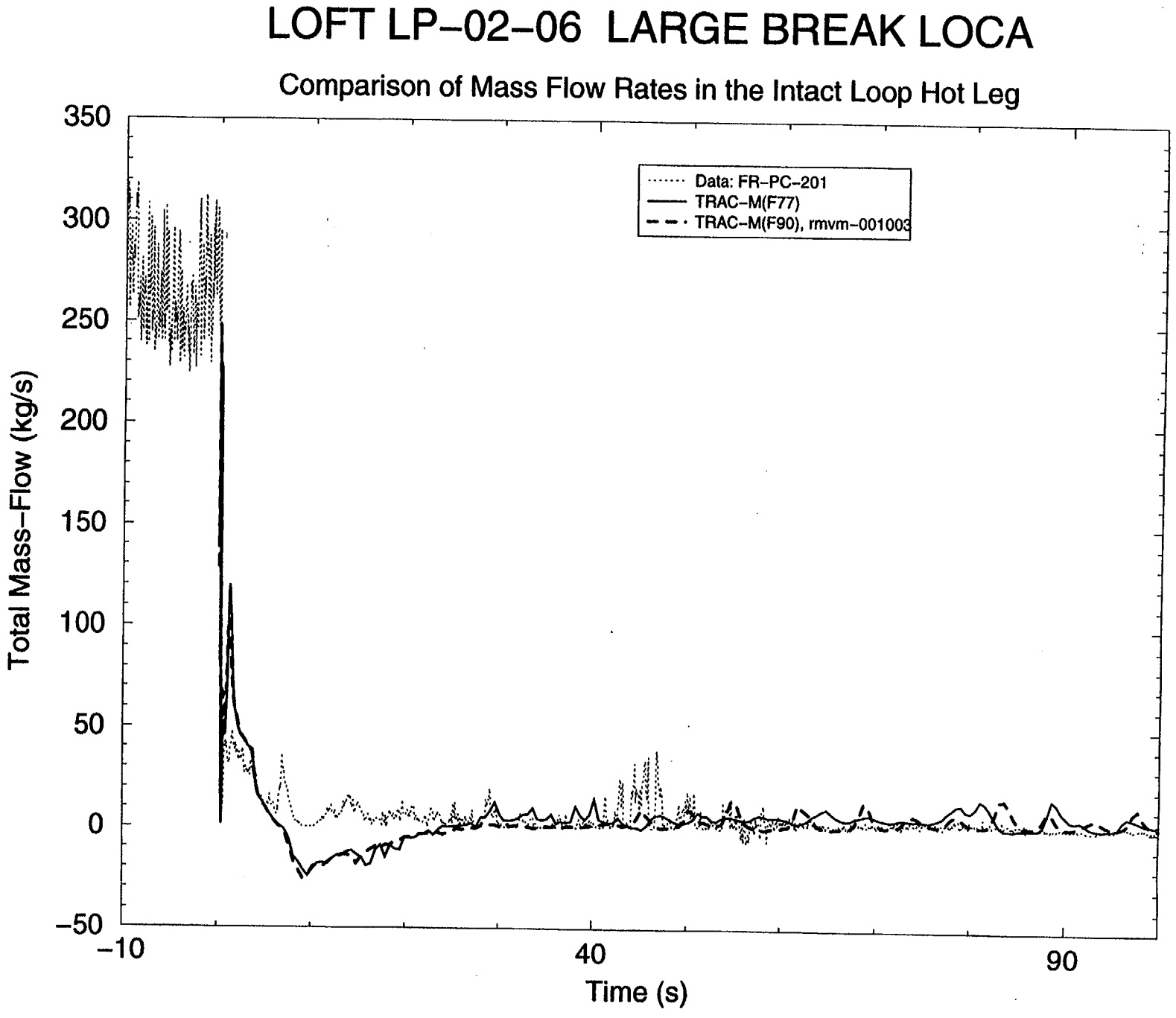

Figure 4.8.11 Comparison of Calculated and Measured Intact Loop Hot Leg Mass Flow Rates

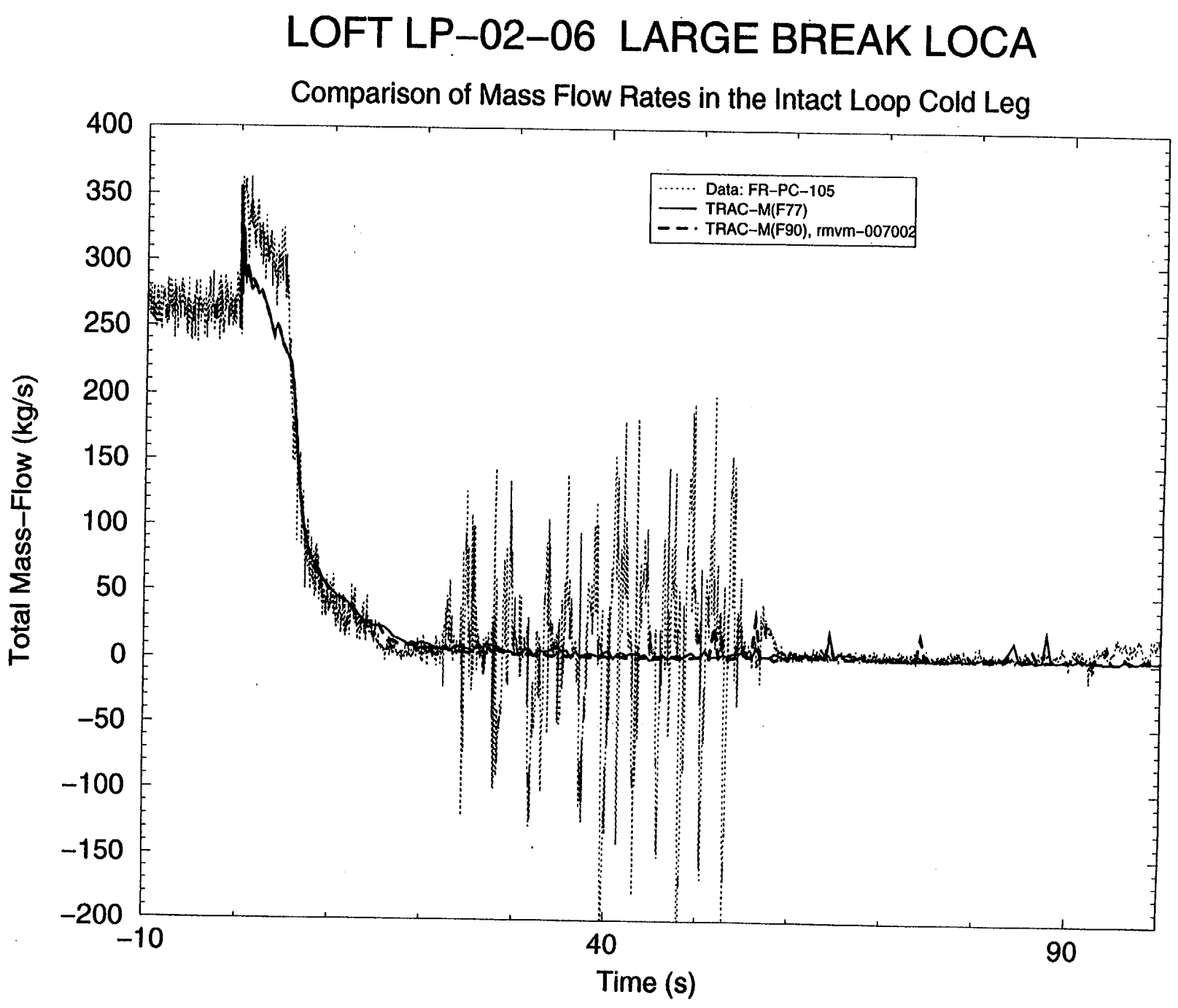

Figure 4.8.12 Comparison of Calculated and Measured Intact Loop Cold Leg Mass Flow Rate

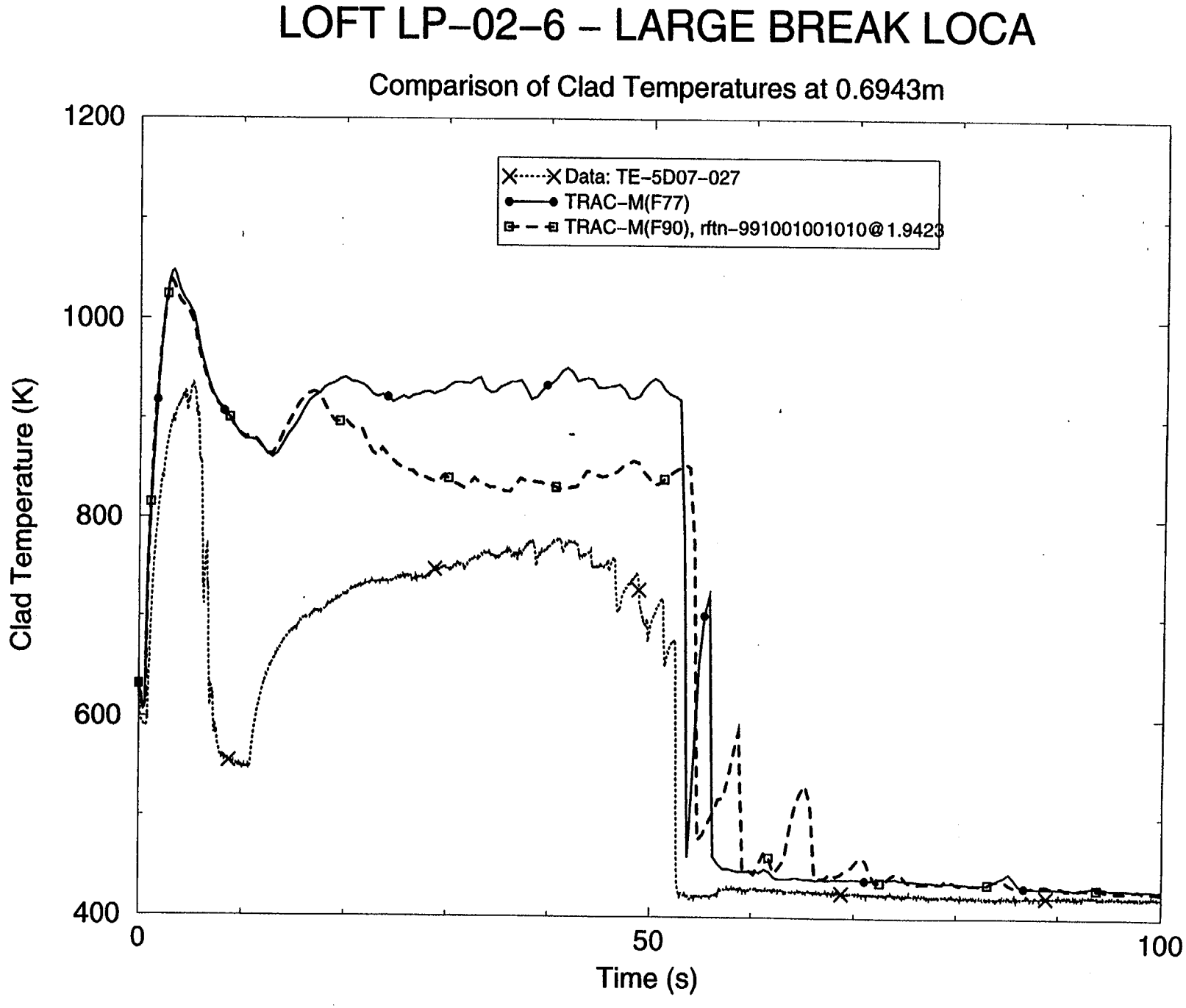

Figure 4.8.13 Comparison of Calculated and Measured Rod Clad Temperatures

4.9 Loss-of-Fluid Test (LOFT), Test L6-1 (Loss of Steam Load)

The Loss-of-Fluid Test (LOFT) facility was a fully operational PWR with instrumentation to measure and provide data on the T/H conditions throughout the system. The LOFT experimental system consisted of five major systems, including the reactor, primary coolant, blowdown suppression, emergency core cooling, and secondary coolant. These systems were heavily instrumented to provide continuous monitoring of the nuclear, thermal, hydraulic, and structural processes occurring during the LOFT experiments. This section presents the results of an assessment of the capabilities of the TRAC codes to predict loss-of-load transients.

4.9.1 Facility Description

The facility was configured to represent a 1/60-scale-by-power (1/44 by volume) model of a typical 3000-MW(t) commercial four-loop PWR. An overview and piping schematic of the LOFT facility are shown in Figs. 4.8.1 and 4.8.2, respectively. References 4.8.1 and 4.8.2 provide descriptions of the LOFT facility in general, and of the primary system in particular.

The reactor system consisted of the reactor vessel and head, core support barrel, upper and lower core support structures, flow skirt, reactor vessel fillers, and nuclear core. The 1.68-m LOFT core was rated at 50 MW(t), and was designed to have the same physical properties as a PWR core. The core contained two basic fuel assembly configurations, square and triangular. The square fuel assemblies contained 225 fuel rod locations, 21 of which were occupied by guide tubes. The triangular assemblies contained 78 fuel rod locations, 8 of which were occupied by guide tubes.

The primary coolant system consisted of two coolant loops connected to the reactor system. Three PWR primary coolant loops were simulated by the single, intact loop in the LOFT experimental system. This single LOFT loop was scaled to have the same volume-to-power ratio as the three PWR loops. The broken loop in the LOFT experimental system simulated the fourth PWR primary coolant loop, the loop where the break was postulated to occur initiating a large or small break LOCA. The intact loop contained a steam generator, primary coolant pumps, pressurizer, primary coolant venturi (flow measuring device), and intact loop piping. The intact loop active steam generator, shown in Fig. 4.9.1, had a secondary side that consists of a U-tube boiler section, a steam dome, and a downcomer. The steam generator secondary side was connected to a main steam flow control valve (MSFCV), condenser, feedwater pump, auxiliary feedwater pump, and a feedwater flow control valve.

The blowdown suppression system simulated the containment backpressure response of commercial PWRs during LOCAs, and provided containment for the blowdown effluent. The major system components were the blowdown suppression header and downcomers, blowdown suppression tank, and blowdown suppression-tank spray system.

The facility's ECCS simulated a commercial plant ECCS. This system included two ECCS trains, each of which contained a high-pressure injection system (HPIS), an accumulator (ACC) system, and a low-pressure injection system (LPIS).

The LOFT facility was highly instrumented. A partial list of the measured parameters includes coolant temperature; coolant level; coolant velocity, momentum, and flow direction;

coolant density; coolant pressure; coolant flows; differential pressure; pump speed; and metal temperatures. The available instrumentation is summarized in Ref. 4.8.2.

4.9.2 Test Procedure

Test L6-1 simulated a loss-of-steam load in a large PWR. The transient was initiated by closing the MSFCV, which increased the steam generator secondary side pressure and the two-phase coolant temperature (at the saturation temperature consistent with the secondary side pressure). The resulting decreased temperature difference between the primary and secondary side coolants then reduced the primary to secondary side heat removal, which increased the primary side temperature and pressure as well.

The pressurizer cycling heater, which was turned on at the beginning of the experiment, was automatically shut off at 6.1 s as the primary side pressure increased above its high-pressure set point. The pressurizer sprayer was initiated at 9.1 s, as the primary side pressure continued to rise above the sprayer low-pressure set point. As the primary side pressure rose, the high primary side pressure reactor core scram set point was reached, causing the reactor core control rod system to scram at 21.8 s. Immediately after the control system scram, the primary side began to depressurize because of the rapid reduction in reactor core power. The depressurization resulted from the primary side cooldown that was caused by the loss of the reactor core heat source while the steam generator provided a heat sink. The rising secondary side pressure (with the MSFCV closed) crossed the MSFCV high-pressure set point, which caused the MSFCV to automatically begin opening at 22.2 s. The secondary side pressure then began to fall until at 31.4 s, when the MSFCV low-pressure set point was crossed. The MSFCV then stopped opening, began closing, and reached its closed state at 40.6 s.

The falling primary side pressure caused the pressurizer sprayer to be turned off at 30.4 s, the pressurizer cycling heater to be turned on at 31.4 s, and the pressurizer backup heater to be turned on at 32.5 s. With the MSFCV closed, the secondary side pressure began to rise again because of the primary side heat source that resulted from decay heat power. Consistent with the MSFCV's high-pressure set point, the MSFCV again opened automatically at 91.2 s. Then, consistent with its low-pressure set point, it automatically closed at 97.8 s, reaching its closed state at 104.4 s. A similar opening and closing of the MSFCV was performed manually (rather than automatically), starting at 312.6 s and ending at 339.4 s with the MSFCV closed. The pressurizer backup heater was turned off at 415.4 s when the primary side pressure rose above the backup heater high-pressure set point. The experiment was terminated at 700 s. No coolant line break was initiated in this experiment, and the blowdown suppression system was not used. During the transient, the broken loop was connected to the intact loop through 1-in. warm-up lines to prevent broken loop coolant stagnation and its potential effect on the vessel's T/H state. Ref. 4.9.1 presents experimental data obtained in this test.

4.9.3 TRAC-M Model

Two TRAC input models have been developed (Ref. 1.2) to model the vessel using (1) 1-D hydro components and (2) a 3-D VESSEL component, respectively. This report presents an assessment of TRAC-M(F77) and TRAC-M(F90) using the input model with the 3-D VESSEL component. Figs. 4.9.2 and 4.9.3 show the respective TRAC-M model plant system loops and the intact loop steam generator modeled by 1-D hydro components. The steam generator is modeled

with separate PIPE, TEE, and heat structure (HSTR) components. Fig. 4.9.4 shows the 3-D VESSEL hydro component and 11 HSTR components. One HSTR component models the fuel rods, and the remaining 10 model the vessel's structural components. The plant model consists of 22 HSTR components, 11 of which are used to model the steam generator.

These TRAC models correspond to the LOFT hardware configuration, with the following exceptions:

- The broken loop quick-opening blowdown valves and blowdown suppression tank were not modeled because they were not used in the L6-1 experiment.

- The LPIS and ACC of the ECC injection system were not modeled because they were not used in the L6 series of experiments. (The HPIS was modeled by FILL component 17, but did not operate during the L6-1 experiment.)

- The pressurizer pressure-operated relief valve (PORV) was not modeled because it did not operate during the L6-1 experiment.

In Fig. 4.9.2, the pressurizer is modeled with PRIZER components, 8 and 13, with PIPE component 9, above PRIZER component 13, PIPE component 12 between the two PRIZER components, and TEE component 1 below the PRIZER components. PIPE component 12 was used between the two PRIZER components to accurately model the pressurizer cycling and backup heaters using the option for direct power deposited in the coolant. The reasons for using two PRIZER components are two-fold:

- The LOFT pressurizer has both cycling and backup heaters that could not be simulated using the PRIZER component heater option.

- The PRIZER component heater option would have uniformly distributed the deposited energy everywhere in the liquid, whereas the energy actually is deposited only in the liquid near the bottom of the pressurizer where the heaters are located.

The pressurizer sprayer inlet line is connected to PIPE component 9 at the top of the pressurizer. The PRIZER component sprayer option cannot simulate the actual LOFT sprayer system because it is a means only for controlling the system pressure, not for modeling the behavior of an actual sprayer. Therefore, the LOFT sprayer was modeled with VALVE component 10 to simulate the sprayer fluid control hardware. The sprayer droplet/mist generating hardware could not be modeled directly and, as the discussion regarding the calculated results will point out later in this section, this hardware may be the most limiting TRAC modeling area for this experiment. Ref. 4.9.1 reports that, when closed, the LOFT sprayer valve has a leakage flow-area-fraction of ~0.025. Because the primary side pressure was accurately predicted with the leakage mass flow of 0.01 kg/s in earlier calculations, adjustments in the valve model were made, and the leakage-flow-area fraction was determined to be 0.00686.

The LOFT pressurizer never reaches an actual steady-state condition because the heater energy source and sprayer energy sink are not in balance. To ensure a steady-state solution that is consistent with experimental conditions at the start of the transient, a trip-controlled direct power

of 5 kW was deposited in the coolant of PIPE component 9 during the steady-state calculation to bring the leaking sprayer liquid to saturation. This small energy addition is terminated at the start of the transient when its controlling trip goes off. Hence, this heater does not affect the anticipated transient portion of the simulation.

In Ref. 4.9.2, Ollikkala reported that the external surface heat losses in the LOFT facility were 6 kW from the pressurizer, 10 kW from the steam-generator secondary side, and a total of 174 kW from the primary system (excluding the pressurizer). These heat losses have been included in the TRAC-M model. As a result, the average heat transfer coefficients on the outside surface areas of the pressurizer, steam generator secondary side, and primary system piping were calculated by assuming that the surrounding air temperature was 305 K.

Evaluation of reactor power was based on a point kinetics model with fuel and coolant temperature reactivity feedback. The TRAC-M default reactor kinetics parameters were used for 6 delayed neutron groups and 11 American Nuclear Society (ANS)-72 decay-heat groups. The delayed neutron and decay heat group concentrations were determined from the L6-1 experiment core power history before the transient.

All control procedures employed in the L6-1 experiment were modeled using the signal variable, control block, and trip control system modeling capability that is available in TRAC-M. The TRAC-M model uses 21 signal variables, 13 control blocks, and 20 trips. Five signal variables define trip signals and the trip set status. A second control parameter evaluation pass is required to determine the trip set status and to evaluate six control blocks that use those signal variables after the trips are evaluated on the first control parameter evaluation pass. The trip set points that trigger control procedure actions are listed in Table 4.9.1, based on information in Refs. 4.9.1, 4.9.3, 4.9.4, and 4.9.5. The modeling of the control procedures employed in the L6-1 experiment is described in Ref. 1.2.

4.9.4 Comparison of Predicted and Measured Results

The L6-1 calculations were performed using both TRAC-M(F77) and TRAC-M(F90). Table 4.9.2 shows the LOFT L6-1 measured initial conditions and the TRAC-M(F77) and TRAC-M(F90) steady-state calculation results after 200 s of problem time evaluation. The calculations show a "Reasonable" agreement between the predicted and measured initial conditions.

The transient calculations were initiated from the last restart data dump of the steady-state calculations at 200 s. The times of the events that occurred during the LOFT L6-1 transient and corresponding calculations by both codes are shown in Table 4.9.3. Small differences in the calculated steam dome pressure and the test data resulted in a large difference in the time at which a set point for opening the MSFCV was crossed in the TRAC calculations.

Figs. 4.9.5 through 4.9.12 compare the TRAC-M(F77) and TRAC-M(F90) predictions and the test data. The agreement between the two code predictions are "Excellent" to "Reasonable" for almost all parameters shown. The only discrepancy occurs in the timing of the second opening of MSFCV, which takes place when the steam dome pressure reaches the set point of 6.9764 Mpa. TRAC-M(F77) predicts the opening of the valve at ~80 s, while TRAC-M(F90) predicts the opening at ~98 s. The agreement between the two sets of pressure predictions for the steam dome is almost "Excellent" (according to Fig. 4.9.12) until the valve opens. However, TRAC-M(F90) predictions are slightly below the TRAC-M(F77) predictions. The pressure trace asymptotically

approaches the set point of 6.9764 Mpa. Hence, a small difference in pressure prediction results in a large difference in the timing of the opening of the valve. Such small differences in pressure predictions are expected, since TRAC-M(F90) includes many error corrections. Consequently, the agreement between valve opening times and subsequent changes in other parameters (caused by different opening times of the valve) are considered "Reasonable."

Agreements between the code predictions and the test data should have been better than is indicated by Figs. 4.9.5 through 4.9.12. Loss of steam load transient is a relatively simple transient, and it should not pose a challenge to code models. Careful examination of the code calculations and test data indicate that the input deck should be improved, and calculations should be repeated. The following recommendations indicate where improvements to the deck can be made:

- Fig. 4.9.5 compares the predicted and measured core power. It is clear that the decay heat used in the input model after the scram is very high compared to the test measurements, and should be corrected. Also, the predicted time of the scram can be improved if the pressure calculations shown in Fig. 4.9.6 are improved. This raises the issue of modeling the pressurizer.

- Examination of the experimental data in Figs. 4.9.10 and 4.9.11 indicates that the steam control valve was not completely closed during the test, as indicated by the control valve fraction of area open and the measured steam flow rates. The input model should have been built to show this leakage since it affects overall system behavior.

- The use of very few cells to model the loop causes high numerical diffusion in the calculated temperatures. The improved input model should have more cells to minimize numerical diffusion.

- Results are very sensitive to calculations of the primary system pressure. The modeling of the pressurizer may be revisited to yield accurate calculations of the pressure.

4.9.5 Conclusions

Agreements between TRAC-M(F77) and TRAC-M(F90) calculations are "Excellent" to "Reasonable," indicating that the conversion from FORTRAN 77 to FORTRAN 90 and the modernization of modules and numerical methods have been successful for this type of applications. Both sets of code predictions do not agree well with the experimental data because the input deck does not accurately model boundary conditions (decay heat and steam flow rate). Some improvements in pressurizer modeling and loop nodalization are also needed.

REFERENCES

4.9.1 Batt, D.L., and J.M. Carpenter, "Experiment Data Report for LOFT Anticipated Transient Experiments L6-1, L6-2, and L6-3," Idaho National Engineering Laboratory Report EGG-2067, NUREG/CR-1797, December 1980.

4.9.2 Ollikkala, H., "Best-Estimate Prediction for LOFT Anticipated Transient Slow and Fast Rod Withdrawal Experimental L6-8B," Idaho National Engineering Laboratory Report EGG-LOFT-5983, August 1982.

4.9.3 Keeler, C.D., "Best-Estimate Prediction for LOFT Nuclear Experiments L6-1, L6-2, L6-3, and L6-5," Idaho National Engineering Laboratory Report EGG-LOFT-5161, October 1980.

4.9.4 Reeder, D.L., "Quick-Look Report on LOFT Nuclear Experiments L6-1, L6-2, and L6-3," Idaho National Engineering Laboratory Report EGG-LOFT-5270, October 1980.

4.9.5 Ollikkala, H., and S.R. Behling, "Post-test Analysis of LOFT Anticipated Transient Experiments L6-1, L6-2, L6-3, and L6-5," Idaho National Engineering Laboratory Report EGG-LOFT-6159, January 1983.

Table 4.9.1 Trip Set Points for Experiment L6-1

Parameter	Set Point
System low-pressure scram (MPa)	14.36
System high-pressure scram (MPa)	15.77
Intact-loop hot-leg high-temperature scram (K)	583.3
Low primary-coolant mass flow (kgs^{-1})	433.5
High core-averaged power scram (MW)	51.5
Steam-generator secondary-side low liquid-level scram (m)	2.0
PORV opening set point (MPa)	16.70
PORV closing set point (MPa)	16.56
Pressurizer spray on	15.24
Pressurizer spray off	14.90
Pressurizer cycling heater on (MPa)	14.75
Pressurizer cycling heater off (MPa)	14.93
Pressurizer backup heater on (MPa)	14.62
Pressurizer backup heater off (MPa)	14.80
HPIS on (MPa)	13.297
HPIS off (MPa)	15.500
MSFCV opening set point before reactor scram (MPa)	5.425
MSFCV opening set point after reactor scram (MPa):	
between 0 and 75 s	6.99
between 75 and 200 s	6.9764
between 200 s and end of transient	6.9464
MSFCV closing set point before reactor scram (MPa)	5.315
MSFCV closing set point after reactor scram (MPa):	
between 0 and 75 s	6.7500
between 75 and 200 s	6.6500
between 200 s and end of transient	6.6000

Table 4.9.2 LOFT Experiment L6-1 Initial Conditions and TRAC-Evaluated Steady-State Calculation Results

Parameter	Measured	TRAC-M(F77)	TRAC-M(F90)
Reactor-core neutronic power (MW)[a]	36.9±0.9	36.9	36.9
Pressurizer pressure (MPa)[a]	14.78±0.20	14.78	14.78
liquid level (m)	1.18±0.07	1.292	1.300
Intact loop			
hot-leg mass flow (kgs^{-1})	478.5±6.3	479.7	479.6
hot-leg temperature (K)	567.5±1.8	567.6	567.6
cold-leg temperature (K)	552.8±1.2	552.8	552.8
Pump impeller rotational speed (rad/s)b	334.0±1.5	333.5	326.6
Steam-generator secondary-side			
steam-dome pressure (MPa)	5.37±0.06	5.3	5.3
downcomer liquid level (m)[d]	3.183±0.034	3.213	3.213
steam mass flow (kgs^{-1})	20.1±0.6	19.57	19.54

[a] Specified steady-state condition
[b] Adjusted to achieve the desired intact-loop hot-leg mass flow
[c] Constrained within 5.425-MPa maximum value and 5.315-MPa minimum value
[d] Constrained to 3.183 m [a downcomer liquid level of 2.9464 + 0.00508 x (core power in MW) = 3.134 m at a 36.9-MW reactor-core power was the specified liquid level for the L6-1 experiment]

Table 4.9.3 LOFT Experiment L6-1 Sequence of Events

Events	Measured Times (s)	TRAC-M(F77) Predictions	TRAC-M(F90) Predictions
MSFCV started to close	2.0±0.1[a]	2.08	2.08
Pressurizer cycling heater off	6.1±0.1	8.37	8.37
Pressurizer spray on	9.1±0.1	10.96	11.17
Reactor-core power scrammed	21.8±0.2	18.29	18.27
MSFCV started to open	22.2±0.2	22.49	22.78
Pressurizer spray off	30.4±0.1	30.08	30.42
Pressurizer cycling heater on	31.4±0.1	31.11	31.53
Pressurizer backup heater on	32.5±0.1	33.23	33.59
MSFCV started to close	33.2±0.2[b]	31.04	31.51
MSFCV started to open	91.2±0.2	81.77	98.53
MSFCV started to close	99.2±0.2[b]	87.90	104.40

[a] The valve closing was reported to have been initiated at 0.0 s; however, pressure data show a ~2-s time delay before any effect of movement in the valve position was observed.

[b] Only the time that the valve was fully closed was reported. The time when the value started to close was estimated to be midway through the valve adjustment time interval.

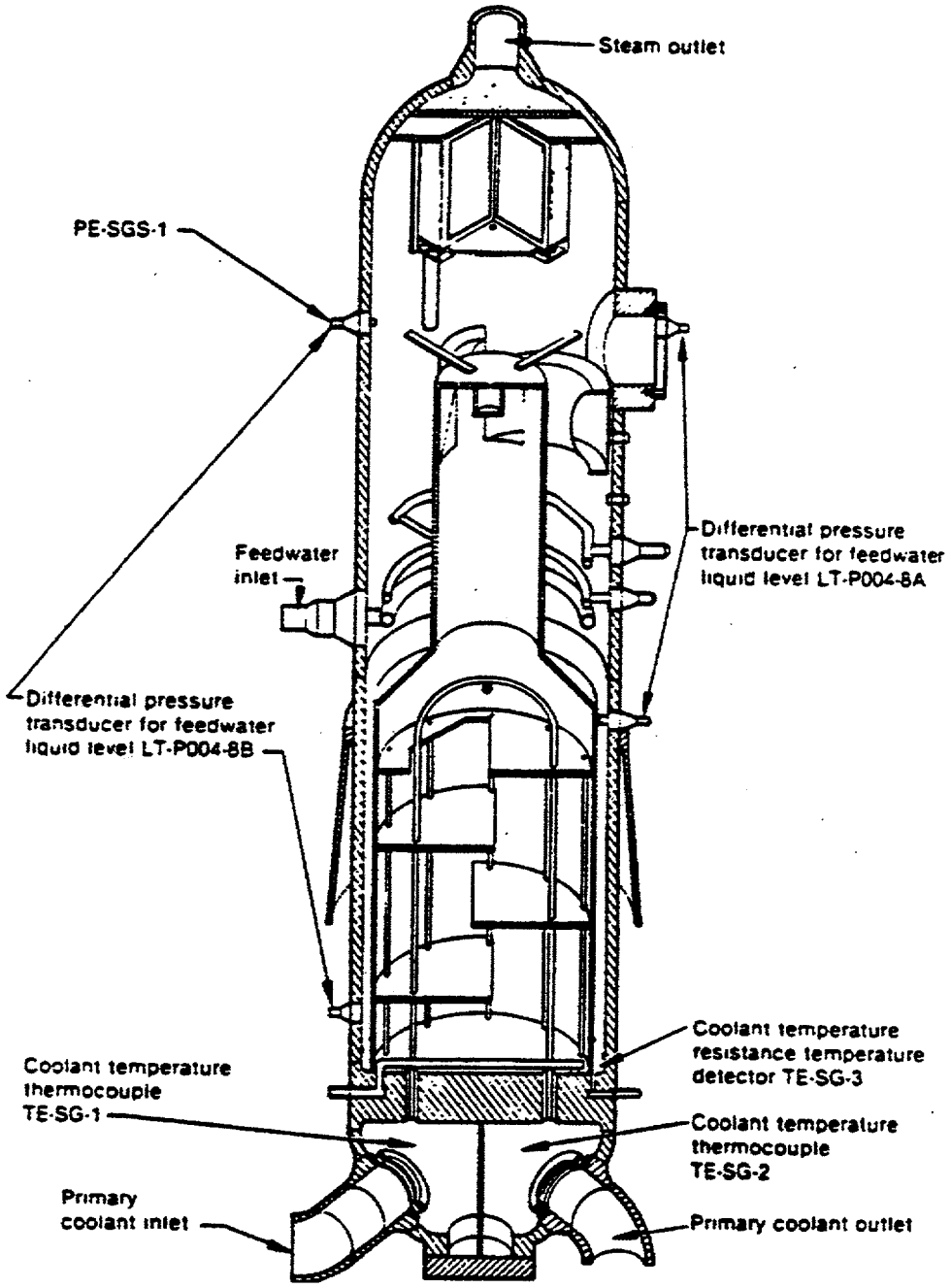

Figure 4.9.1 Intact-Loop Steam Generator in the LOFT Facility

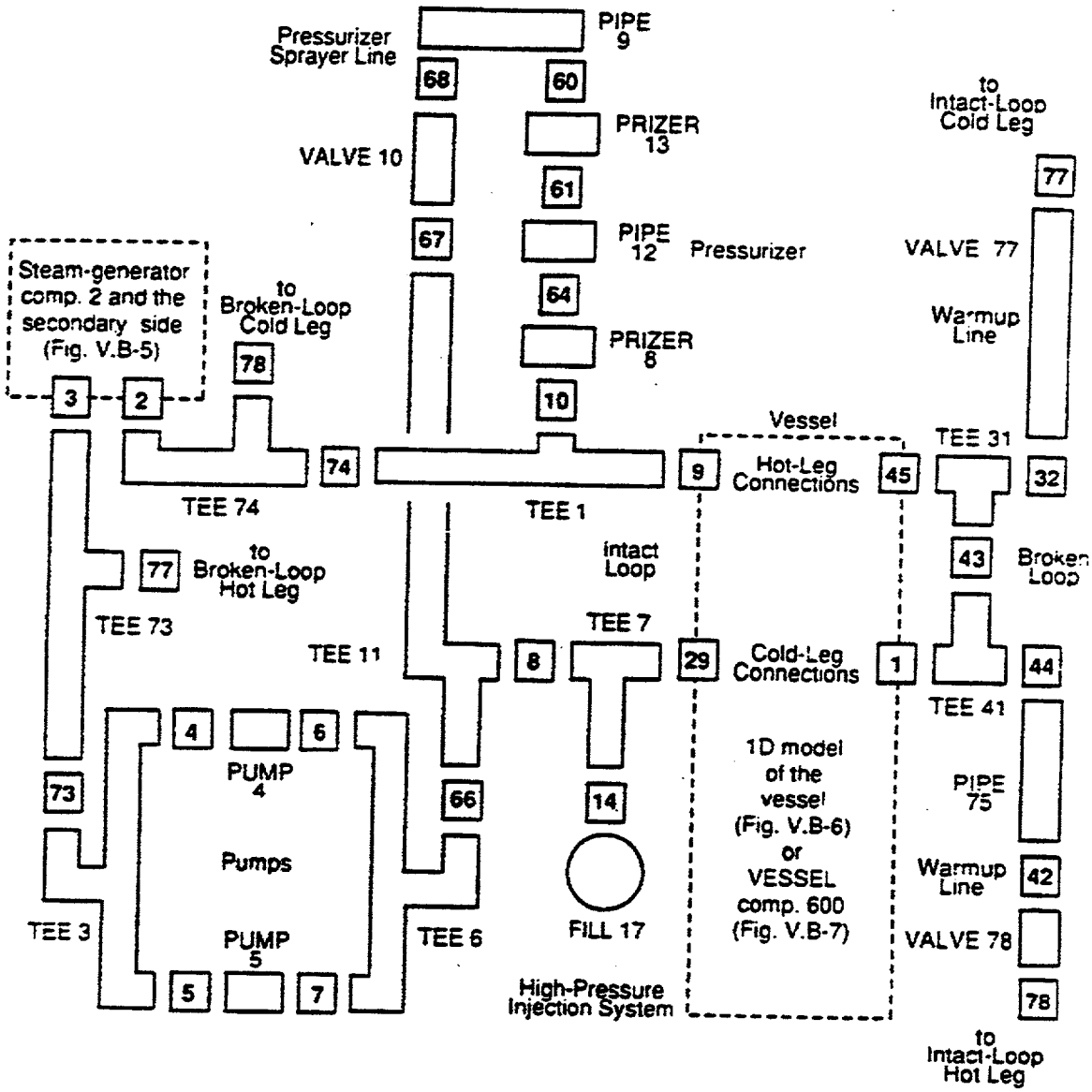

Figure 4.9.2 TRAC Model of the LOFT Facility

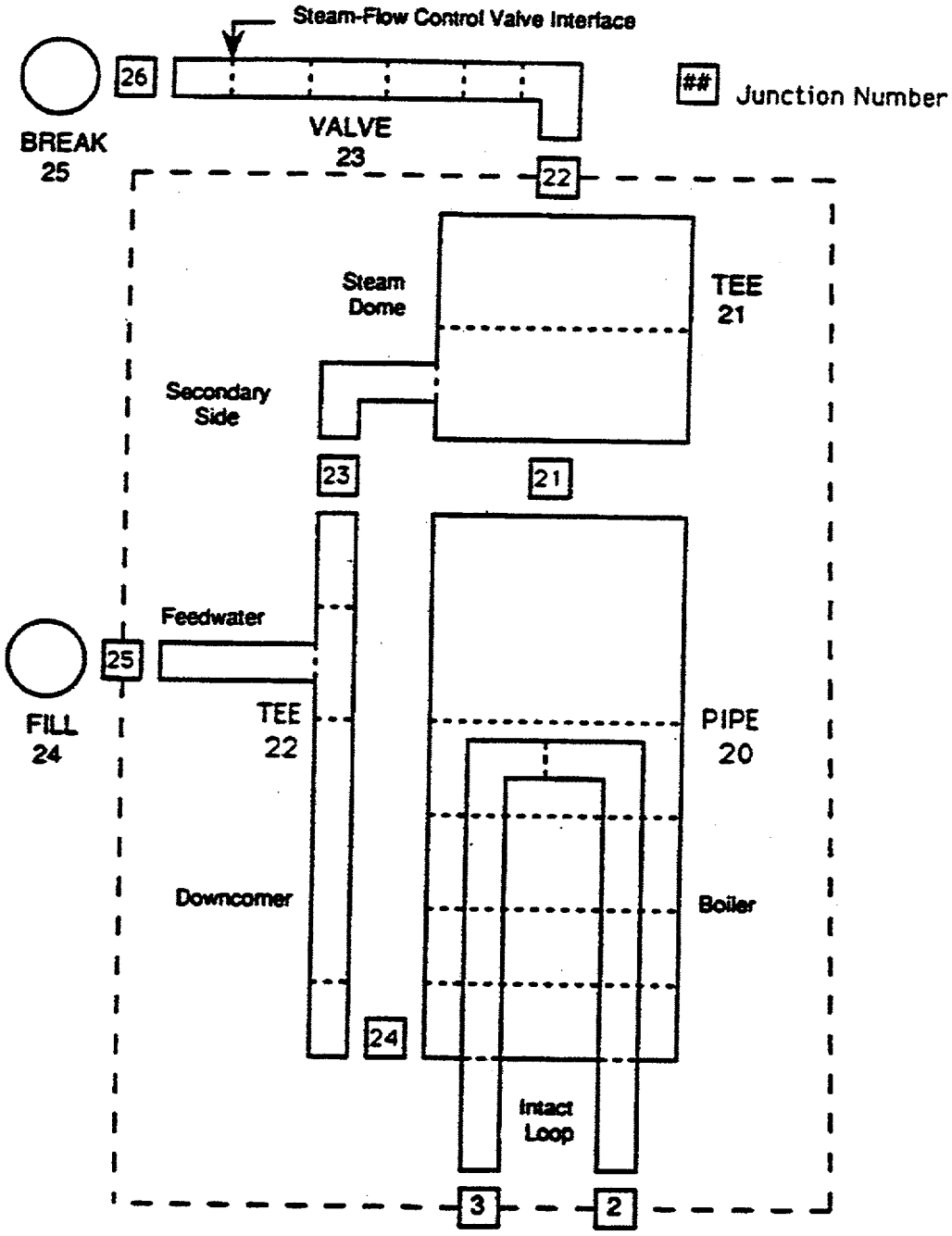

Figure 4.9.3 TRAC Model for the LOFT Facility Intact-Loop Steam Generator

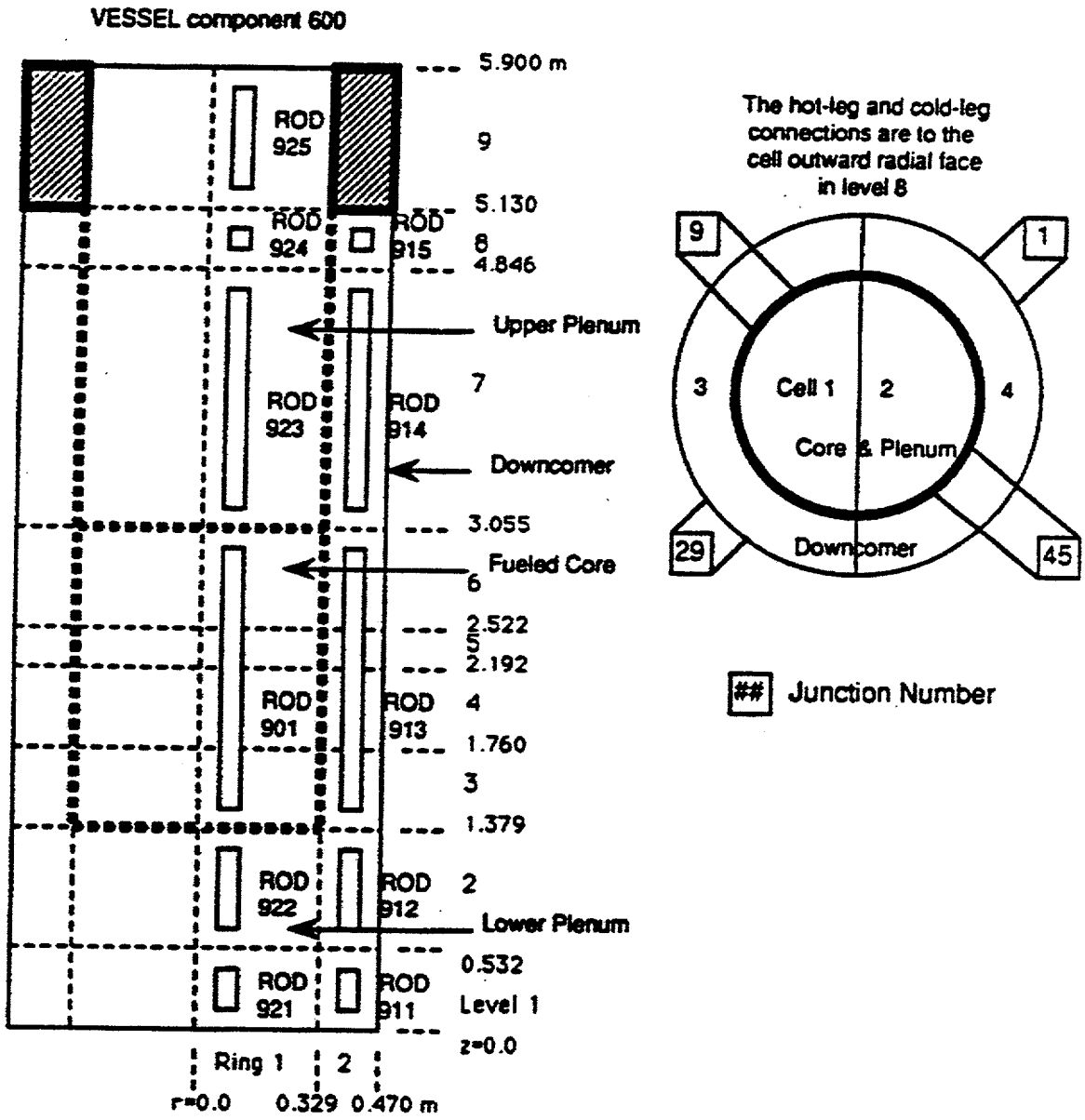

Figure 4.9.4 3-D Vessel, Fueled-Core Rod, and Structure Rod Components Modeling the LOFT Facility Vessel

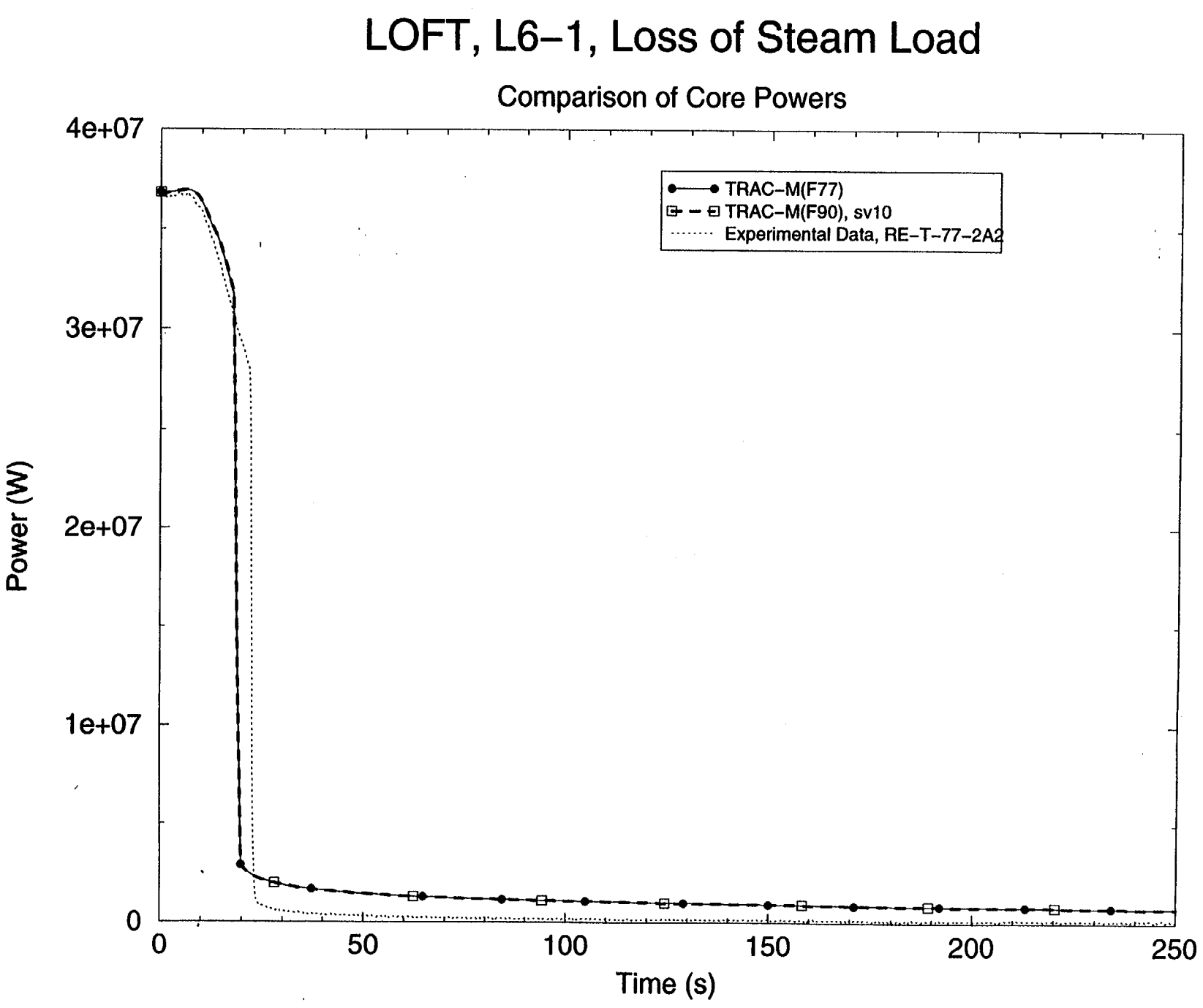

Figure 4.9.5 Comparison of Core Powers

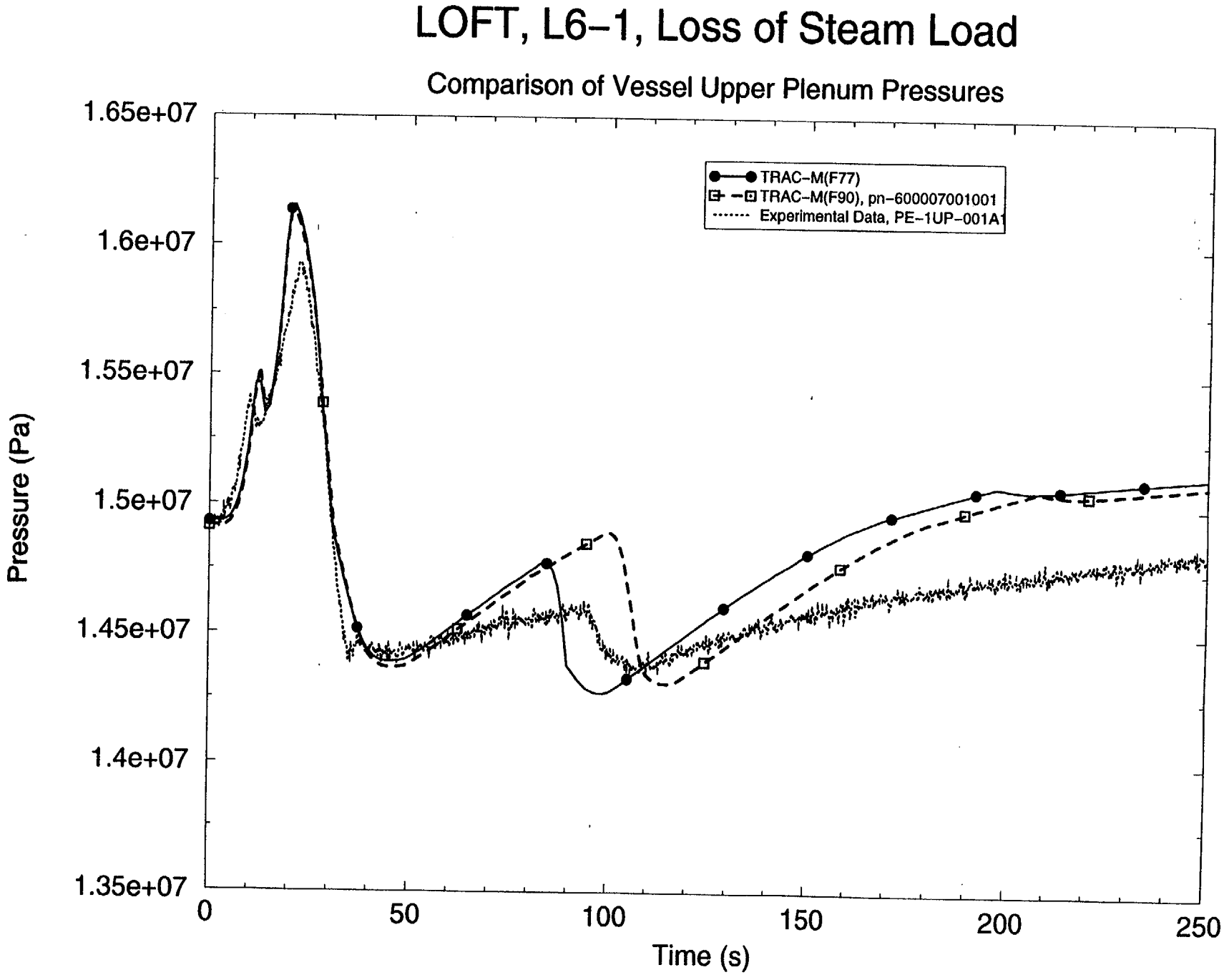

Figure 4.9.6 Comparison of Vessel Upper-Plenum Pressures

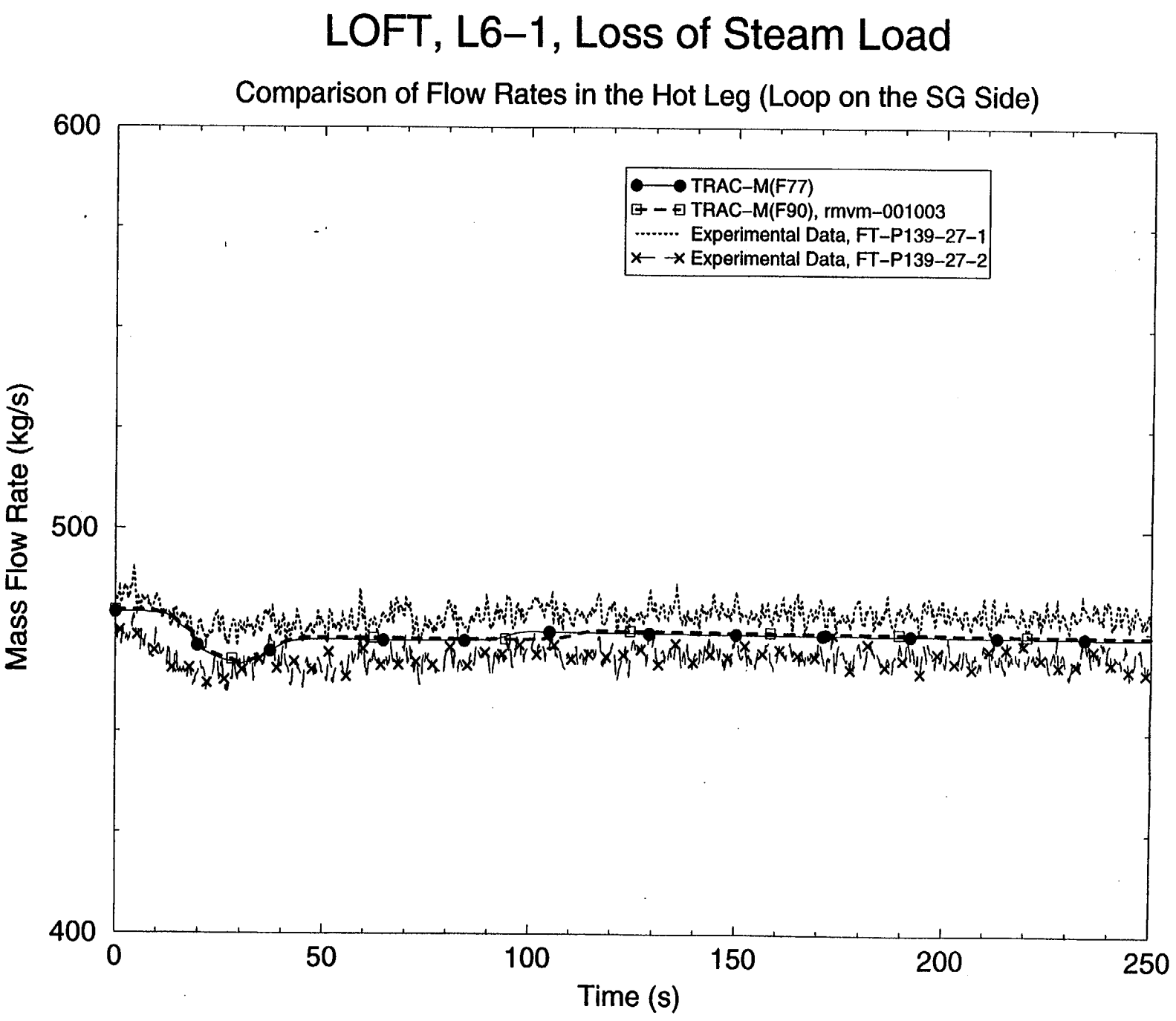

Figure 4.9.7 Comparison of Flow Rates in the Hot Leg of the Loop on the Steam Generator Side

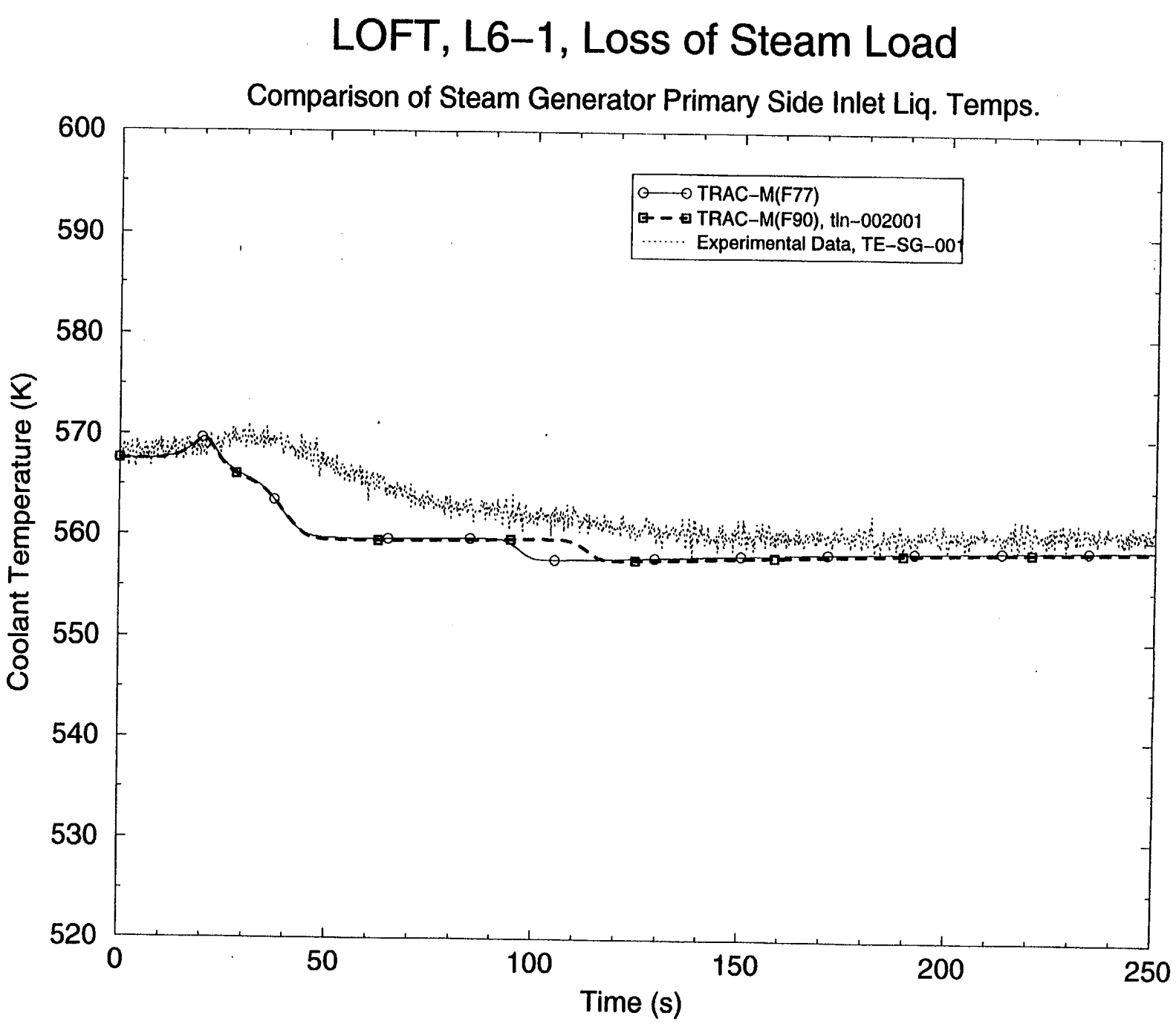

Figure 4.9.8 Comparison of Steam Generator Primary Side Inlet Liquid Temperatures

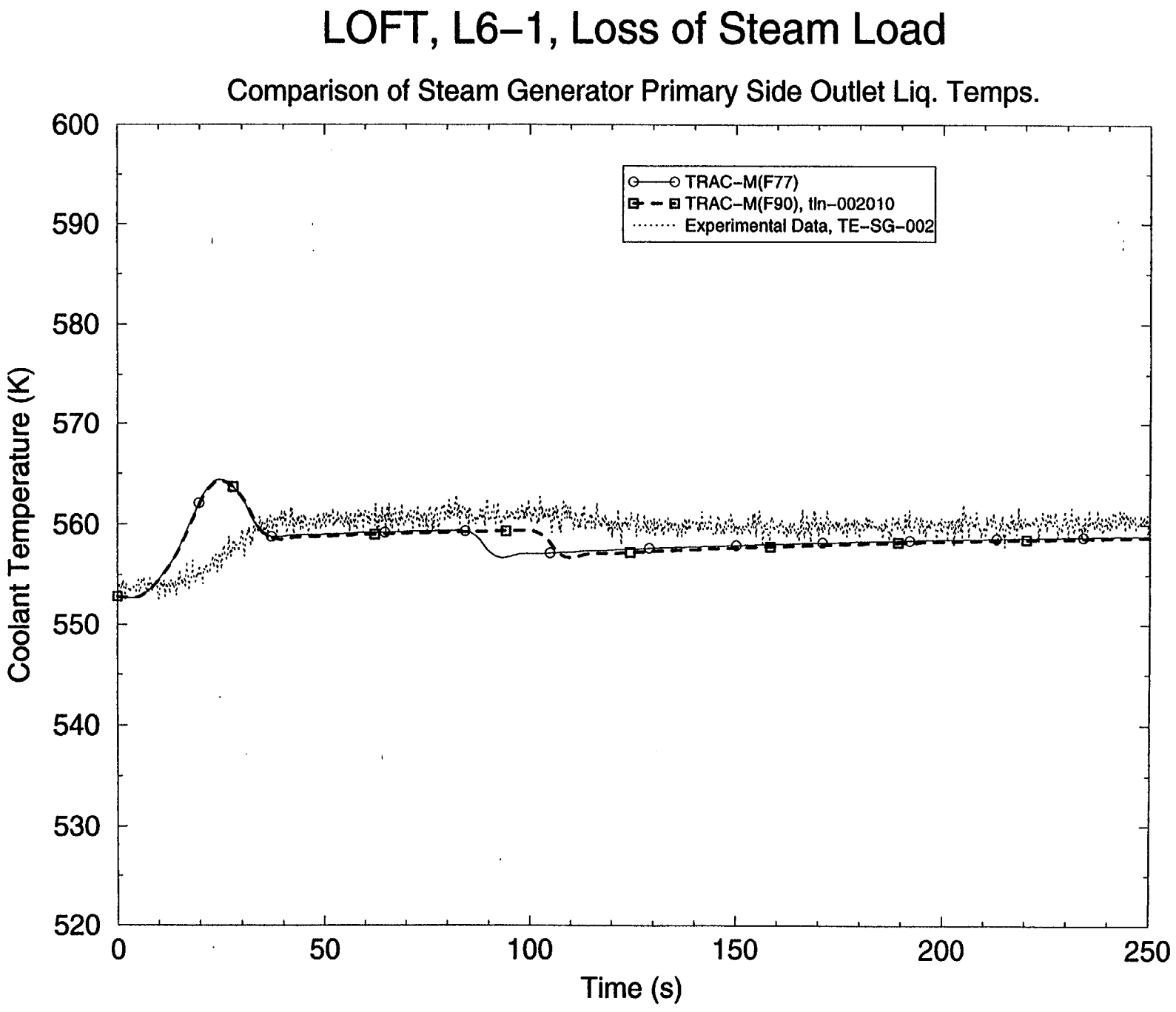

Figure 4.9.9 Comparison of Steam Generator Primary Side Outlet Liquid Temperatures

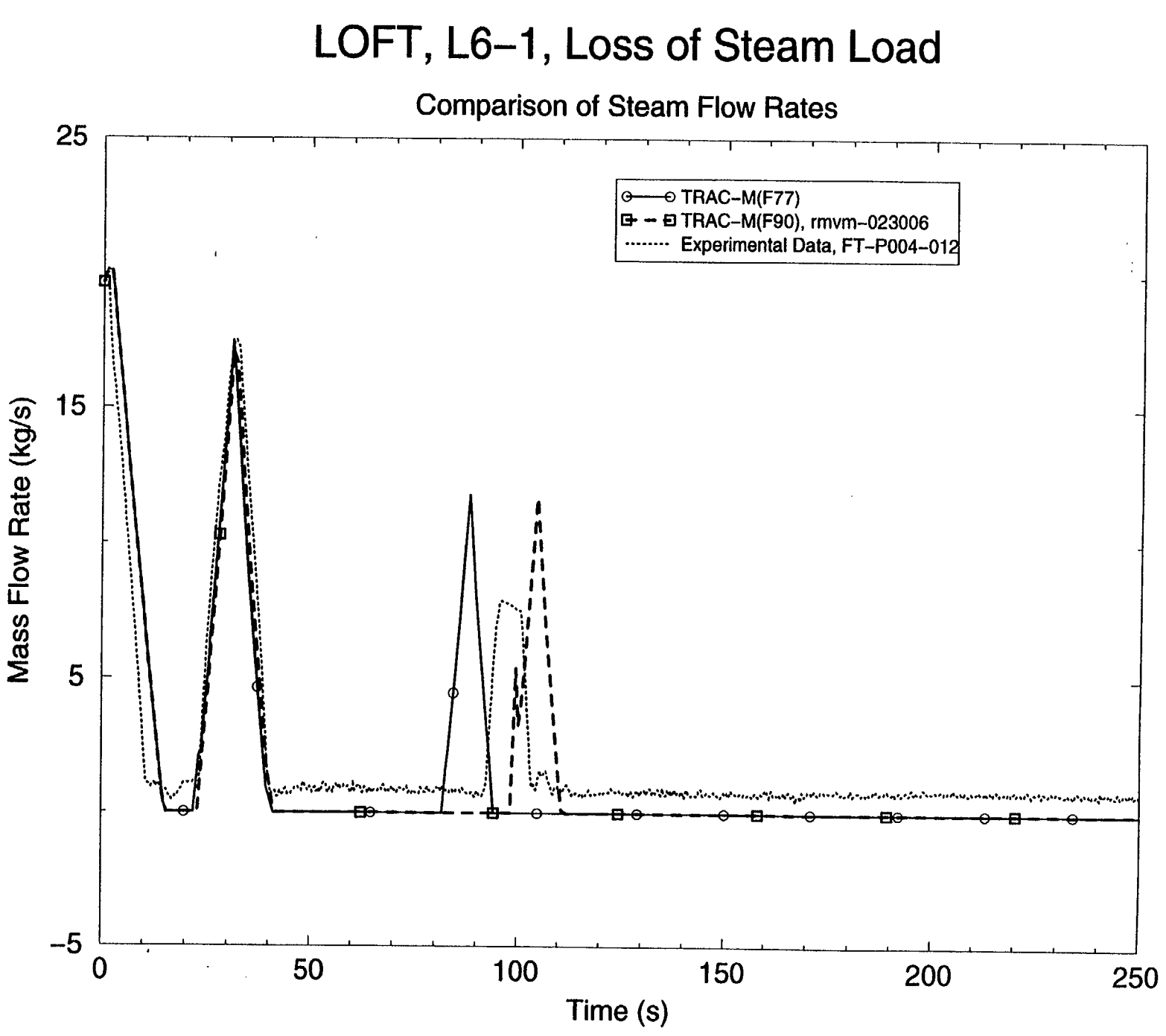

Figure 4.9.10 Comparison of Steam Flow Rates

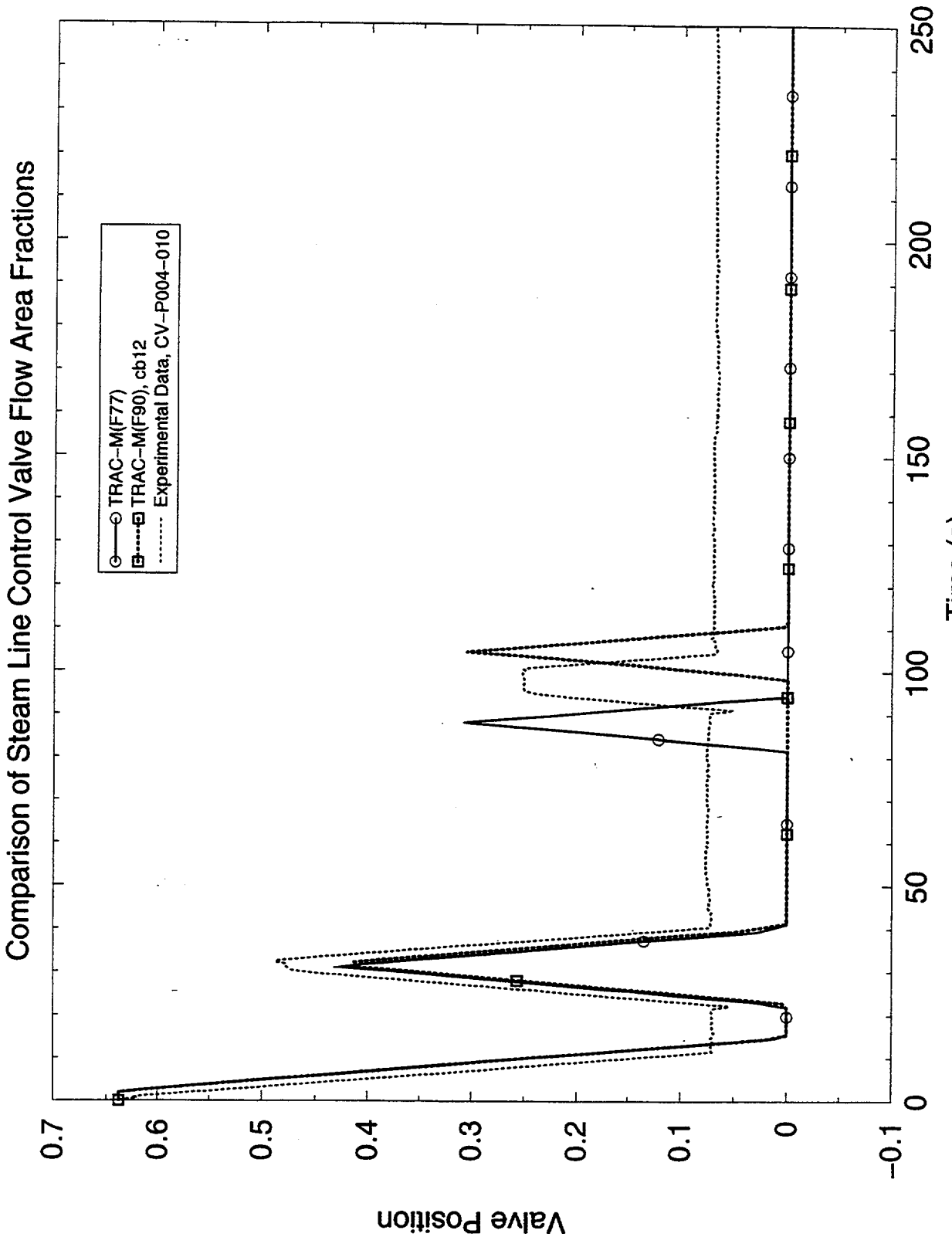

Figure 4.9.11 Comparison of Steam Line Control Valve Flow Area Restrictions

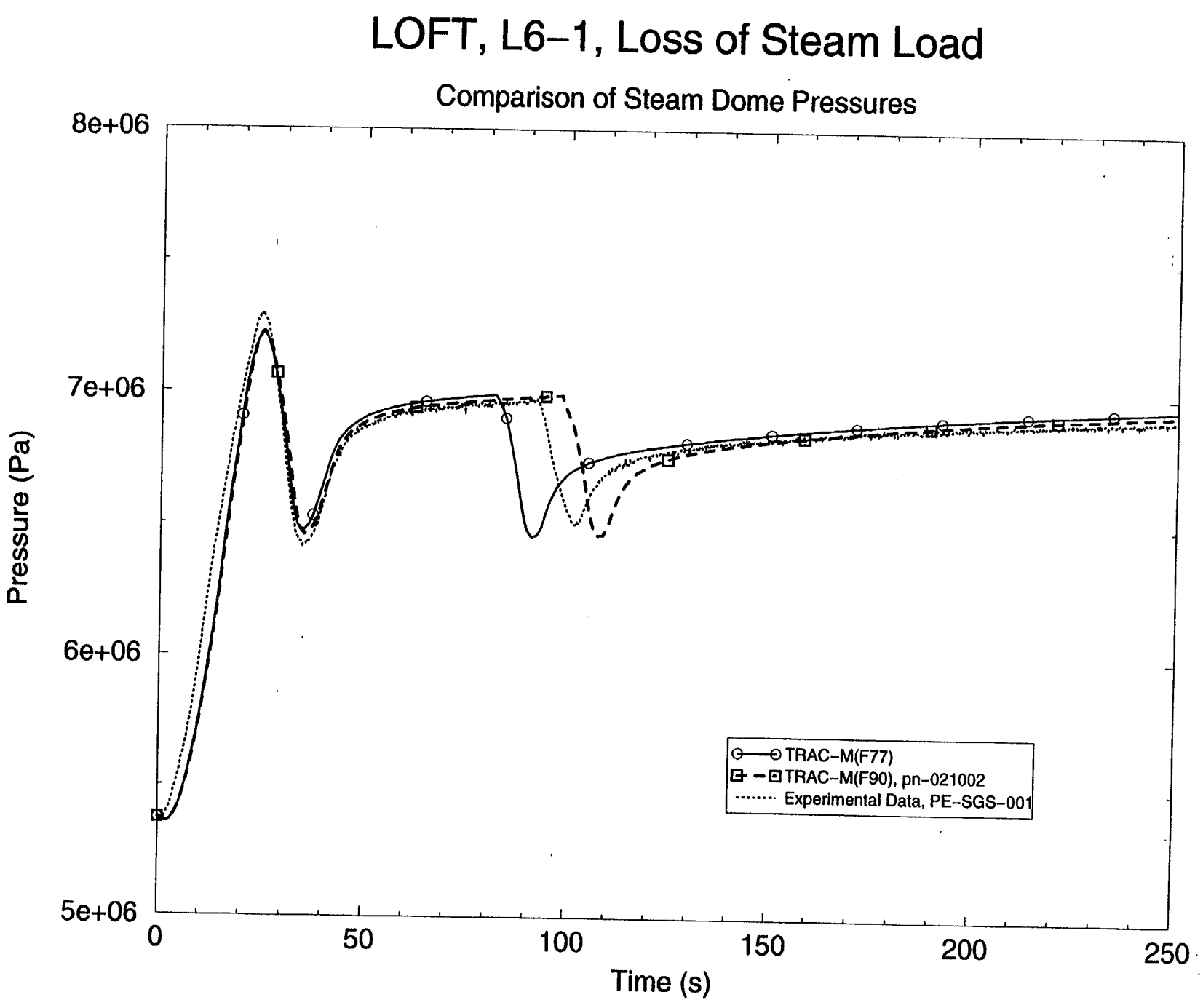

Figure 4.9.12 Comparison of Steam Dome Pressures

5. Assessment of Integration of BWR Components

Heaters are used in boiling-water reactor (BWR) steam supply systems either to raise the feedwater heater temperature, or to condense the steam exiting turbines. This section presents an assessment of the integration of the heater component from TRAC-B to TRAC-M.

5.1 Heater (HEATR) Component

Fig. 5.1.1 shows a schematic of a typical two-zone, horizontal, closed feedwater heater, which consists of a shell and a bank of folded tubes. This type of heater heats feedwater passing through its tubes by means of steam or condensate on the shell side. The inlet and outlet to and from the tubes are located at a tube sheet at one end of the heater where the feedwater enters and leaves through the divided water box. The tubes are supported by baffle plates, which also promote the steam crossflow across the tube bank rather than permitting parallel flow. Film condensation is the mode of heat transfer inside the condensing region.

It is important to emphasize that different behavior is expected for vertical and horizontal heaters, since the tube orientation influences the water film thickness and, therefore, the heat transfer resistance. During the normal operation of a heater, the condensate level inside the condensing region is maintained above the inlet to the subcooling region, such that this region is characterized by the presence of a continuous liquid condensate, rather than steam or a two-phase mixture. The higher steam pressure in the shell region drives the liquid condensate into the drain cooler zone. Again, the baffle plates force crossflow over the tubes in this region. The heat transfer mode expected inside the drain cooler zone is, therefore, turbulent convection inside and outside the tube. Figs. 5.1.1 and 5.1.2 illustrate the geometry of this typical feedwater heater.

Heater designs are plant-specific, since these off-the-shelf items are chosen by the architect/ engineer (A/E) rather than supplied by the reactor vendor. Thus, the design and operational data are scarce and limited only to the information published in the plant safety analysis reports. Simulation of a typical feedwater heater with realistic design and operational data is critical for use in verifying the correct integration of the heater model into the TRAC-M code. Consequently, a decision was made to "reverse-engineer" the design and operational data for a typical feedwater heater from a plant safety analysis report, in order to identify key design parameters such as tube diameters, tube thickness, shell diameter, and total heat transfer area in the subcooling and condensing zones.

The second point heater of the River Bend Station was chosen as the target feedwater heater to be modeled. Fig. 5.1.3 shows the heat balance and flows for the first and the second point heaters of River Bend Station taken from the Updated Safety Analysis Report (USAR) of the River Bend Station (Ref. 5.1.1). Although the use of two high-pressure (vertical) heaters and three low-pressure heaters for each of the three turbines in a BWR/6 turbine island is a typical arrangement, the second point heater is a horizontal U-tube type heater with internal drain cooling. Since the feedwater heater specifications are taken from a USAR, analysis in this section is performed using English units.

Fig. 5.1.4 shows a typical plot of temperature vs. enthalpy (or distance along the feedwater tube) for horizontal heaters.

Some common terms that the industry frequently uses in defining heater specifications are also used in Fig. 5.1.4. Since these terms are frequently used in the discussions throughout this report, it is important to understand their definitions:

Heater Duty is the net heat that is transferred to the feedwater (usually expressed in Btu per hr).

Design Maximum Working Pressure is the pressure for which the tube and shell sides are structurally designed.

Operating Pressure is the pressure for which the shell side is thermally designed and rated. The tube side pressure is the normal discharge pressure of either the steam generator feed or the condensate pump.

Terminal Temperature Difference (TTD) is the difference between the saturation temperature corresponding to the entering extraction steam and the outlet feedwater temperature (usually expressed in degrees F). The value could be either positive or negative, and is calculated as $TTD = (T_1-T_6)$, where the subscripts refer to locations in Fig. 5.1.4.

Drain Cooler Approach (DCA) is the difference between the temperatures of the drain water leaving the shell side of the heater and the feedwater entering on the tube side. This value is calculated as $DCA = (T_3-T_4)$, where the subscripts refer to locations in Fig. 5.1.4.

Logarithmic Mean Temperature Difference (LMTD) is the ratio of the difference between the initial temperature difference and the terminal temperature difference to the Napieran Logarithm of the ratio of the initial temperature difference to the terminal temperature difference in degrees F. This value is calculated as $LMTD = [(T_1-T_4) - (T_1-T_6)]/\ln [T_1-T_4) / (T_1-T_6)]$, where the subscripts refer to locations in Fig. 5.1.4.

Tube Side Pressure Drop consists of the friction loss through the tubes, including inlet and outlet channel losses.

Shell Side Pressure Drop is the pressure loss through the zones of the heater, and does not include any static losses.

The heat transfer mechanisms of interest for modeling are condensation in the shell region, convective heat transfer inside the drain cooler region and feedwater tubes, and conduction across the walls of U-tubes. The HEATR component is based on the TEE component, which allows the two vapor streams (steam from the turbine exhaust and condensate from the high-pressure heater) to join at the shell region represented by the junction cell (JCELL) of the TEE component. The feedwater flow inside the U-tubes was modeled with a separate PIPE component.

Fig. 5.1.5 shows the schematic of TRAC nodalization for a feedwater heater. Cell 1 of the HEATR component is the JCELL, which represents the shell region, while Cells 2, 3, and 4 represent the drain cooler region. The HEATR component contains appropriate correlations for condensation and convective heat transfer, as well as a drain control valve, such that the

downstream flow area of the cell at the drain outlet can be adjusted by a control system. Adjusting the drain control valve flow area via a control system requires knowledge of the condensate level inside the shell region, which was interpolated from a table of shell liquid level versus the shell void fraction, which is required as input to TRAC-B or TRAC-M. A phase-separation model inside the shell region then allowed only the condensate to flow from the shell region (Cell 1) into the drain cooler region (Cell 2) as long as the condensate level was maintained above the inlet to the drain cooler. However, always maintaining a condensate level above the drain cooler inlet required a control system action to regulate the drain flow. Consequently, a control system was built to adjust the flow area of the drain control valve (Cell 5) based on the condensate level error (i.e., the difference between the condensate level set point and the actual condensate level). This control system action to maintain a steady condensate level inside the shell region was critical for accurate modeling of the steady state and transient behavior of the feedwater heaters.

5.1.1 Requirements

This section presents the four functional requirements that were identified and implemented for the HEATR component into TRAC-M, along with its input and output (I/O) requirements. These requirements emphasize the design features that the new HEATR component in TRAC-M must possess in order to match the current capabilities of the HEATR component in TRAC-B. In other words, the following functional requirements must be considered during the design of the HEATR component in order to achieve a fully functional BWR heater model.

Requirement HEATR 1: The Hydraulics

The HEATR component model in TRAC-M will rely on the TEE component to model the shell side flow, as does the current HEATR component in TRAC-B. Thus, the TEE component modules and subroutines performing standard tasks (such as input, output, dump, restart, and graphics) will also be used by the HEATR component to perform the same tasks. This new component in TRAC-M will continue to use the generic two-fluid equations and numerical scheme for one-dimensional components, as do the other one-dimensional hydraulic components. The HEATR and TEE components should produce identical solutions when all heater-specific models (such as heat transfer correlations) are excluded from the HEATR component.

Requirement HEATR 2: Shell Liquid Level

During a normal operation, the condensate level inside the condensing zone always remains above the inlet to the drain cooler zone so that no vapor is entrained. The HEATR component in TRAC-B correlates the liquid level inside the condensing zone versus the void fraction (assuming that all vapor and water are separated) using a table provided by the user. The HEATR component in TRAC-M shall inherit the same method of correlating the shell liquid level from the void fraction. The phase separation model, which simulates the flow from the shell region to the drain cooler, will be tested for TRAC-M and TRAC-B, and the results should be identical.

Requirement HEATR 3: Drain Flow Control Valve

Maintaining a steady water level inside the condensing zone is essential to the operation of any heater. A steady water level inside the shell volume is the result of carefully controlling and

balancing the drain outlet flow rate to match the rate at which the steam inside the shell volume is condensed. In both codes, the flow area representing the drain cooler outlet can be controlled through the use of a user-defined control system. This system should give the TRAC-M user the capability to control the water level in the condensing zone by controlling the drain cooler outlet flow rate. Testing with a sinusoidal driving force should produce a sinusoidal change in flow area.

Requirement HEATR 4: Shell-Side Heat Transfer

To accurately model the heat transfer processes in a feedwater heater, heat-transfer correlations appropriate to condensation on horizontal and vertical tubes banks were implemented into TRAC-B. The same correlations will be incorporated into the TRAC-M HEATR component. In addition to the condensation correlations, a correlation for single-phase (liquid) heat transfer convection across tube banks was implemented in TRAC-B to better describe the behavior in the liquid-filled regions of the feedwater heater. The same correlation will also be implemented in the TRAC-M HEATR component.

A realistic simulation of a feedwater heater will help to verify that the heat exchange rate between the TRAC-M HEATR component (which represents the shell side) and the PIPE component (which represents the U-tubes) is consistent with the feedwater heater specifications. A three-way comparison between the specifications of the heater being simulated and both TRAC-B and TRAC-M will be made. Various parameters discussed in the requirements (such as terminal temperature difference, drain cooler approach, steam flow rate, and heater duty) will be used in this comparison. The code results should agree reasonably well with the heater specifications.

5.1.2 Verification Testing and Assessment

This section presents the results of the verification testing and assessment of the integration of the heater component from TRAC-B to TRAC-M(F90). The results show that the integration of the heater component has been correctly performed.

Test HEATR 1. The Hydraulics

The flow through a typical BWR feedwater heater geometry was simulated using the TRAC-M TEE and HEATR components, and the results were compared. As long as the same result is obtained for a given flow problem, this ensures that the design and implementation steps involving hydraulics to meet Requirement HEATR 1 are free from any error.

Four input decks were built. Input decks TeeSS.inp (steady-state) and Tee.inp (restart-transient) simulated all liquid flow through the heater geometry. Later, the same flow through the feedwater heater geometry was simulated with input decks HeatrSS.inp (steady-state), and Heatr.inp (restart-transient). In this instance, the TEE component was replaced with the new HEATR component. The results obtained for these tests were identical (NULL difference), thereby meeting the acceptance criteria for this test. See Fig. 5.1.6.

Test HEATR 2. Shell Liquid Level

An input was set up using the typical feedwater heater geometry with the entire heater component flooded with liquid at 350°F and 225 psia. To simulate the conditions inside the shell region with the condensate level above and below the drain cooler inlet, air was injected into the shell region from the top to force the liquid to flow into the drain cooler. The use of air (rather than water vapor) helped to eliminate condensation effects and to isolate the changes in the solution that are attributable to the changing shell liquid level.

As the air replaces the liquid inside the shell region, the shell liquid level should decrease until the liquid level reaches the drain cooler inlet. Once the liquid level clears the drain cooler inlet, only air should flow from the shell region into the drain cooler, and the shell liquid level should remain just below the drain cooler inlet.

Initially, a steady state was obtained for both TRAC-B and TRAC-M using input decks LiqLevelBSS.inp and LiqLevelMSS.inp. Following the steady-state runs, two transient calculations for each code were restarted, in which the liquid was drained from the shell region by the force of air injection. The shell liquid levels predicted by TRAC-B and TRAC-M are depicted in Fig. 5.1.7. The third curve in Fig. 5.1.7 is the signal variable defined for the shell liquid level. This plot verifies that the signal variable is properly implemented and works as designed.

The other variables of interest in this test calculation are the cell average void fraction inside the shell region, and the cell edge void fraction defined at the drain cooler inlet. Fig. 5.1.8 compares these void fractions predicted by the two codes. Notice that the cell edge void fraction at the drain cooler inlet calculated by TRAC-B indicates a small liquid entrainment into the drain cooler. By contrast consistent with the phase-separation model, TRAC-M predicts zero liquid fraction at the drain cooler inlet after the shell liquid level reaches the inlet and remains below it. Although some entrainment is physically expected, no physical model to address this process exists in TRAC-B. Therefore, the small liquid void fraction seen in Fig. 5.1.8 is attributable to different numerics in TRAC-B and TRAC-M.

The last variable worthy of comparison between the two codes is the time step size (see Fig. 5.1.9), which is momentarily reduced to 0.025 s when the cell edge void fraction at the drain cooler inlet makes the transition from zero to one, and is recovered back to 0.25 s, which is the maximum time step size specified as input. A comparison of the time step size between the two codes reveals that TRAC-B (unlike TRAC-M) has difficulty with the transition of the cell edge void fraction at the drain cooler inlet following the uncovering of the drain cooler inlet, and the time step size in TRAC-B is not recovered.

Test HEATR 3. Drain Flow Control Valve

In this test, a control system was built to drive the drain control valve flow area following a sinusoidal function. The location of the drain valve and the control block output (which would be the area fraction multiplying the actual valve flow area) were specified using the input variables. The control system used in input deck DrainValve.inp follows the function given by the following equation:

$$f(t) = f_0 + \sin\frac{2\pi t}{T} \qquad (5.1.1)$$

where $f_0 = 0.5$ and $T = 20$ s.

Following the driving function given by Equation 5.1.1, the flow area of the drain valve should initially be half of the full available flow area, and should oscillate as a sine wave with a period of 20 seconds. Both the flow area fraction (a control block output) and the flow area of the drain control valve are plotted in Fig. 5.1.10. As can be seen from the figure, the valve flow area behaves as expected, fully satisfying Requirement HEATR 3.

Building a condensate level controller is essential before taking any steps to design and implement the shell-side condensation model. Using the CON (cb10) and PI (cb20) control blocks, a condensate level controller was built as shown in Fig. 5.1.11. This controller is essential to simulate the typical feedwater heater that will be used to verify the design and implementation of the shell-side condensation model.

Test HEATR 4. Shell-Side Heat Transfer

This test is designed to fulfill the Requirements identified as HEATR 4 and CNSYS 5.4 (in Section 5.5). Two sets of input decks were built. Figs. 5.1.5 and 5.1.11 show the nodalization and control system diagrams used in these analyses, respectively. Each set contains two input decks, one for TRAC-B and the other for TRAC-M. The first set of input decks, ShellHTB.inp and ShellHTM.inp, simulated the feedwater heater operating conditions without the condensate from the high-presure (HP) heater. The second set of input decks, DrainFlwB.inp and DrainFlwM.inp, included this condensate.

The steam temperature, pressure, and flow rate from the turbine at the shell inlet, the condensate flow rate from the HP heater, the feedwater inlet temperature, and the flow rate were fixed as boundary conditions. (See Table 5.1.1.) Four variables were selected for a comparison between TRAC-B and TRAC-M. Specifically, these variables were the shell condensate level, the drain mass flow rate, the drain cooler approach, and the feedwater temperature rise.

As shown in Fig. 5.1.12, the condensate level inside the shell reached the setpoint in the calculations carried out by both codes. The shell void fraction corresponding to this liquid level (0.897) was accurately predicted by both codes. Note that the heater specifications indicate a steady-state operation. The codes first calculate transient behavior, and converge to steady-state values in about 250 s. The rate at which the condensate flows into the drain cooler is equal to the sum of the condensate flow rate from the HP heater and the condensation rate of the steam flow from the turbine. In tests ShellHTB.inp and ShellHTM.inp, the condensate flow rate from the HP heater was zero. Thus, the rate at which the condensate flows into the drain cooler region was equal to the rate at which the steam flow from the turbine was condensed inside the shell region. As can be seen in Fig. 5.1.13, a comparison between the two codes showed that both predicted the same drain flow rate into the drain cooler region, indicating that the vapor inside the shell region

was condensed at the same rate. This flow rate agreed reasonably well with the 323568-lbm/h steam flow rate of the typical heater model specification.

From Figs. 5.1.12 and 5.1.14, one could conclude that TRAC-B had a difficult time in arriving at a steady flow and maintaining a steady shell condensate level (because of rather unstable vapor condensation), while TRAC-M displayed a stable solution. The other indication of this oscillatory vapor condensation predicted by TRAC-B was seen in the drain cooler approach (T_3 - T_4). As shown in Fig. 5.1.14, the temperature predicted by TRAC-B for the condensate exiting the drain cooler region oscillated following the oscillatory flow of condensate into the drain cooler region, while the same temperature predicted by TRAC-M showed no signs of oscillation.

Perhaps, the most important variable compared between the two codes was the temperature of the feedwater leaving the heater. Comparing the feedwater exit temperature between the codes was another way to compare the heat load, since the feedwater flow rate, inlet pressure, and temperature were all fixed as boundary conditions. Fig. 5.1.15 depicts the feedwater exit temperatures predicted by TRAC-B and TRAC-M, which are reasonably close to each other, indicating the same heat load.

The same test was repeated after the condensate flow from the HP heater was included as a flow boundary (662537 lb_m/h, 400°F and 375.45 BTU/lb_m at 278.8 psia) to the side arm of the HEATR component. The setpoint for the shell condensate level was not changed. Therefore, the shell void fraction and shell liquid level remained the same when the tests were repeated with the addition of drain flow from the downstream heater. Three variables worthy of comparison for the repeated tests were the drain flow rate, drain cooler approach, and feedwater temperature rise.

Under steady-state conditions, the drain flow rate would be the sum of the condensate flow rate from the HP heater and the steam flow from the turbine into the shell region. As shown in Fig. 5.1.16, both TRAC-B and TRAC-M predicted this flow rate reasonably close to the flow rate (986105 lb_m/h) specified for the typical feedwater heater used as the basis for these tests.

On the other hand, the drain cooler approach was predicted differently by the two codes, as depicted in Fig. 5.1.17. TRAC-B predicted a temperature closer to the temperature specified for the drain exiting the typical feedwater heater (i.e., 6.1°F), while the drain cooler approach predicted by TRAC-M was almost 12°F. A brief investigation indicated that the use of cell edge hydraulic diameters in the TRAC-M heat-transfer correlations resulted in heat-transfer coefficients inside the drain cooler region that were three times smaller than those predicted by TRAC-B (1000 W/m^2K vs. 3000 W/m^2K). Smaller heat-transfer coefficients drove the temperatures inside the drain cooler region higher, since the heat load determined by the heat-transfer inside the tubes had to be maintained. To remedy this deficiency, it is highly recommended that the heat structure (HTSTR) component in TRAC-M be modified to use volume average hydraulic diameters and fluid velocities. It is planned to change the coding in TRAC-M to eliminate this deficiency. Nonetheless, the most important variable was the feedwater temperature rise, and both codes predicted this temperature rise reasonably close to each other, as shown in Fig. 5.1.18. The specified temperature rise (ΔT = 44°F) for the typical

feedwater was used as the basis for the test. The code results agree reasonably well with the heater specifications, thereby satisfying Requirement HEATR 4, and they also show that the functionality of Requirement CNSYS 5.4 is satisfied.

5.1.3 Conclusion

The heater (HEATR) component is correctly implemented in TRAC-M.

REFERENCES

5.1.1 "River Bend Station Updated Safety Analysis Report," Vol. 17, Chapter 10.

Table 5.1.1 Typical Feedwater Heater Boundary Conditions

Bled Steam from Turbine	Flow Rate (lb_m/h)	323,568.00
	Enthalpy (BTU/lb_m)	1,101.96
	Temperature (^oF)	392.19
	Pressure (psia)	226.00
Condensate from HP Heater	Flow Rate (lb_m/h)	662,537.00
	Enthalpy (BTU/lb_m)	375.45
	Temperature (^oF)	400.32
	Pressure (psia)	247.00
Feedwater Flow	Flow Rate (lb_m/h)	6,204,817.00
	Enthalpy (BTU/lb_m)	314.62
	Temperature (^oF)	342.77
	Pressure (psia)	410.00

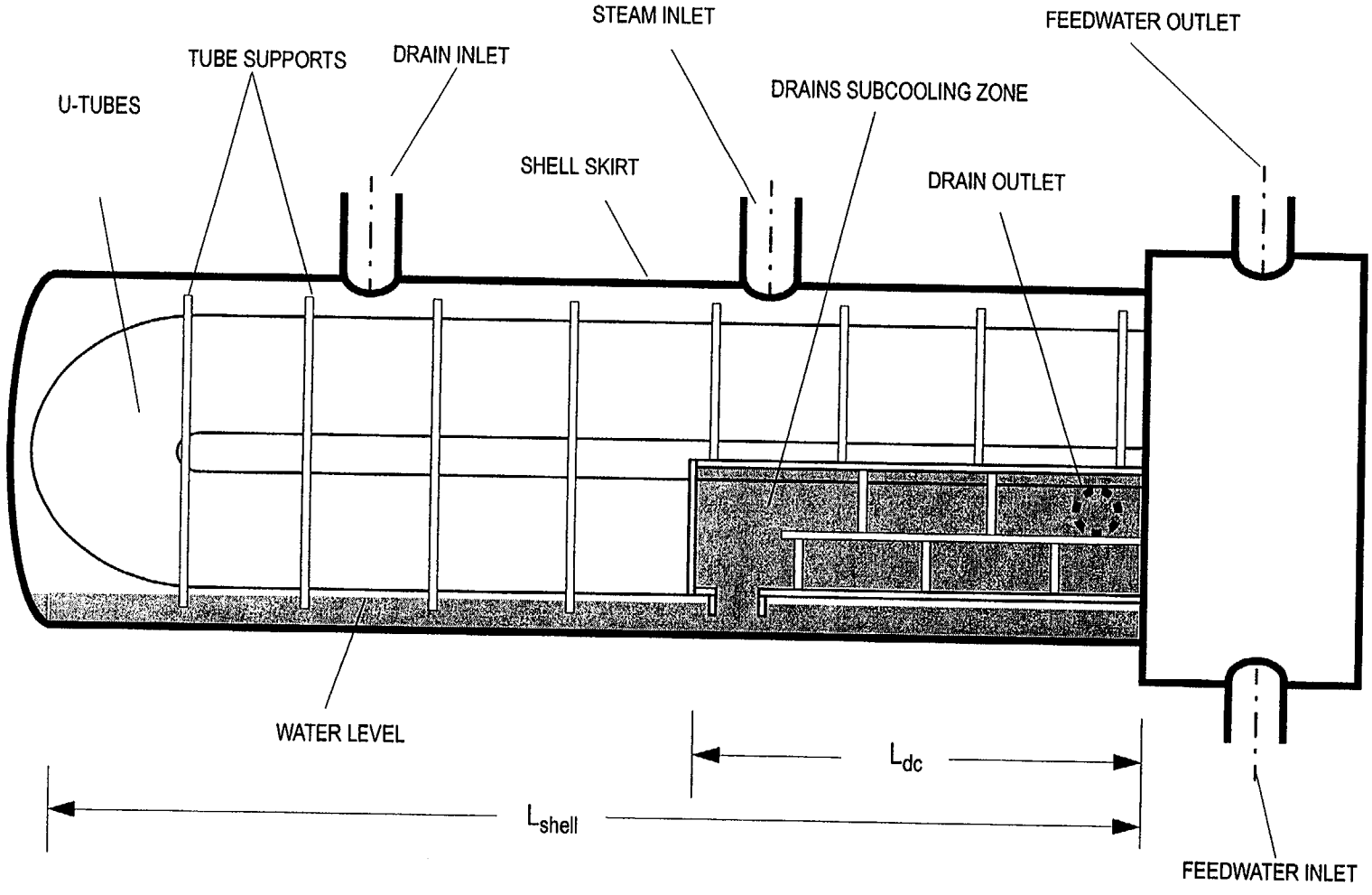

Figure 5.1.1 Typical Two-Zone Feedwater Heater (condensing and subcooling zones)

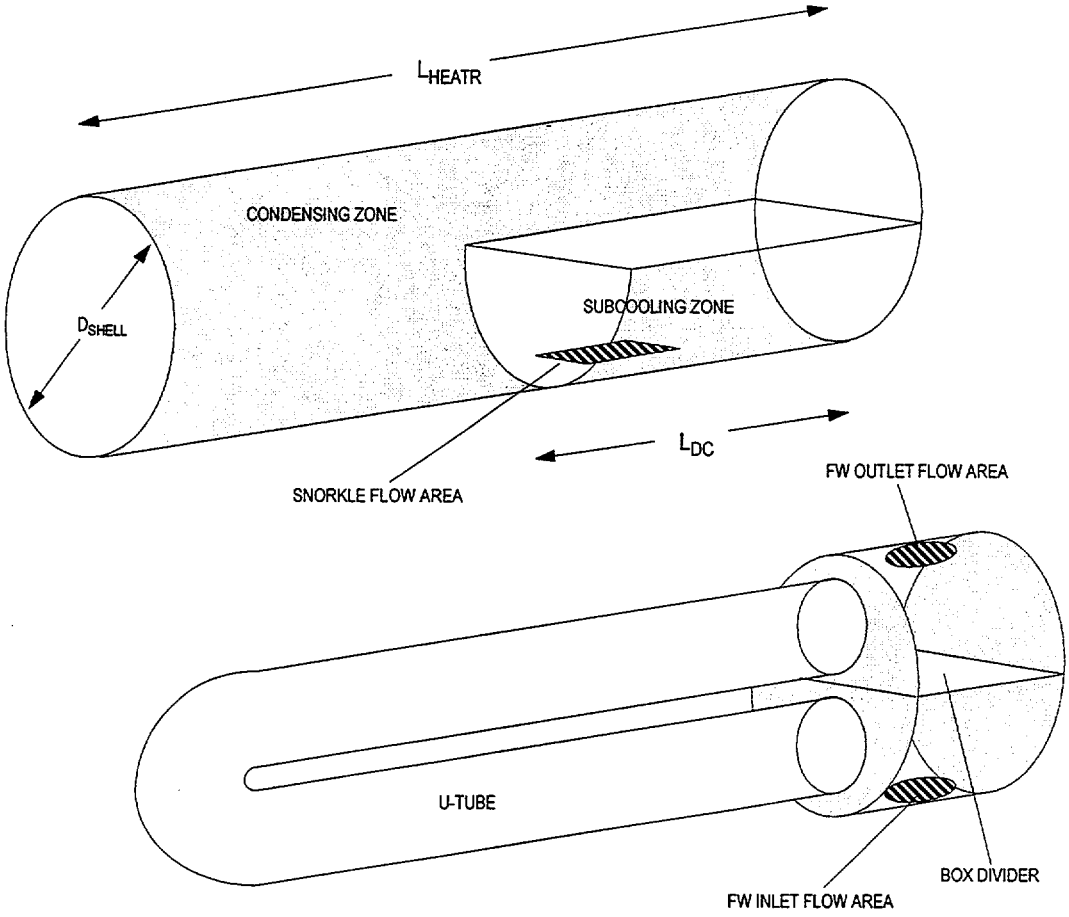

Figure 5.1.2 Sketch of a Simple Feedwater Heater

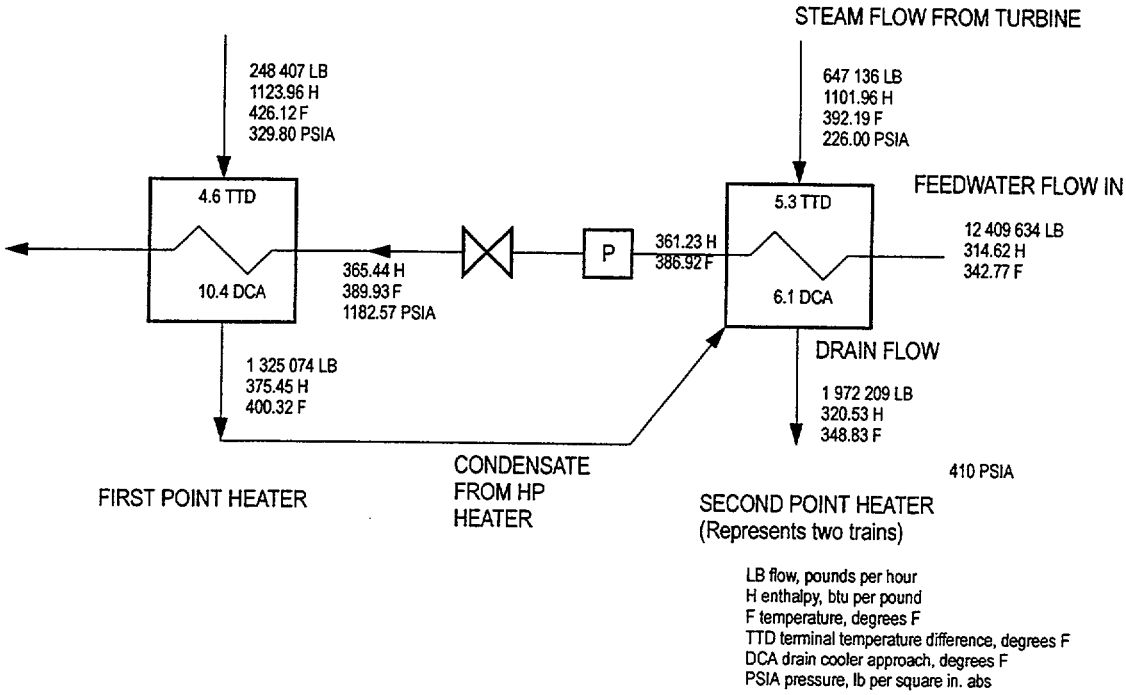

Figure 5.1.3 Heat Balance and Flows for the First and Second Point Heaters of River Bend Station

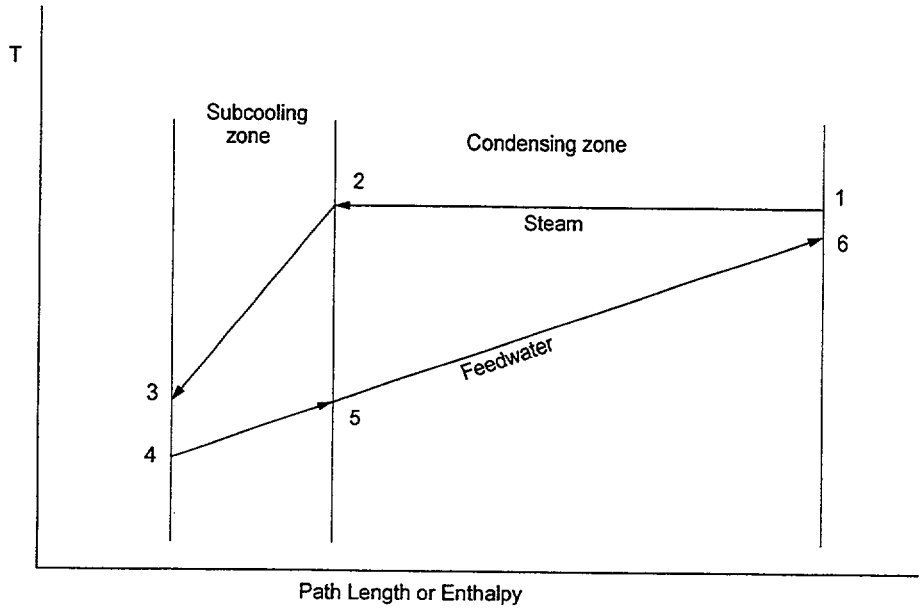

Figure 5.1.4 Temperature-Path Length Diagram for a Two-Zone Closed Heater

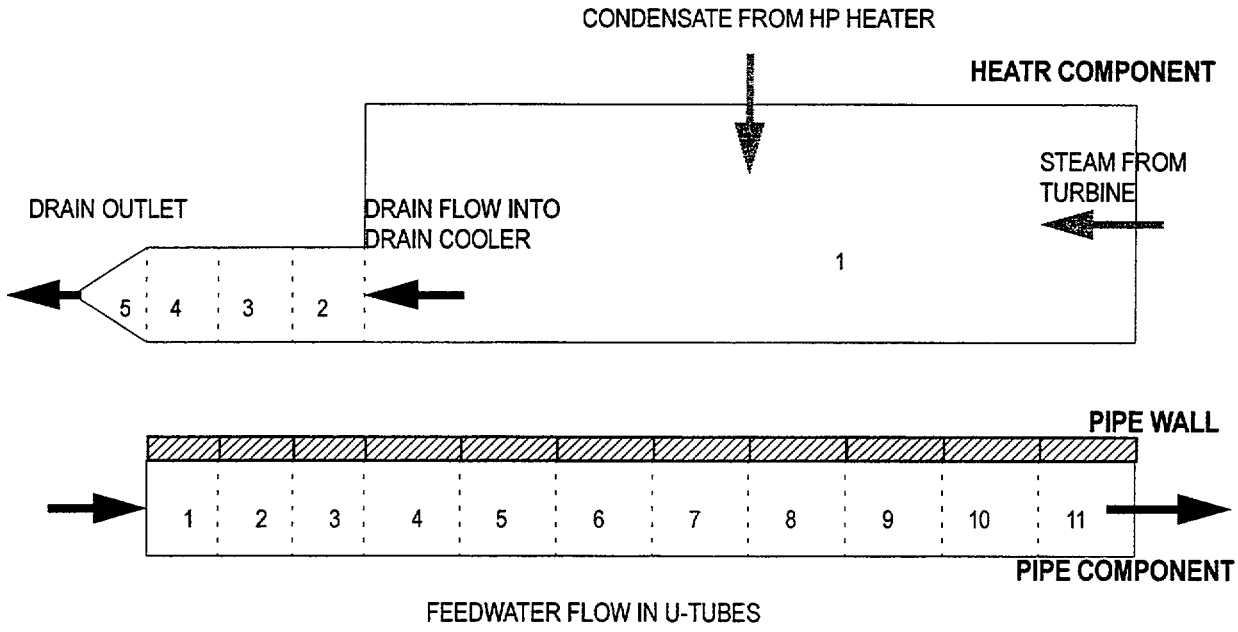

Figure 5.1.5 Schematic of a Two-Zone Closed Feedwater Heater

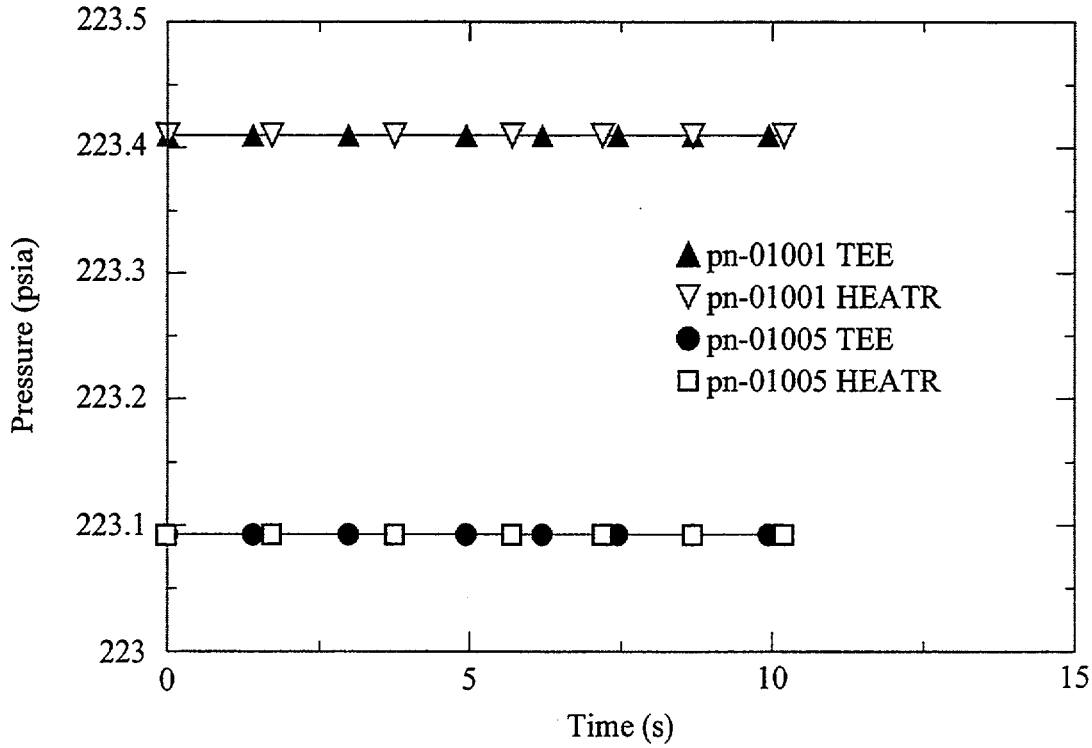

Figure 5.1.6 Comparison of Shell and Drain Cooler Pressures

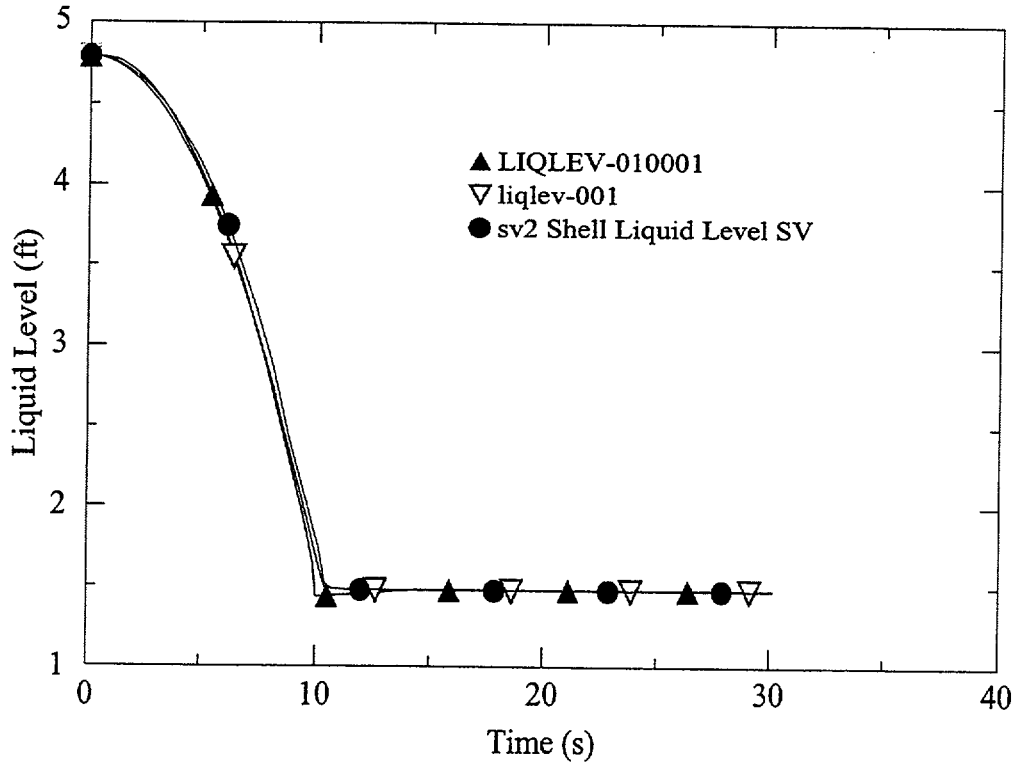

Figure 5.1.7 Shell Liquid Level

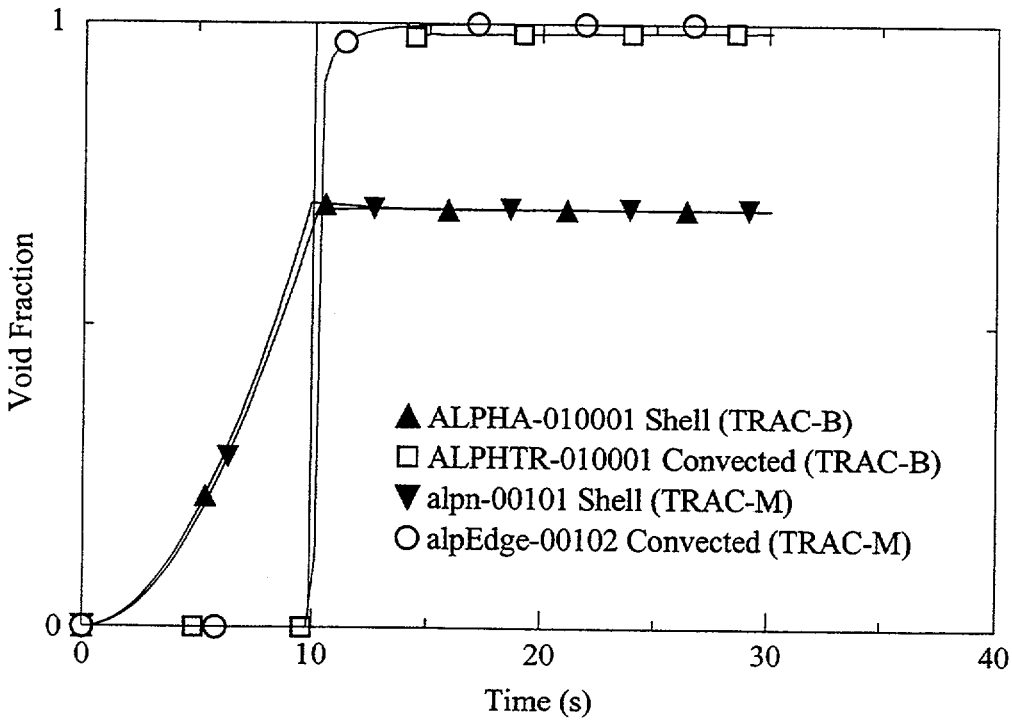

Figure 5.1.8 Cell Edge Void Fraction Defined at the Drain Cooler Inlet

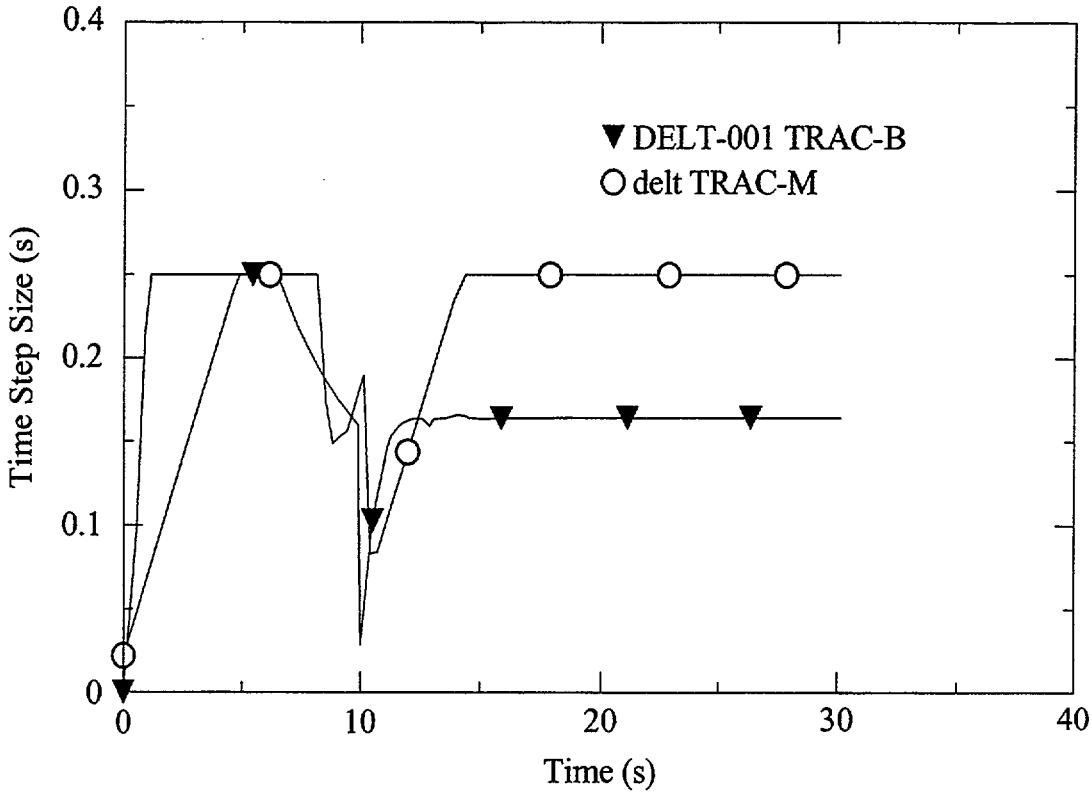

Figure 5.1.9 Timestep Size Used by TRAC-B and TRAC-M

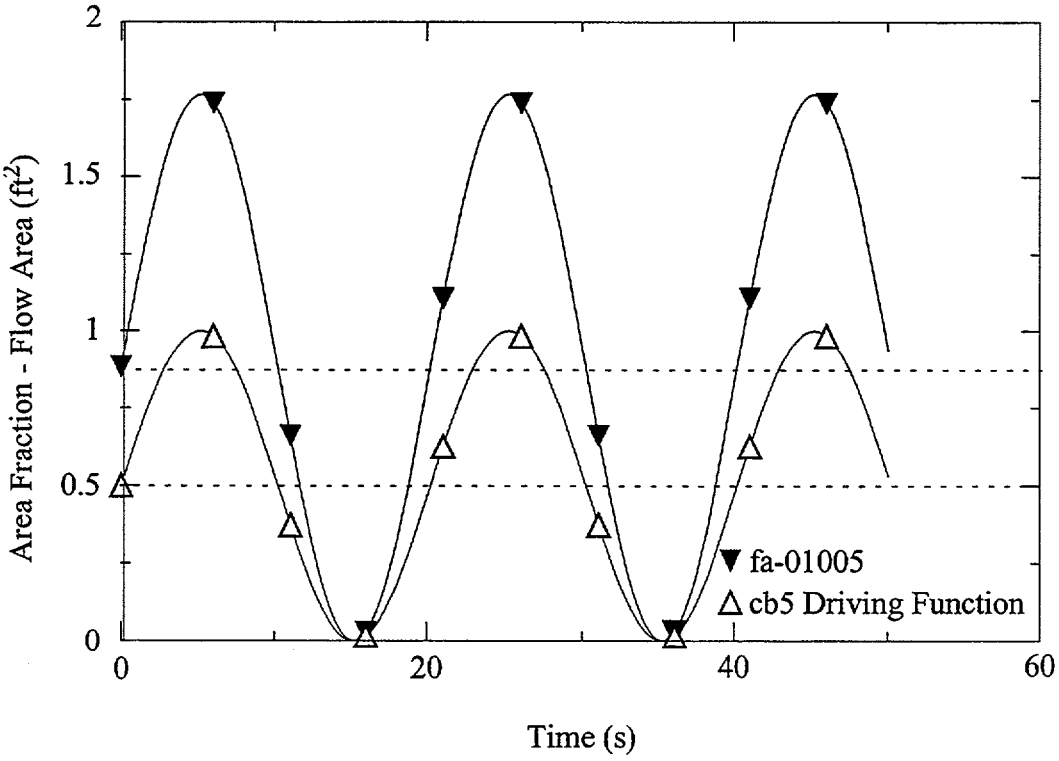

Figure 5.1.10 Drain Valve Flow Area Driven by Equation 5.1.1

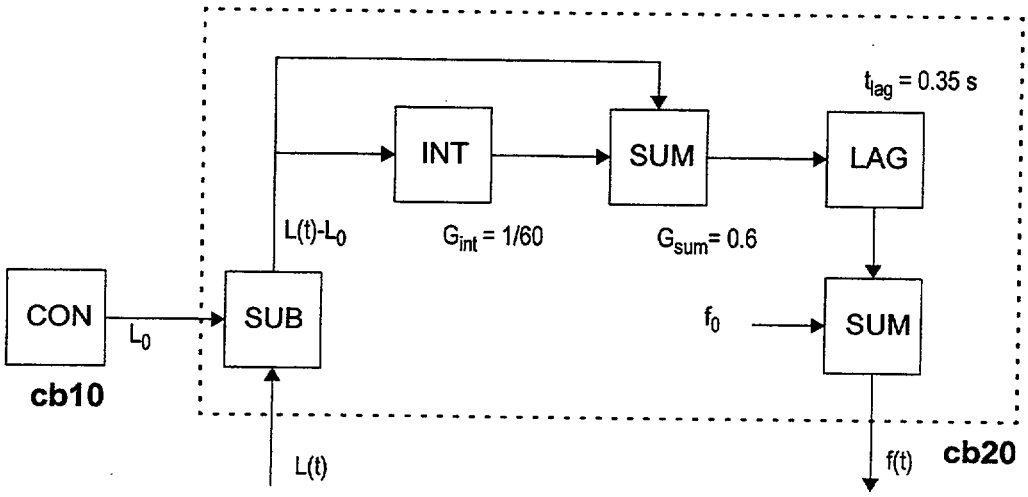

Figure 5.1.11 Shell Condensate Level Controller

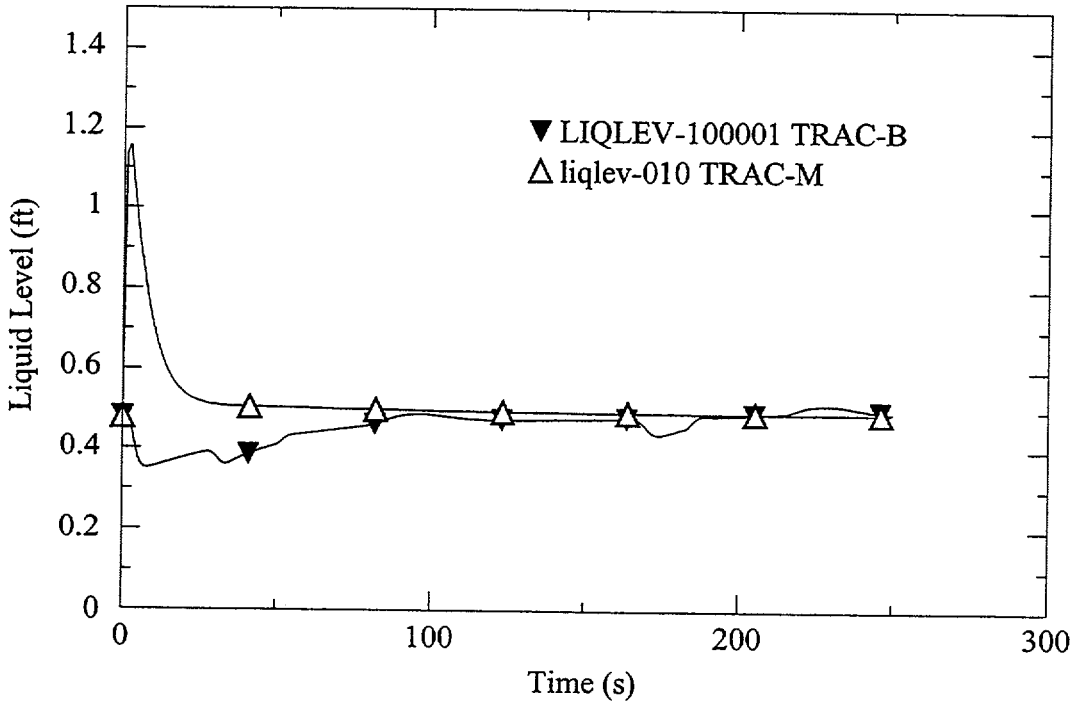

Figure 5.1.12 Condensate Level (no condensate flow from the HP heater)

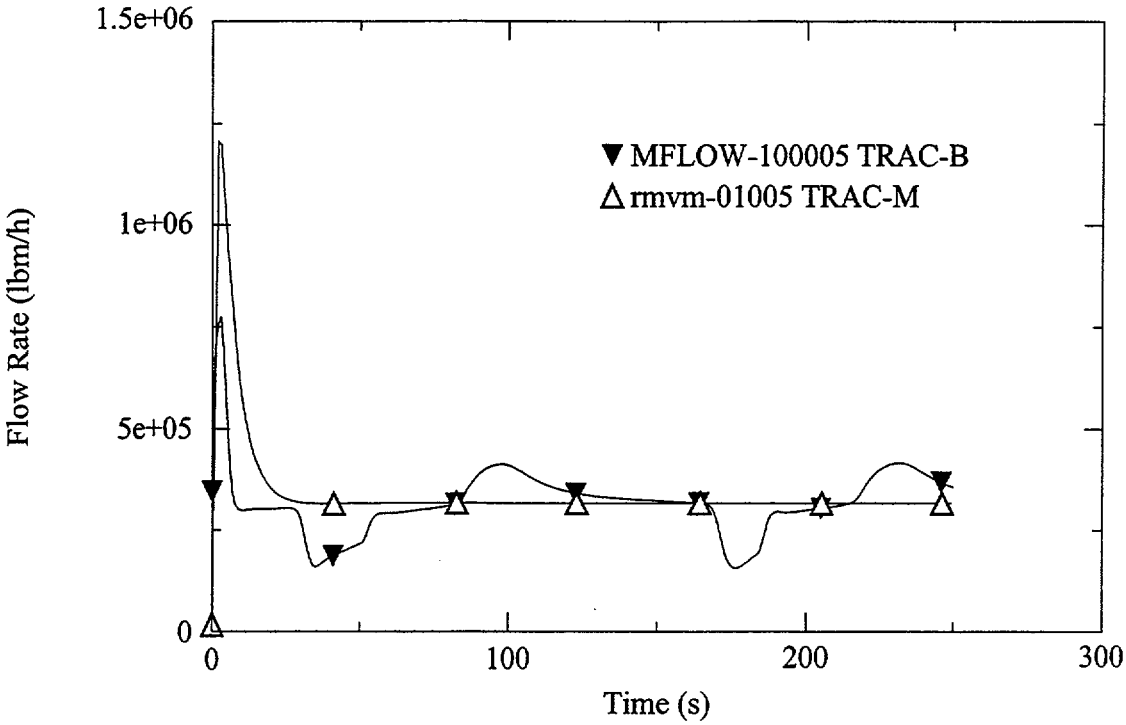

Figure 5.1.13 Drain Flow Rate (no condensate flow from the HP heater)

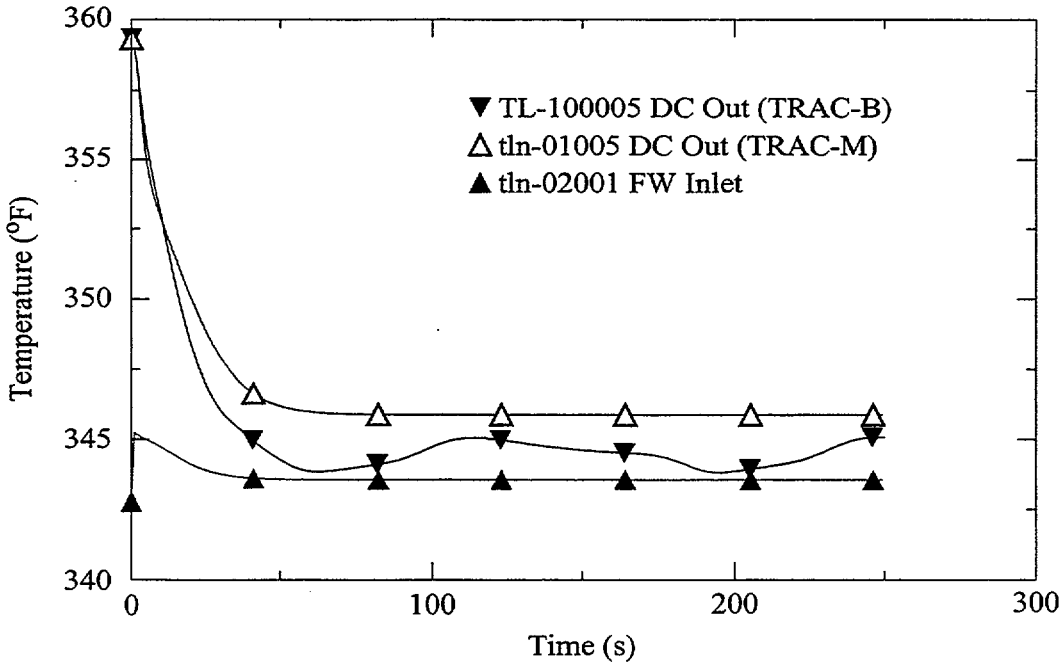

Figure 5.1.14 Drain Cooler Approach (no condensate flow from the HP heater)

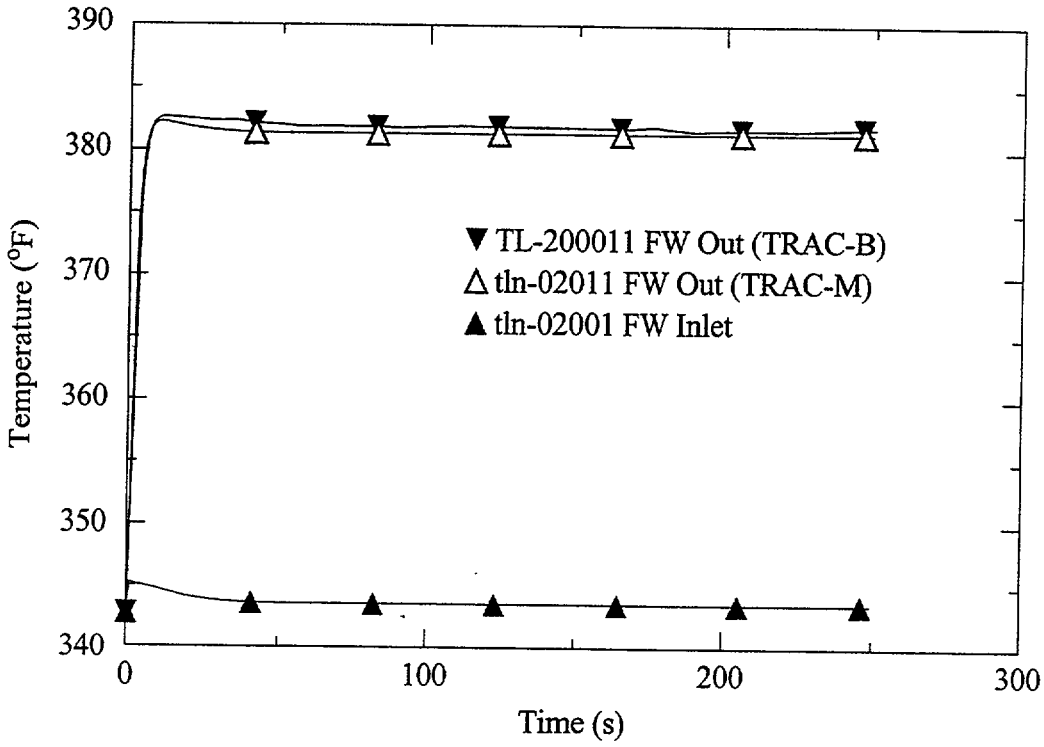

Figure 5.1.15 Feedwater Temperature Rise (no condensate flow from the HP heater)

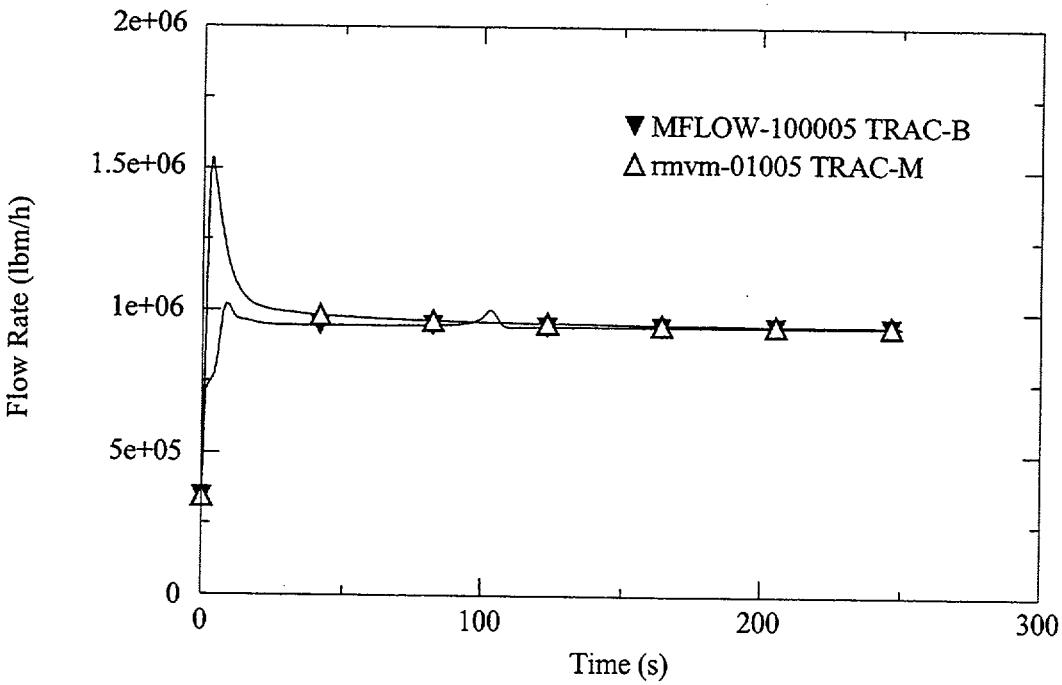

Figure 5.1.16 Drain Flow Rate

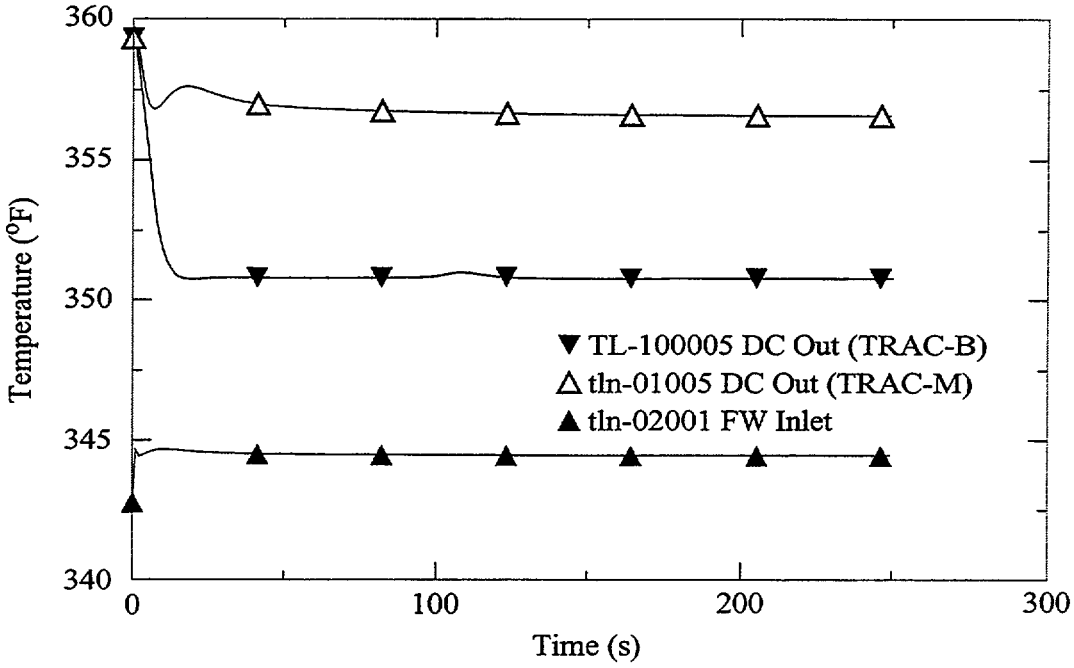

Figure 5.1.17 Drain Cooler Approach

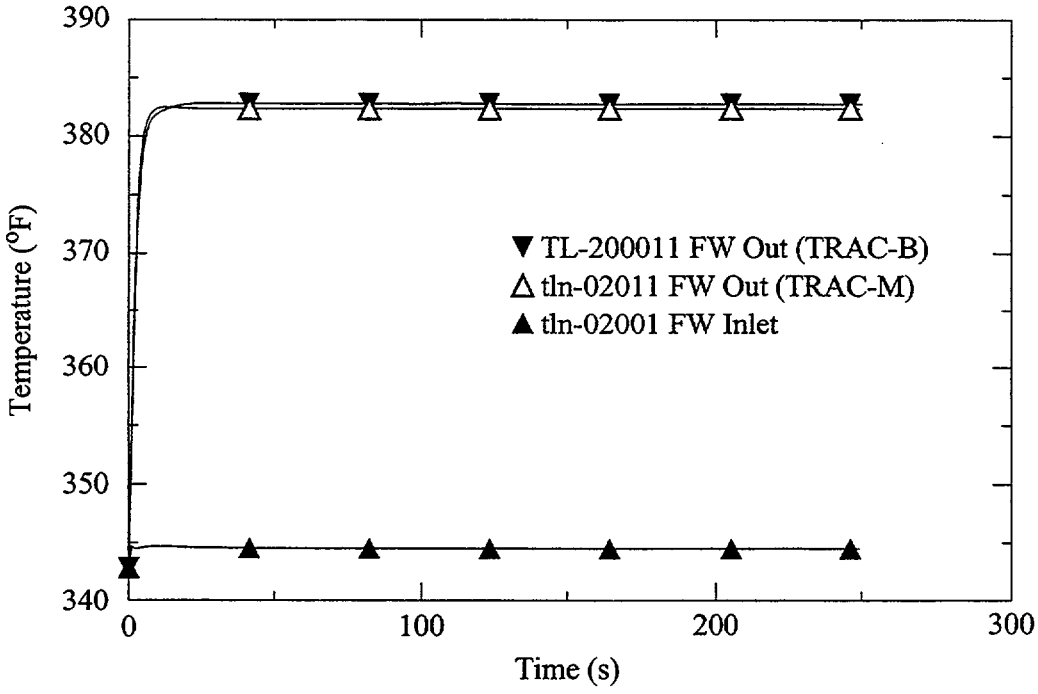

Figure 5.1.18 Feedwater Temperature Rise

5.2 Jet Pump (JETP) Component

Jet pumps are used inside the reactor pressure vessels of some BWRs, as part of the reactor recirculation system. Specifically, BWR/3 to BWR/6 designs have been equipped with jet pumps. Typically, such BWRs have 20 jet pumps, divided into two groups of 10, with each group supplying the flow to half (i.e., 180 degrees) of the core. In such configurations, the jet pumps are located inside the reactor vessel, in the downcomer annulus between the core shroud and the reactor vessel wall.

Jet pumps receive two input flows, including a high-pressure drive (or nozzle) flow and a low-pressure entrained stream referred to as suction flow. The jet pumps then mix these two streams into a single medium-pressure exit flow.

As the flow emerges from the jet pump nozzle with a high velocity and high momentum, it entrains a large quantity of low-velocity, low-momentum downcomer flow into the jet pump throat section. At rated conditions, the suction flow is typically about twice the magnitude of the drive flow. The two streams then merge in the mixing section, and the diffuser section recovers some of the velocity head as static head.

The drive flow is taken from one of two recirculation lines that exit the vessel through a penetration in the lower downcomer. The drive flow is then pumped to a higher pressure, using a variable-speed recirculation pump (BWR/3,4, some BWR/5s) or a two-speed pump and flow control valve combination (some BWR/5s, BWR/6), and is finally distributed through a manifold into a number of risers. Each riser penetrates the vessel low in the downcomer annulus, and continues to rise until it is capped with a rams head flow divider, which directs the flow from the riser to two jet pump nozzles. Using jet pumps, a small flow is pumped to a high head so that a large flow can receive a medium head. Only one-third of the core flow passes through the recirculation pumps, while two-thirds of the flow does not leave the reactor vessel.

5.2.1 Requirements

The following seven requirements provide a road map for creating a JETP component in TRAC-M from the TEE component, in the same way that the JETP component in TRAC-B was originally developed from the TRAC-B TEE component. These requirements define the critical elements of the current JETP component in TRAC-B, which are necessary to provide TRAC-M with the same capabilities of the JETP component in TRAC-B.

Requirement JETP 1. The Hydraulics

The JETP component model in TRAC-M will be based on the TEE component model, as is the current JETP component in TRAC-B. Thus, the JETP component will use the TEE component procedures and modules to perform standard tasks, such as input, output, dump, restart, and graphics. The schematic of a JETP component is shown in Fig. 5.2.1. This new component in TRAC-M will use the generic two-fluid (TF) equations and numerical scheme for one-dimensional components, together with the existing constitutive relations of TRAC-M for wall drag, interfacial shear, and heat transfer, which are also used by the TEE component. Therefore, the new JETP component should produce solutions that are identical to those generated by the TEE component, when all JETP-specific models are excluded. (JETP-specific models are discussed in the following additional requirements.)

Requirement JETP 2. Reversible Pressure Gains and Losses

The JETP component must accurately predict the reversible pressure changes across smooth area changes (such as nozzle and diffuser sections).

Requirement JETP 3. Pressure Rise Associated With the Mixing of Suction and Drive Flows

The JETP component in TRAC-M must accurately predict the pressure rise associated with the mixing of suction and drive flows.

Requirement JETP 4. Irreversible Pressure Losses

The current JETP component in TRAC-B models 1) geometry using one-sixth scale jet pump data, 2) irreversible losses attributable to incomplete mixing, and 3) additional information correlated as flow-dependent formulas. The JETP component in TRAC-M will model the irreversible losses in the same manner as TRAC-B. The performance of the JETP component in TRAC-M must match the performance of the current JETP component in TRAC-B.

Requirement JETP 5. Multiple Jet Pumps

The current JETP component in TRAC-B is capable of modeling a single jet pump assembly or multiple jet pumps in parallel lumped together. The JETP component in TRAC-M will also have this capability.

Requirement JETP 6. Flow and Conduction Coupling with the Reactor Vessel

In most TRAC-B plant models, the JETP component is connected across the downcomer region of a VESSEL component with standard vessel sources. In addition to a hydraulic coupling to the downcomer region of a VESSEL component, the current JETP component in TRAC-B allows specifying a wall heat transfer between its hydraulic cells and a VESSEL component. Therefore, the JETP component in TRAC-M should allow its component junctions to be defined as standard sources to the VESSEL component, and should also be capable of conducting heat between its hydraulic cells and outside hydraulic cells (usually a VESSEL component) through its heat-conducting walls.

Requirement JETP 7. Scalability

The current JETP component in TRAC-B was primarily developed using the one-sixth scale INEL jet pump data. The accuracy of the JETP component in TRAC-B was tested using the same data. The design and testing of the JETP component in TRAC-M will also rely on the one-sixth scale jet pump data obtained by the Idaho National Engineering Laboratory (INEL). However, like the current JETP component model in TRAC-B, the JETP component in TRAC-M should be sufficiently general that it can be applied to full-scale BWR jet pumps.

5.2.2 Verification Testing and Assessment

The purpose of verification testing is to systematically test the JETP component in TRAC-M to verify that it meets the software requirements defined in Section 5.2.1.

Test JETP 1. The Hydraulics

The new JETP component should produce the same answer as the TEE component for a given flow problem when all JETP-specific models are excluded from the solution. To verify this, both the JETP and TEE components will be used to simulate a flow in a manner that is similar to one of the one-sixth scale INEL jet pump tests (Ref. 5.2.1). The JETP hydraulics test will be considered successful only after it is verified that the results from the steady-state and transient runs are identical for both the JETP and TEE components of TRAC-M. Fig. 5.2.1 shows a schematic of the jet pump nodalization that will be used in the JETP tests. In this nodalization, the primary leg has two cells in the mixing region, one in the diffuser, and one in the tail pipe. The side leg has one cell to model the nozzle, one to model the *rams head*, and one to model a section of the riser.

Comparison of the outputs from the calculations showed that both the JETP and TEE components yielded identical solutions. Fig. 5.2.2 shows that the pressures predicted by both components were *identical*.

Test JETP 2. Reversible Pressure Gains and Losses

For horizontal flows with no wall friction, the equation of motion yields a Bernoulli-type equation that relates pressure losses between cells that are adjacent to the reversible pressure changes.

$$P_{j+1} - P_j = \frac{1}{2}(\rho_{j+1} V_{j+1}^2 - \rho_j V_j^2) \tag{5.2.1}$$

where P is the pressure, V is the fluid velocity and ρ is the fluid density. Subscripts refer to cell numbers.

The term "reversible" is used here because the pressure loss associated with a contraction can be regained by a pressure rise at an expansion of the same magnitude. For properly calculated reversible losses across area changes at the jet pump diffuser and across inter-component junctions, the mechanical energy per unit mass, the so-called Bernoulli number, should be identical for every cell, as follows:

$$\frac{P_1}{\rho_1} + \frac{1}{2}V_1^2 = \frac{P_2}{\rho_2} + \frac{1}{2}V_2^2 = \ldots = \frac{P_N}{\rho_N} + \frac{1}{2}V_N^2 \tag{5.2.2}$$

The elevation head term is not included in the above equation, since this test considers the flow through a horizontal JETP component (thereby simplifying the computation of the Bernoulli number in TRAC-M). The Bernoulli numbers for mesh cells across the diffuser and the nozzle

sections will be compared. For the successful completion of this test, the Bernoulli numbers for these cells should be the same.

The input description of the scaled jet pump assembly from Test JETP 1 was modified to simulate the flow through a horizontal jet pump. Thus, the elevation term could be excluded from the Bernoulli expression computed for cells in the diffuser and the nozzle sections of the jet pump.

Fig. 5.2.3 depicts the Bernoulli expression computed using Equation 5.2.1 for Cells 2, 3, and 4 across the diffuser and the tail pipe sections, as well as for Cells 6, 7, and 8 across the nozzle and the riser sections (see Fig. 5.2.1 for cell numbers). The upper straight line in Fig. 5.2.3 corresponds to the Bernoulli expression for the cells across the diffuser, and the Bernoulli expression for these cells indicates that TRAC-M predicts the reversible pressure gain associated with the flow area across the diffuser reasonably well. The lower straight line corresponds to the Bernoulli expression for the cells across the nozzle, and the Bernoulli expression for these cells indicates that the reversible pressure loss between the nozzle (Cell 6) and the *rams head* (Cell 7) is slightly higher than the actual Bernoulli loss. Nonetheless, this is a small deviation, and it should be absorbed by the loss coefficients for the irreversible changes across the nozzle.

Test JETP 3. Pressure Rise Associated With the Mixing of Suction and Drive Flows

The implementation of the TEE component momentum source term of TRAC-M will be verified using an analytical calculation to ensure that it can accurately predict the pressure rise associated with the mixing of suction and drive flows.

Fig. 5.2.4 illustrates the mixing of suction and drive line flows. The equations of motion at Faces 2 and 6 are coupled through the convection terms, because the angle between the side leg and the low-numbered mesh-cell end of the primary leg is 0° (i.e., less than 90°). Therefore, the pressure rise associated with the mixing of the two streams is accounted for between the centers of Cells 1 and 2. In a TRAC model, the position of Face 2 must be chosen far enough downstream that the velocity at Face 2 can be assumed to be uniform. In other words, the suction and drive flows fully mix at Face 2. If only one cell is used to describe the throat section, the pressure rise associated with the expansion in the first half of the cell describing the diffuser section will interfere with the pressure rise associated with the mixing of the two streams with different velocities. Therefore, two cells will be used in the JETP tests to describe the throat section, to enable this test to verify the pressure rise associated with the mixing of the suction and drive flows.

The pressure rise associated with the mixing of the suction and drive line flows in the throat, and the reversible changes in pressure associated with the area change across the diffuser, will be calculated assuming constant density. This is a valid assumption, since the fluid used in the steady-state tests is subcooled, and its density is essentially constant throughout the jet pump at any point.

$$V_1A_1 - V_6A_6 - V_2A_2 = 0 \qquad (5.2.3)$$

where A is the cross-sectional area and $A_1 + A_6 = A_2$. Subscripts refer to the Face numbers in Fig. 5.2.4.

In the above equation, the positive direction of the flow at Face 6 is assumed to be to the left for consistency with the TEE component side arm. A uniform mixture velocity will then be determined as follows:

$$V_2 = \frac{A_1}{A_2}V_1 - \frac{A_6}{A_2}V_6 \tag{5.2.4}$$

Once the uniform mixture velocity is known, the pressure rise from Cell 1 to Cell 2 associated with the mixing of the two streams will be estimated from a force balance across the staggered momentum cell, neglecting the force on the pipe wall:

$$\rho(V_1)^2A_1 + \rho(V_6)^2A_6 - \rho(V_2)^2A_2 + P_1\bar{A}_1 - P_2\bar{A}_2 = 0 \tag{5.2.5}$$

The elevation head term is not included in the above equation, since this test will consider only the flow through a horizontal JETP component.

$$\frac{P_2 - P_1}{\rho} = \frac{A_1}{A_2}(V_1)^2 + \frac{A_6}{A_2}(V_6)^2 - (V_2)^2 \tag{5.2.6}$$

The pressure rise from Cell 1 to Cell 2 for the fluid conditions of INEL Test 96 will be predicted with Equation 5.2.6 and TRAC-M. These predictions will then be compared, excluding from the solution any frictional losses and all additional losses, since Equation 5.2.6 accounts for no losses.

Although the pressure rise predicted by TRAC-M will include the non-linear variations of fluid properties, it should compare reasonably well with the pressure rise predicted with Equation 5.2.6.

Test JETP 3 requires that a jet pump flow problem be simulated with both TRAC-B and TRAC-M, and the pressure rise associated with the mixing of the suction and drive line flows be compared against each other and against the pressure rise predicted by Equation 5.2.6.

The INEL jet pump Test No. 96, used in Test JETP 1, was used here, with the exception that this time, the jet pump component was positioned horizontally, and the jet pump component loss coefficients were set to zero. Irreversible pressure losses were excluded, thereby setting the loss coefficients to zero, since Equation 5.2.6 accounts for no losses. The volume flow rate at the jet pump discharge for Test No. 96 was known from the data. Thus, the fluid velocity corresponding to this volume flow could be calculated and applied as a flow boundary condition at the jet pump discharge.

Assuming a constant fluid density, V_6 and V_2 were found to be:

$$V_6 = \frac{A_9}{A_6}V_9 = \frac{8.0425 \cdot 10^{-4}\text{m}^2}{1.6286 \cdot 10^{-4}\text{m}^2}(4.9860\text{m/s}) = 24.6223\text{m/s} \tag{5.2.7}$$

$$V_2 = \frac{A_5}{A_2}V_5 = \frac{4.0715 \cdot 10^{-3}\text{m}^2}{6.6052 \cdot 10^{-4}\text{m}^2}(1.6328\text{m/s}) = 10.0647\text{m/s} \tag{5.2.8}$$

Using Equation 5.2.6, the pressure rise from Cell 1 to Cell 2 could be predicted as follows:

$$\frac{P_2 - P_1}{\rho} = \frac{4.9766 \cdot 10^{-4}\text{m}^2}{6.6052 \cdot 10^{-4}\text{m}^2}(5.3008\text{m/s})^2 + \frac{1.6286 \cdot 10^{-4}\text{m}^2}{6.6052 \cdot 10^{-4}\text{m}^2}(24.6223\text{m/s})^2 - (10.0647\text{m/s})^2 \tag{5.2.9}$$

$$P_2 - P_1 = \left(69.3531\frac{\text{m}^2}{\text{s}^2}\right)\left(739.8\frac{\text{kg}}{\text{m}^3}\right) = 51.30\text{KPa} \tag{5.2.10}$$

where the fluid density was evaluated at 7.479 MPa and 560 K.

TRAC-M predicted P_1 and P_2 to be 7.45881 MPa and 7.51008 MPa, respectively. That is, a pressure rise from Cell 1 to Cell 2 of 51.27 KPa is very close to the value shown in Equation 5.2.10. This result satisfies Requirement JETP 3.

Test JETP 4. Irreversible Pressure Losses

The JETP components of both TRAC-B and TRAC-M will be used to simulate the conditions of INEL Tests 96, 99, 149, 161, 167, and 214 (Ref. 5.2.1). The results of the code calculations will be compared against the pressure drop data, corrected for biases in measurement. A point-by-point comparison of pressure changes along the JETP component (i.e., $\Delta P_{c2 \rightarrow c1}$, $\Delta P_{c3 \rightarrow c2}$, etc...) with data from the INEL experiment will estimate the irreversible pressure losses, which together with the reversible pressure changes and the pressure rise associated with the mixing of the suction and drive line flows should yield an accurate total pressure change across the jet pump.

For these tests, the jet pump M and N ratios will be calculated and plotted against the INEL data.

The N-ratio is the ratio of the specific energy increase of the suction flow to the specific energy decrease of the driving flow. It accounts for the elevation head, and discounts the kinetic head associated with the discharge flow. That is:

$$N = \frac{P_{ds} - P_{su}}{P_{dr} - P_{ds} + 0.5\rho V_{dr}^2} \tag{5.2.11}$$

where

P_{su} the fluid pressure at the jet pump suction

P_{ds} the fluid pressure at the jet pump discharge

P_{dr} the fluid pressure at the jet pump drive line

V_{dr} the fluid velocity at the jet pump drive line

The M-ratio is defined as the ratio of the driven mass flow (suction flow) to the driving mass flow through the nozzle:

$$M = \frac{\text{Suction Mass Flow}}{\text{Drive Line Mass Flow}} \tag{5.2.12}$$

These ratios define the performance of the jet pump, and can be used to calculate its efficiency, as follows:

$$\eta = MN \tag{5.2.13}$$

Fig. 5.2.5 illustrates the six steady-state flow regimes that can exist within the jet pump under normal and abnormal BWR operating conditions. Six test points from INEL Tests 96, 99, 149, 161, 167, and 214 were tested. These tests were selected because the error in M-N ratios were small. The M-N ratios for both the positive and negative drive flows, covering Jet Pump Flow Regimes 1 to 5 were computed. Tables 5.2.1 and 5.2.2 present the parameters measured in the INEL test data. Tables 5.2.3 and 5.2.4 present boundary conditions applied in TRAC-M.

Figs. 5.2.6 and 5.2.7 verify that the irreversible losses from TRAC-B were appropriately implemented into TRAC-M. The error bars in Figs. 5.2.6 and 5.2.7 represent the mean N-ratios for the 95% confidence limits from the test data.

Additional tests were performed to verify how well the JETP components in TRAC-B and TRAC-M would compare with the INEL data and each other. Two tests were performed, one with a positive drive flow (i.e., Flow Regimes 1, 2, and 3), and another with a negative drive flow (i.e., Flow Regimes 4 and 5). These two tests covered a range of $-1 < M < 3$ for both negative and positive drive flows. Figs. 5.2.8 and 5.2.9 summarize the results obtained with TRAC-B and

TRAC-M for the one-sixth scale INEL jet pump tests. These results indicate that both the TRAC-B and TRAC-M predictions degrade for high jet flows (i.e., $2 < M < 3$). An effort to identify the reason for the degradation of the TRAC-M results in this range led to the evaluation of the momentum convection term in the stabilizer momentum equations. This evaluation revealed that the tilde velocity ($\tilde{V}$) at the junction next to the BREAK component (the jet pump suction boundary) was not updated during the back substitution stage of the stabilizer momentum equations. This failure leads to an extra pressure drop attributable to the $V \cdot \nabla\tilde{V}$ term in the stabilizer momentum equations, which is evaluated at the first cell face between Cell 1 of the JETP component and the BREAK component (simulating the suction pressure boundary condition). This problem with the stabilizer momentum equations will be corrected.

Test JETP 5. Multiple Jet Pumps

This test was designed to ensure that the JETP component meets the requirement that it must be capable of modeling multiple jet pumps in parallel lumped together (see Requirement JETP 5).

Two decks were built, one for a JETP component representing a single jet pump (i.e., NJETP=1), and another for a JETP component representing 10 jet pumps (i.e., NJETP=10). Since the flow areas and volumes of a single JETP component are scaled up for NJETP jet pumps, the volumes defined for the boundary components (BREAK and FILL) had to be scaled up accordingly.

TRAC-M was executed in both a steady-state and a null transient mode with each deck. Figs. 5.2.10 and 5.2.11 show the pressures and liquid velocities from the null transient. Fig. 5.2.10 compares pressures at the discharge (Cell 4) and the jet pump riser section (Cell 7), while Fig. 5.2.11 compares the liquid velocity at the suction inlet (Face 1). The comparison of these variables indicates that they were identical whether NJETP=1 or NJETP>1. As expected, the mass flow rate through the JETP component representing 10 jet pumps (19.52 kg/s when NJETP=10) was 10 times the mass flow through the JETP component representing a single jet pump (1.952 kg/s when NJETP=1), as shown in Fig. 5.2.12. Thus, modeling multiple jet pumps with a single JETP component was verified.

Test JETP 6. Flow and Conduction Coupling with the Reactor Vessel

This test requires that the JETP component be tested as a part of an integral BWR recirculation system. Along with the JETP component, this simulation includes BWR components, such as fuel channels (CHAN), separators (SEPD), and feedwater heaters (HEATR). The same requirement also applies to these components. The Peach Bottom Turbine Trip transient presented in Section 7.2 demonstrates that this requirement has been met.

Test JETP 7. Scalability

A full-scale jet pump model was simulated in this test. The dimensions of the full-scale jet pump, shown in Table 5.2.5, were determined from Ref. 5.2.2. In developing input decks, the same type of boundary components (BREAK and FILL components) used in the simulation of the

INEL jet pump tests were also used for the full-scale jet pump. A drive line flow of 200 liter/s was estimated from Ref. 5.2.2 and set at the drive line boundary. The discharge flow was parametrically increased from 300 liter/s to 750 liter/s at 7.05 MPa to obtain a range of $0.5 < M < 2.5$.

Fig. 5.2.13 depicts the N ratios obtained using both TRAC-B and TRAC-M. The two codes yield different predictions because they rely on different wall friction formulations. In previous tests performed with the INEL tests, the velocities were smaller, and the contribution of the wall drag was small. In a full-scale jet pump, this contribution is larger and, hence, the differences in the predictions are larger.

The data included in Fig. 5.2.13 were estimated from Ref. 5.2.2; however, the boundary conditions and losses were not available in that reference. In order to better judge how well the JETP component can model the performance of full-scale jet pumps, more complete data on full-scale jet pumps must be made available.

5.2.3 Conclusions

These tests show that the JETP component is correctly implemented in TRAC-M. The scalability concern is a functionality issue rather than an implementation issue. If the performance of a full-scale jet pump leads to important differences in the predictions of transients in plants, further research on jet pump modeling may be warranted.

REFERENCES

5.2.1. Crapo, H.S., "One-Sixth Scale Model BWR Jet Pump Test," Idaho National Engineering Report, EGG-LOFT-6063, November 1979.

5.2.2. Kudirka, A.A., and Gluntz, D.M., "Development of Jet Pumps for Boiling-Water Reactor Recirculation Systems," *Journal of Engineering for Power*, pp.7–12, January 1974.

Table 5.2.1 The INEL Tests with Positive Drive Flow

	Positive Drive Flow ($W_j > 0$)		
Parameters	**No. 96**	**No. 99**	**No. 149**
W_j (l/s)	4.010	4.110	4.099
W_s (l/s)	2.638	0.	-3.318
M-ratio	0.658	0.	-0.809
N-ratio	0.470	0.703	2.076
P_1 (MPa)	7.6935	7.7073	7.8983
P_2 (MPa)	7.4796	7.4796	7.6796
P_5 (MPa)	7.5570	7.5845	7.8416

Table 5.2.2 Boundary Conditions for Negative Flow Tests

Component		**No. 161**	**No. 167**	**No. 214**
FILL 2	V_J (m/s)	$-5.3043\ 10^0$	$-5.2173\ 10^0$	$-5.2098\ 10^0$
	T_J (K)	559	559	561
BREAK 3	P_S (Pa)	$7.6796\ 10^6$	$7.6796\ 10^6$	$7.6796\ 10^6$
	T_S (K)	559	559	561
FILL 4	V_D (m/s)	$-2.0585\ 10^0$	$-1.0306\ 10^0$	$-2.1343\ 10^{-1}$
	T_D (K)	559	559	561

Table 5.2.3 The INEL Tests with Negative Drive Flow

	Negative Drive Flow ($W_j < 0$)		
Parameters	**No. 161**	**No. 167**	**No. 214**
W_j (l/s)	-4.266	-4.196	-4.190
W_s (l/s)	-4.115	0.	3.321
M-ratio	0.965	0.	-0.793
N-ratio	-0.275	-0.044	0.008
P_1 (MPa)	7.7252	7.5862	7.4558
P_2 (MPa)	7.8796	7.8796	7.8797
P_5 (MPa)	7.9380	7.8983	7.8825

Table 5.2.4 Boundary Conditions for Positive Flow Tests

Component		**No. 96**	**No. 99**	**No. 149**
FILL 2	V_J (m/s)	$4.9860\ 10^0$	$5.1104\ 10^0$	$5.0967\ 10^0$
	T_J (K)	560	558	560
BREAK 3	P_S (Pa)	$7.4796\ 10^6$	$7.4796\ 10^6$	$7.6796\ 10^6$
	T_S (K)	560	558	560
FILL 4	V_D (m/s)	$1.6328\ 10^0$	$1.0095\ 10^0$	$1.9182\ 10^{-1}$
	T_D (K)	560	558	560

Table 5.2.5 Full-Scale Jet Pump Dimensions

	Cell/Face No.	Length (m)	Area (m^2)	Volume (m^3)
Primary Arm	1	$4.1800\ 10^{-1}$	$1.9945\ 10^{-2}$	$9.6892\ 10^{-3}$
	2	$1.1440\ 10^{0}$	$2.3180\ 10^{-2}$	$3.6370\ 10^{-2}$
	3	$3.0527\ 10^{0}$	$4.1260\ 10^{-2}$	$2.3525\ 10^{-1}$
	4	$6.9379\ 10^{-1}$	$1.1960\ 10^{-1}$	$8.2977\ 10^{-2}$
	5		$1.1960\ 10^{-1}$	
Side Arm	6	$5.0000\ 10^{-1}$	$3.2350\ 10^{-3}$	$5.8433\ 10^{-3}$
	7	$5.0000\ 10^{-1}$	$2.3170\ 10^{-2}$	$1.1585\ 10^{-2}$
	8		$2.3170\ 10^{-2}$	

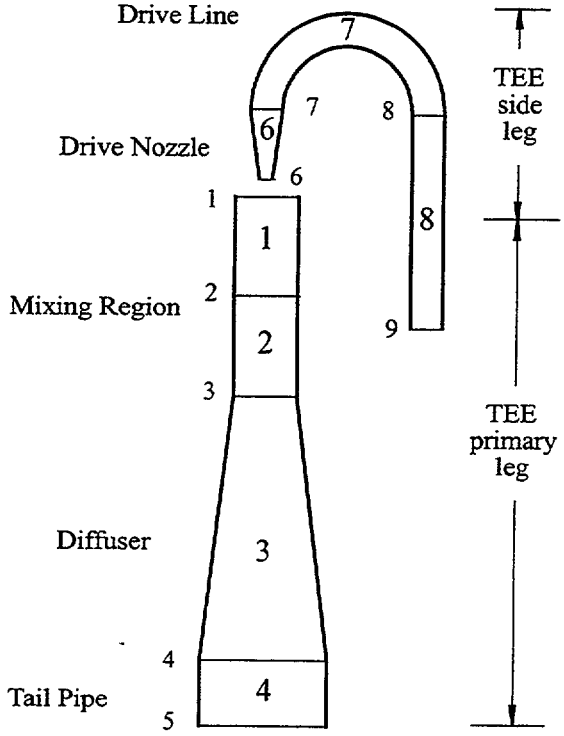

Figure 5.2.1 Schematic of a JETP Component

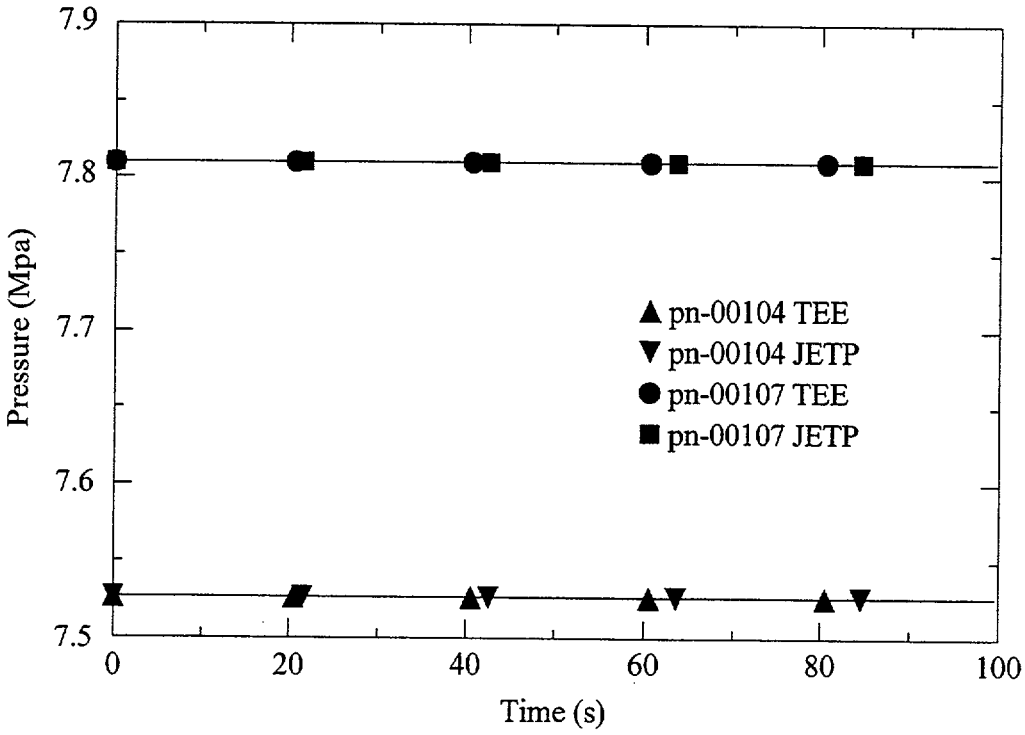

Figure 5.2.2 Comparison of Discharge and Drive Line Pressures

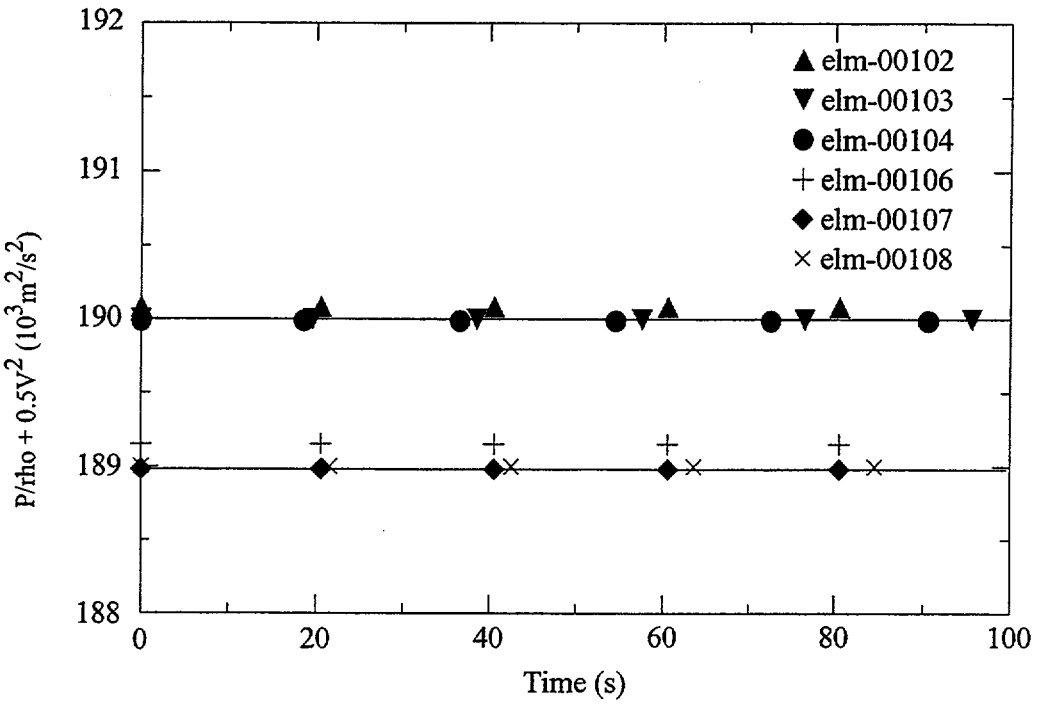

Figure 5.2.3 Bernoulli Losses and Gains Across Diffuser and Nozzle

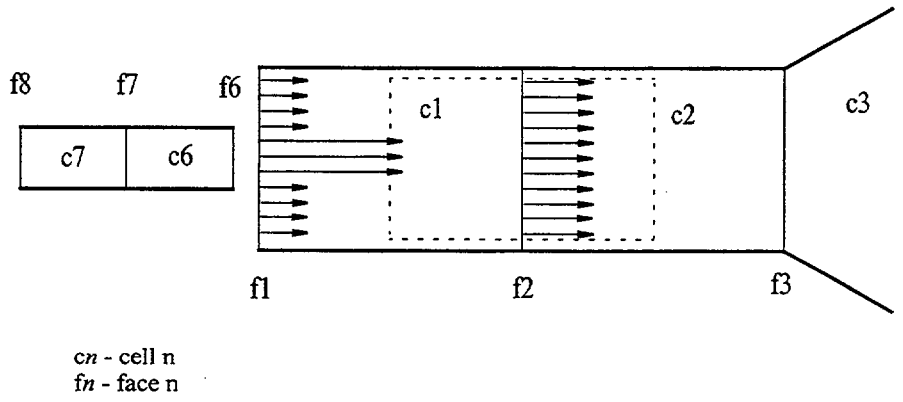

Figure 5.2.4 Mixing of Suction and Drive Line Flows

(a) Positive drive line flow

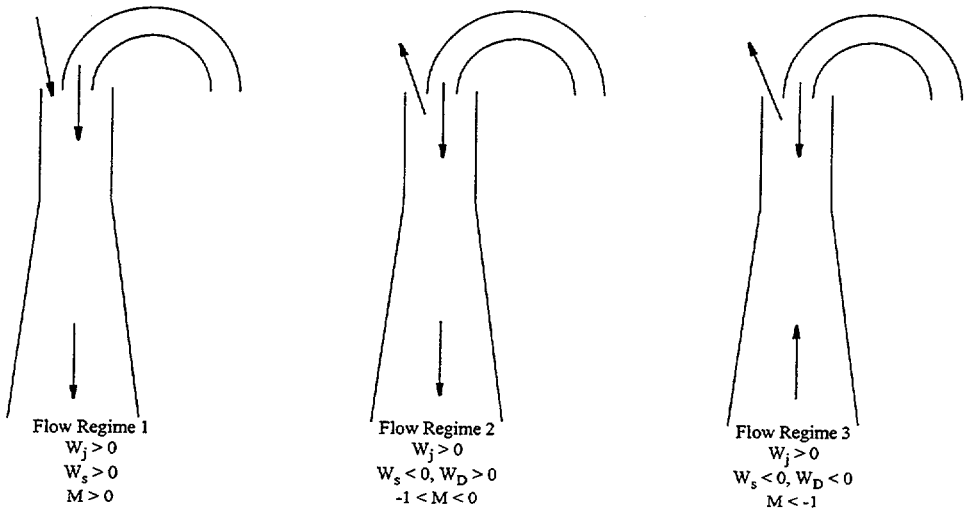

(b) Negative drive line flow

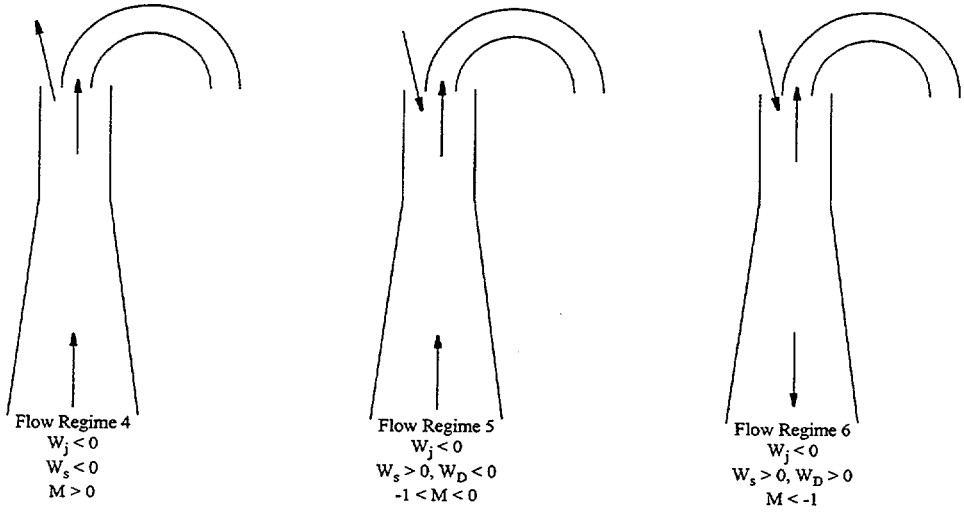

Figure 5.2.5 Jet Pump Flow Regimes

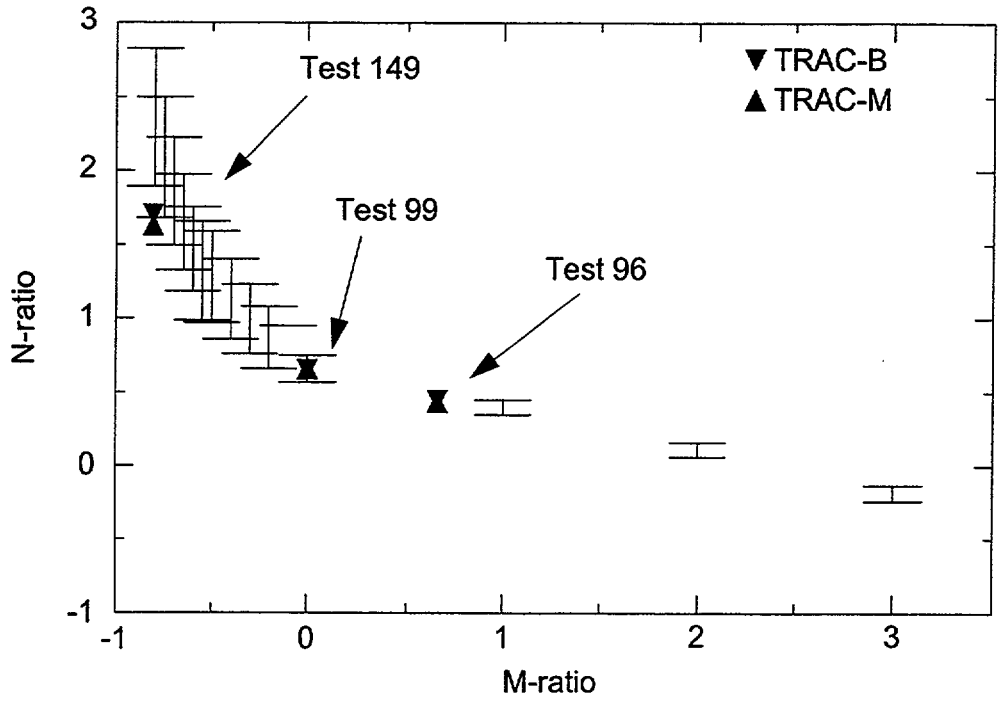

Figure 5.2.6 INEL Tests with Positive Drive Flow

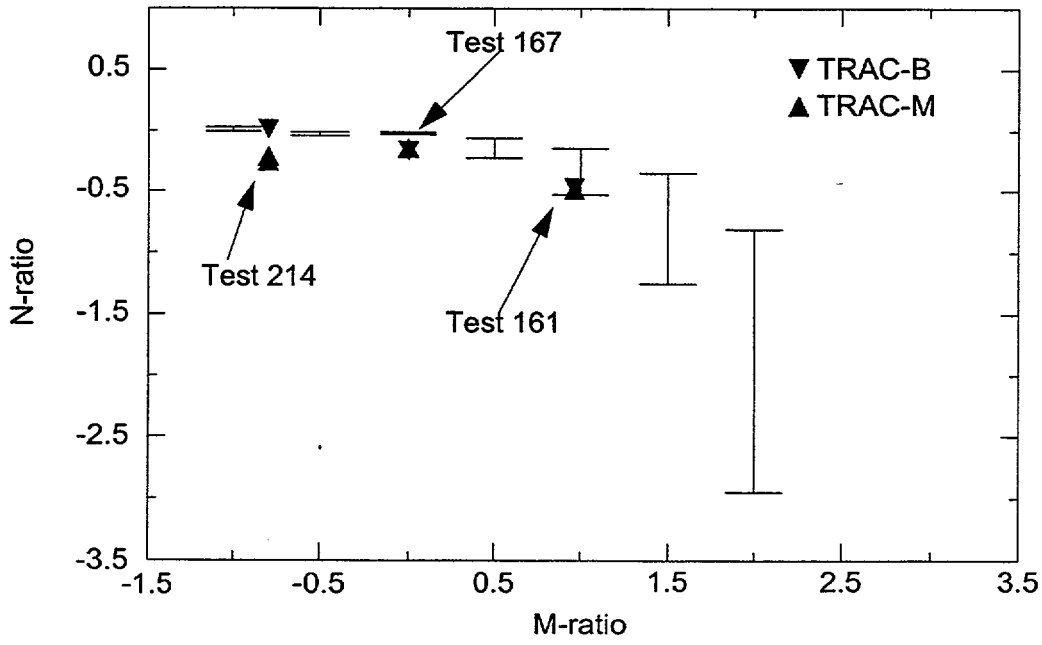

Figure 5.2.7 INEL Tests with Negative Drive Flow

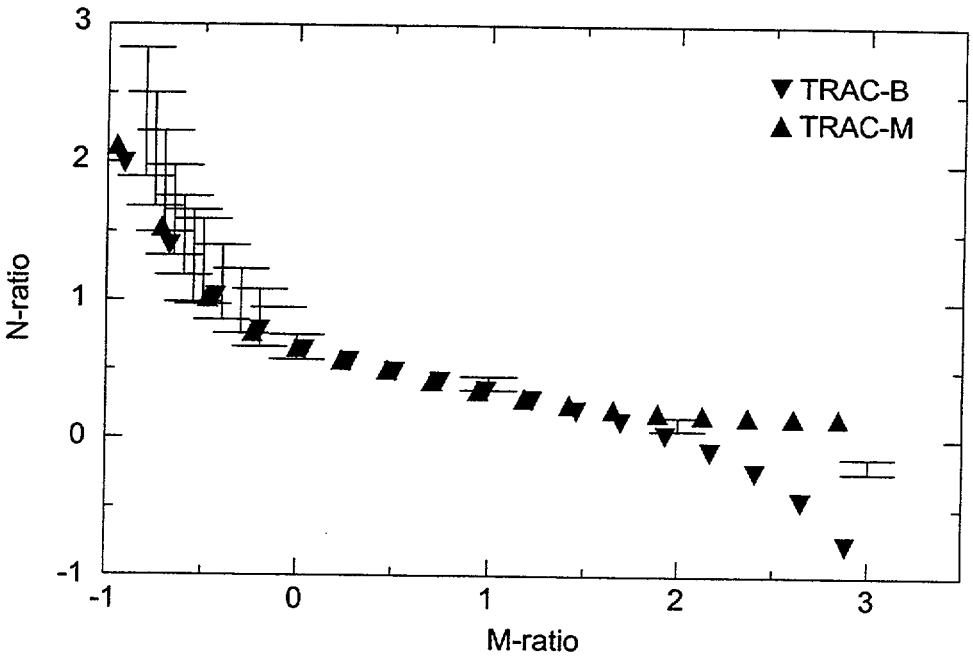

Figure 5.2.8 Comparison of TRAC-B and TRAC-M vs. the INEL Data

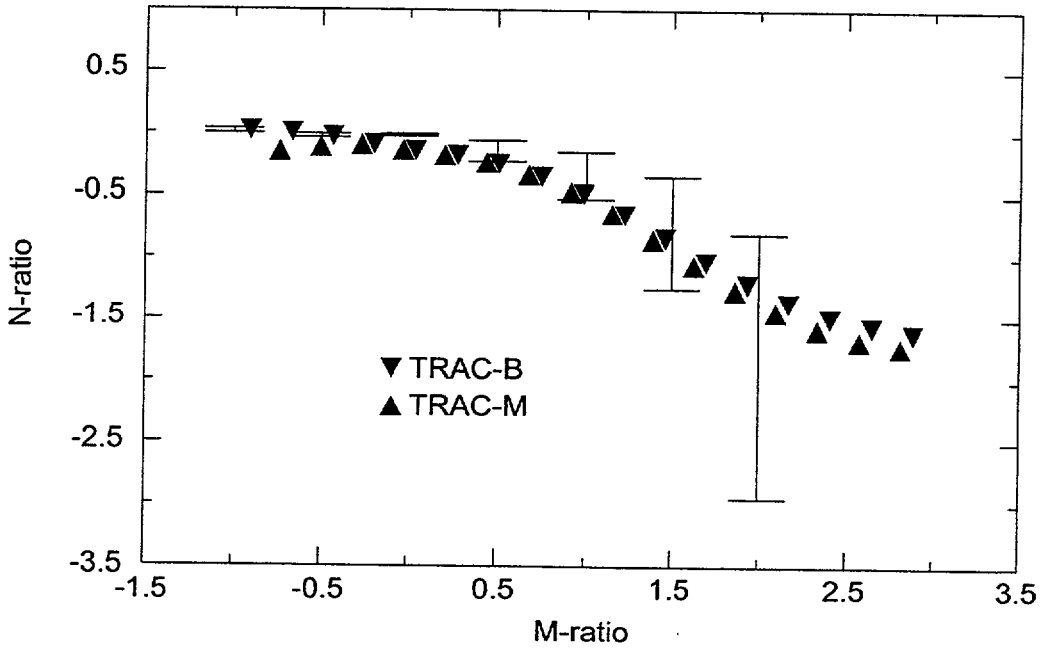

Figure 5.2.9 Comparison of TRAC-B and TRAC-M vs. the INEL Data

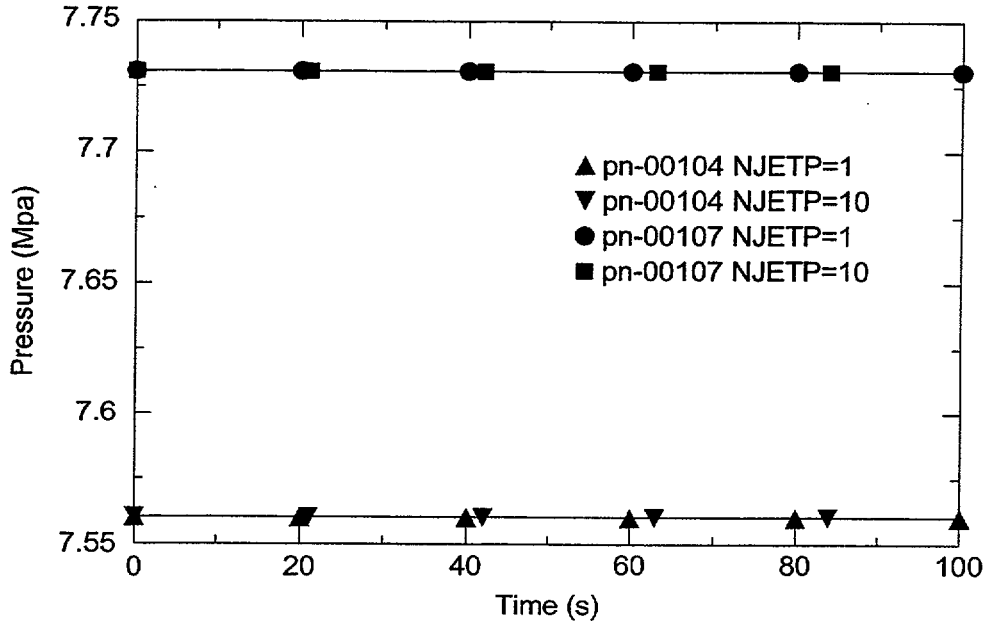

Figure 5.2.10 Pressures of Single vs. Lumped Jet Pump(s)

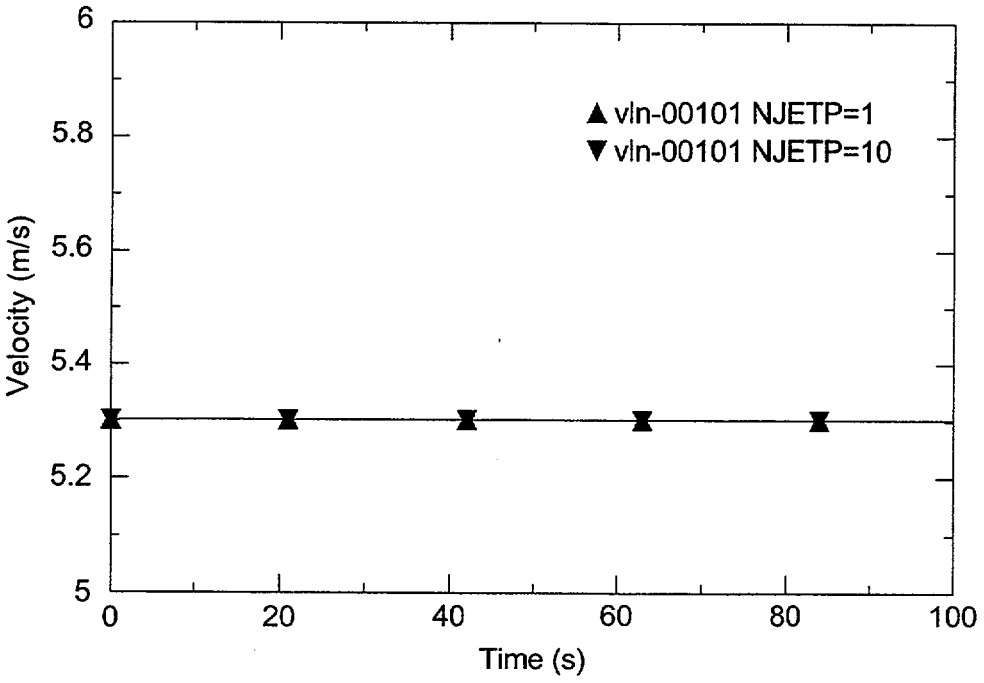

Figure 5.2.11 Velocities of Single vs. Lumped Jet Pump(s)

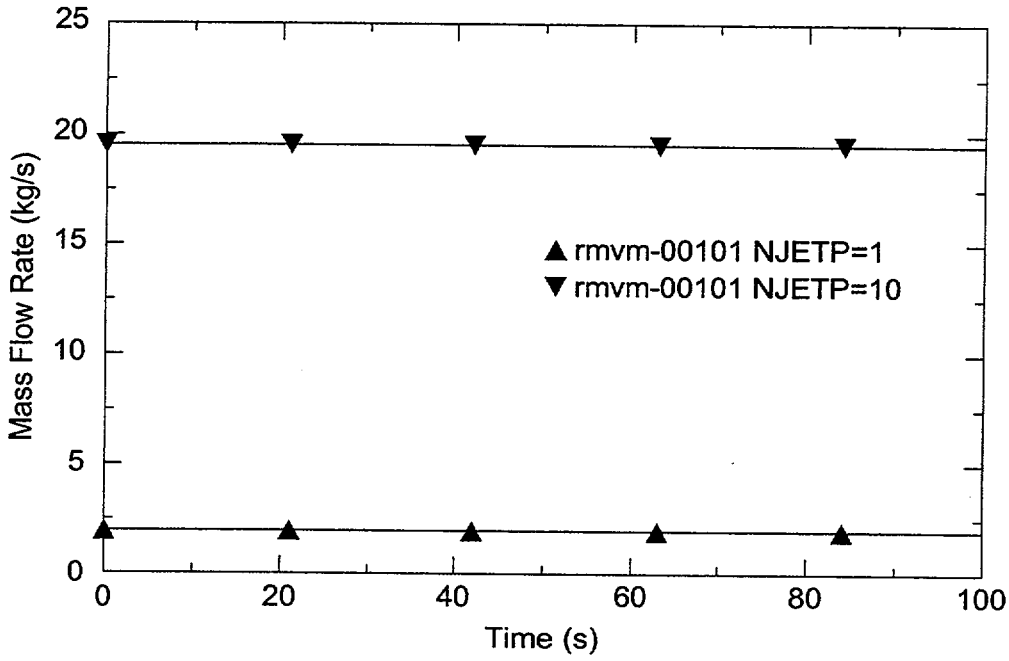

Figure 5.2.12 Mass Flow Rate of Single vs. Lumped Jet Pump(s)

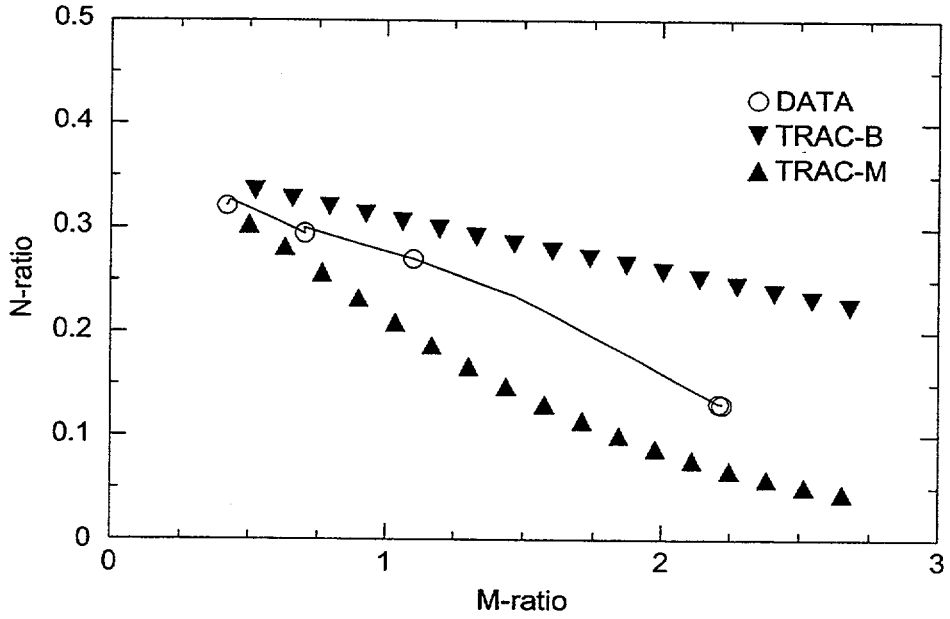

Figure 5.2.13 M-N Ratio for Full-Scale Jet Pumps

5.3 Fuel Channel (CHAN) Component

The fuel channel (CHAN) is a one-dimensional, two-fluid, six-equation component in TRAC-B (Ref. 5.3.1) that provides hydraulic communication in the BWR between the vessel's upper and lower plena and the core bypass, as shown in Fig. 5.3.1.

Each CHAN component in TRAC-B represents as many actual fuel bundles as the user specifies. A BWR/6-218 plant has 624 bundles that are commonly modeled using one to six different CHAN components. Each CHAN component can contain 1 to 64 rods, surrounded by a housing (canister). There is one convection and one radiation heat transfer coefficient for both water and steam at each hydraulic junction of each rod and canister that is modeled by the code. Because conduction nodes are placed at junctions, calls to heat transfer correlation evaluation subroutines are made once with the hydraulic conditions from the cell below the junction, and once with conditions from the cell above the junction. Results from the two calls are averaged based on the half-cell lengths of the two adjoining cells.

TRAC-B internally calculates the rod-to-rod and rod-to-canister thermal radiation view factors and beam lengths. It also has models that calculate the absorption of radiation energy by the steam and water in each hydraulic cell.

5.3.1 Requirements

Some of the models that affect the results of the CHAN component output in TRAC-B will not be ported to TRAC-M. Specifically, the TRAC-B models that will not be ported include the interfacial drag and flow regime identification, interfacial heat transfer, wall friction, and metal-water reaction. Also, only part of the differences between TRAC-B and TRAC-M wall heat transfer will be ported, as explained below. The CHAN component rod and canister wall material types will use those already in TRAC-M. In this version of TRAC-M, the PWR physics of TRAC-P will be used.

The fine mesh reflood model in TRAC-B will also not be ported to TRAC-M during this development phase, since TRAC-M has a fine mesh reflood model for the ROD and SLAB components. In addition, the CHAN component will use the radial conduction solution method from TRAC-M.

The TRAC-M CHAN heat structures will be based on the ROD and SLAB heat structures currently in TRAC-M. This is significant because the TRAC-M heat structures include power history/reactivity information instead of the power peaking factors used in TRAC-B. Also, the TRAC-B reactor power description is separate from its heat structure input, so the TRAC-M method of processing power input will be used for the CHAN component.

The development philosophy is to use TRAC-M coding to perform the tasks since it already has the compatible data structure and FORTRAN 90 coding format.

Thus, this implementation will use three categories of models, including 1) TRAC-B and TRAC-M models that will be incorporated into the new TRAC-M CHAN component and tested, 2) TRAC-B models (which are similar to existing TRAC-M models) that will not be ported, but will be tested, and 3) TRAC-B models (which are similar to existing TRAC-M models) that will not be ported or tested during this development phase. Table 5.3.1 summarizes the second and third categories of models.

Table 5.3.2 lists requirements for the CHAN models that will be implemented into TRAC-M and tested. The testing range of the CHAN component will be from a low-pressure, low-flow, and high-void fraction, to BWR operating conditions. The steady-state BWR operating conditions include a pressure of about 7 MPa, a mass flux at the bottom of the channel of about 1000 kg/m^2-s, and an exit void fraction of 70 to 80%.

5.3.2 Verification Testing and Assessment

This section presents the results of the verification testing and assessment of the integration of the CHAN component from TRAC-B to TRAC-M(F90). The results show that the integration of the CHAN component has been correctly performed.

Requirement 1: CHAN Hydraulics

The flow in the new CHAN component should have the same flow rate as a PIPE component when subjected to the same differential pressure, provided that the only difference between the two components is the name. To verify this, a CHAN component and a PIPE component (with two cells each) will be placed between two vessel cells (see Fig. 5.3.2). In this exercise with TRAC-M, a transient calculation using the restart feature will also be performed.

The test will start from stagnant subcooled liquid conditions in the vessel, and will run to 10 s. A restart at 5 s will also run to 10 s. All components will contain subcooled liquid. Pressure in all other components will have an initial pressure of 7 MPA. The only flow path from the FILL and vessel lower plenum to the upper plenum will be through the PIPE and CHAN components.

The CHAN hydraulics test will be considered successful only after it is verified that the velocities in both the PIPE and the CHAN components are identical (i.e., use of the CHAN component does not alter the hydraulic solution). Thus, the CHAN component will be a proven PIPE-class component.

The CHAN hydraulics test was successful because the exit velocities of both the PIPE and CHAN components are identical, as shown in Fig. 5.3.3. A restart at 5 s reproduced the initial results to the end of the run at 10 s. Thus, the modeling of CHAN component hydraulics was verified.

Requirement 2: CHAN Canister Leakage Path

BWR fuel canisters have holes drilled near the bottom to allow flow from the bundle into the core bypass. The plan is that leakage from the TRAC-M CHAN component will be calculated implicitly, instead of explicitly as it was in TRAC-B. Details of the new leak capabilities are not known, but TRAC-M needs the ability to define the elevation difference between the center of the CHAN leak cell and the center of the VESSEL cell that receives the fluid. Fig. 5.3.4 illustrates cell 1 of a CHAN leaking to cell 1 in a VESSEL. The momentum equation must account for the gravity head difference between the centers of the two cells.

After the leak coding becomes available, a leak will be placed between CHAN 25 cell 1 and VESSEL 12 level 2. The leakage rate calculated with TRAC-M will be compared to that calculated by a similar TRAC-B model. The leakage rate is expected to differ because of differences between the implicit and explicit models. The test will show that the two flow rates

can be made the same over a range of conditions by adjusting the leakage path "K loss coefficient." The total flow should also be conserved.

TRAC-M users will be able to model CCFL at the leak using the flexible CCFL input currently implemented in TRAC-M.

Requirement 3: CHAN Double-Sided Canister Wall Heat Transfer

The CHAN canister wall must be able to transfer energy from the fluid inside of the CHAN component to the fluid in a surrounding VESSEL or PIPE component. The TRAC-M SLAB component has the features needed for the CHAN canister wall.

Test Heat Transfer to Pipe (1-D component)

The first problem is proposed to check the ability of the code to conduct energy through the CHAN wall to a 1-D component, as shown in Fig. 5.3.5. This test consists of PIPE component 8 with one cell, PIPE component 25 with two cells, and PIPE component 24 with three cells. FILL and BREAK components act as boundaries, providing a boundary pressure of 7 MPa. The fluid in PIPE component 24 is stagnant, and has an initial temperature of 509 K (50 degrees subcooled). FILL component 12 sends fluid through PIPE component 25 at 13.3 m/s, with a temperature of 554 K (5 degrees subcooled). Initially, a SLAB heat structure is placed between PIPE components 24 and 25. Heat will be conducted from the flowing hot water to the stagnant colder water.

Next, the SLAB and PIPE component 25 will be replaced with CHAN component 25 so that a standalone SLAB will no longer be needed. The test will be repeated, and the results should not change. Again, this test is intended to confirm that the CHAN wall energy transfer capability goal has been met.

Results of the 1-D test, shown in Fig. 5.3.6, demonstrate that the heat-up is the same for the two problems.

Test Heat Transfer to Vessel (3-D Component)

A modified Zion input file will be set up, as shown in Fig. 5.3.7, and will initially be run with a SLAB and a PIPE representing the core, and then switched to a CHAN. The exit pressure will be set to 7 MPa, and the inlet flow will be ramped from 0 to 17,000 kg/s during the first 100 s. The temperature of the liquid in FILL component 1, PIPE/CHAN component 25, and VESSEL level 1 will be 5 degrees subcooled (554 K). The BREAK component 5 will have pressure of 7 MPa. The temperature of the other VESSEL levels will be 50 degrees subcooled (509 K), and the VESSEL liquid temperature will rise as energy is conducted from the water inside the PIPE or CHAN component to the water in the VESSEL.

The heatup rate of the VESSEL cells should remain the same with the SLAB and PIPE core as with the CHAN. This will verify that the CHAN wall energy successfully transfers to a 3-D component.

The rise in the liquid temperature of VESSEL level 3 is shown in Fig. 5.3.8. Heat transfer rates to the VESSEL were the same with a PIPE/SLAB as with a CHAN component. Thus, the modeling of the canister wall heat transfer in the CHAN component was verified.

Requirement 4: CHAN Multiple Rods

This step checks the multiple fuel rod convective heat transfer capability of the TRAC-M CHAN component. A one-rod model and a four-rod model will be used in a CHAN component with a FILL at the inlet and a BREAK at the outlet, as shown in Fig. 5.3.9.

This test consists of one rod in a one-cell CHAN component filled with stagnant steam at a temperature of 319 K and a pressure of 0.01 MPa. The rod power will be set at 100 W. Next, the 1x1 rod bundle will be changed to a 2x2 rod bundle, with no change in the total power. The rate of rod temperature increase should drop by a factor of about 4.

Fig. 5.3.10 shows the temperature rise of the centerline of rod 1 in each case. With four rods, the heatup was about four times slower, as expected. Four rods heated up 109 K in 2000 s, whereas heatup using one rod was 408 K in the same amount of time. Thus, the modeling of multiple rods in the CHAN component was verified.

Requirement 5: CHAN Multiple Channels

A CHAN component represents one rod bundle in a core lattice consisting of many rod bundles. To do this, the NCHANS capability of TRAC-B will be added to TRAC-M. NCHANS is the number of identical fuel assemblies represented by a given CHAN component, and it affects the total leakage mass flow and total core flow and energy exchange to the VESSEL cells.

CHAN component 25, shown in Fig. 5.3.7, will be changed from representing 1 fuel bundle to representing 10 bundles. Thus, the flow rate through PIPE component 25 should drop by a factor of 10, since the lower plenum inlet flow is fixed and there are now 10 flow passages from the lower plenum to the upper plenum. However, the total energy transfer to the VESSEL will likely increase because of the increased canister surface area.

The model illustrated in Fig. 5.3.7 with the CHAN component (no SLAB or PIPE in the core) was used to test Requirement 5. The variable "NPIPES" in the CHAN input file was changed from 1 to 10. If the coding is correct, this change should cause the velocity through the rod bundle to drop by a factor of 10 because the inlet flow is fixed by the FILL.

The problem output showed that the CHAN liquid velocity dropped from 13.3 m/s to 1.33 m/s when NPIPES was changed from 1 to 10. This result verified the multiple CHAN coding.

Also, as expected, the drop in liquid velocity reduced the canister inside convection coefficient; however, 10 CHAN components caused the VESSEL liquid temperature to rise much faster than it did with 1 CHAN, as shown in Fig. 5.3.11. This is due to the increased canister surface area in contact with the vessel fluid.

Requirement 6: CHAN Boiling Transition

TRAC-P contains only the Biasi correlation to calculate the CHF for the ROD and SLAB components (variable ICHF is hardwired to 1 for SLABS and RODS). For other components, ICHF is a user input that may be 0 or 1. An input value of 1 means that the Biasi correlation should be used, while a value of 0 means that the fluid should be treated as a homogenous mixture, ignoring CHF.

TRAC-B users have the option to select ICHF values of (0) homogeneous mixture with CHF occurring at 50 K wall superheat; (1) Biasi/Zuber with Zuber used for low-flow conditions; (2) Biasi/Zuber where Biasi has been reformulated into a boiling length correlation; or (3) the CISE-GE boiling length correlation. When a boiling length correlation is used, the code checks the predicted critical quality against the local equilibrium quality, and the predicted critical wall temperature (at the critical heat flux) against the local wall temperature. Nucleate boiling is not allowed if either of the critical values are exceeded.

The ability to set ICHF to 1, 2, or 3 will be added as an option to the CHAN, ROD, and SLAB components, while ICHF values of 2 and 3 will be added for the other components.

A modified version of the model shown in Fig. 5.3.9 will be used, with the BREAK pressure set to 7.0 MPA, the inlet FILL velocity set to 10 m/s, the subcooling set to 0, and the initial void fraction set to 0.85. The FILL velocity will be held constant, while the void fraction is ramped from 0.85 to 1.0 over a 500 s time period. The total rod bundle power will be ramped from 1 W at time zero to 2 MW at 500 s.

These tests will show the effect of ICHF on the TRAC-M results, which will differ from the TRAC-B results because of many other differences between the two codes (such as the interfacial drag models).

The simple one-cell CHAN problem was run using both TRAC-M and TRAC-B with ICHF =1, 2, and 3. ICHF is the critical heat flux flag. When ICHF equals 1, the Biasi correlation is used to predict the critical heat flux, provided that the mass flux is above 300 kg/s-m^2. When ICHF equals 2, the critical quality form of the Biasi correlation is used, and when ICHF equals 3, the CISE-GE critical quality correlation is used. If ICHF equals 2 or 3, departure from nucleate boiling is predicted when the local thermodynamic equilibrium quality exceeds the critical quality. When ICHF equals 1, 2, or 3 the local wall temperature is compared with the critical wall temperature based on the critical heat flux predicted by the Biasi correlation. Departure from nucleate boiling occurs when the critical temperature exceeds the local temperature. When departure from nucleate boiling is predicted, post-CHF correlations are used to obtain the wall heat transfer coefficients.

As described above, this one-celled CHAN problem held the FILL velocity constant, while the void fraction was ramped from 0.85 to 1.0 over a 500 s time period. This ramping caused the inlet mass flux to drop from an initial value of 1422 kg/s-m^2 to 367 at 500 s. The total rod bundle power was also ramped from 1 W at time zero to 2 MW at 500 s; however, the mass flux was large enough that the Zuber correlation did not influence the results.

In addition, the critical quality correlations are not active when the height of the point in question is less than one meter from the start of boiling in the rod bundle, as it was in this test with the length of the CHAN cell set to 1.5 m.

TRAC-B and TRAC-M results are shown in Figs. 5.3.12 and 5.3.13, respectively. The two plots are similar, with the exception that the post-CHF temperatures predicted by TRAC-M are lower. This implies that the post-CHF heat transfer coefficients are smaller in the TRAC-B code. At 200 s, TRAC-B calculated liquid and vapor heat transfer coefficients of 39 and 2580 W/m^2-K, respectively, while TRAC-M calculated values of 825 and 3170 W/m^2-K. Differences in constitutive relations between the two codes also resulted in different velocity and void profiles.

Thus, the modeling of the BWR boiling transition in the TRAC-M CHAN component was verified.

Requirement 7: CHAN Radiation Heat Transfer

The simple TRAC-M input nodalization illustrated in Fig. 5.3.9 will be modified to verify that the CHAN component meets the requirements shown in Table 5.3.3. An analytical solution or GOTA tests will be used to verify that the coding was performed correctly. These tests may also be considered as part of "Validation Tests" for the CHAN component.

Analytical Solution

TRAC-M will be used to model a powered rod surrounded by a cooled wall in order to obtain results for which there is an analytical solution. The analytical solution (Ref. 5.3.2) is as follows:

$$Q_{rod} = \frac{A_{rod}\sigma(T_{rod}^{\ 4} - T_{wall}^{4})}{(1/\varepsilon_{rod}) + (A_{rod}/A_{wall})[(1/\varepsilon_{wall}) - 1]} \qquad (5.3.1)$$

where:

Q = energy transfer

A = surface area

σ = Stefan-Boltzmann coefficient, 5.729e-8 W/m^2K^4

T_{rod} = rod surface temperature

T_{wall} = surrounding wall temperature

This equation is valid when the rod view factor is 1.0.

GOTA Test

After rod-to-rod, rod-to-channel, and rod-to-steam and water radiation capabilities will be added to TRAC-M. GOTA Test 27 (Ref. 5.3.3) will be simulated, and TRAC-B and TRAC-M output will be compared with the measured rod data.

Data taken in the GOTA test facility in Sweden is very useful for validating radiation heat transfer in rod bundles because it was taken under steady-state conditions at high temperature with a high-temperature gradient. A 64-rod bundle was filled with steam near atmospheric pressure. The geometry of the test section is shown in Fig. 5.3.14. Power was applied to the rods, and the canister walls were maintained at 373 K by cooling them with water on the outside. Over half of the rods were instrumented. The peak temperature in the bundle was 1224 K, and the data uncertainty was believed to be less than 5 K. Fig. 5.3.15 shows the rod temperature profile diagonally across the bundle with data uncertainty bands.

A one-cell CHAN model of five rod groups is developed. Rod groups are shown in Fig. 5.3.14. The water rod has been lumped with two other low-powered rods as rod group 5. A

zero-velocity FILL is attached to the bottom of the CHAN component, and a BREAK sets the pressure at the top.

This test will confirm whether the radiation network coding is working properly, and it will also provide a comparison with experimental data.

Radiation has nine sub-level requirements, as described in the following paragraphs.

Requirement 7.1: Surface Emissivity Changes

Surface emissivity must change to 0.96 when the surface quenches because of the presence of liquid film. A quenched surface is defined to be one with heat transfer regime identifiers less than 3 (i.e., nucleate boiling or forced convection to single-phase liquid). The surface emissivity is set to 0.96 if the surface is in heat transfer regime of 7, 11, or 12, (i.e., convection to two-phase mixture, condensation, and liquid natural convection, respectively).

This test problem consisted of a CHAN component with one rod and one cell. The rod and canister emissivities were specified to be 0.7, and the initial cell void fraction was 0.95. The pressure was set at 1.e4 Pa by a BREAK connected to the top of the CHAN component, which also had a void fraction of 0.95. A zero-velocity fill was attached to the bottom of the CHAN component. The initial temperatures of the rod and canister were 1000 and 550 K, respectively. Power generation in the rod was a constant 1 kW.

On the outside of the canister, a convective boundary condition was specified. The liquid and vapor heat transfer coefficients were 100 W/m^2K, and the reference temperature was 250 K.

The canister was initially in transition boiling and, for about 40 s, cycled between transition boiling and nucleate boiling before entering regime 1 (forced convection to a single-phase liquid) or regime 12 (liquid natural convection). The cycling is caused by void fraction oscillations near a value of 1.0. When the canister wall regime was nucleate boiling (2), the rod radiation heat flux was about 10% larger than when it was in transition boiling, as shown in Fig. 5.3.16. The larger rod heat flux was caused by the larger value of canister wall emissivity when the canister was quenched. (Note that oscillations between regimes 2 and 3 were also observed when the CHAN component was replaced with a PIPE and SLAB.) This test confirms that rod quenching effects on radiation were coded as intended.

Requirement 7.2: Anisotropic Reflection Correction

Anisotropic reflection correction factors were built into TRAC-M, using the values recommend by Tien et al. (Ref. 5.3.4) of 0.15 for the rods and 0.5 for the canister. The problem was run in debugger mode so that it could be stopped in subroutine IRADNET in order to set the anisotropic reflection to 0.0. This was necessary in order to obtain a rod-to-wall view factor of 1.0.

In order to test this requirement, TRAC-M was used to model a powered rod surrounded by a cooled wall. The rod had an internal power of 1 kW, and a surface area of 0.038485 m^2. The rod and canister emissivity were set to 0.96, and the rod-to-wall view factor was set to 1.0. The wall surface temperature was controlled at 350 K with a surface area of 0.1 m^2. The steady-state rod surface temperature calculated by the analytical method, Equation 5.3.1, was 835.8 K when radiation is the only method of transferring energy from the rod to the wall.

The code calculated a surface temperature of 832.24 K. This included both radiation and convection components. The code also calculated 18.2 W of energy transfer by convection. When Q in Equation 5.3.1 was reduced by this amount, the equation gave a rod temperature of 832.1 K which was the temperature attributed to the radiation component of the heat transfer. Thus, radiation test results indicate that the radiation coding in TRAC-M is working properly and is therefore verified.

Equation 5.3.1 is not valid when the rod view factor is not 1.0. With anisotropic reflection active, the view factor from the rod to the wall is 0.85, and the predicted steady-state temperature is 866 K.

Requirement 7.3: Rod Grouping

Users are able to specify various rod groupings, including the rod group to which every rod in the bundle is assigned. One rod group in a one-rod bundle was used for Requirement 7.1. Five rod groups in a 64-rod bundle are shown in Fig. 5.3.17. The water rod has been lumped with two other low-powered rods as rod group 5. A one-cell CHAN component represents the bundle mid-section in the TRAC model. A zero-velocity FILL is attached to the bottom of the CHAN component, and a BREAK sets the pressure at the top.

The TRAC-M results are closer to the data than the TRAC-B results. The TRAC-M vapor heat transfer coefficients were about a factor of 5 smaller than the TRAC-B values (5 and 26 W/ m^2-K, respectively). Thus, the ability of the TRAC-M CHAN component to model radiation with multiple rod groups has been verified.

Requirement 7.4: View Factors

The code calculates view factors for rods in 1x1 to 8x8 rod bundles. The user specifies the number of rods in each row, the rod radius, and the inside perimeter of the canister.

The view factors calculated by TRAC-B for the five-rod group GOTA test are shown in Table 5.3.4. The canister wall is the sixth radiation surface. Table 5.3.5 shows view factors for TRAC-M. Within five significant figures, TRAC-M and TRAC-B values are the same, and the acceptability of the view factor coding is confirmed.

Requirement 7.5: Beam Lengths

The code calculates beam lengths, and uses them to estimate the amount of radiation energy absorbed by the fluid. Beam lengths for TRAC-B and TRAC-M are shown for the GOTA problem in Tables 5.3.6 and 5.3.7, respectively. These lengths are the same within five significant figures, and the acceptability of the beam length coding is confirmed.

Requirement 7.6: Radiation Cut-Off

This case used the same input file used for Requirement 7.1, with the exception that the rod used in this case contained no power generation. In this case, the CHAN component was filled with condensate and liquid from the BREAK. The plot of rod radiation heat flux versus time is given in Fig. 5.3.18. At about 157 s, the flux briefly reaches a value of zero. This decrease

resulted from the radiation criterion which states, "skip radiation when the maximum difference between the wall temperatures in the network and the fluid saturation temperature is less than 100 K." The reason for the cutoff is to save computer CPU time. During BWR transients, as the fuel rod temperature approaches the saturation temperature, convection dominates radiation.

Radiation reactivated when the temperature difference exceeded 100 K, and terminated again as the rod temperature continued to drop (as shown in Fig. 5.3.18). This test verified that radiation cutoff coding is working as intended.

Requirement 7.7: Radiation Absorption by Steam and Water

An input file was developed from the previous file, with the exception that the pressure was increased to 10 MPa to increase the ability of the steam to absorb radiation energy. The initial steam temperature was set to 600 K, the void fraction was set to 1.0, and the exit BREAK was replaced with a zero-velocity fill.

Three cases were executed with (1) both convection and radiation on, (2) radiation but no convection, and (3) no convection or radiation. The model was deactivated by recompiling the code with the models disabled. Fig. 5.3.19 shows that, with both models inactive, the steam temperature did not rise. When radiation was activated, the temperature did rise and, with both models activated, the steam heated at an even faster rate.

Next, water was added to the CHAN cell. In addition, the rod temperature was set to 1400 K, the canister temperature to 800 K, and the cell pressure to 0.01 MPa. The void fraction was set to 1.0, 0.99, and 0.9, and the radiation heat flux to the canister was monitored (convection was set to zero). Water and steam temperatures were set to the saturation temperature (319 K).

With no water present, the heat flux to the canister wall was negative. At a void fraction of 0.99, the canister heat flux decreased, and was positive at a void fraction of 0.9. This indicates that the water was shielding the canister enough that more radiant energy was being lost from the wall to the water than was being absorbed from the rod. Fig. 5.3.20 illustrates the results. The trends of the results show that the absorption coding is working as intended.

Requirement 7.8: Steam Emissivities

The steam emissivities and absorptivities were checked in the TRAC-B and TRAC-M debugger using the GOTA input file. Numerical values were identical in both codes. Thus, TRAC-M coding is working as intended.

Requirement 7.9: Compatibility With the Convection Model

The CHAN component calculates radiation from structures to liquid when conditions are such that radiation is important. Therefore, subroutine HTCOR includes checks designed to skip enhanced convection attributable to radiant energy absorption by the liquid whenever the component under consideration involves a CHAN component. Skipping enhanced convection was verified in the debugger.

Requirement 8: CHAN Input/Output

The input and output of the TRAC-M CHAN component will look as similar as practical to that of TRAC-B.

5.3.3 Conclusions

These tests demonstrate that the CHAN component is correctly implemented in TRAC-M.

REFERENCES

5.3.1 Giles, M.M., et al., "TRAC-BF1/MOD1: Users Guide," EGG-2626, Vol. 2, R4, NUREG/CR-4356, U.S. Nuclear Regulatory Commission, February 1992.

5.3.2 Eckert, E.R.G., and R.M. Drake, *Heat and Mass Transfer*, McGraw-Hill Book Co., Inc., 1959, page 405.

5.3.3 Nilsson, L., L. Gustafson, and R. Harju, "Experimental Investigation of Cooling by Top Spray and Bottom Flooding of a Simulated 64-Rod Bundle for a BWR, Part 2," Studsvic Report, STUDSVIC/RL-78/59, Norhav S-046, June 30, 1978.

5.3.4 Tien, C.L, et al., "Surface Radiation Exchange in Rod Bundles," *Transactions of ASME, 101,* 1979, p. 378.

Table 5.3.1 TRAC-B CHAN Models That Will Not Be Ported

Models that will NOT be ported, but will be tested	Models that will NOT be ported or tested	Comment
Leak Path Flow		The CHAN component in TRAC-M will use the single-junction model being developed at LANL.
	Subcooled Boiling	The subcooled boiling model in TRAC-B is different than the one in TRAC-M. TRAC-M uses a critical temperature model, while TRAC-B uses a critical enthalpy model.
	Countercurrent Flow Limitation (CCFL)	CCFL can be important at the top of the BWR fuel bundle, at the bundle leakage holes during spray cooling, and at the bundle inlet orifice (a vertical orifice known as the side-entry-orifice) during lower plenum refill. TRAC-M allows users to specify up to 10 sets of CCFL correlation constants, and any set may be invoked at any junction. This capability is deemed satisfactory for the CHAN component.
	Fine Mesh Rezoning During Reflood	The TRAC-M SLAB and ROD components already have this capability. Therefore, the CHAN component will inherit this capability. The TRAC-B reflood model was originally taken from TRAC-P.
	Metal-Water-Reaction	TRAC-M has a model similar to the model currently used in TRAC-B.
	Material Types	TRAC-M already has all of the necessary material types.
	Direct Heating of Fluid	TRAC-B direct heating is specified as a fraction in the core power input data, which is separate from the CHAN input data. In TRAC-M, direct heating is part of the TEE or PIPE input, and reactor power is part of the HSTR input. This method of treating reactor power will not be changed during this development effort. After power input is modularized, the direct heating of the CHAN component plus vessel water will be allowed. The BWR core bypass water (in the vessel) needs to have a direct heating term added.
	Fuel-Clad Interaction	Both codes have similar fuel-clad interaction models. The one in TRAC-M will be used.
	Interfacial Drag and Heat Transfer and Wall Friction	TRAC-B uses a drift flux-based interfacial friction model, instead of the drag-based model used in TRAC-M.

Table 5.3.2 CHAN Requirements

Requirement	Sub-Level Requirement	Requirement Statement
CHAN 1		The CHAN component must provide a fluid passage between lower and upper plenums. The flow rate shall be identical to that in a PIPE component.
CHAN 2		Leakage from the CHAN component to the VESSEL bypass must be allowed.
CHAN 3		The canister walls must calculate heat convection on both the inside and outside.
CHAN 4		A user-specified number of rods must be accommodated inside the CHAN component.
CHAN 5		Users must be able to specify how many fuel bundles each CHAN component represents.
CHAN 6		The departure from nucleate boiling must be calculated using a boiling length correlation.
CHAN 7		Radiation heat transfer must be considered inside each CHAN component.
	CHAN 7.1	Surface emissivity must change when the surface quenches.
	CHAN 7.2	Reflected radiant energy must be anisotropic.
	CHAN 7.3	Users must be able to specify various rod groupings, including the rod locations in the bundle for each group.
	CHAN 7.4	The code must calculate the average view factors for each group of rods.
	CHAN 7.5	The code must calculate the average beam lengths for each group of rods.
	CHAN 7.6	The code must have a built-in criterion below which radiation will not be calculated.
	CHAN 7.7	The code must allow radiation absorption by the fluid in the rod bundle.
	CHAN 7.8	The code must calculate emissivities for steam and water.
	CHAN 7.9	Radiation from a wall to liquid in the wall heat transfer convection logic must be set to zero when the surface-to-surface radiation model is active.
CHAN 8		The format for TRAC-M input and output must follow the TRAC-B input and output.

Table 5.3.3 CHAN Radiation Requirements

Sub-Level Requirement	Requirement Statement	GOTA Deck Modifications and Output Evaluation
CHAN 7.1	Surface emissivity must change when the surface quenches.	Set the rod temperature to 1000 K, and cool the canister with liquid present. Verify that the rod radiation increases when the canister heat transfer regime indicates that the surface is wet.
CHAN 7.2	Anisotropic reflection must be considered.	Show the effect of anisotropic reflection.
CHAN 7.3	Users must be able to specify various rod groupings, including rod locations in the bundle for each group.	Show the radial temperature profile inside the GOTA bundle using five rod groups.
CHAN 7.4	The code calculates view factors.	Verify that the view factors calculated by TRAC-M are the same as those calculated by TRAC-B.
CHAN 7.5	The code calculates beam lengths.	Verify that the two codes calculate the same beam lengths.
CHAN 7.6	Users specify criteria below which radiation is not calculated.	Use water flow to lower the rod temperatures so that nucleate boiling results. Verify that the radiation model deactivates.
CHAN 7.7	Consider radiation to steam and water.	Show the effect of radiation on the steam temperature in the bundle. Also, show that increasing the amount of water reduces the radiation from the rods to the canister.
CHAN 7.8	Steam and water emissivities are calculated by the code.	Verify that the two codes calculate the same emissivities.
CHAN 7.9	Compatibility with convection model.	Verify (in the debugger) that radiation to liquid is terminated in the convection model when the new radiation model is in use so that double accounting of the energy transfer does not occur.

Table 5.3.4 TRAC-B View Factors for GOTA Test with 5 Rod Groups

i/j	1	2	3	4	5	6
1	0.44862846	0.10499371	0.04087847	0.00348879	0.00270504	0.39930553
2	0.06299623	0.50697181	0.13791402	0.01719264	0.00618810	0.26873720
3	0.03065886	0.17239253	0.61064303	0.11868582	0.03105298	0.03656678
4	0.00322042	0.02645021	0.14607486	0.75900174	0.05733681	0.00791596
5	0.01082014	0.04125398	0.16561592	0.2484591	0.52479799	0.00905247
6	0.34403905	0.38590372	0.04200760	0.0073870	0.00194989	0.21871105

Table 5.3.5 TRAC-M View Factors for GOTA Test with 5 Rod Groups

i/j	1	2	3	4	5	6
1	0.44863	0.10499	0.040878	0.0034888	0.0027050	0.39931
2	0.062996	0.50697	0.13791	0.017193	0.0061881	0.26874
3	0.030659	0.17239	0.61064	0.11869	0.031053	0.036567
4	0.0032204	0.026450	0.14607	0.75900	0.057337	0.007916
5	0.010820	0.041254	0.16562	0.24846	0.52480	0.0090525
6	0.34404	0.38590	0.042008	0.0073887	0.0019499	0.21871

Table 5.3.6 TRAC-B Beam Lengths for GOTA Test with 5 Rod Groups

i/j	1	2	3	4	5	6
1	0.00213230	0.00903721	0.01830990	0.03143364	0.02741477	0.00866181
2	0.00903721	0.00234390	0.01089230	0.02544208	0.01866668	0.00945001
3	0.01830990	0.01089230	0.00196553	0.01297744	0.01221999	0.02495431

Table 5.3.6 TRAC-B Beam Lengths for GOTA Test with 5 Rod Groups (Continued)

i/j	1	2	3	4	5	6
4	0.03143364	0.02544208	0.01297744	0.00364178	0.01012619	0.04379207
5	0.02741477	0.01866668	0.01221999	0.01012619	0.00072944	0.04446172
6	0.00866181	0.00945001	0.02495431	0.04379207	0.04446172	0.02371800

Table 5.3.7 TRAC-M Beam Lengths for GOTA Test with 5 Rod Groups

i/j	1	2	3	4	5	6
1	0.0021323	0.0090372	0.018310	0.031434	0.027415	0.0086618
2	0.0090372	0.0023439	0.010892	0.025442	0.018667	0.0094500
3	0.018310	0.010892	0.0019655	0.012977	0.012220	0.024954
4	0.031434	0.025442	0.012977	0.0036418	0.010126	0.043792
5	0.027415	0.018667	0.012220	0.010126	0.00072944	0.044462
6	0.0086618	0.0094500	0.024954	0.043792	0.044462	0.023718

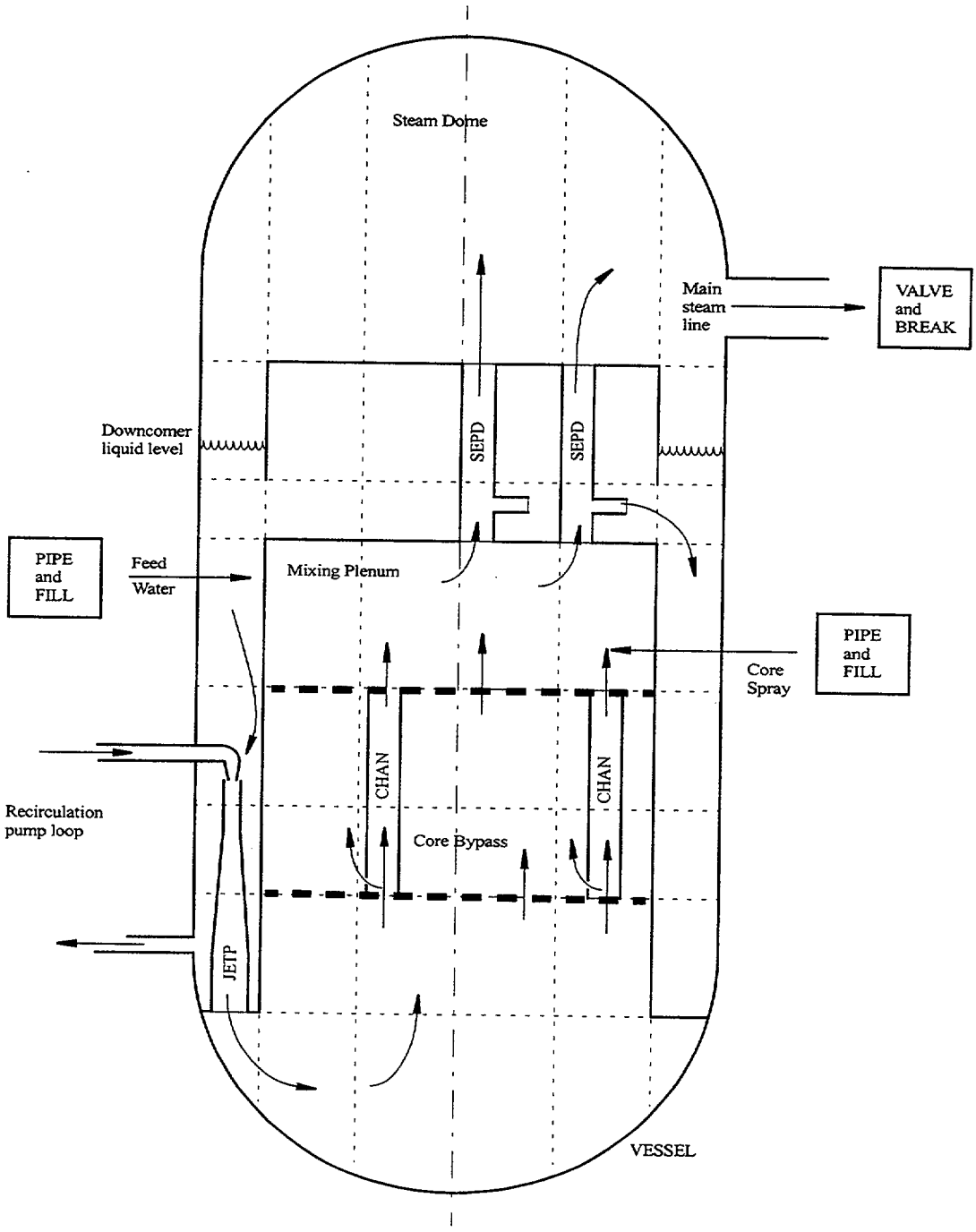

Figure 5.3.1 Boiling-Water Reactor Schematic

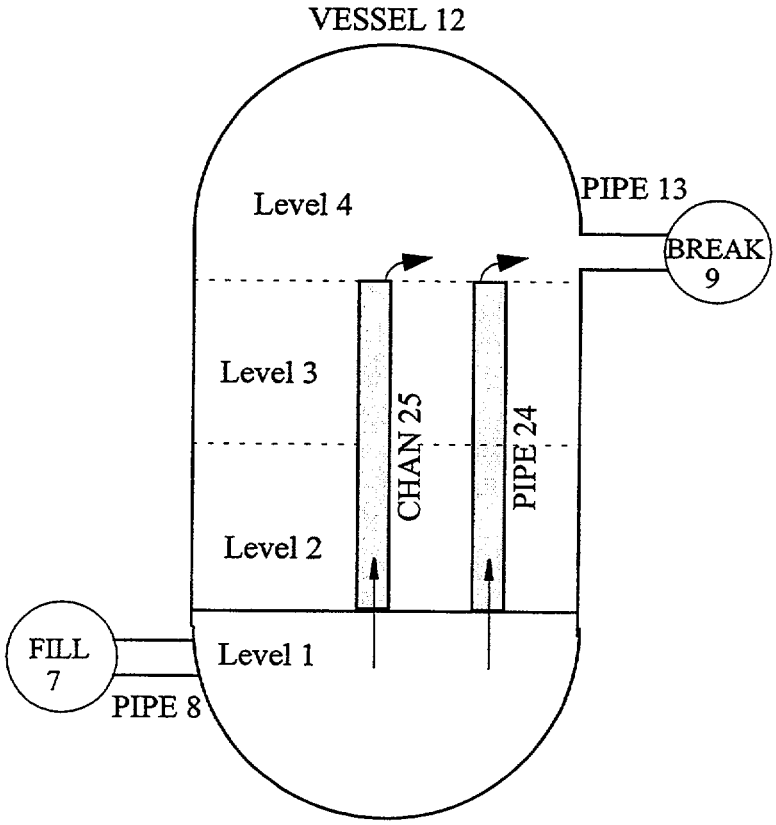

Figure 5.3.2 Hydraulic and Heat Transfer Test Nodalization Diagram

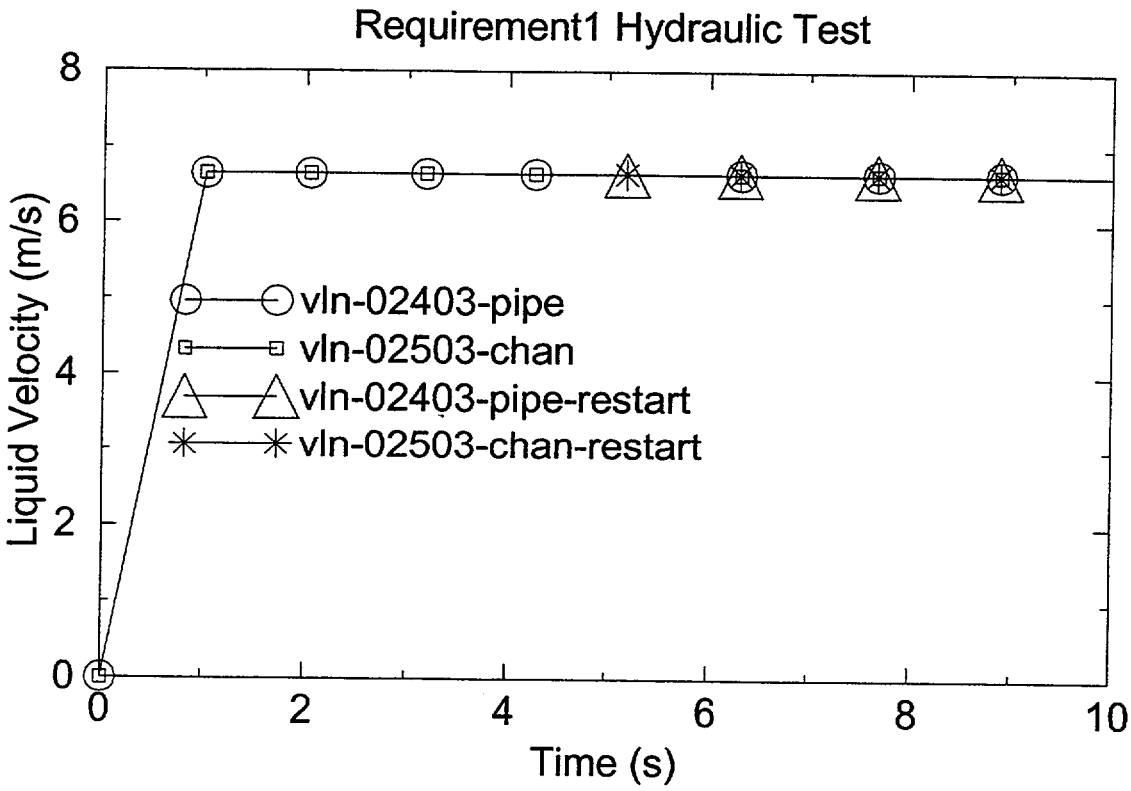

Figure 5.3.3 Results of Requirement 1 Test

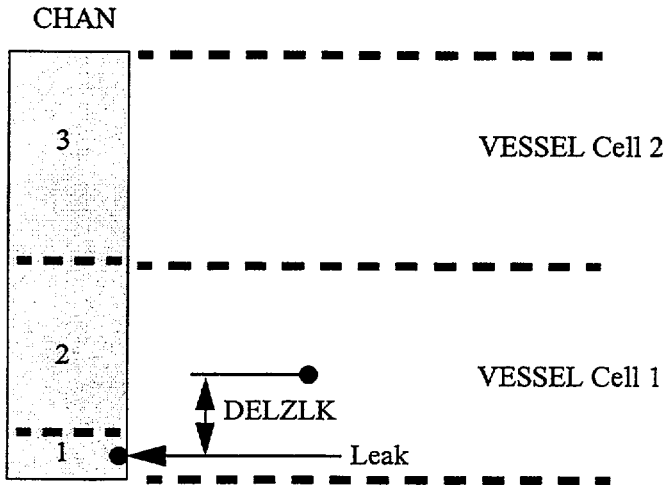

Figure 5.3.4 CHAN Cell Leaking to a VESSEL Cell

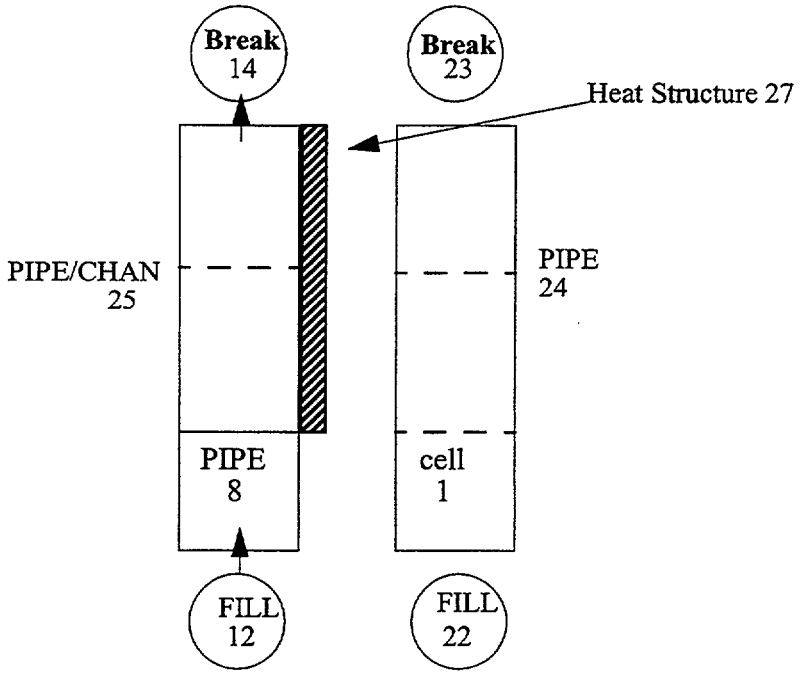

Figure 5.3.5 Requirement 3 (1-D Test)

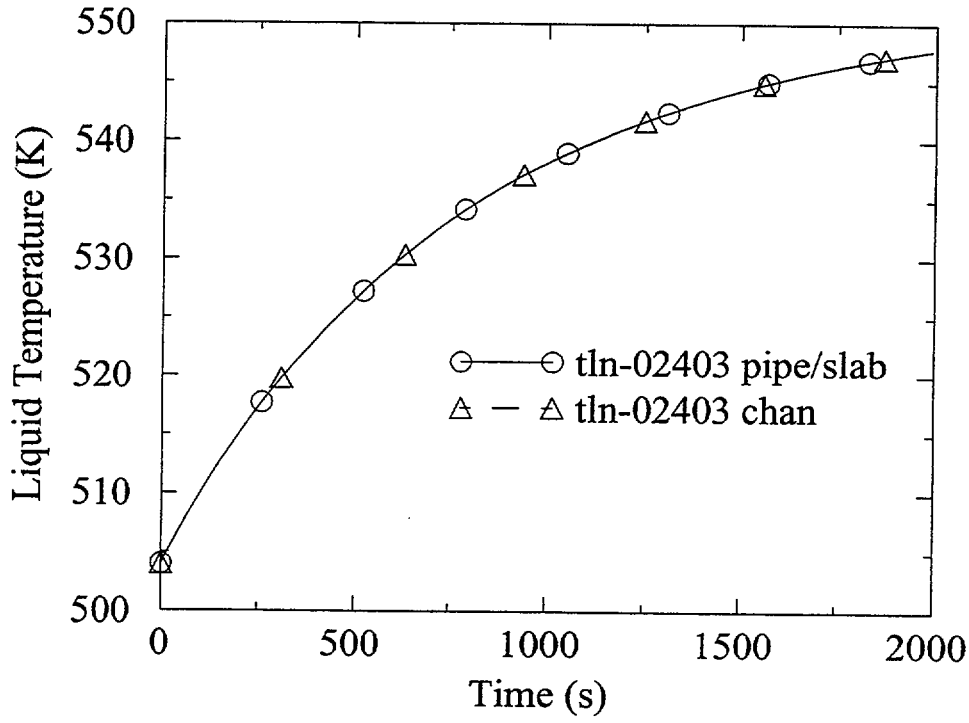

Figure 5.3.6 Requirement 3 1-D Results

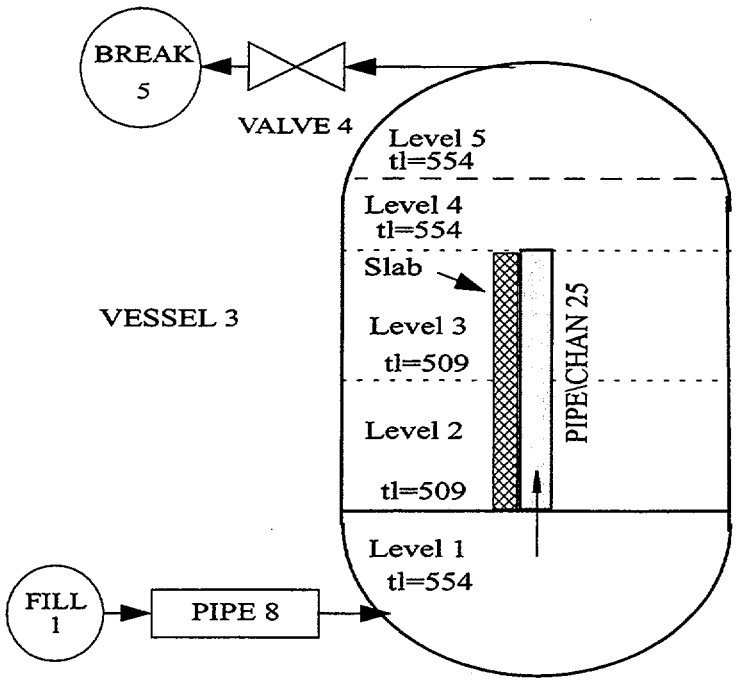

Figure 5.3.7 3-D Requirement 3 Nodalization Diagram

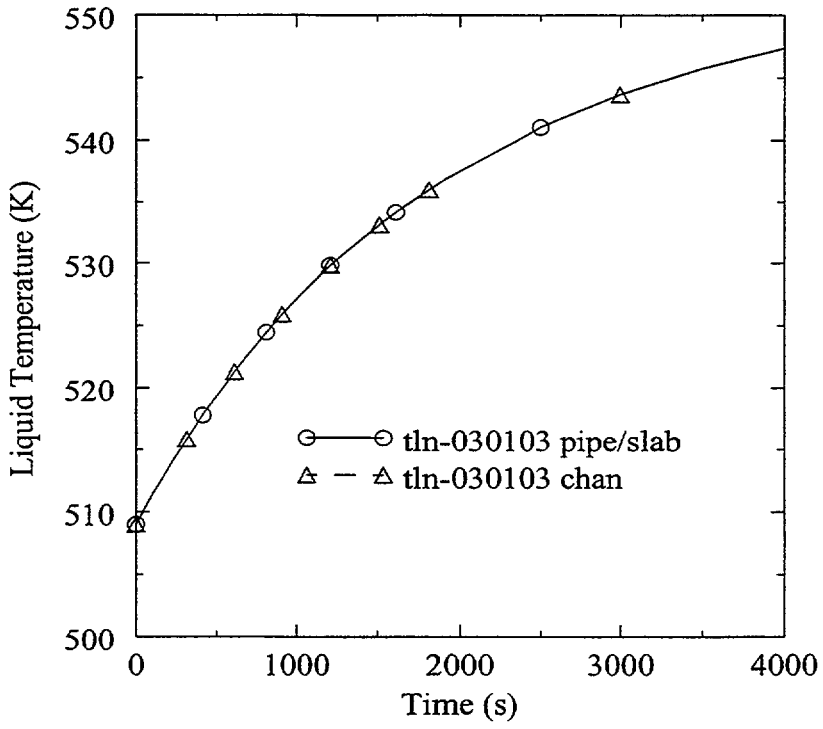

Figure 5.3.8 3-D Results for Requirement 3

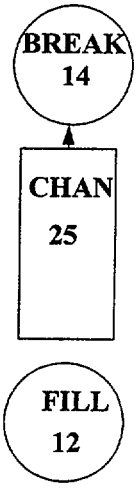

Figure 5.3.9 One Cell CHAN with FILL and BREAK

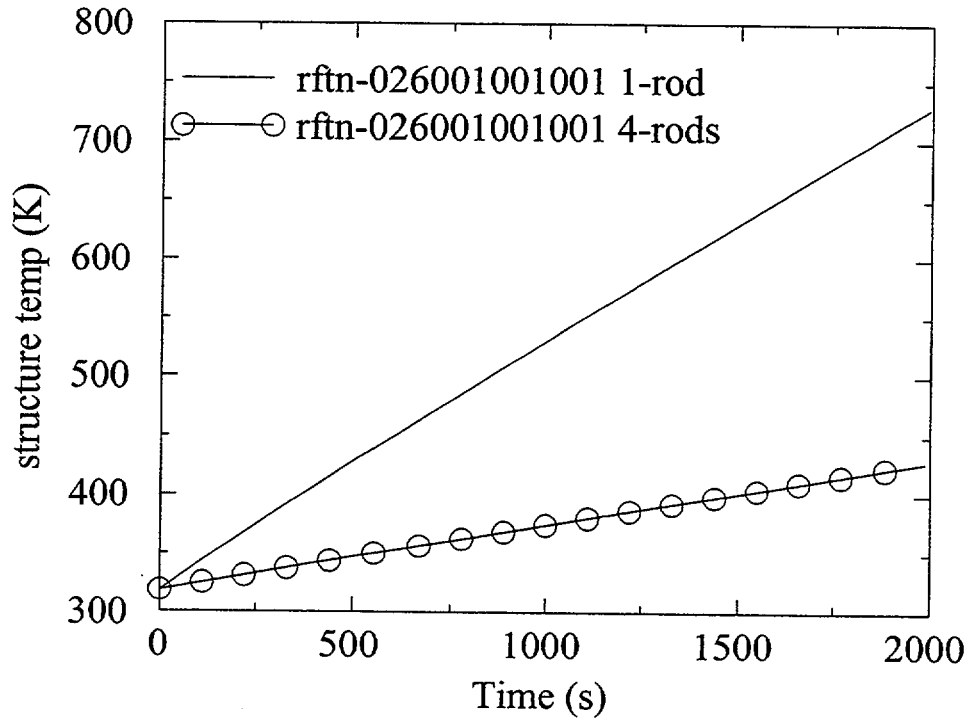

Figure 5.3.10 Effect of Multiple Rods (Requirement 4) on Rod Heat-Up

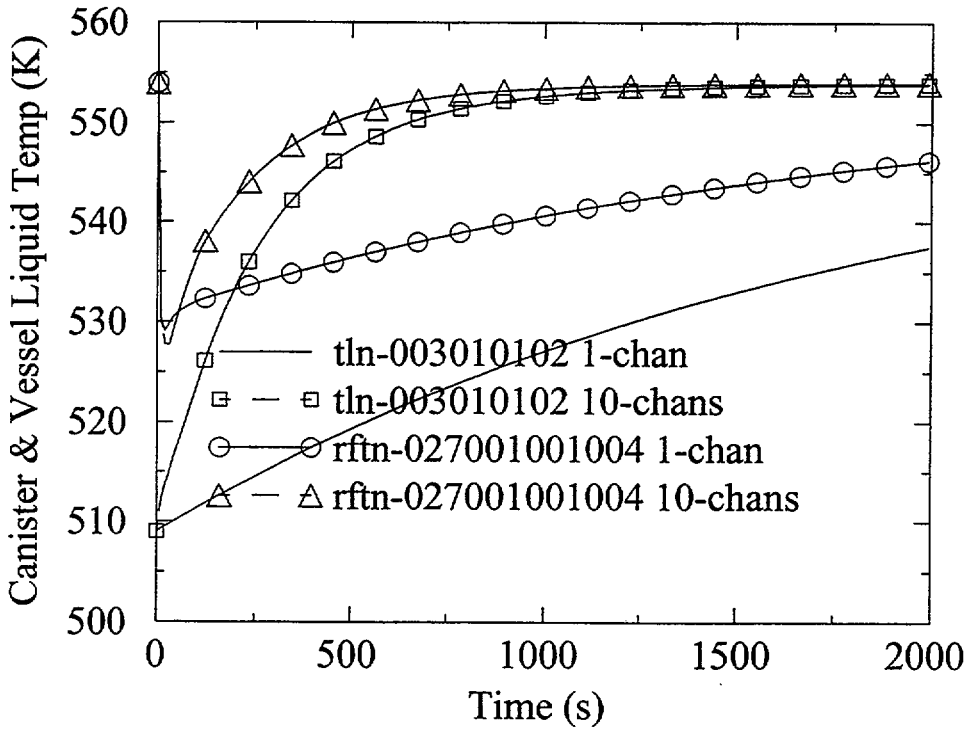

Figure 5.3.11 Vessel and Canister Wall Temperatures with 1 CHAN Compared to 10 CHANs

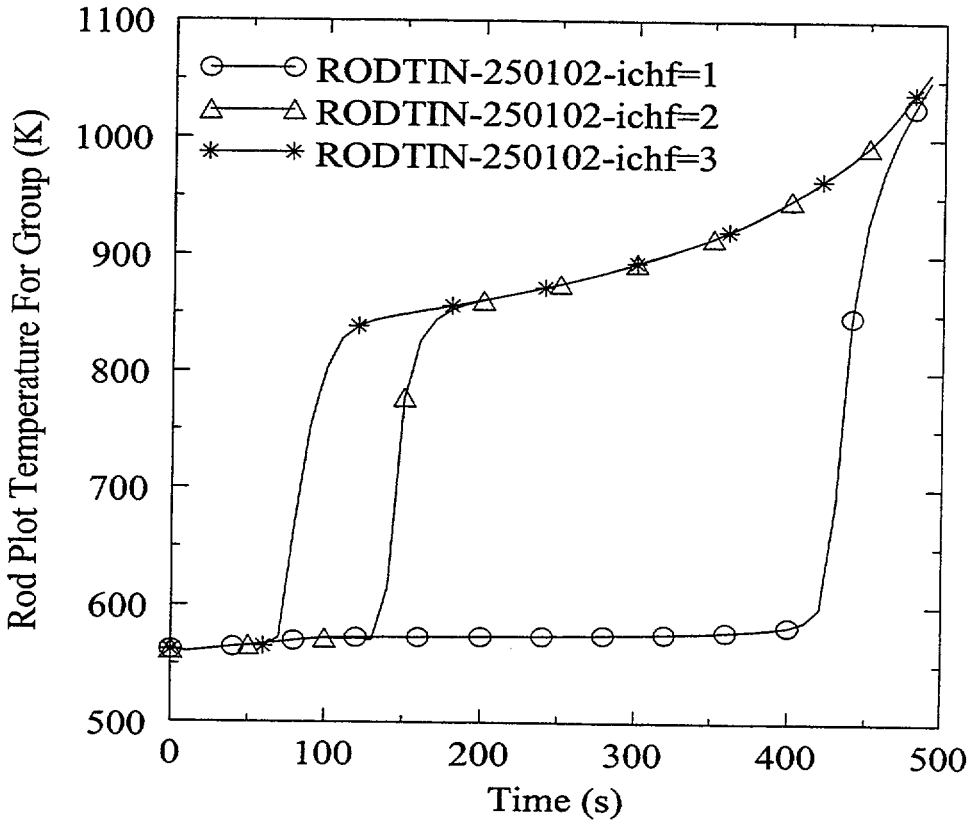

Figure 5.3.12 TRAC-B Results for Requirement 6

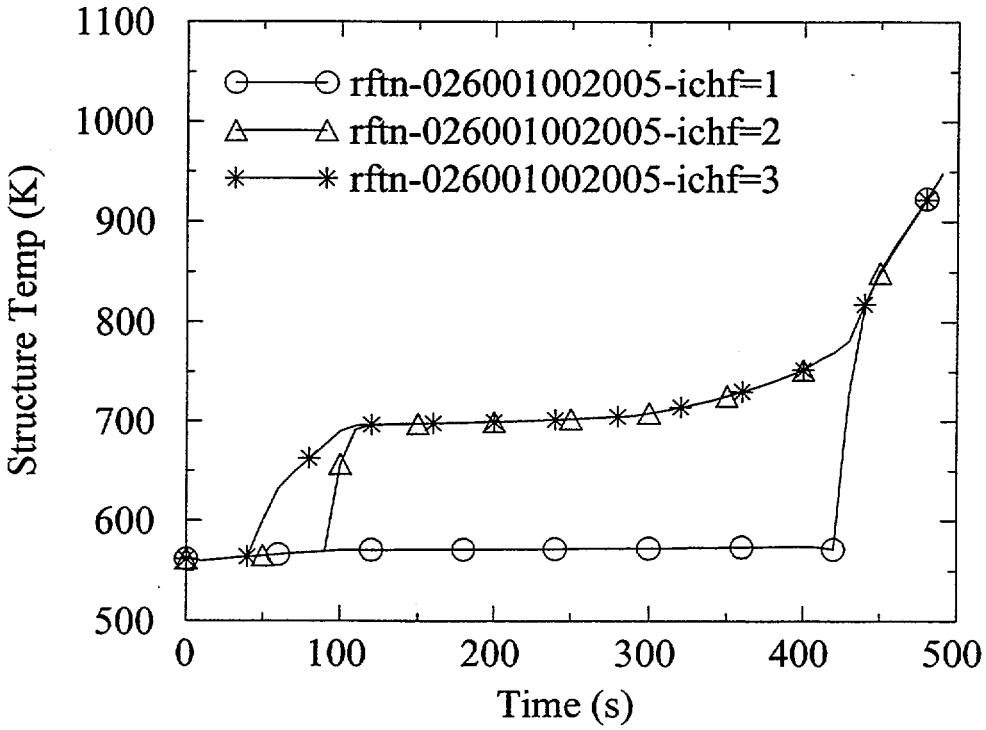

Figure 5.3.13 TRAC-M Results for Requirement 6

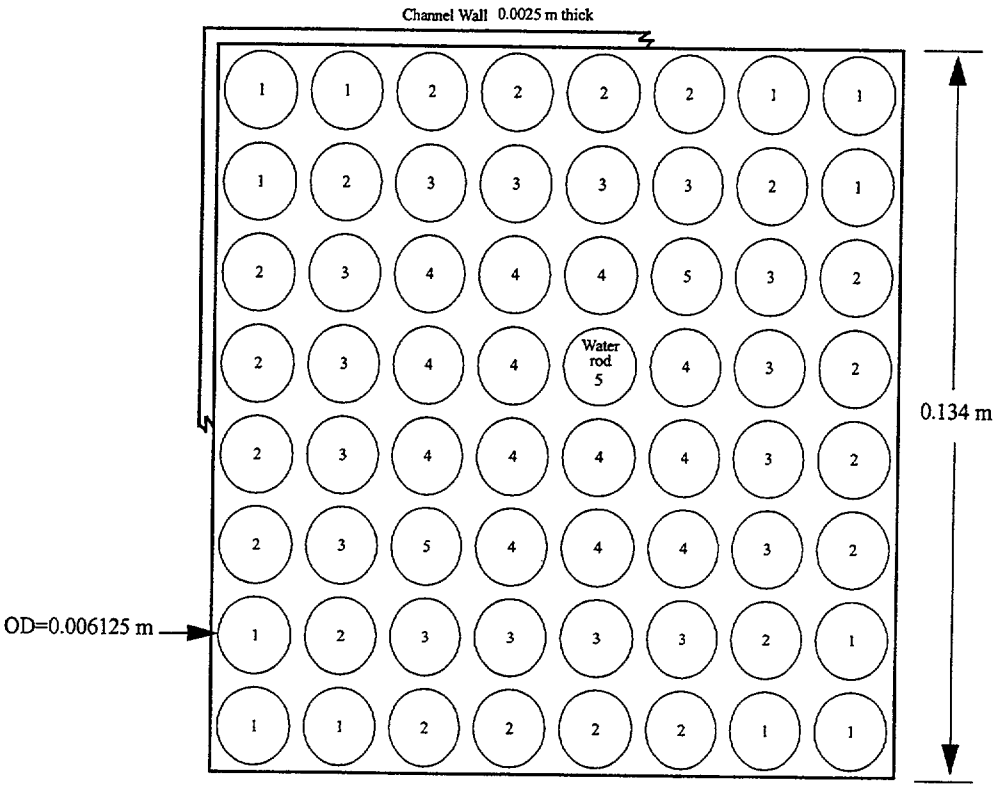

Figure 5.3.14 Geometry of GOTA Radiation Test Model Section

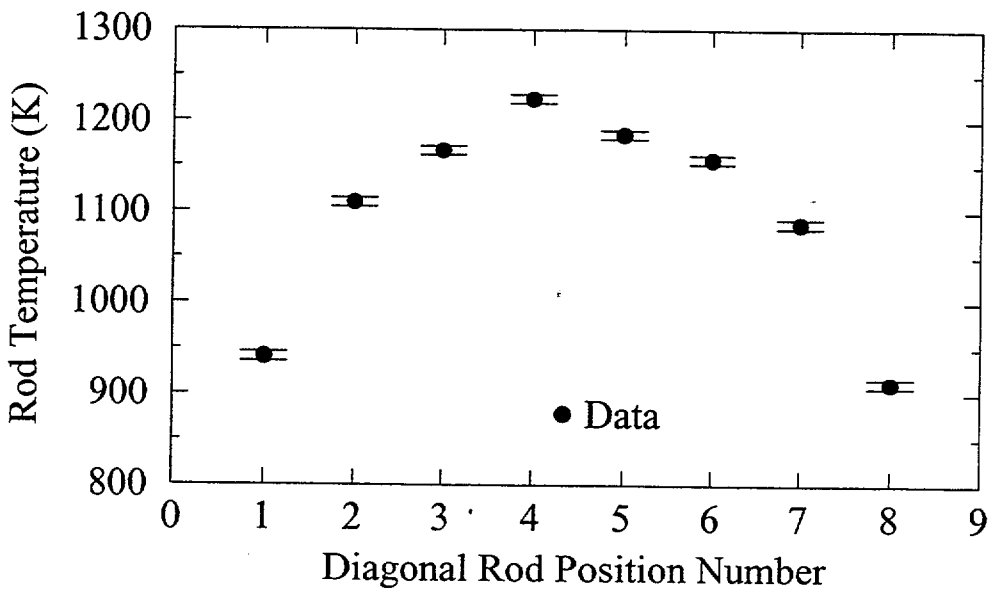

Figure 5.3.15 GOTA Radiation Test 27 Results

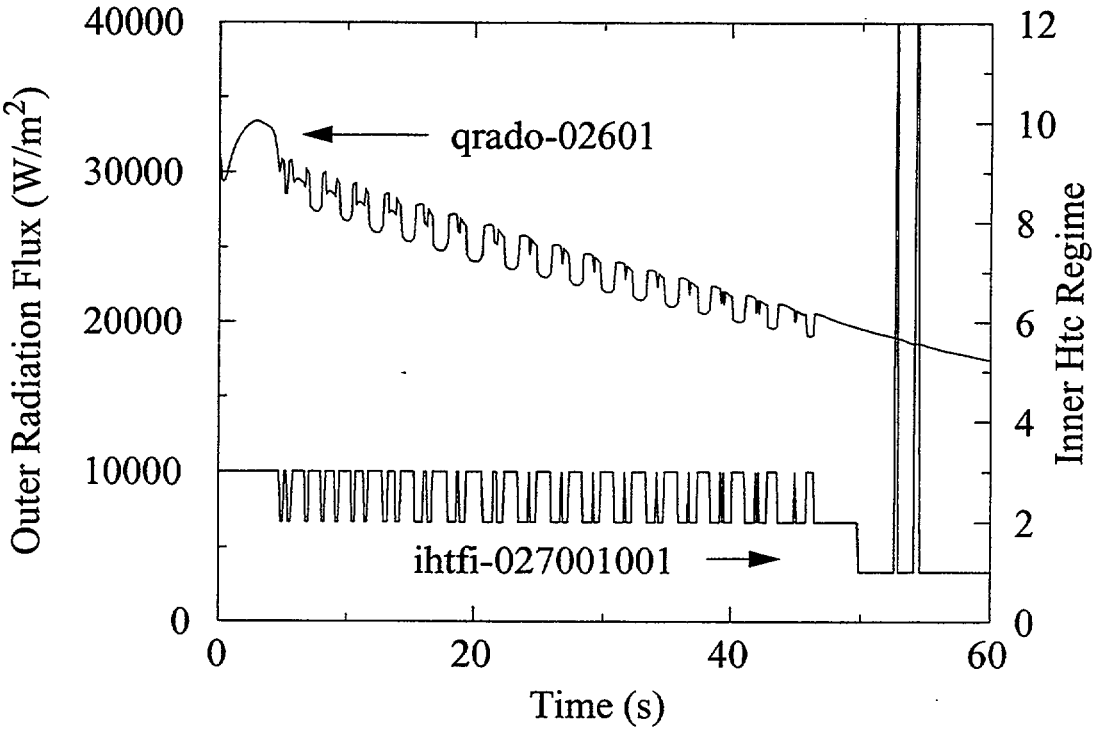

Figure 5.3.16 Effect of Canister Quenching on Rod Radiation (Requirement 7.1)

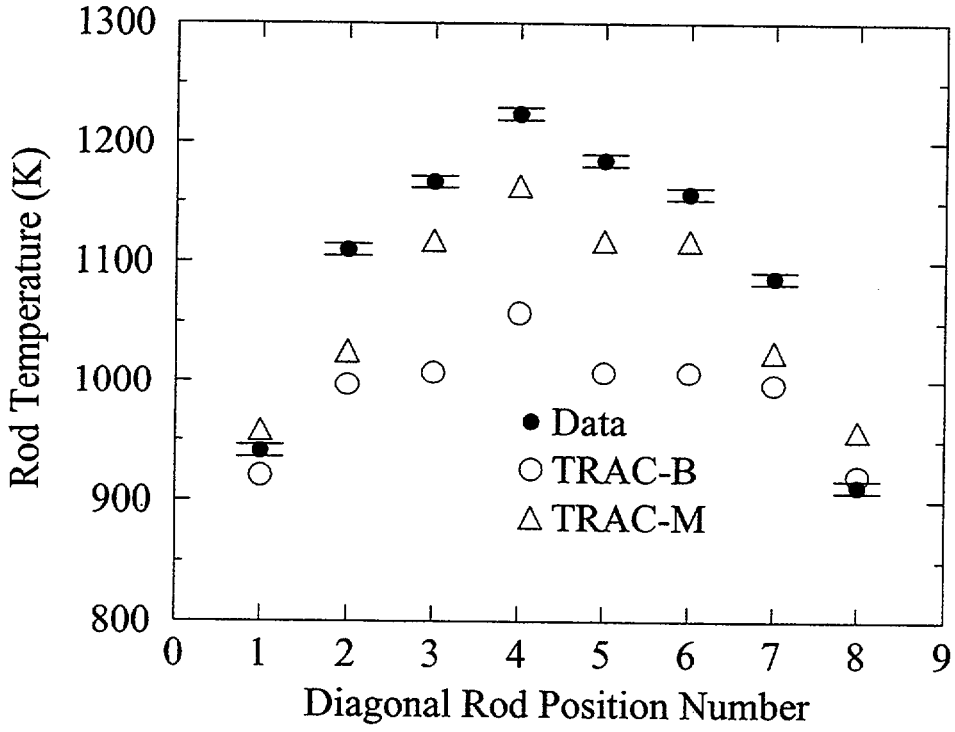

Figure 5.3.17 GOTA Radiation Test 27 Results with 5 Rod Groups

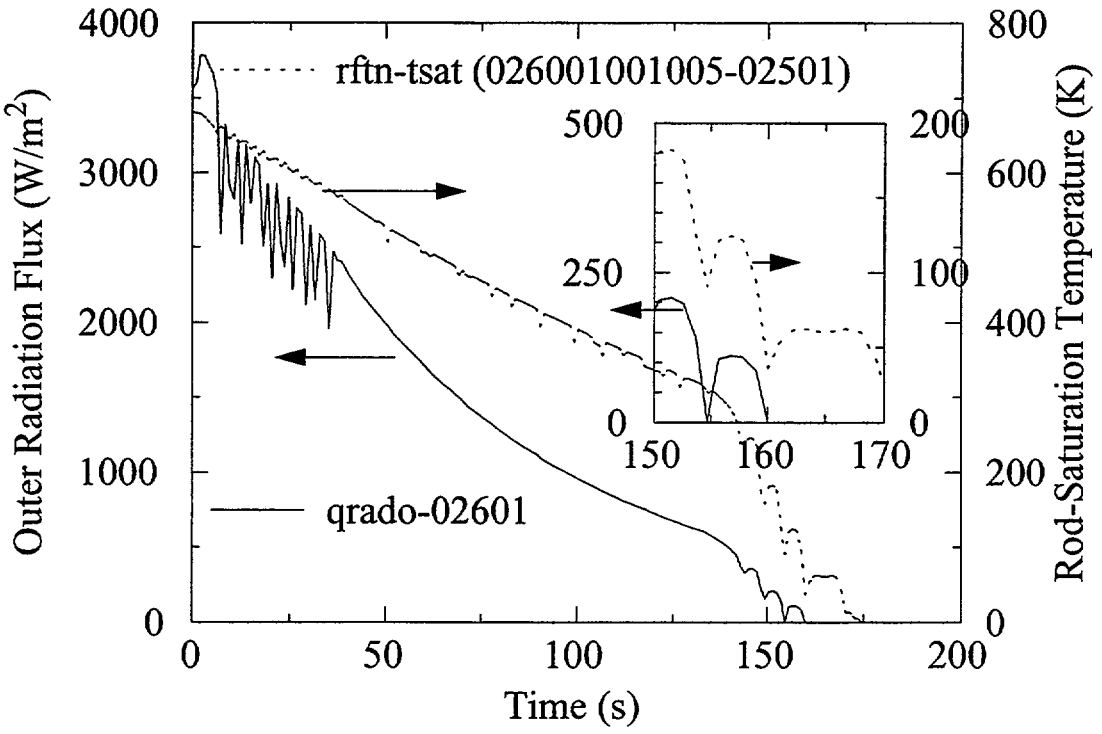

Figure 5.3.18 Demonstration of Radiation Cut-Off (Requirement 7.6)

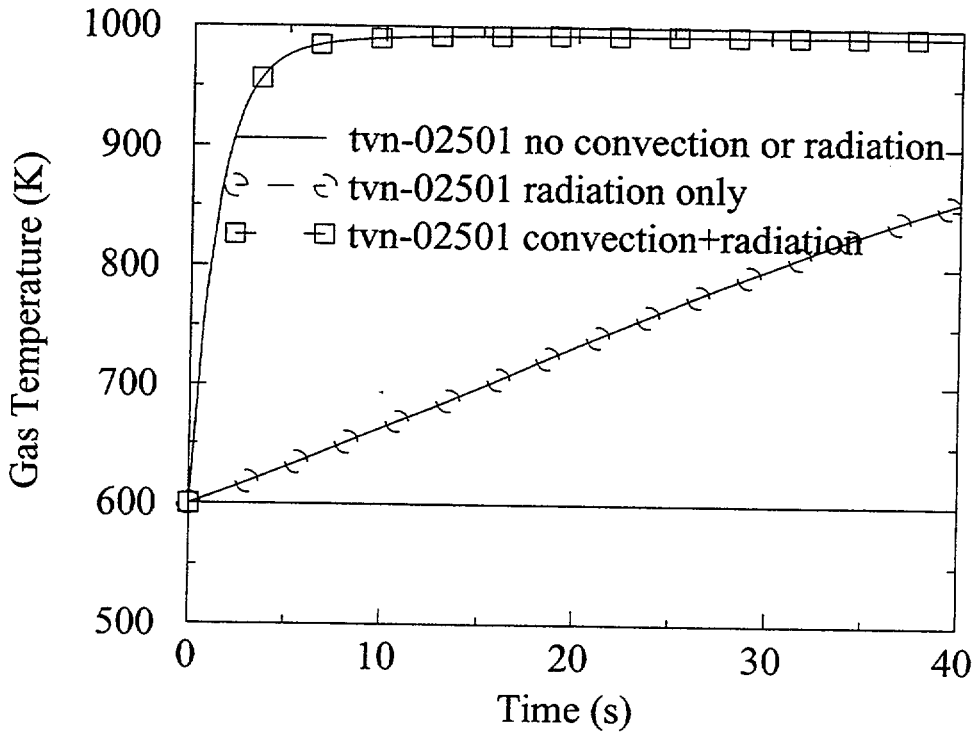

Figure 5.3.19 Demonstration of Energy Absorption by Steam (Requirement 7.7)

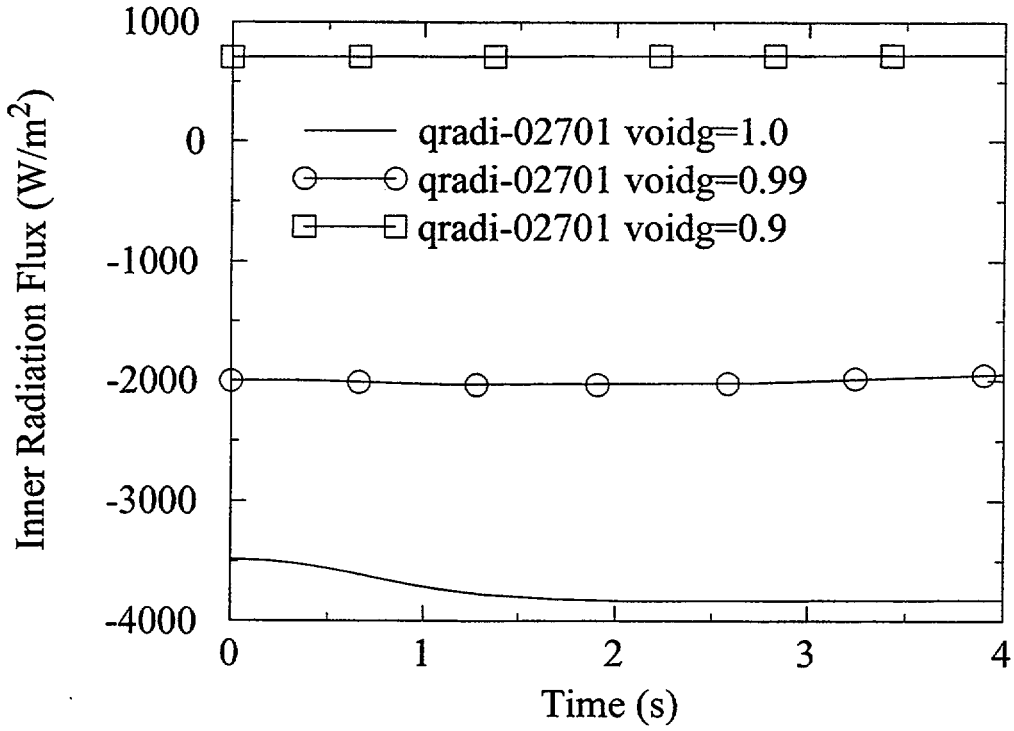

Figure 5.3.20 Effect of Water on the Radiation to the Canister Wall (Requirement 7.7)

5.4 Level Tracking (LTRCK) Model

The tracking of liquid and two-phase levels is essential for accurate predictions of the liquid inventories during a LOCA and transient events. Originally, the finite volume approximations to the equations governing two-phase flow in TRAC assumed a void fraction that is uniformly distributed throughout each fluid volume. In vertical flows, this assumption results in solutions to the governing equations that over-calculate cell-to-cell fluid mass convection. Over-estimating fluid convection introduces large errors, especially in the large finite volumes contained in the TRAC VESSEL component. For transients where a distinct two-phase region develops below a steam region, the step change in void fraction across the two-phase steam interface becomes dissipated as liquid is artificially convected upward into the above steam region.

Most BWR transients rely on accurate prediction of water levels. It is especially important to simulate the behavior of the downcomer liquid level during recirculation line breaks. For instance, accurate prediction of the timing for uncovering the jet pump suction inlet as the water level decreases in the downcomer is essential to determine the rate at which the system will depressurize and, thus, the history of the vessel water inventory. As the water level in the downcomer decreases during a recirculation line small break, only liquid should enter the jet pump suction until the liquid level in the downcomer cell above the jet pump suction (the donor cell) falls below the suction inlet. Thereafter, the fluid entering the suction inlet should be mostly vapor. Without the level tracking model, vapor will enter the jet pump inlet at the moment that vapor first appears in the donor cell, resulting in a premature uncovering of the jet pump suction. Proper use of level tracking in TRAC eliminates this problem. Thus, level tracking significantly improves the ability of TRAC to predict the rapid depressurization that occurs in a recirculation line break transient as vapor is allowed to flow out of the break. Without level tracking, TRAC cannot predict this behavior because of the "smearing" of the void fraction in the downcomer. In addition, reliance on the cell average void fractions for the evaluation of the constitutive relationships will not enable the code to distinguish between the two situations illustrated in Fig. 5.4.1, where the interfacial heat transfer conditions are markedly different.

The level tracking method was originally developed cooperatively by General Electric and the Idaho National Engineering Laboratory (INEL) to simulate the sharp void fraction gradients that develop across two-phase steam interfaces in TRAC-B simulations (Ref. 5.4.1). The TRAC-B level tracking model enables the code to track a two-phase level inside a vertically oriented 1-D component or a stack of vertical cells in a 3-D vessel component. The model predicts the two-phase level location, and calculates the above- and below-level void fractions. These non-cell-centered void fractions are then used to correct the flux of fluid mass and energy when a two-phase level is present.

As part of the consolidation effort, the TRAC-BF1 water level tracking model will be implemented into TRAC-M. The software requirements for this model are provided in the following section.

5.4.1 Requirements

The current TRAC-BF1 level tracking model performs several calculational steps to track the two-phase level and correct the solution of the hydraulic equations. The model first detects the existence of a two-phase level within a stack of vertical cells in either a 1-D or a 3-D component

for a normal or an inverted void fraction profile. The model then predicts the above- and below-level void fractions, the level position, and the level velocity. Based on the level position and velocity, the model examines the possibility of a level to cross a cell boundary during the next time step. If the level is predicted to cross a cell boundary, the model calculates the cell junction phasic velocities, and these data are then passed to the hydraulic solution scheme. These functional features of the model will be preserved during the consolidation. In addition, the input and output features of the TRAC-BF1 level tracking option will be included in TRAC-M when the water level tracking model is exercised.

Requirement LTRCK 1.0: Tracking of Two-Phase Level In Vertical Flow Regions

The level tracking model will calculate the location of the two-phase level in all vertical regions with either a normal or an inverted void profile. The model should track both liquid and two-phase levels that are increasing or decreasing in the 1-D or 3-D components. The model is required to track levels that propagate across cell boundaries, as well as across junctions that connect two components. Based on the predicted level location, the model should calculate the above- and below-level void fractions, level velocities, and cell junction phasic velocities.

In order to provide detailed requirements, two sub-requirements are specified for the level tracking model used with either normal or inverted void profiles. These requirements are described below.

Requirement LTRCK 1.1: Tracking of Two-Phase Level With Normal Void Profile

Level Detection Logic

The level tracking model will determine the two-phase level position with a normal void profile. A normal void profile has the void fraction increasing from the bottom to the top of the flow channel. The following criteria will be used to determine the existence of the two-phase level.

As shown in Fig. 5.4.2, if the two-phase level exists inside cell j,

$$(\alpha_{j+1}-\alpha_j) > \Delta\alpha_{\text{cut-off}} \quad \text{or} \quad (\alpha_j-\alpha_{j-1}) > \Delta\alpha_{\text{cut-off}} \quad \text{and} \quad \alpha_{j+1} > \alpha_{\text{cut-off}} \tag{5.4.1}$$

provided that no level exists in cell j+1 or cell j-1. Here, $\Delta\alpha_{\text{cut-off}}$ and $\alpha_{\text{cut-off}}$ are predetermined cut-off values, which have default values of 0.2 and 0.7 or are specified by the user. The nomenclature for the level tracking model is presented in Table 5.4.1.

Above-and Below-Level Void Fraction Determination

The below-level void fraction in cell j is assumed to equal the void fraction in cell j-1, and the above-level void fraction equals the void fraction of cell j+1, if the velocity from the previous time step at the top of cell j is downward. Conversely, when the velocity at the cell junction is upward, the liquid entrainment tends to lower the above-level void fraction. In this situation, an entrainment correlation developed by Rosen (Ref. 5.4.2) is employed to predict the liquid entrainment.

The entrained liquid mass flux is expressed as follows:

$$G_{lent} = \left[3. \times 10^{-5}(CK^{0.5} + 530.CK^{2.1})\left(\frac{\rho_l - \rho_g}{\rho_g}\right)^{0.5}\right] J_g \rho_g \tag{5.4.2}$$

where

$$CK = \frac{2.\ DMAX\, J_g}{\left[VCRIT\left(\frac{\sigma}{g(\rho_l - \rho_g)}\right)^{0.5}\right]} \tag{5.4.3}$$

$$VCRIT = 2.\left(\frac{\sigma g(\rho_l - \rho_g)}{\rho_g^2}\right)^{0.25} \tag{5.4.4}$$

$$DMAX = 0.3375\left[\frac{\rho_g V_g^2}{g(\rho_l - \rho_g)}\right] \tag{5.4.5}$$

In Equation 5.4.2, G_{lent} is calculated using donor cell-averaged values for ρ_l, ρ_g, and σ at cell j. The value of J_g is set equal to the value where

$$J_g = \alpha_{j+1} V_g \tag{5.4.6}$$

and

$$V_g = V_{g,j+1/2}\left(\frac{A_{j+1/2}}{A_j}\right) . \tag{5.4.7}$$

$V_{g,\,j+1/2}$ is the junction vapor phasic velocity calculated by the momentum solution solver and passed to the level tracking subroutine.

Using the conservation of mass, the liquid mass flux out of the top of the cell j is equal to

$$G_{lent} = (1 - \alpha_j^+)\rho_l V_l \tag{5.4.8}$$

from which the above-level void fraction, α_j^+, is computed to be

$$\alpha_j^+ = 1 - \frac{G_{lent}}{\rho_l V_l} \tag{5.4.9}$$

and

$$V_l = V_{l,j+1/2}\left(\frac{A_{j+1/2}}{A_j}\right) \tag{5.4.10}$$

Two-Phase Level Position, Velocity, and Cell Boundary Crossing Determination

With the calculated above- and below-level void fractions determined in the previous section, the level position inside a cell is now calculated as follows:

$$L_j = \Delta z_j\left(\frac{\alpha^+{}_j - \alpha_j}{\alpha^+{}_j - \alpha^-{}_j}\right) \tag{5.4.11}$$

In the above equation, α_j is the cell average void fraction and $\alpha^-{}_j$ and $\alpha^+{}_j$ are the below and above level void fractions, respectively (Fig. 5.4.3). The level velocity can then readily be calculated by taking the derivative of Equation 5.4.11.

$$V_{\text{level},j} = \frac{\Delta z_j \frac{d\alpha_j}{dt} - L_j \frac{d\alpha^-{}_j}{dt} - (\Delta z_j - L_j)\frac{d\alpha^+{}_j}{dt}}{\alpha^-{}_j - \alpha^+{}_j} \tag{5.4.12}$$

With the level velocity, two criteria are used to determine if a level will cross an axial cell boundary. For a rising level, $V_{\text{level},j} > 0$, the condition is

$$(\alpha_j - \alpha_j^-) < \delta\alpha_{\text{level}} \tag{5.4.13}$$

If $V_{\text{level},j} < 0$, the criteria for a falling level is

$$(\alpha_j^+ - \alpha_j) < \delta\alpha_{\text{level}} \tag{5.4.14}$$

The parameter, $\delta\alpha_{\text{level}}$, is user-defined with a default value of 0.02 (Ref. 5.4.1).

The second criteria is employed to test the possibility that the mixture level will advance into the adjacent cell during the next time step. The criteria for a rising level to advance to the next cell is

$$\frac{\Delta z_j - L_j}{|V_{\text{level},j}|} < \Delta t \tag{5.4.15}$$

For a decreasing water level, the same criteria is

$$\frac{L_j}{|V_{level,j}|} < \Delta t \tag{5.4.16}$$

Cell Junction Phasic Velocity Determination

There is a discontinuous change in the void fraction and phasic velocity at the cell boundary when a two-phase level crosses a cell boundary. When this occurs, the level tracking model modifies the phasic velocities to stabilize the numerics. The modified level velocities are determined from the jump conditions

$$V_{\text{level},j} = \frac{J_g^- - J_g^+}{\alpha_j^- - \alpha_j^+} \tag{5.4.17}$$

or

$$V_{\text{level},j} = \frac{J_\ell^- - J_\ell^+}{\alpha_j^+ - \alpha_j^-} \tag{5.4.18}$$

For a rising level that will cross a cell boundary at the next time step, the liquid velocity at the boundary is calculated using Equation 5.4.18. The modified previous time step junction liquid velocity becomes

$$(V_\ell)^n_{j-1/2} = \frac{(\alpha^+_j - \alpha^-_j)V_{\text{level},j} + (1-\alpha_j^+)(V_\ell)^n_{j+1/2}}{1-\alpha^-_j} \tag{5.4.19}$$

For a decreasing level that will cross a cell boundary at the next time step, the modified previous time junction vapor velocity at the boundary is calculated from Equation 5.4.17, as follows.

$$(V_g)^n_{j-1/2} = \frac{\alpha^-_j (V_g)^n_{j-1/2} - (\alpha^-_j - \alpha^n_j)V_{\text{level},j}}{\alpha} \tag{5.4.20}$$

One should note that the use of Equations 5.4.19 and 5.4.20, based on the jump discontinuity condition, are expected to introduce radical changes in the interfacial shear, resulting in instantaneous changes in pressure, vapor velocity, and liquid velocity. Further assessment of the model will indicate significance of these discontinuities and if needed, necessity of improvements.

Requirement LTRCK 1.2: Tracking of Two-Phase Levels In Inverted Void Profiles

The level tracking model will track water levels in vertical components with inverted void profiles. That is, when area contractions are contained in vertical regions, the steam velocities can prevent the down-flow of liquid across the area change, causing the development of levels in the

adjacent cells. The model should track the location of the levels in the adjacent cells, as well as the void discontinuities in these two regions.

The importance of this requirement is that because of the large area restrictions at the core inlet and outlet of a BWR, countercurrent flow limitations (CCFLs) may inhibit the draining of liquid across these boundaries. This hydraulic condition would result in steam regions developing below the two-phase regions in the vessel lower plenum, core, and upper plenum. The level tracking will, therefore, be able to track the two-phase levels under these inverted void profile conditions.

Level Detection Logic

An inverted void profile typically appears during a LOCA when liquid collects in pools on the upper or lower tie plates of a BWR reactor pressure vessel. Thus, the level tracking model first checks for the presence of flow restrictions by calculating the area ratios for a cell-to-cell junction (see Ref. 5.4.1) when

$$E = \frac{A_{j+1/2} - A_{j+3/2}}{A_{j+3/2}} \tag{5.4.21}$$

$$B = \frac{A_{j+1/2} - A_{j-1/2}}{A_{j-1/2}} \tag{5.4.22}$$

If E is greater than 0.5, a flag is set for an area reduction above cell j; if B is greater than 0.5, a flag is set for a area reduction below cell j. In either case, the code logic automatically initiates a search for a void profile inversion. As it does if the inlet or outlet cell flow area is less than 1.E-10 m^2, then, if

$$\alpha_j - \alpha_{j+1} > \Delta\alpha_{\text{cut-off, inverted}} \tag{5.4.23}$$

the void inversion is above Cell, j.

If

$$\alpha_{j-1} - \alpha_j > \Delta\alpha_{\text{cut-off, inverted}} \tag{5.4.24}$$

the void inversion is below cell j. Here, $\Delta\alpha_{\text{cut-off, inverted}}$ is a user-input, predetermined cut-off value with a default value of 0.1. For the case with cell j below the void inversion, the model assumes the existence of a two-phase level if the criterion is satisfied where

$$(0.999 - \alpha_j) > \Delta\alpha_{\text{cut-off}} \quad or \quad (\alpha_j - \alpha_{j-1}) > \Delta\alpha_{\text{cut-off}} \tag{5.4.25}$$

For the case with cell j above the void inversion, the model assumes the existence of a two-phase level if

$$(\alpha_{j+1} - \alpha_j) > \Delta\alpha_{\text{cut-off}} \quad \text{or} \quad (\alpha_j - 0.001) > \Delta\alpha_{\text{cut-off}} \text{ and } \alpha_{j+1} > \alpha_{\text{cut-off}} \tag{5.4.26}$$

Above- and Below-Level Void Fraction Determination

For the case with a flow area reduction at the top of cell j, Rosen's entrainment correlation (Ref. 5.4.2) will be employed with the modified vapor volumetric flux density to calculate the above-level void fraction. The J_g term of Equation 5.4.2 is calculated as

$$J_g = 0.999 V_g \tag{5.4.27}$$

For the case with a two-phase level occurring above a void fraction inversion or bottom cell area reduction, the below-cell void fraction will be calculated using the drift flux approximation, where

$$\alpha_j^- = \frac{J_g^-}{C_0 J^- + V_{gj}} \tag{5.4.28}$$

$$V_{gj} = 1.41\left(\frac{\Delta\rho g\sigma}{\rho_l^2}\right)^{1/4} \tag{5.4.29}$$

$$C_0 = C_\infty - (C_\infty - 1)\sqrt{\frac{\rho_g}{\rho_l}} \tag{5.4.30}$$

$$C_\infty = 1.395 - 0.15\ln(Re) \tag{5.4.31}$$

and the Reynolds number (Re) is calculated as

$$Re = \frac{GD_h}{\mu_\ell} \tag{5.4.32}$$

The volume fluxes, J^-_g and J^-, are calculated using junction-donored velocities from the bottom of cell j, and void fractions from either cell j-1 or the previous-time step cell j void fraction.

Two-Phase Level Position, Velocity, and Cell Boundary Crossing Determination

The same methods used to evaluate normal void profiles are applicable to inverted void profiles.

Cell Junction Phasic Velocity Determination

The same methods used to evaluate normal void profiles are applicable to inverted void profiles.

Requirement LTRCK 2: Interaction With Thermal-Hydraulic Equations

The finite volume equations in TRAC-M will be modified to use the above- and below-level void fractions when a two-phase level is present in vertically oriented components, using the same methodology employed in TRAC-B. The use of above- and below-level void fractions from the level tracking model will preclude the "smearing" of the void fraction across two-phase steam interfaces. The inertia terms in the momentum equations will also be corrected using the same methodology that is employed in TRAC-B.

Requirement LTRCK 2.1: Above- and Below-Level Void Fractions as Donor Quantities

When a two-phase level exists in cell j or j+1, as illustrated in Fig. 5.4.4, the previous time step level flux terms are defined using the following equation, which specifies how the donor cell flux terms are computed using the below-and above-level void fraction:

$$(\alpha\rho V)^n_{f,\,j+1/2} = \begin{cases} (\alpha\rho)^n_{f,j} \quad V^n_{f,\,j+1/2} & , \quad \text{if } V^n_{f,\,j+1/2} > 0 \text{ and no level exists in cell j} \\ (\alpha\rho)^n_{f,\,j+1} \quad V^n_{f,\,j+1/2} & , \quad \text{if } V^n_{f,\,j+1/2} < 0 \text{ and a level exists in cell j} \\ \alpha^{+}_{f,j}\rho^n_{f,j} \quad V^n_{f,\,j+1/2} & , \quad \text{if } V^n_{f,\,j+1/2} > 0 \text{ and a level exists in cell j} \\ (\alpha\rho)^n_{f,\,j+1} \quad V^n_{f,\,j+1/2} & , \quad \text{if } V^n_{f,\,j+1/2} < 0 \text{ and no level exists in cell j+1} \\ (\alpha\rho)^n_{j} \quad V^n_{f,\,j+1/2} & , \quad \text{if } V^n_{f,\,j+1/2} > 0 \text{ and a level exists in cell j+1} \\ \alpha^{-}_{f,\,j+1}\rho^n_{f,\,j+1} \quad V^n_{f,\,j+1/2} & , \quad \text{if } V^n_{f,\,j+1/2} < 0 \text{ and a level exists in cell j+1} \end{cases} \qquad (5.4.33)$$

where $f = \ell, g$

The flux of $(\alpha\rho eV)$ in the energy equations will also be modified similarly.

Since TRAC-B deactivates the Courant Limit Violating (CLV) numerics when the level tracking option is active, TRAC-M will also deactivate the SETS method and use the semi-implicit method. This is necessary because the level tracking model is an explicit scheme.

Requirement LTRCK 2.2: Inertial Terms in the Momentum Equations

The modifications to the inertial terms in the basic momentum equations of TRAC-B will be implemented into the basic momentum equations of TRAC-M as follows:

$$(\alpha\rho)_{f,\,j+1/2} = \frac{A_1\Delta z_j\rho_{f,j} + A_2\Delta z_{j+1}\rho_{f,\,j+1}}{\Delta z_{j+1} + \Delta z_j} \qquad (5.4.34)$$

where

$$A_1 = \begin{cases} \alpha_{f,j}, & \text{no mixture level between j and j+1/2;} \\ \dfrac{[L_j - (\Delta z_j/2)]\alpha_{f,j} + (\Delta z_j - L_j)\alpha^+_{f,j}}{\Delta z_j/2}, & \text{mixture level between j and j+1/2.} \end{cases} \quad (5.4.35)$$

$$A_2 = \begin{cases} \alpha_{f,j+1}, & \text{no mixture level between j+1/2 and j+1;} \\ \dfrac{[(\Delta z_{j+1}/2) - L_{j+1}]\alpha^+_{f,j+1} + L_{j+1}\alpha^-_{f,j+1}}{\Delta z_{j+1}/2}, & \text{mixture level between j+1/2 and j+1.} \end{cases} \quad (5.4.36)$$

In the above equations, f becomes ℓ for liquid, and g for gas phases.

Requirement LTRCK 2.3: VESSEL Boundary Condition

The level tracking model will also be implemented into the selection of boundary conditions that are used for the vessel source connections. This requires an additional vessel source input to specify the axial location of the connection within the vessel cell. When a source is connected to a vessel cell containing a two-phase level, the vessel void fraction stored in the boundary array will depend on the location of the two-phase level. As shown in Fig. 5.4.3, the vessel void fraction stored in the boundary array is

$$\alpha_{vessel} = \begin{cases} \alpha^+_j & for\ L_j \le Z_{\text{junction}} - r \\ \alpha^-_j & for\ L_j \ge Z_{\text{junction}} + r \\ \xi\alpha^+_j + (1-\xi)\alpha^-_j & for\ Z_{\text{junction}} - r < L_j < Z_{\text{junction}} + r \end{cases} \quad (5.4.37)$$

where $\xi = \dfrac{A_{\text{level}}}{A_{\text{total}}}$, A_{level} is the flow area of source connection above level, and A_{total} is the flow area of the source connection.

Requirement LTRCK 2.4: Interfacial Heat Transfer in Partially Filled Cells

The level tracking model corrects the interfacial heat transfer coefficients for a partially filled cell, as illustrated in Fig. 5.4.2, ignoring the vapor space heat exchange when the flow is stratified and the level tracking is activated. If the above-level void fraction is greater than 0.999, TRAC-B then calculates the total interfacial heat transfer per unit volume for a partially filled cell as two components (one below the level, and one at the free surface).

Below the level, the interfacial heat transfer is calculated from Equations 5.4.38 and 5.4.39, where the heat transfer coefficients, $h^-_{i\ell}$ and h^-_{ig}, are predicted using the below-level void fraction.

$$(Ah)^-_{i\ell} = \frac{L_j}{\Delta z_j} Vol_j \frac{1}{d_i} h^-_{i\ell} \quad (5.4.38)$$

$$(Ah)^{-}_{ig} = \frac{L_j}{\Delta z_j} Vol_j \frac{1}{d_i} h^{-}_{ig} \tag{5.4.39}$$

At the location of the level, the interfacial heat transfer is calculated from

$$(Ah)^{L}_{i\ell} = A\, h^{L}_{i\ell} \tag{5.4.40}$$

$$(Ah)^{L}_{ig} = A\, h^{L}_{ig} \tag{5.4.41}$$

where the heat transfer coefficients at the level are given by

$$h^{L}_{i\ell} = \frac{k_\ell}{k_a}\ 1.027\ |T_\ell - T_s|^{\frac{1}{3}} \tag{5.4.42}$$

$$h^{L}_{ig} = \frac{k_g}{k_a}\ 1.027\ |T_g - T_s|^{\frac{1}{3}} \tag{5.4.43}$$

The total heat transfer coefficient for a partially filled cell with $\alpha^{+} \geq 0.999$ is given by

$$(Ah)_{i\ell} = (Ah)^{-}_{i\ell} + (Ah)^{L}_{i\ell} \tag{5.4.44}$$

$$(Ah)_{ig} = (Ah)^{-}_{ig} + (Ah)^{L}_{ig} \tag{5.4.45}$$

It is important to mention that the above model is not intended to replace the interfacial area model for stratified flows in TRAC-M. However, modifications to the TRAC-M model will be made to correct the interfacial heat transfer area at and below the free surface. The position of the free surface and the volume of two-phase mixture below the free surface will be determined by the level tracking model.

Requirement LTRCK 3.0: Input, Output, and Restart Requirement

The input and output of TRAC-M will be modified to accommodate the addition of a level tracking option for all of the applicable 1-D and 3-D components. The following parameters will be made available for the output:

- ILEV: Two-phase level flag
- ALPA: Above-level void fraction
- ALPB: Below-level void fraction
- DZLEV: Height of two-phase level above bottom of the cell
- VLEV: Propagation velocity of two-phase level

For the input, the ILEV and DZLEV variables are required for applicable components. In addition, the 1-D source center line elevation versus the 3-D vessel cell height, ZFRAC, is also required for each 1-D connection with the VESSEL component.

Table 5.4.2 summarizes the requirements for the Level Tracking (LTRCK) model.

5.4.2 Verification Testing and Assessment

As identified in Table 5.4.2, the LTRCK model has three major software requirements, divided into six sub-requirements. A total of 19 test problems are designed to examine the code according to the requirements, as summarized in Table 5.4.3. The test problems are discussed in detail below.

5.4.2.1 Verification Tests for Requirements LTRCK 1.1, 2.1, and 2.2

Requirement LTRCK 1.1 requires that both 1-D and 3-D level tracking models must be able to track a two-phase water level for a normal void fraction distribution. In addition, Requirements LTRCK 2.1 and 2.2 require that the model must be able to provide the correct feedback to the hydraulic solution. Test Problems 1 through 11 are employed to test the code for several different component types and nodalizations. These first 11 test problems are discussed below, as they pertain to the software requirements identified as LTRCK 1.1, 2.1, and 2.2.

Test Problem 1. Single Pipe Component Fill and Drain Test Problem

This test problem is designed to test the TRAC-M 1-D level tracking model for a PIPE component, and to examine the software requirements of LTRCK 1.1, 2.1, and 2.2. As shown in Fig. 5.4.5, the test problem consists of a vertical PIPE component with 10 axial nodes, a BREAK component with a constant pressure, and a FILL component that provides a velocity boundary. The PIPE is 3 m high, and each cell has a height of 0.3 m and a volume of 0.09 m^3. Each cell edge has a flow area of 0.3 m^2, with a zero friction loss coefficient and 0.1 m hydraulic diameter. The pressure of the BREAK component is set to a value of 1.01325E+5 Pa.

In order to establish a slow fill and drain transient, a liquid velocity versus time table is provided to the FILL component as follows:

0.0 seconds < time < 39.0 seconds, VL = 0.05 m/sec

39.0 seconds < time < 42.0 seconds, linear ramp from 0.05 m/sec to -0.05 m/sec

42.0 seconds < time < 80.0 seconds, VL = -0.05 m/sec

The TRAC-M air-water option is activated to eliminate the level calculation uncertainties that are introduced during the transient. In this way, an analytical solution can be obtained for the water level height, to allow a comparison between the TRAC-M results and the analytical solution. In order to verify the code against Requirements LTRCK 2.1 and 2.2, the Cell 1 pressure calculated by the TRAC-M code is compared with the TRAC-BF1 results for the same test problem. The results will be acceptable if the calculated TRAC-M water level matches the TRAC-BF1 results, and the pressure of node #1 shows the same behavior as the TRAC-BF1 results.

Fig. 5.4.6 shows the water level height calculated by TRAC-BF1. An identical result is obtained with TRAC-M, as shown in Fig. 5.4.7. This proves that the TRAC-M code is able to track the position of a two-phase water level in a vertical flow region for a normal void profile. Thus, the code meets Requirement LTRCK 1.1.

The PIPE bottom cell pressure calculated by TRAC-BF1 with and without level tracking are shown in Figs. 5.4.8 and 5.4.9, respectively. Undesirable results are observed from these two plots. Without the level tracking model activated, TRAC-BF1 predicts a reasonable pressure profile. However, with the level tracking model, the code predicts large pressure spikes when the level is present in the upper half of each cell. This is not expected, since the original INEL report provided a reasonable pressure profile.

Errors found in the original TRAC-B level tracking model were corrected as the model was implemented in TRAC-M. These corrections also included a new level correction relaxation scheme in TRAC-M. Figs. 5.4.10 and 5.4.11 show the bottom cell pressure calculated using TRAC-M with and without the level tracking model. It should be noted that the code is able to predict a reasonable pressure profile without level tracking; however, the implemented level tracking model introduces insignificant pressure fluctuations when the level crosses the cell boundary.

Test Problem 2. Single Valve Component Fill and Drain Test

This problem is designed to test the 1-D level tracking capability for the VALVE component. The geometry and hydraulic conditions are identical to Test Problem 1. The valve adjustable flow area is set at cell face #6 with a constant flow area of 0.3 m^2, which is the same as the cell edge area. The results will be acceptable if the pressure of node #1 matches the result of Test Problem 1. Fig. 5.4.12 shows the calculated VALVE component bottom cell pressure profile. Comparing it with Fig. 5.4.11, one can see that they are identical, which verifies that the level tracking model is functional for the VALVE component.

Test Problem 3. Single Pressurizer Component Fill and Drain Test

This test problem is designed to examine the 1-D level tracking capability for the PRIZER component. The geometry, nodalization, and hydraulic conditions are identical to those of Test Problem 1. All of the pressurizer component-specific options are deactivated. The results will be acceptable if the pressure of node #1 matches the result of Test Problem 1. Fig. 5.4.13 shows the calculated PRIZER component bottom cell pressure profile. Comparison with Fig. 5.4.11 demonstrates that the results are identical for the period of time during which the level is rising, while slight differences are observed when the level recedes. Since no abnormal pressure fluctuations are observed, the results are considered acceptable, and the level tracking model is considered functional for the PRIZER component.

Test Problem 4. Single Pump Component Fill and Drain Test

This test problem is designed to examine the 1-D level tracking capability for the PUMP component, in case it is extended by a user to model a pump and the connected pipe lines. The geometry, nodalization, and hydraulic conditions are identical to those of Test Problem 1. The pump component type IPMPTY is set to 0, and the reverse rotation is allowed. The results will be

acceptable if the pressure of node #1 matches the result of Test Problem 1. Fig. 5.4.14 shows the calculated PUMP component bottom cell pressure profile. It should be noted that the pressure has a slightly different trend than that shown in Fig. 5.4.10 at the beginning of the transient and during the period of time when the level is receding. However, since no abnormal pressure fluctuations are observed, the results are considered acceptable.

Test Problem 5. Single CHAN Component Fill and Drain Test

This test problem is designed to examine the 1-D level tracking capability for the CHAN component. The geometry, nodalization, and hydraulic conditions are identical to those of Test Problem 1, and the rod power is set to zero. The results will be acceptable if the pressure of node #1 matches the results of Test Problem 1.

This test is not yet completed. The TRAC-M code did not run and gave some error messages. The errors are being researched and will be corrected when they are found.

This analysis will be completed with the next version of the code. Fig. 5.4.15 will show verification and test results. It is intentionally left blank in this report.

Test Problem 6. TEE Component Fill and Drain Test

This test problem is designed to examine the 1-D level tracking capability in both the primary tube and the side arm of a TEE component. As shown in Fig. 5.4.16, the primary tube of the TEE component has 11 nodes with a cell height of 0.3 m, a cell edge flow area of 0.3 m^2, and a hydraulic diameter of 0.1 m. By contrast, The side arm has 10 nodes, all of which have the same geometric dimensions. Both FILL components are set with a liquid velocity versus time table, which is the same as that used in Test Problem 1. The level tracking at the junction cell is deactivated by default.

The results will be considered acceptable if the pressures of node #1 of the primary tube and the last cell of the side arm match the node #1 pressure of Test Problem 1. The same fill and drain process occurs in the TEE side arm and the main tube at the same time. Figs. 5.4.17 and 5.4.18 show the calculated main tube and side arm bottom cell pressure profiles, respectively. It should be noted that these two pressure profiles agree well with the results shown in Fig. 5.4.11. Thus, the level tracking model is functional for the TEE component.

Test Problem 7. JETP Component Fill and Drain Test

This test problem is designed to examine the 1-D level tracking capability for the JETP component. The hydraulic condition and geometric dimensions of the JETP component are identical to those of Test Problem 6. Since the JETP component is based on the TEE component, the level tracking model is functional for the JETP component.

Test Problem 8. Two-PIPE Fill and Drain Test

This problem is designed to examine the inter-component level-crossing capability of the 1-D level tracking model. The boundary conditions are the same as those of Test Problem 1. Each PIPE component has five nodes, and two PIPEs are vertically connected with each other. All of the nodes have the same geometry and zero cell edge loss coefficients. The calculated level flag (ILEV) term should have an instant transition from one PIPE component to another. The level

height versus time and the bottom node cell center pressure should match those of Test Problem 1 for acceptance of this test. This test problem repeats the same transient analyzed in Test Problem 1 using two TRAC-M PIPE components. Fig. 5.4.19 shows the calculated bottom cell pressure profile. The water level crosses the component junction at 27.5 s and 52.5 s. Good agreement is observed between Figs. 5.4.19 and Fig. 5.4.10, which verifies that the inter-component level crossing was properly implemented in TRAC-M.

Test Problem 9. Single-Ring Vessel Fill and Drain Test

This test problem is designed to test the 3-D level tracking capability of the model, as well as the ability to predict the correct pressure and level position. The hydraulic conditions are identical to those of Test Problem 1, while the PIPE component is replaced by a VESSEL component with a radius of 0.5 m. Two PIPE components are connected to the bottom and top of the VESSEL component to perform the fill and drain functions. The results will be acceptable if the calculated TRAC-M water level matches the TRAC-BF1 results, and the pressure of node #1 shows the same behavior as the TRAC-BF1 results.

The transient is analyzed using TRAC-BF1 and TRAC-M with and without the level tracking model activated. Fig. 5.4.20 shows the water level height calculated by TRAC-BF1. A similar result is obtained from the TRAC-M code, as shown in Fig. 5.4.21, which verifies that TRAC-M is able to track the position of a two-phase water level in a vertical flow region for a normal void profile using the VESSEL component. Thus, the code meets Requirement LTRCK 1.1.

The PIPE bottom cell pressure calculated by the TRAC-BF1 code with and without level tracking are shown in Figs. 5.4.22 and 5.4.23, respectively. Unlike the 1-D PIPE fill and drain transient, without the level tracking model activated, TRAC-BF1 provides an undesirable pressure profile. The level tracking model used in TRAC-BF1 improves the pressure response somewhat; however, the pressure fluctuations remain as the level crosses the cell boundaries.

Figs. 5.4.24 and 5.4.25 show the bottom cell pressure calculated using TRAC-M with and without the level tracking model, respectively. It should be noted that the code is able to predict a reasonable pressure profile without level tracking.

The test results of this test problem show that the implemented 3-D level tracking model is able to track the level position. Improvements made in the level tracking model in TRAC-M produce reasonable pressure profiles.

Test Problem 10. Multiple-Ring/Azimuthal Cell Vessel Fill and Drain Test

This test problem is designed to test the 3-D level tracking capability in a vessel component with multiple rings and azimuthal nodes. As shown in Fig. 5.4.26, the test problem consists of a 3-D vessel component with two rings and two azimuthal sectors, six PIPE components providing the vessel fluid inlet/outlet flow paths, four FILL components, and two BREAK components. The 3-D VESSEL component has 10 axial levels with an even axial height of 0.3 m. The outer radius is 0.4 m for the first ring, and 0.7 m for the second ring cell. Each ring cell is divided into two identical azimuthal sectors, and all of the PIPE components have the same geometrical dimensions as in Test Problem 1.

The water initially fills the first level and half of the second level of the vessel component and all four PIPE components connecting with the vessel component at the bottom. The pressure is set to a constant (i.e., 1.013E+5 Pa) for the two BREAK components. In order to provide a uniform water level across the ring cells, two different liquid velocities are provided to the FILL components for the inner and the outer ring cells. A uniform liquid temperature of 300 K is assumed, and the air-water option is used to eliminate the uncertainties that are introduced through the interfacial mass transfer.

Since the correctness of the 3-D level tracking model is verified by Test Problem 9, the calculation results are considered acceptable if the code can be successfully executed to predict the level position. Fig. 5.4.27 shows the calculated water level, which demonstrates that the level tracking model is functional for a vessel component with multiple rings and azimuthal sectors.

Test Problem 11. Two-Vessel Fill and Drain Test Problem

This problem is used to test the 3-D level tracking capability for the case with multiple vessel components. Three PIPE components are employed to connect two identical VESSEL components, and all components are vertically connected together. One PIPE component connects the bottom of VESSEL #1 to a FILL component where a flow rate is specified. The second PIPE component connects VESSEL #1 and VESSEL #2 components, and the third PIPE component connects the top of VESSEL #2 to a BREAK component where a pressure is specified. Each VESSEL component has 1 ring and 10 axial levels. The outer radius of the ring is 0.4 m, and each axial level has the same height of 0.3 m. The geometrical dimensions of these three identical PIPE components are the same as in Test Problem 1. Initially, the bottom PIPE component and the first level of VESSEL #1 are filled with water, and the second level of VESSEL #1 is partially filled to provide a void fraction of 0.5. The FILL component connecting the bottom PIPE is given a velocity versus time table to control the fill and drain process.

The results of this test demonstrate that the code successfully simulates the entire transient in which the water first fills the lower vessel component, then the connecting PIPE component and finally the upper vessel component. The level then recedes into the lower vessel component at the end of the transient. Fig. 5.4.28 shows the water level height through the entire test. Since the code is able to predict a reasonable water level height, the results are considered acceptable, and the code is verified in its ability to track a water level when two vessel components are present.

5.4.2.2 Verification Tests and Their Assessment for Requirement LTRCK 1.2

Requirement LTRCK 1.2 specifies that the level tracking model is to track the water level for vertical components with an inverted void fraction distribution. Test Problems 12 and 13 are used to verify the correct implementation of this capability.

Test Problem 12. 1-D Inverted Void Fraction Profile Level Tracking Test

This problem is designed to test the 1-D level tracking capability for an inverted void fraction profile. A VALVE component is employed to establish an initial inverted void profile. As shown in Fig. 5.4.29, a VALVE component with the same geometrical dimensions as that of Test Problem 2 is provided with the following initial void fraction distribution:

- Cell #1, #2 and #6 have a void fraction of 0.0.
- Cell #3 and #7 have a void fraction of 0.5.
- All other cells have a void fraction of 1.0.
- The VALVE is initially closed at cell edge #6, and is suddenly opened at 50 s with a throat area of 0.003 m^2.

The results will be considered acceptable if the code is able to predict two water levels in the same component as long as there is water above the valve throat. After the water above the valve throat drains to the bottom, the code should only predict a single water level. The calculated water level heights above and below the throat area are shown in Fig. 5.4.30. It should be that the code predicts two water levels in the same component before t = 50 s, and is able to track two water levels above and below the throat. At t = 50 s, the throat area is abruptly changed. At ~ t = 60 s the water above the throat is completely drained, and the code predicts only one level. These results are deemed to be acceptable. Thus, the test verifies that the code meets Requirement LTRCK 1.2 for the 1-D level tracking model.

Test Problem 13. Vessel Inverted Void Fraction Level Tracking Test

Using a single-ring vessel component with the same geometrical dimension and same initial condition as in Test Problem 12, this problem is designed to test the 3-D level tracking model for the inverted void profile. Cell edge #6 of the VESSEL component has a flow area of 0.003 m^2, while the water above cell edge #6 gradually flows downward. Some of the air that is initially below the area reduction flows upward to maintain the pressure balance.

The results will be considered acceptable if the code is able to identify two water levels in the same component. After the water above the area reduction (cell # 6) drains to the bottom, the code should only predict a single water level.

Fig. 5.4.31 shows the water level below and above the flow area reduction. Since the code is able to track two levels initially present in the component, including the disappearance of the level above the flow area reduction, the results are considered acceptable, and the code meets Requirement LTRCK 1.2 for the 3-D level tracking model.

5.4.2.3 Verification Tests and Their Assessment for Requirement LTRCK 2.3

Requirement LTRCK 2.3 specifies that the level tracking model be able to provide the correct 3-D to 1-D donor cell void fraction based on the level position and the 1-D junction elevation. Test problems 14 and 15 are used to test this capability, as discussed below.

Test Problem 14. 3-D to 1-D Above-Level Suction Test

This problem is used to test the 3-D to 1-D donor cell void fraction calculation for a vertical PIPE component connected to the top of a cell that is partially filled with water. As shown in Fig. 5.4.32, a single-ring vessel component with 10 axial nodes is initially filled with water to level 6, while the void fraction of that level is 0.5. A four-node PIPE #1 component is connected

to the top of level 6, with a low-pressure boundary set by a BREAK #1 component. Another PIPE #2 component is connected at the top of the vessel component to provide a high-pressure boundary condition. During the transient, the air flows from the high-pressure BREAK #2 component to the low-pressure BREAK #1 component. It is expected that the void fraction inside the four-node PIPE should be close to 1.0.

The results will be acceptable if the void fraction of the first cell of the PIPE #1 component is close or equal to one. The calculated void fraction of the first cell of the PIPE #1 component is shown in Fig. 5.4.33. It should be noted that the void fraction remains at the value of 1.0 throughout the entire transient. Thus, the results are considered acceptable, thereby verifying the donor cell void fraction calculation.

Test Problem 15. 3-D to 1-D Below-Level Suction Test

For this test, as shown in Fig. 5.4.34, the vessel component and initial conditions are identical to those of Test Problem 14. A PIPE component is connected to the bottom of level 6, with a FILL velocity boundary, and the PIPE is initially filled with water. Another PIPE component is connected to the bottom level with a FILL velocity boundary. During the transient, the water inside the vessel is drained through the PIPE #2 component. Positive velocity will be specified in FILL #3, while negative velocity will be specified in FILL #2. PIPE #1 and BREAK #1 components provide a pressure source of air from the top of the vessel component. During the transient, the level inside the vessel component descends below level 6, and the void fraction of the PIPE #2 component connected to the bottom of level 6 will not contain air until the water level recedes below that level.

The results will be acceptable if the calculated void fraction inside the PIPE #2 component is close to zero before the level descends to level 5, and increases to 1.0 as the level further descends.

Calculated void fractions of the first cell in PIPE #2 and in level 6 of the VESSEL component are shown in Fig. 5.4.35. It should be noted that the void fraction in PIPE #2, Cell #1, remains at the value of 0.0 until the water level recedes, at which time the void gradually increases to the value of 1.0 and remains 1.0 throughout the remainder of the transient. Thus, the results are considered acceptable, and verify the 3-D to 1-D donor cell void fraction calculation.

5.4.2.4 Verification Tests and Their Assessment for Requirement LTRCK 2.4

The level tracking model requires modification of the interfacial heat transfer coefficient of a node with a water level. In order to verify the proper implementation, Test Problems 16 and 17 are employed to test the proper modifications to the interfacial heat transfer coefficient model. These test problems are discussed below.

Test Problem 16. 1-D PIPE Cold Water Injection Test

This test is designed to examine the modified interfacial heat transfer based on the water level. The test is a simple 10-cell vertical PIPE-filling transient. Each cell is 0.1 m high, with a flow area of 0.1 m^2. The FILL component connected to the bottom of the PIPE component injects the 333 K water into the PIPE, which is initially filled with 373 K vapor. The BREAK component at

the PIPE outlet maintains a constant pressure of 1 atm, and a constant vapor temperature of 373 K.

The transient will be simulated with and without level tracking activated, and the steam flow rate from the BREAK into the PIPE will be compared for the two cases. The water level propagates upward with a speed of 0.1 m/sec. At the interface, the steam condenses on the surface of the liquid. The condensation at the interface results in a low-pressure region adjacent to the level, which causes the extraction of the steam from the cell above. However, when the liquid surface temperature is raised to saturation, the steam condensation rate remains constant, so that no significant steam flow should be observed at the top of the PIPE component. It is expected that the run with level tracking will have a stable steam mass flow rate from the BREAK component to the PIPE component, while the run without level tracking will show a fluctuating mass flow. The results will be acceptable if the TRAC-M results are comparable with the TRAC-BF1 results.

Fig. 5.4.36 shows the calculated steam mass flow rate across the top of the PIPE component from the BREAK component. Without the level tracking model activated, TRAC-B predicts an unrealistic mass flow rate profile. Fig. 5.4.37 shows the mass flow rate calculated by the code with the level tracking model activated. It should be noted that the mass flow rate profile was improved; however, several fluctuations in the mass flow rate occurred when the level crossed the cell boundary.

With the level tracking model activated, TRAC-M provides a reasonable steam mass flow rate profile, as shown in Fig. 5.4.38. Good agreement is observed between the TRAC-B and TRAC-M results with the level tracking model activated when fluctuations in TRAC-B calculations are disregarded. Test results show that the TRAC-M code meets Requirement LTRCK 2.4.

Test Problem 17. 3-D VESSEL Cold Water Injection Test

A single-ring vessel component with the same dimension as the PIPE component of Test Problem 16 is connected with two PIPE components to the bottom and the top. The bottom PIPE component has two identical cells, with a cell edge flow area of 0.1 m^2 and a cell height of 0.1 m. The PIPE component is initially filled with 333 K water. The FILL component injects cold water into the PIPE with a speed of 0.1 m/sec. The vessel component is initially filled with the saturated steam at 373 K, and a constant pressure boundary is set for the PIPE connected at the top of the vessel. In a similar manner as in Test Problem 16, the results will be acceptable if the TRAC-M results are comparable with the TRAC-BF1 results.

An attempt was made to use an equivalent TRAC-BF1 input deck to compare the results. However, the TRAC-BF1 code failed to run for this case, while TRAC-M successfully executed through the entire transient. Fig. 5.4.39 shows the calculated steam supply mass flow rate without the level tracking model activated, while Fig. 5.4.40 shows the results with level tracking activated. It should be noted that the differences between these results are insignificant, and the TRAC-M level tracking model does not produce any adverse impacts on the mass flow rate profile. Therefore, the results are considered acceptable, and verify that the code meets Requirement LTRCK 2.4 for the 3-D vessel component.

5.4.2.5 Verification Tests and Their Assessment for Requirement LTRCK 3.0

Requirement LTRCK 3.0 specifies that the code must be able to restart with the level tracking model activated. In addition, proper input and output modifications should be made to accommodate the level tracking model. Test Problems 18 and 19 are used to test the input, output, and restart options, as discussed below.

Test Problem 18. 1-D Level Tracking Restart Test

In order to test the TRAC-M restart capability with the 1-D level tracking option activated, Test Problem 1 will be rerun, and then terminated at 40.0 s. A restart run will be performed to continue the transient to 80.0 s. The results will be compared with the results of Test Problem 1. If good agreement is obtained between these two runs, the TRAC-M 1-D level tracking restart capability will be considered acceptable.

Fig. 5.4.41 shows the cell 1 pressure from 0.0 s to 80.0 s, while Fig. 5.4.42 shows the cell 1 pressure from 0.0 s to 40.0 s. A restart run was performed at 40 s, and the calculated cell pressure was plotted in Fig. 5.4.43. The results demonstrate that the code is able to properly restart and produce identical results.

Test Problem 19. 3-D Level Tracking Restart Test

In a manner similar to Test Problem 18, this problem is designed to test the TRAC-M restart capability with the 3-D level tracking option activated. Test Problem 9 will be rerun, and then terminated at 50.0 s. A restart run will be performed to continue the transient to 100.0 s. If good agreement is obtained between the results of the restart run and the results of the original Test Problem 9, the TRAC-M 3-D level tracking restart capability will be considered acceptable.

Fig. 5.4.44 shows the level 1 pressure from 0.0 s to 80.0 s, while Fig. 5.4.45 shows the cell 1 pressure from 0.0 s to 40.0 s. A restart run was performed at 40 seconds, and the calculated level 1 pressure was plotted in Fig. 5.4.46. The results demonstrate that the code is able to restart and produces identical results, and verify that the new code is able to perform a restart calculation for 3-D components.

5.4.3 Conclusions

A total of 15 sets of test problems were successfully executed to verify the proper implementation of the level tracking model in TRAC-M. The results demonstrate that the code meets most of the requirements specified in the Software Requirement Specifications and associated tests listed in Tables 5.4.1 and 5.4.2, respectively.

Some code errors have been found in executing Test Problem 5. These tests will be executed using a future version of the code after the errors are corrected.

REFERENCES

5.4.1 Wade, N.L. et al., "TRAC/BF1-MOD1 Models and Correlations," U.S. Nuclear Regulatory Commission, NUREG/CR-4391, August 1992.

5.4.2 Rosen, A., et al., *Teploenergetikia*, 11, p. 59, 1976.

Table 5.4.1 LTRCK Nomenclature

α_j	Cell j average void fraction
α_{j+1}	Cell j+1 average void fraction
α_{j-1}	Cell j-1 average void fraction
α_j^+	Cell j above level void fraction
α_j^-	Cell j below level void fraction
$A_{j+1/2}$	Cell j top junction flow area (m^2)
$A_{j-1/2}$	Cell j bottom junction flow area (m^2)
$A_{j+3/2}$	Cell j+1 top junction flow area (m^2)
D_h	Cell j center hydraulic diameter (m)
G	Mass velocity (kg/sec m^2)
ΔZ_j	Cell j height (m)
L_j	Cell j two-phase level height (m)
J_g	Vapor volumetric flux density
J_g^-	Below level vapor volumetric flux density
V_g	Vapor velocity (m/sec)
V_{gj}	Below level vapor drift velocity (m/sec)
$V_{\text{level},j}$	Two-phase level velocity (m/sec)
ρ_g	Vapor density (kg/m^3)
ρ_l	Liquid density (kg/m^3)
σ	Surface tension (N/m)
μ_ℓ	Liquid viscosity (kg/m*sec)

Table 5.4.2 Requirements for Two-Phase Level Tracking Model

Requirement ID	Sub-Requirement	Requirement
LTRCK 1.0	LTRCK 1.1	The level tracking model will determine two-phase levels in vertically oriented components with normal void profiles. TRAC-M results will be the same as (or very close to) TRAC-B results in the test problems.
	LTRCK 1.2	The level tracking model will determine two-phase levels in vertically oriented components with inverted void profiles. TRAC-M results will be the same as (or very close to) TRAC-B results in the test problems.
LTRCK 2.0	LTRCK 2.1	The mass and energy flux terms will be modified to use above- and below-level void fractions when a two-phase level is present. TRAC-M results will be the same as (or very close to) TRAC-B results in the test problems.
	LTRCK 2.2	The inertial terms in the momentum equations will be modified to use above- and below-level void fractions when a two-phase level is present. TRAC-M results will be the same as (or very close to) TRAC-B results in the test problems.
	LTRCK 2.3	The component junction between 1-D and 3-D components will be modified to use above- and below-level void fractions when a two-phase level is present. TRAC-M results will be the same as (or very close to) TRAC-B results in the test problems.
	LTRCK 2.4	The flow regime map for interfacial heat transfer will be modified to use above- and below-level void fractions when a two-phase level is present. TRAC-M results will be the same as (or very close to) TRAC-B results in the test problems.
LTRCK 3.0		The input, output, and graphics modules of TRAC-M will be modified to accommodate the level tracking model input, output, and graphics. Restart will function the same as in TRAC-B.

Table 5.4.3 Test Problem Summary

Level Tracking Requirements	Test Problem	Test Problem Summary
LTRCK 1.1. Tracking of Two-Phase Level with Normal Void Profile LTRCK 2.1. Above- and Below-Level Void Fractions As Donor Quantities LTRCK 2.2. Inertial Terms in the Momentum Equations	1	FILL-PIPE-BREAK fill and drain test problem to test the level tracking in a PIPE component
	2	FILL-VALVE-BREAK fill and drain test problem to test the level tracking in VALVE component
	3	FILL-PRIZER-BREAK fill and drain test problem to test the level tracking in PRIZER component
	4	FILL-PUMP-BREAK fill and drain test problem to test the level tracking in PUMP component
	5	FILL-CHAN-BREAK fill and drain test problem to test the level tracking in the CHAN component
	6	FILL-TEE-BREAK fill and drain test problem to test the level tracking in the TEE primary and the side tube
	7	FILL-JETP-BREAK fill and drain test problem to test the level tracking in the primary and side tubes of the JETP component
	8	FILL-PIPE-PIPE-BREAK test problem to test the inter-component level crossing
	9	Single ring vessel fill and drain test problem to test the 3-D level tracking model
	10	Two-vessel fill and drain test to test the level tracking in multiple vessel components connected with the PIPE components
	11	3-D vessel fill and drain test to test the level tracking in a VESSEL component with multiple rings and azimuthal sectors
LTRCK 1.2. Tracking of two-phase level with inverted void profile (2.1 and 2.2)	12	FILL-VALVE-BREAK water leaking test problem
	13	Vessel stagnant water column leaking test problem
LTRCK 2.3. Vessel Boundary Condition	14	VESSEL-PIPE above-level test to test the VESSEL-to-PIPE void fraction for a connection above the level
	15	VESSEL-PIPE below-level test to test the VESSEL-to-PIPE void fraction for a connection below the level
LTRCK 2.4. Interfacial Heat Transfer in Partially Filled Cells	16	FILL-PIPE-BREAK subcooled water draining problem to test the 1-D component two-phase level front condensation calculation
	17	Single-ring vessel subcooled water draining problem.
LTRCK 3.0. Input, Output and Restart Requirement	18	Stop test problem #1 at 40 seconds, followed by a restart
	19	Stop test problem #9 at 40 seconds, followed by a restart

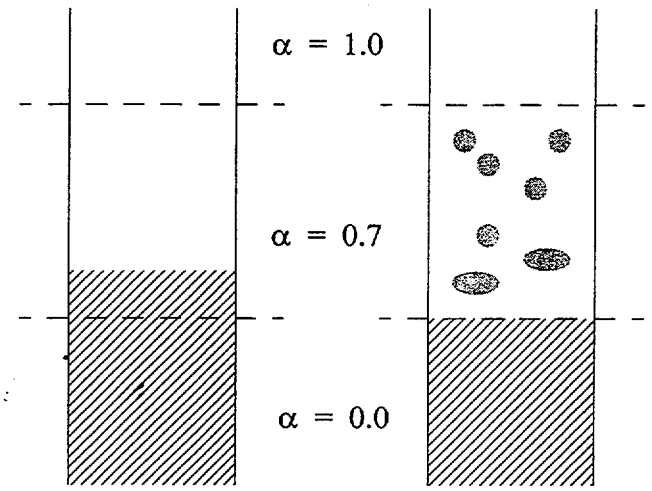

Figure 5.4.1 Flow Regime Dilemma

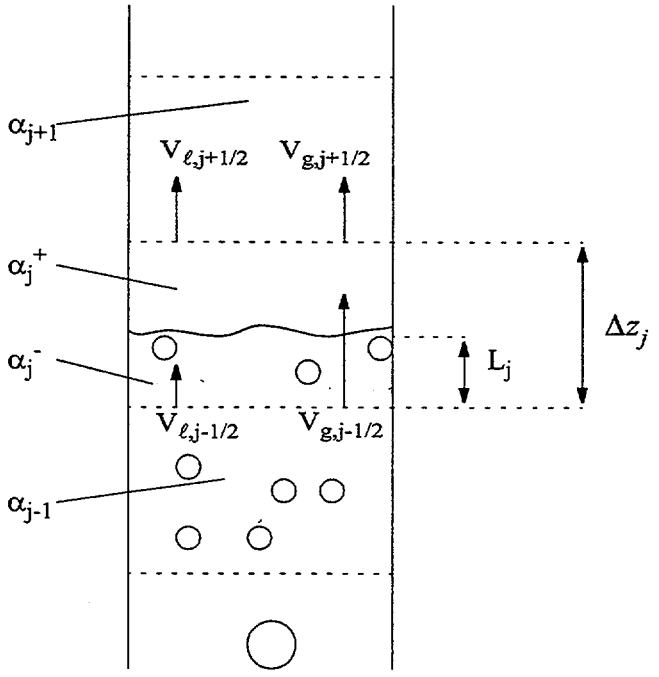

Figure 5.4.2 Two-Phase Level in Vertical Flows

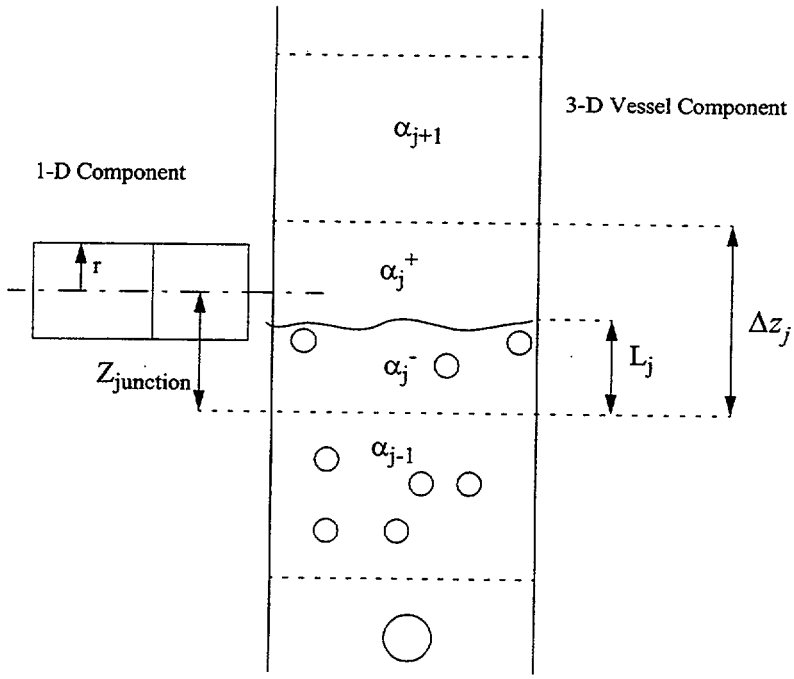

Figure 5.4.3 1-D and 3-D Component Connection with Two-Phase Level

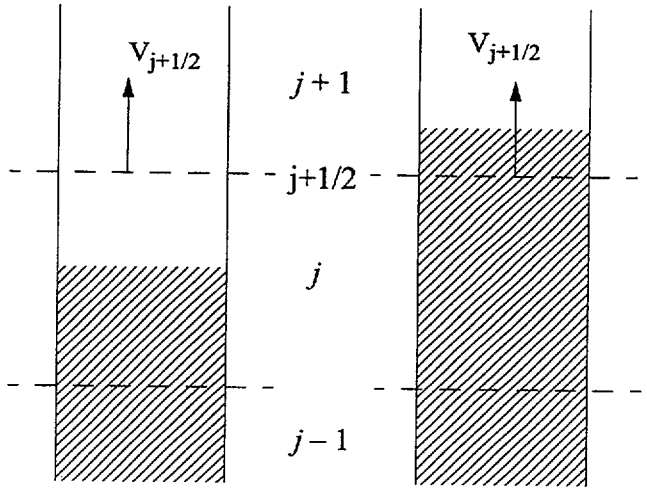

Figure 5.4.4 Flux Terms Above and Below a Two-Phase Level

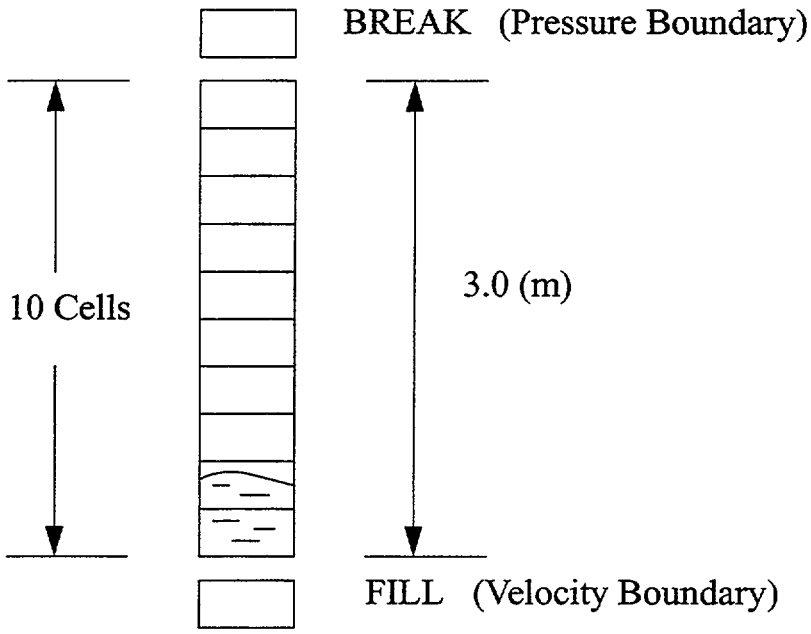

Figure 5.4.5 Single-Pipe Fill and Drain Test Problem

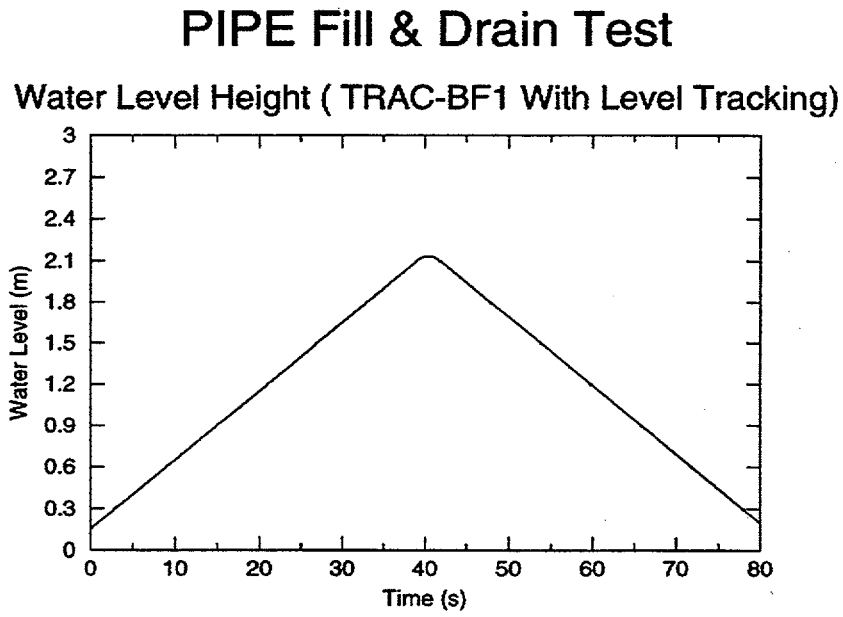

Figure 5.4.6 Pipe Fill & Drain Test, Water Level Height, TRAC-BF1 with Level Tracking

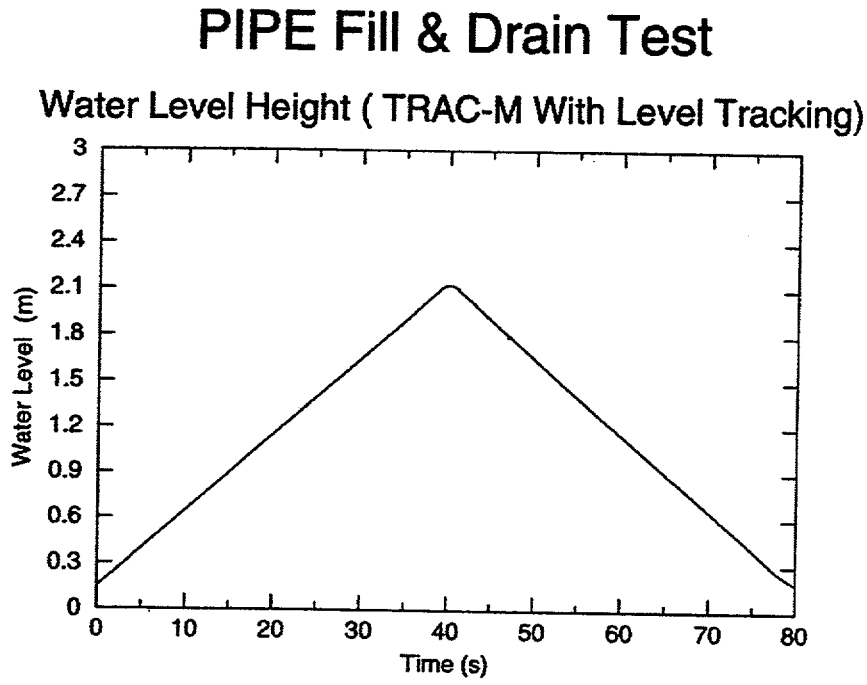

Figure 5.4.7 Pipe Fill & Drain Test, Water Level Height, TRAC-M with Level Tracking

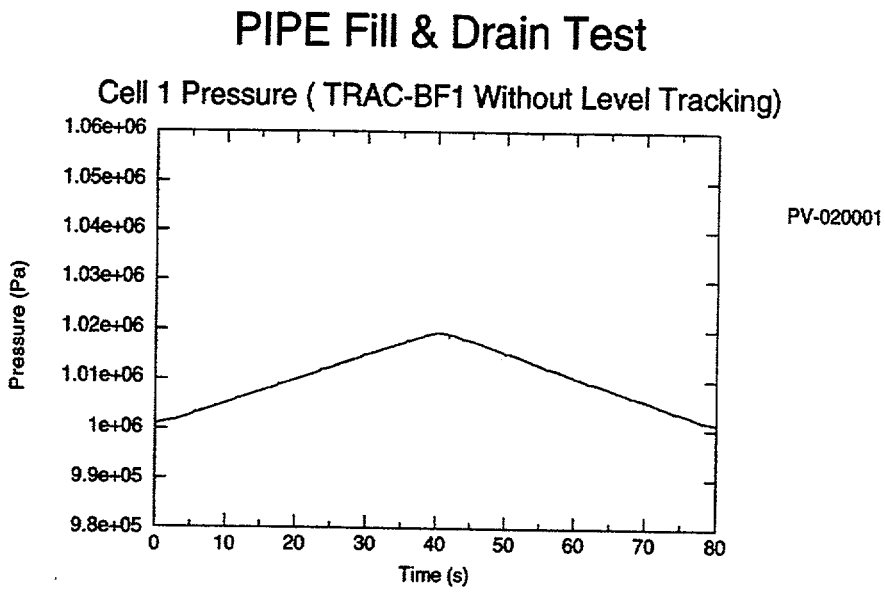

Figure 5.4.8 Pipe Fill & Drain Test, Pressure in Cell #1, TRAC-BF1 without Level Tracking

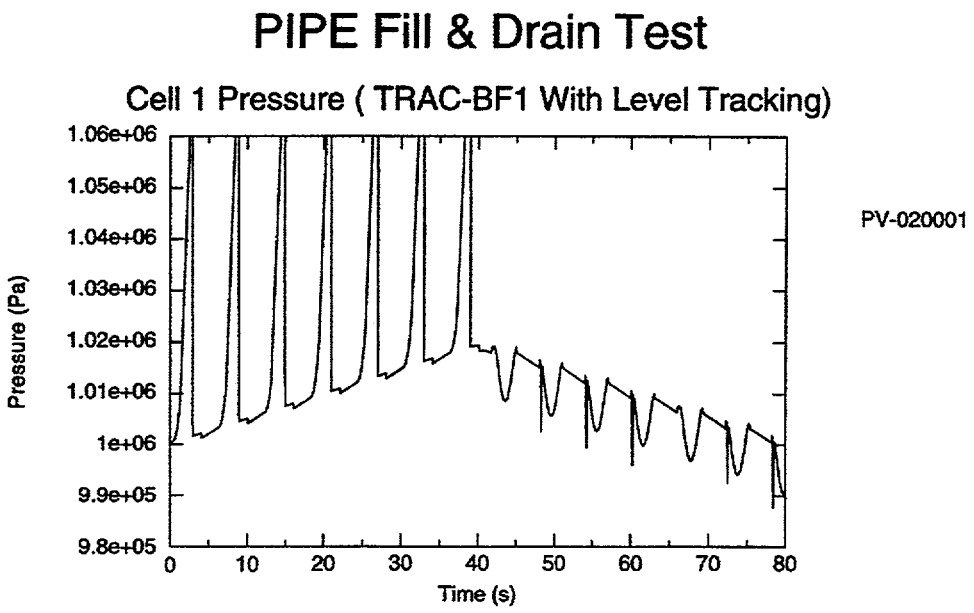

Figure 5.4.9 Pipe Fill & Drain Test, Pressure in Cell #1, TRAC-BF1 with Level Tracking

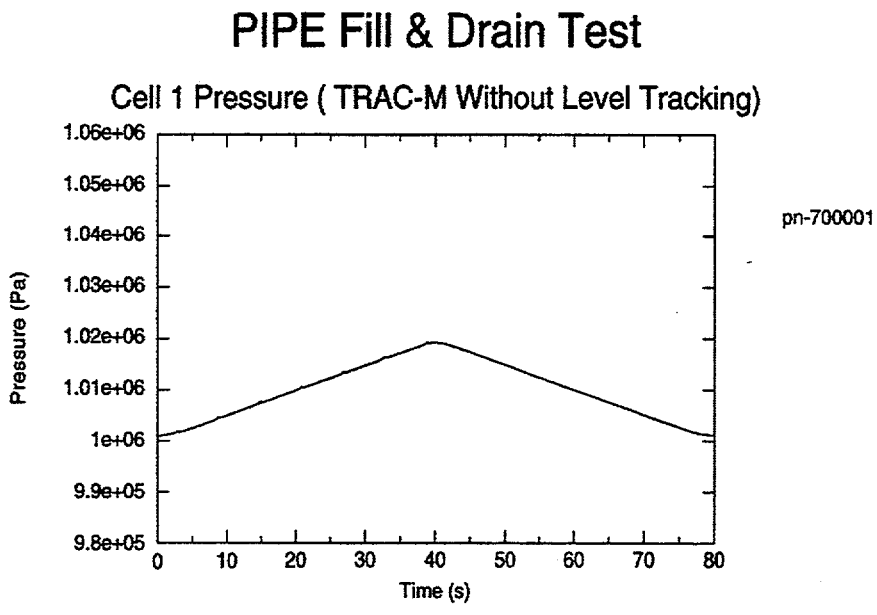

Figure 5.4.10 Pipe Fill & Drain Test, Pressure in Cell #1, TRAC-M without Level Tracking

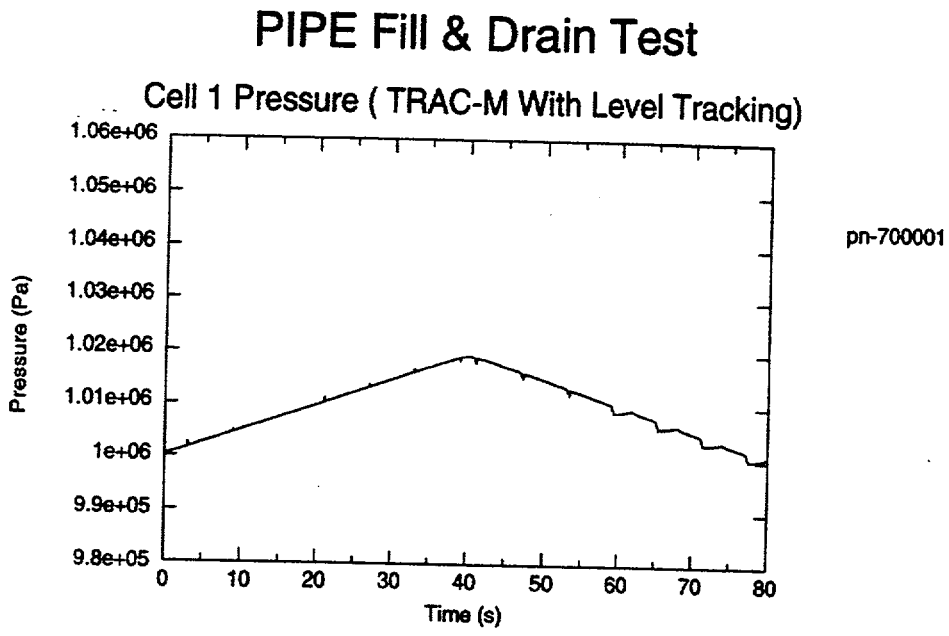

Figure 5.4.11 Pipe Fill & Drain Test, Pressure in Cell #1, TRAC-M with Level Tracking

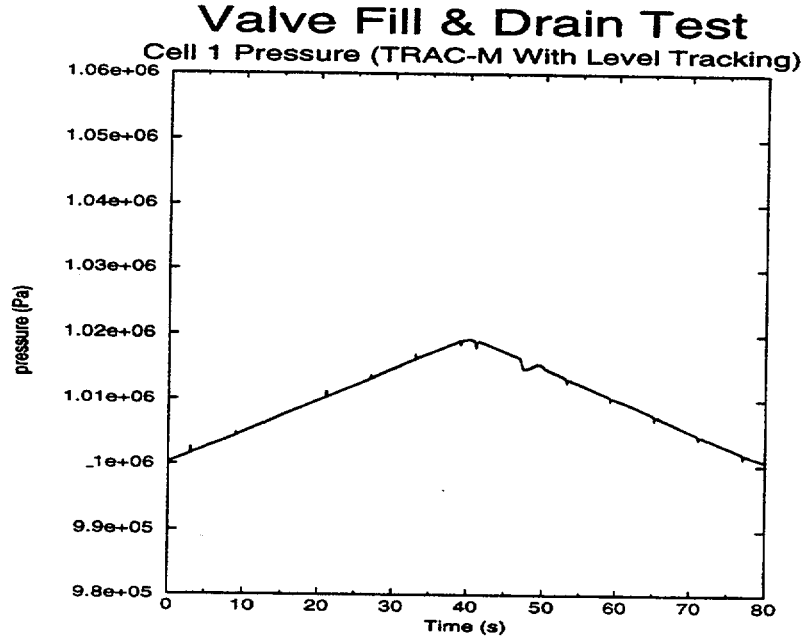

Figure 5.4.12 Valve Fill & Drain Test, Pressure in Cell #1, TRAC-M with Level Tracking

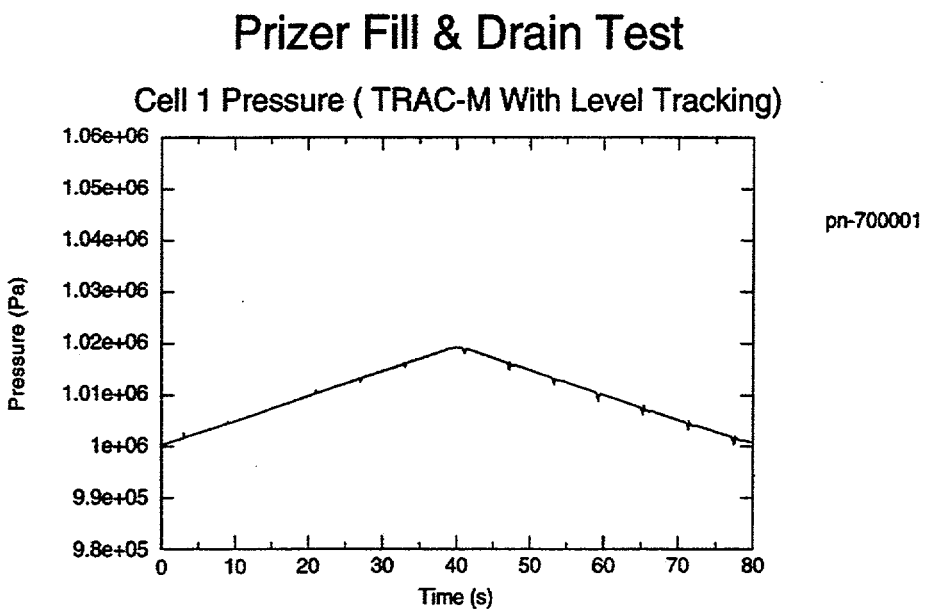

Figure 5.4.13 Prizer Fill & Drain Test, Pressure in Cell #1, TRAC-M with Level Tracking

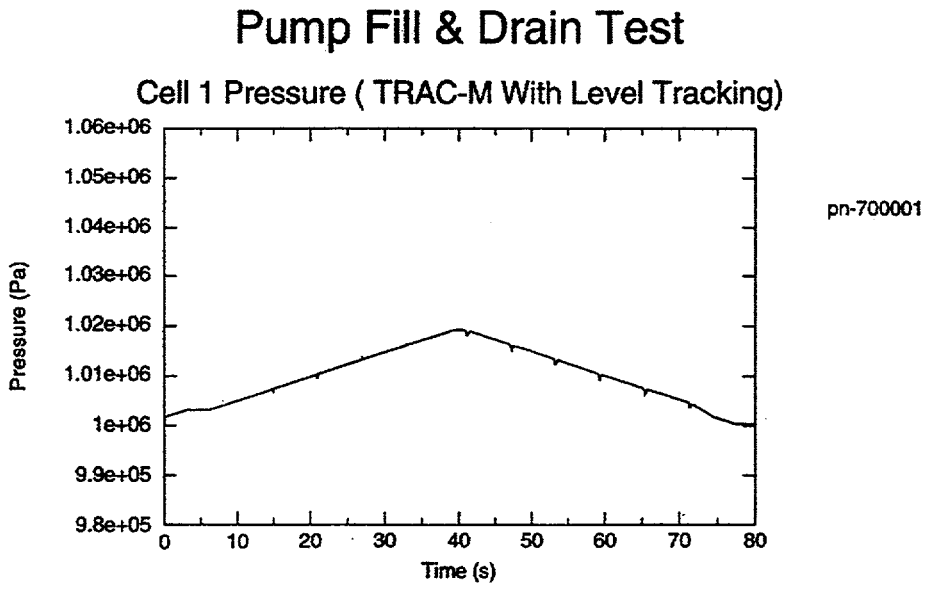

Figure 5.4.14 Pump Fill & Drain Test, Pressure in Cell #1, TRAC-M with Level Tracking

[THIS FIGURE IS INTENTIONALLY LEFT BLANK]

Figure 5.4.15 Intentionally Left Blank

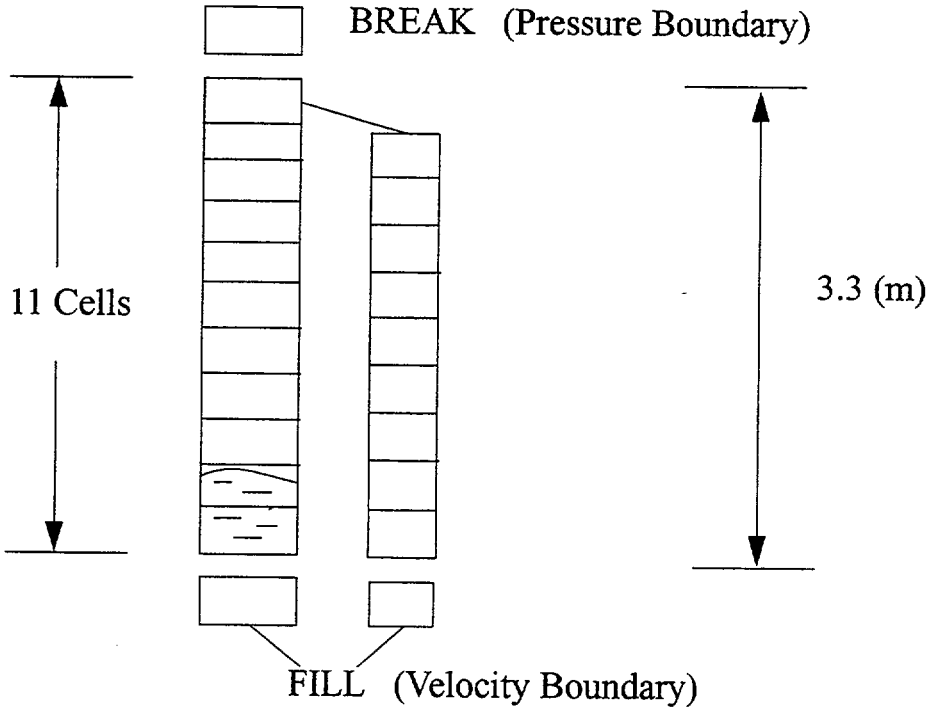

Figure 5.4.16 TEE Component Fill and Drain Test Problem Nodalization